Università degli studi di Catania

Facoltà di Scienze Matematiche, Fisiche e Naturali
Dipartimento di Scienze Biologiche, Geologiche ed Ambientali

Doctor of Philosophy Thesis

Approaches to earthquake scenarios validation using seismic site response

"Evoluzione Geologica di Orogeni di Tipo Mediterraneo"

XXIV Ciclo

Author:
Dr. Francesco Panzera

Advisers:
Prof. Giuseppe Lombardo
(Università degli Studi di Catania – Dip. di Scienze Biologiche, Geologiche ed Ambientali)
Dr. Rosaria Rigano
(Università degli Studi di Catania – Dip. di Scienze Biologiche, Geologiche ed Ambientali)
Dr. Antonio Rovelli
(Istituto Nazionale di Geofisica e Vulcanologia – Roma)

Acknowledgements

My first thanks go to my Advisor Prof. Giuseppe Lombardo for his sustain and help, for his courtesy and scientific suggestions.

Thanks to the co-tutor Dr. Antonio Rovelli, for his prestigious help, the precious suggestions and his sound problem solving ability.

Thanks to Dr. Rosaria Rigano for her ever available courtesy and the advises for the software use.

Finally thanks to Raffaella and my Family, that support me in the everyday life and in this studying career.

"La ragione umana viene afflitta da domande che non può respingere,
perché le sono assegnate dalla natura della ragione stessa,
e a cui però non può neanche dare risposta,
perché esse superano ogni capacità della ragione umana."
I.Kant

Table of contents

Introduction

In order to mitigate the risk from earthquake and to ensure the safety of the buildings under earthquake loading, local seismic response has been taken into consideration in many design code (e.g. EUROCODE8, 2003; Norme tecniche per le costruzioni, 2008). The increasing of importance of this problem, in particular in recent years, has been generated from the damage on structure linked to landslides, liquefaction and amplification of the seismic ground motion in the shallow soil layers observed in earthquakes that affect many large cities. The first step in seismic risk reduction is the compilation of the seismic hazard map on the base of the effects of historical earthquakes, seismic source zone model, seismic rate, ground motion attenuation relationships and other existing information. The quality of the first step may be improved considerably through detailed seismic response analysis at local scale. A reliable evaluation of ground motion at one site requires the analysis of the following three steps: seismic radiation released by the source; path and attenuation effects in the wave propagation from the source to the city; local effects linked to elastic and anelastic properties of soil deposits interposed between the bedrock and the surface.

In particular, seismic sources in eastern Sicily were studied by several authors who estimated, also through numerical simulations, potential shaking parameters for different earthquake inputs (Langer *et al.*, 1999; Zollo *et al.*, 1999; Azzaro and Barbano, 2000; Barbano and Rigano, 2001; Laurenzano *et al.*, 2004; Laurenzano and Priolo, 2005). As far as the second step is concerned, the evaluation of the seismic input at the bedrock, by taking into account both the source features of a scenario earthquake and the attenuation, was carried out by De Lorenzo *et al.* (2004), Giampiccolo *et al.* (2002, 2003, 2004). A significant improvement to the knowledge of the seismotectonic setting in south-eastern Sicily was achieved through the analysis of the 13 December 1990 earthquake and its aftershocks.

These events are, indeed, the first digital set of seismic data for the area, therefore allowing investigations on the spectral source parameters and estimate of attenuation and seismic scaling laws in south-eastern Sicily (Amato *et al.*, 1995; Di Bona *et al.*, 1995; Giardini *et al.*, 1995; Scognamiglio *et al.*, 2005). The estimate of ground motion features at the surface was performed using numerical modeling as well as noise measurements. In particular, for Catania, Biondi and Maugeri (2005), Lombardo *et al.* (2004, 2006), Catalano *et al.* (2005), Lombardo and Rigano (2007) evaluated the local seismic response in test sectors of the urban area, whereas preliminary estimates of site response in the whole Catania area were obtained by Giampiccolo *et al.* (2001), Lombardo *et al.* (2001), Priolo *et al.* (2005). Further investigations on the local effects due to fault zones (Rigano *et al.*, 2008) as well as natural cavities (Lombardo and Rigano, 2009; Lanzo *et al.*, 2006; Sgarlato *et al.*, 2011) have been recently performed and others are still in progress. While the main study of the seismic site effects at Siracusa was performed in the frame of a project called "Scenari di pericolosità sismica ad Augusta, Siracusa e Noto" (Decanini and Panza, 2000).

Catania and Siracusa are located on the eastern coast of Sicily (southern Italy). The high level of seismicity that affects the area (**Fig. 1**), together with the considerably high density of inhabitants, contribute to classifying these towns amongst those with the highest seismic risk in Italy. The potential severity of damage to which their historic-architectural patrimony could be subjected to is also not negligible. The seismic activity of the investigated area is particularly high as testified by the historical earthquakes that occurred in 1169, 1542, 1693, 1818, 1908 as well as the recent one that occurred in 1990, all having intensity ranging between the VI and XI MCS scale (Working Group CPTI, 2004). The manuscript identifies and briefly describes the methods considered suitable for the hazard and seismic site response assessment, and provides an illustration and discussion through practical applications to Catania and Siracusa. In particular, a detailed probabilistic seismic hazard analysis for the towns of Catania and Siracusa using two probabilistic approaches "site" method (Albarello and Mucciarelli, 2002) and the "seismotectonic" methodology (Cornell, 1968; Esteva,

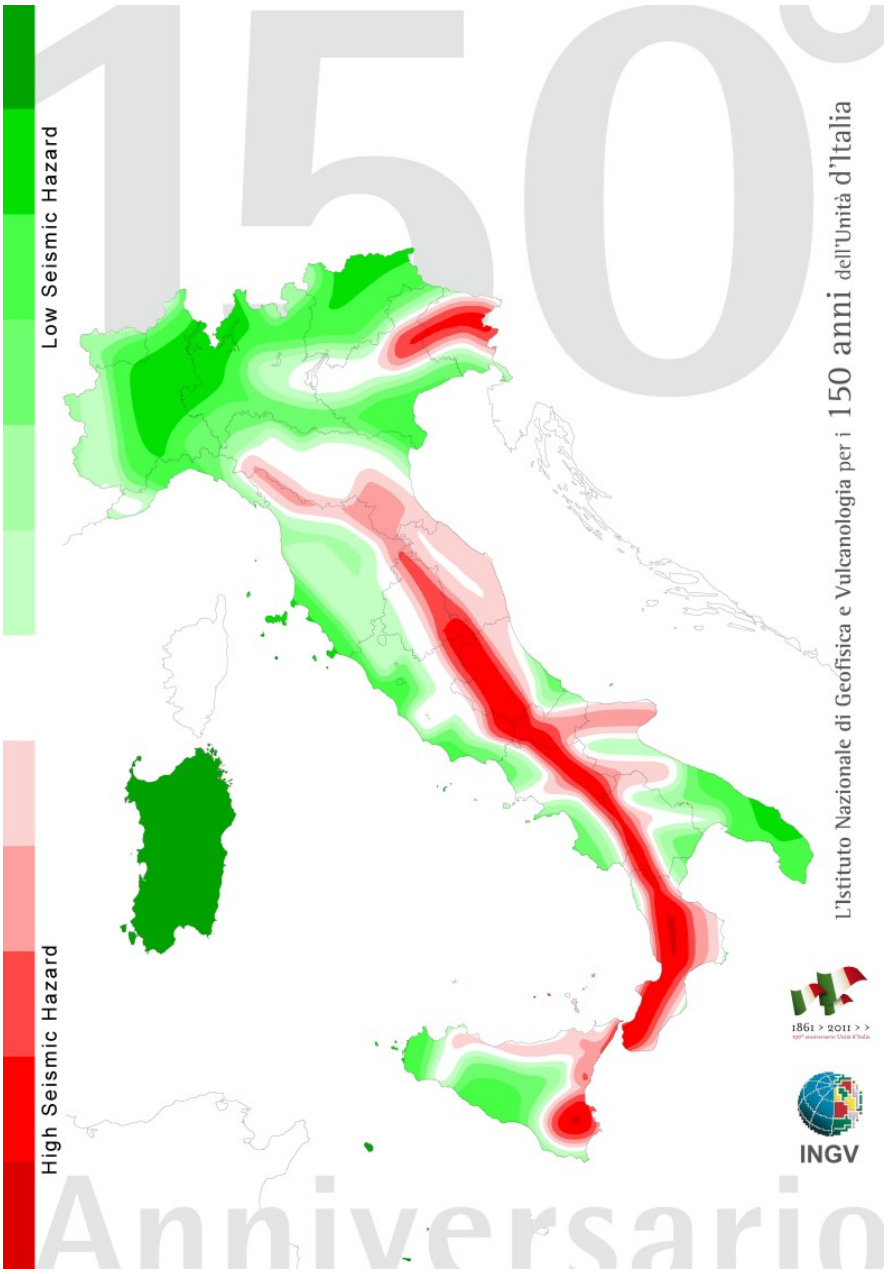

Fig. 1. *Hazard map of Italian national territory*

1967), taking into account different seismogenic sources, was performed. Therefore, the seismic site response of the two cities, considering that numerous observations in earthquake-affected areas have shown that seismic impact are in some way influenced by the local subsoil structure, was assessed. The soil amplification of the sites are investigated using different approaches: either numerically and instrumentally. The first method requires detailed information

about the site's subsoil stratigraphy and geotechnical soil parameters. The second method presumes the availability of instrumental data (earthquakes or noise) at the ground surface and possibly at an additional reference site. The role of topographic features on seismic waves amplification was, particularly, examined testing different methodology.

Chapter I

Seismic Hazard

Seismic hazard analysis (SHA) is usually performed to obtain the possible effects due to an earthquake of the future (and the related uncertainties) at a specific site in term of displacement, velocity and/or acceleration. It is commonly used to describe the severity of ground motion at a particular site without consideration of the consequences (Kramer, 1996). It can be performed using either a *deterministic* (DSHA) or a *probabilistic* (PSHA) approach. The DSHA uses individual earthquake sources and single-valued events to establish a particular scenario that describes the hazard. Typically, a seismic source location, an earthquake of specified size and a ground motion attenuation relationship are required. However, this approach does not provide information on the occurrence probability of an earthquake parameter (acceleration, magnitude) during a finite period of time (e.g., the useful lifetime of a particular structure or facility). PSHA, being a statistical approach, needs to identify a suitable time interval having good completeness of information. On the other hand, PSHA allows to estimate the probability when an intensity measurement (e.g., peak acceleration) could exceed a defined value during a given time (e.g., 50 years) (McGuire, 2004). It accounts for all possible combinations of magnitude-location of shocks and models describing the effects and the occurrence rate of all earthquakes that could affect an area.

1.1. Probabilistic Seismic Hazard

PSHA provides a framework in which it is possible to identify, quantify and combine uncertainties in the size, location and rate of occurrence of earthquakes, seismogenic source geometry, and in the ground motion as a function of the size and location of earthquakes (Kramer, 1996). Following the traditional approach proposed by Esteva-Cornell in 1968, PSHA consists of four steps: 1. identification and characterization of earthquake sources (these might be fault sources or areal

sources within which earthquakes are to be equally likely to occur at any location; 2. evaluation of temporal distribution of earthquake recurrence assuming that earthquakes occur independently; 3. characterization of the ground motion produced at a site by earthquakes of different size occurring at different locations in each seismic source; 4. computation of the probability that a specified ground motion level at a site will be equalled or exceeded during a specific time period (**Fig. 1.1.1**).

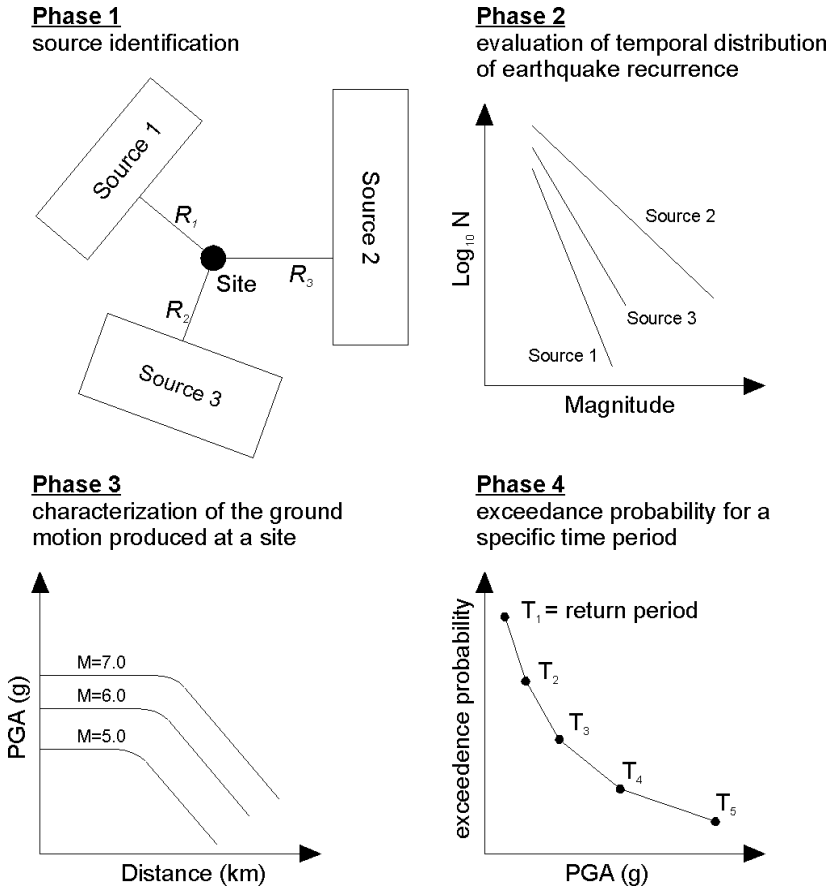

Fig. 1.1.1. *Phases of a probabilistic seismic hazard assessment (modified from Kramer, 1996).*

The probabilistic formulation in terms of exceedence rates λ of a ground shaking parameter m^* considering all the potential magnitudes, in the range M_{min} to M_{max}, and source-to-site distances, having value vary from R_{max} to R_{min}, have the form:

$$\lambda_{m^*} = \sum_{i=1}^{N_S} v_i \int_{M_{min}}^{M_{max}} \int_{R_{min}}^{R_{max}} \int_{\varepsilon} P[m > m^* | = M, R, \varepsilon] \, f_m f_r f_\epsilon \, dm dr d\varepsilon \qquad (1.1)$$

where υ_i is the mean annual rate of earthquake occurrence greater than a minimum magnitude M_{min} for each one of the N_S potential earthquake sources. The $P[m > m^*|= M, R, \varepsilon]$ function is the probability that a specific earthquake parameter (m), given the magnitude (M), the distance (R) and the uncertainties (ε), exceeds a ground motion parameter (m^*) at a specific site. The f_m, f_r and f_ε, lastly, are the probability density function of magnitude, distance and for the ground motion variability respectively.

Taking into account a Poisson process the probability to observe a given ground motion parameter value during a specified exposure time, t, can be estimated using the formula:

$$P[N \geq 1] = 1 - P[N \geq 0] = 1 - e^{-m^* t} \qquad (1.2)$$

The results of a PSHA can be summarized by *seismic hazard curves*, which show the probability of exceedance versus a specific ground motion parameter (e.g. peak ground acceleration, PGA). The PSHA results, however, can be illustrated using *uniform hazard spectrum* (UHS) obtained by computing the ground motion at a suite of spectral periods.

Another important problem in PSHA regards the treatment of uncertainties that can be distinct in aleatory uncertainty, related to the unpredictability of natural phenomena, and epistemic uncertainty, connect to mathematical models and values of the parameters of each model used. For the reduction of the epistemic uncertainty a logic tree approach proposed by Senior Seismic Hazard Analysis Committee (SSHAC, 1997) can be used.

1.2. Deterministic Seismic Hazard

A deterministic ground motion scenario was intended as maps representing the ground-shaking severity over a municipal area with appropriate hazard descriptors (Faccioli and Pessina, 2003). A "reference" earthquake, of specified magnitude (or epicentral intensity) on a specified seismic source (e.g a fault) was assumed, and the zonation map of the ground-shaking distribution in the city through 1D, 2D or 3D ground motion simulation for the selected hazard parameters was build (**Fig. 1.2.1**). A strong requirement for DSHA was that the "reference" earthquake

should be the "true" maximum historical earthquake affecting the city. If the site under study had historically been exposed to earthquakes of significantly different intensity, two or more different deterministic scenarios could be considered. After choosing the "reference" earthquake, another problems concern its source location. The historical observations, in particular, are often unwell documented and the location of the source tends to be controversial. In a deterministic analysis, it is usually prudent to test alternative source hypotheses, but for any given scenario the preferred hypothesis for the seismic source had to be clearly indicated and justified.

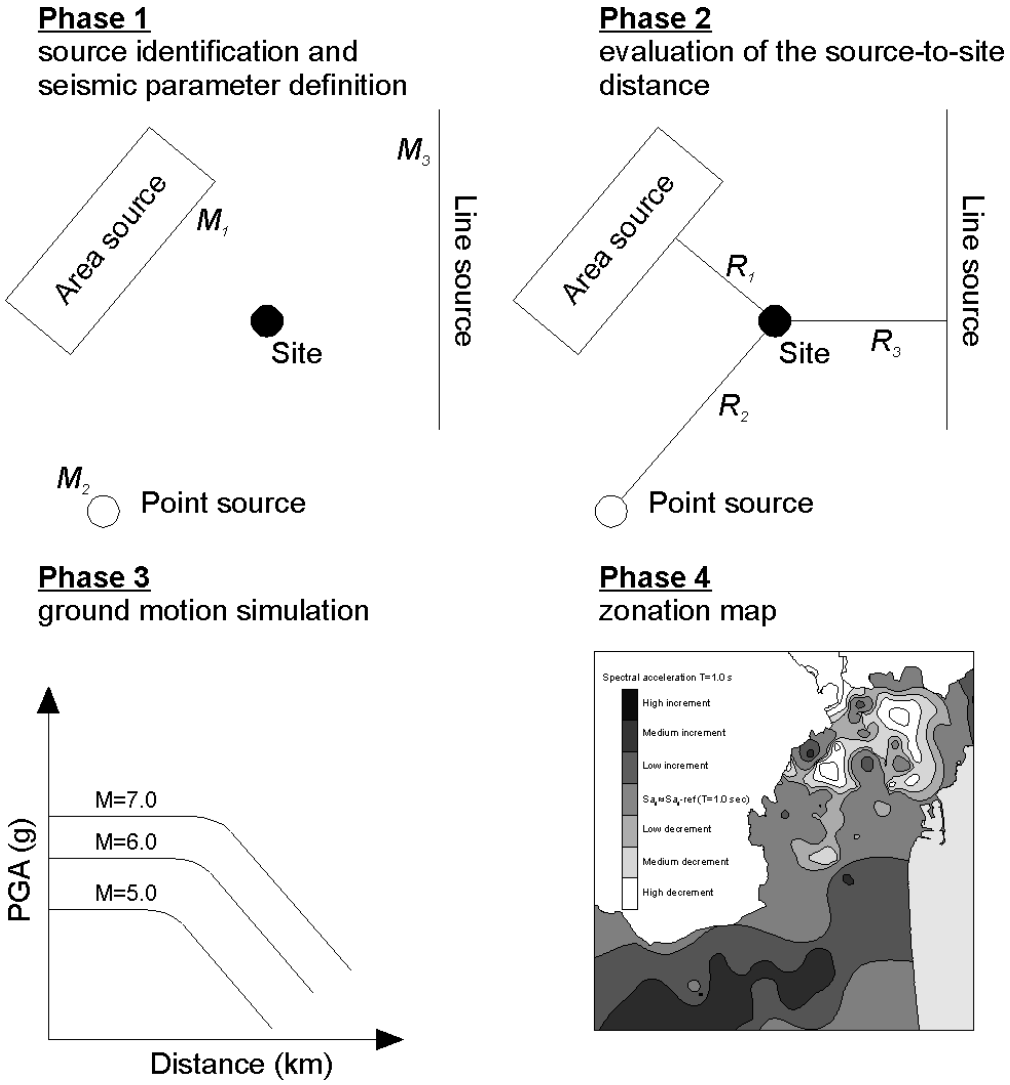

Fig.1.2.1. *Phases of a deterministic seismic hazard assessment (modified from Kramer, 1996).*

The deterministic spectrum, lastly, is associated to the largest historical earthquake, which occurred on a specific fault, with a specific magnitude at a specific distance, while the constant hazard spectrum does not represent a specific event but a kind of weighted combination of many different events originating on different geological features. This is essentially the principal difference between the deterministic and the probabilistic hazard assessment (Faccioli and Pessina, 2003).

Chapter II

Seismic Site Effect

According to Seed and Idriss (1982) the seismic wave motion generated by an earthquake in a site with free-field conditions (in the absence of buildings) depends on a set of physical phenomena that can be summarized as follows: speed of fault rupture, source mechanism of the earthquake, magnitude of the earthquake, distance of the site from the source of energy release, geologic characteristics of the rocks along the wave transmission path from the source to the site, wave interference effects related to the path direction and local soil conditions at the site (**Fig. 2.1**).

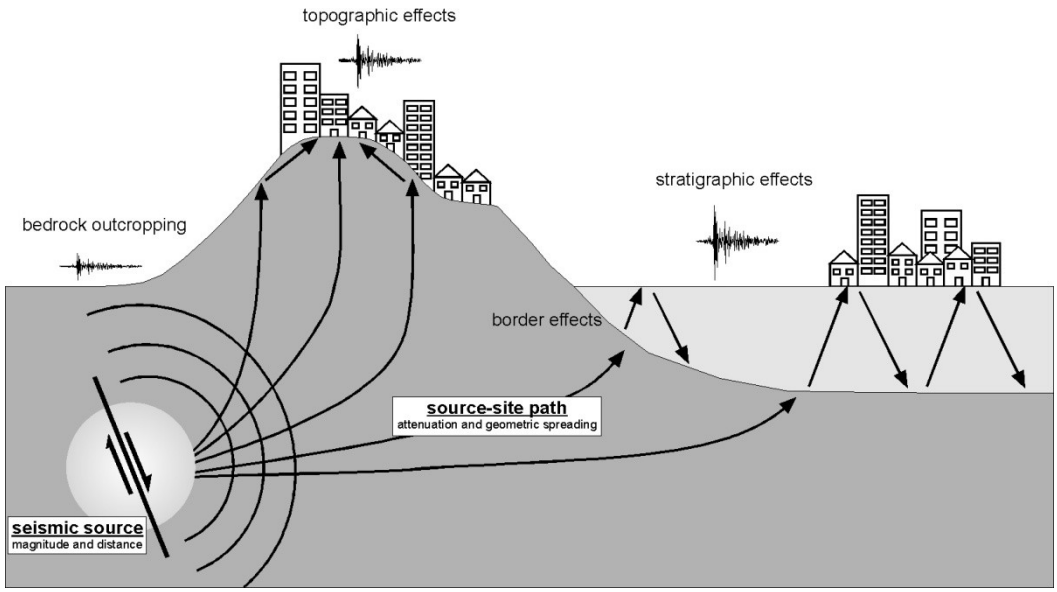

Fig. 2.1. *Factors responsible for the ground motion shaking*

According to the foregoing a seismic signal spectrum S(ω), to a generic site, can be represented by the following equation:

$$S(\omega) = G(\omega)\, R(\omega)\, I(\omega)\, T(\omega) \qquad (2.1)$$

In *2.1* equation G(ω) represents all the characteristics of the source, R(ω) the path from the source to the site of seismic waves, I(ω) is the instrumental

response, while T(ω) is the transfer function of the site. The term T(ω), transfer function of the site, is a clear and effective representation of local seismic response and it is characteristic of each site.

The local seismic response is clearly influenced by seismic site effects that can be subdivided into *primary seismic site effects* and *secondary seismic site effects*. A definition of both terms is given by Wang and Law (1994). *Primary seismic site effects* are connect to modification in amplitude, in frequency content, or in time duration of the seismic waves transmitted through the ground material. Examples of this type of site effect are wave-field effects, amplification/filtering effects of soft ground, and resonance effects. *Secondary seismic site effects* are phenomena induced by earthquake as well as seismic liquefaction of the soil, ground collapse (e.g. earthquake-induced collapse of underground cavity), and seismic landslide forced by slope instability.

The main factors, connect to *primary seismic site effects*, which have influence on local seismic response, are the result of multiple physical phenomena (reflections, diffraction, focusing, resonance, etc.), that the waves suffer for the presence of the heterogeneity and discontinuity of the shallow layers. These effects can be distinguished in: stratigraphic effects (or 1D), edge effects (or valley), and topographic effects related to lateral heterogeneity, such as the presence of faults and/or stratigraphic contact (**Fig. 2.1**). The latter can be interpreted in part as a topographical effect (fault scarps) and partly as a result of the edge (e.g. fault gouge). This subdivision is also very significant from practical point of view, since different categories also correspond to different methods and tools for quantitative assessment of local seismic response.

The behavior of a site, therefore, in terms of energy distribution at different frequency, depends on the local characteristics of the formations crossed by the seismic waves, the geometry of the subsurface and surface morphology how recent earthquakes (e.g., Mexico 1985, Loma Prieta 1989, L'Aquila 2008) has shown. It is then important to define the seismic site response in order to reduce the effects of earthquakes.

2.1. Soft surface layers effects

The earthquake damage is generally larger over soft sediments than on firm bedrock outcrops. This is particularly important because most of urban area are located along river valleys where deep alluvial deposits outcrop. In this condition the main seismic site effect is called stratigraphic or 1D. The so-called stratigraphic effects are related to changes that the seismic wave motion undergoes when it incides vertically to a flat deposit with horizontally layered structure. In this condition, the fundamental phenomenon responsible for the amplification of motion over soft sediments is the trapping of body seismic waves due to the impedance contrast between sediments and the underlying bedrock. For each soil layer the impedance is defined as the product of mass density (ρ) and shear wave velocity (V_S). The impedance ratio (α) between bedrock and overlying sediments can be calculated using the equation:

$$\alpha = \frac{\rho_B V_{S,B}}{\rho_S V_{S,S}} \qquad (2.2)$$

where the numerator of the equation is the bedrock impedance whereas the denominator is relate to soil deposits impedance. The resonance frequencies at which amplification take place depends on the geometry (in particular thickness, H) and dynamic soil properties (in particular shear wave velocity, V_S, and damping factor, ξ) of the sedimentary soil layers (**Fig. 2.1.1**).

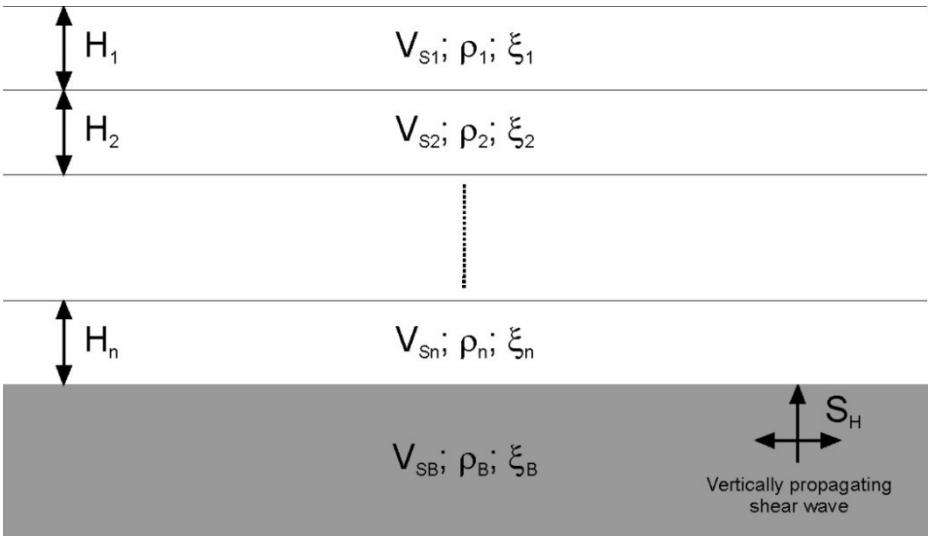

Fig. 2.1.1. *One dimensional layered soil deposits system*

The i_{th} resonance frequency of the soil profile is given:

$$F_i = (2i + 1)\frac{V_S}{4H} \qquad (2.3)$$

where i = 0, 1, 2…, ∞. For i = 0 the lowest resonance frequency is determined, called *"fundamental or natural site frequency"*. The level of amplification (A) is controlled mainly by the damping factor, ξ, of the soil layers, that it is maxima in correspondence of the fundamental frequency.

$$A_{max} = \frac{1}{\frac{1}{\alpha}+\frac{\pi\xi}{2}} \qquad (2.4)$$

Another important feature in seismic site response analysis is connect to nonlinear behavior of soft soils. The application of weak-motion data or ambient seismic noise for the study of structural earthquake damage, leads to the consideration of possible nonlinear effects that are caused by strong earthquake. Nonlinear site effects are one of the most important and controversial problems because the determination of the threshold acceleration or shear strain γ, beyond which soil nonlinearity becomes observable, is quite difficult (Özel *et al.*, 2002). The nonlinear behavior of strain dependent shear modulus $G(\gamma)$ can usually be expressed by a relation between shear stress, τ, and shear strain, γ:

$$G(\gamma) = \frac{\tau}{\gamma} = \frac{G_0}{1+\frac{\gamma}{\gamma_{ref}}} \qquad (2.5)$$

where G_0 is shear modulus for smallest shear strains and γ_{ref} is reference shear strain. The characteristic curves of shear modulus G can be described by hyperbolic relationships proposed by Yokota *et al.* (1981):

$$\frac{G(\gamma)}{G_0} = \frac{1}{1+\alpha\gamma(\%)^{\beta}} \qquad (2.6)$$

in which constants α and β, depending on the type of soil material. A same relationship was obtained for strain dependent damping $\xi(\gamma)$:

$$\xi(\gamma) = \eta exp\left[-\lambda\frac{G(\gamma)}{G_0}\right] \qquad (2.7)$$

with the constants η and λ depending on the type of soil material. The G_0 reduction functions and damping ratio functions due to the response to a cyclic

shear deformations can be obtained from resonant column test and through cyclic loading torsional shear test (**Fig. 2.1.2**).

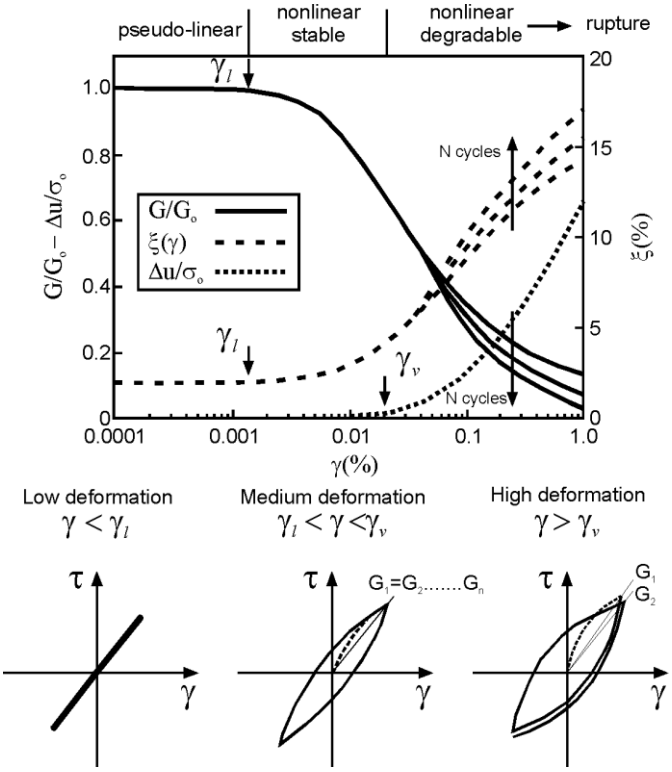

Fig. 2.1.2. *Behavior of shear modulus, G, and damping factor, ξ, dependent on shear strain γ (modified from Lanzo and Silvestri, 1999).*

Other factors that play a role in the nonlinear behavior of a soil site during an earthquake are the intensity of earthquake shaking and the source-to-site distance. Response spectra of larger magnitude events, indeed, have their highest amplification at longer periods, while for events with smaller magnitudes this is shifted into the short-period range. Distant earthquake records, moreover, have little energy at high frequencies, while local earthquakes have higher frequency contents (Wang and Law, 1994; Lang and Schwarz, 2000).

2.2. Topographic effects

Amplification of the ground motion in a topographic irregularity is generally linked to the focalization of seismic waves at its topmost part due to the existence of diffraction, reflection, and conversion of the incident waves (Bard, 1982). The

amplification effects at the topmost part of a hill are frequency-dependent so that resonance phenomena occur when the wavelength of the incident wave is comparable to the horizontal dimension of the hill. The theoretical resonance frequency (f_0) expected for a topographic effect can be calculated using the relationship:

$$f_0 = \frac{V_S}{L} \qquad (2.8)$$

where L is the width of the hill and Vs is the shear wave velocity of the outcropping lithotypes (Bouchon, 1973; Géli *et al.*, 1988). In addition, the influence of the topography on ground motion is linked to the sharpness of the ridge crest (Géli *et al.*, 1988; Bard and Riepl-Thomas, 1999). Slope inclination is a sensitive feature of site response because it determines the angle of reflection and diffraction of seismic waves (**Fig. 2.2.1**). Going into more details, steep slopes tend to pack and focus the reflected seismic waves at the slope crest, while gentle slopes scatter the diffracted seismic waves (Boore, 1973; Ashford *et al.*, 1997).

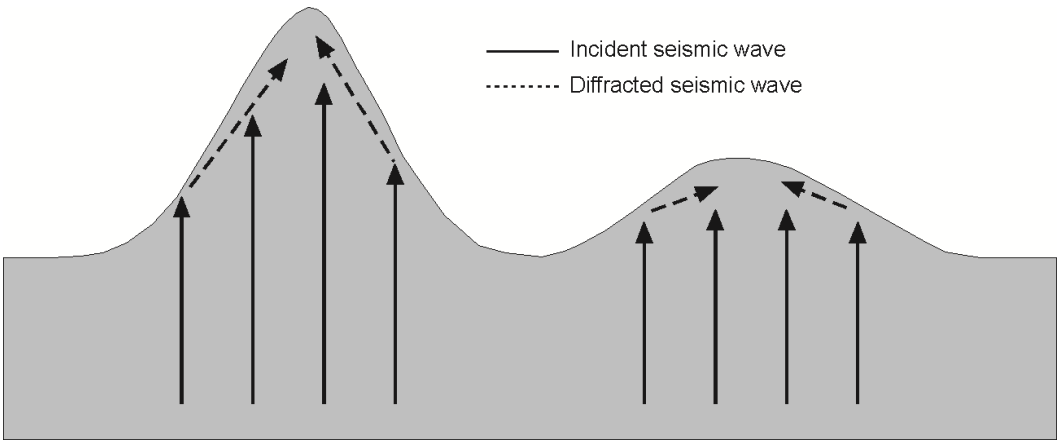

Fig. 2.2.1. *Impact of slope angle on propagation of diffracted seismic waves.*

The upper part of a hill shows increasing resonant motion with respect to the whole of the structure. This ground-motion amplification mechanism at ridge crests is in principle similar to the well-known effects in the seismic design of buildings, which appears to apply at a larger scale to mountains as well (Buech *et al.*, 2010). Moreover, significant directional effects, transverse to the major axis of

the ridge, are often observed (e.g. Spudich *et al.*, 1996; Le Brun *et al.*, 1999; Pischiutta *et al.*, 2010; Marzorati *et al.*, 2011). Several analytical and numerical methods have been developed to study incoming seismic waves when crossing a hill shaped morphology (*e.g.*, LeBrun *et al.*, 1999; Paolucci, 2002).

Another important aspect concerns the difficulty to distinguish between a purely topographic effect and the influence of different local lithology amplification. Performing measurements along a cross section in the French Alps, Pedersen *et al.*, (1994) observed that ground motion amplitude caused by topography variations can be in some instances smaller than the amplification linked to stratigraphic effects.

2.3. Basin effects

In the case of sediment-filled basins, where the soils are laterally bounded by rock, the assumptions of simple stratigraphic effects are not valid and two (2D) or three dimensional (3D) site effects should be taken into account. In this condition diffraction phenomena and wave conversions taking place at the boundaries of the basin whereas trapping and focusing of energy are observed inside the soil layered structure (Bindi *et al.*, 2011). The multiple reflection of energy and the propagation back and forward of the basin induced surface waves can lead to a dramatic increase in damage due to amplification of ground motion and the extension of its duration has been observed in many basins (*e.g.* Kawase, 1996; Di Giulio *et al.* 2003; Bindi *et al.*, 2011).

To identify valleys whose seismic behaviour is characterized by 2-D resonance, Bard and Bouchon (1985) introduced the concept of the shape ratio. The shape ratio is defined as the ratio of the maximum sediment thickness h to the valley half-width l and it is also connect to the impedance ratio between bedrock and sediment fill. In other word for a specific impedance ratio exist a critical shape ratio above which 2D effect take place (**Fig. 2.3.1a**).

Three fundamental modes were identified in a shaped valley considering the model proposed by Roten *et al.* (2006) and the results of the simulation obtained by Bard and Bouchon (1985) for valley seismic behavior on incident SH, SV and

P-waves. The phase of the fundamental mode *SH*, is the same across the valley, and the amplification reaches its maximum in the valley centre. The *SV* fundamental mode is characterized by a maximum amplification in the centre for the perpendicular component and a central node and two maxima for the vertical component. The SV phase is the same across the valley for the perpendicular component, while the phase of the vertical motion changes at the valley centre. The *P* fundamental mode behaves just vice-versa (**Fig. 2.3.1b and c**).

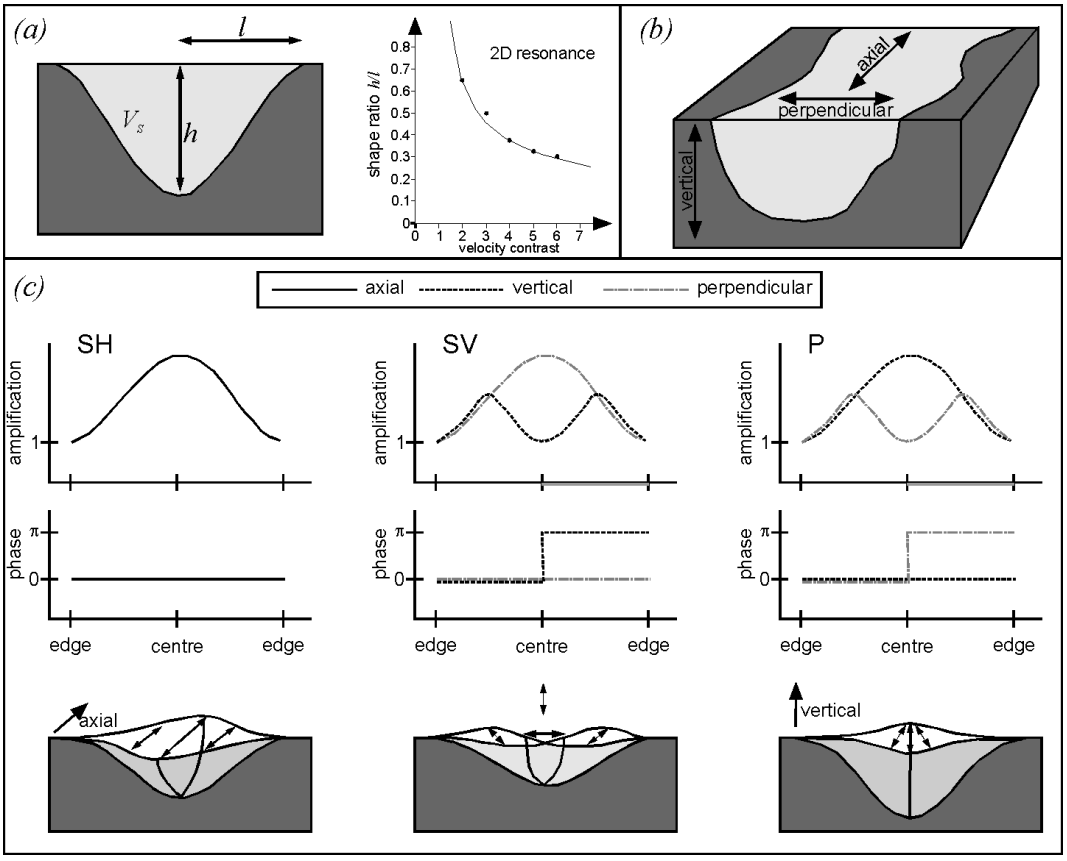

Fig. 2.3.2. *(a) Shape ratio as a function of the velocity contrast for the SH case. (b) Nomenclature of principle direction in the valley. (c) Amplification, phase and particle motion of the three fundamental modes of a valley in its principal directions (modified from Bard and Bouchon 1985; Roten et al. 2006).*

2.4. Method for estimating site effects

Local site effects are considered to be the most significant factor in the modification of predicted rock outcrop motions. The most useful tools used to

propose a guideline for urban planners to mitigate earthquake risk is the seismic microzonation which deals with geology, geophysics, geotechnical engineering and civil administration (Ansal *et al.*, 2004). In recent years many methods are proposed to do the microzonation study of different city in the world (Faccioli *et al.*, 1991; Faccioli and Pessina 2001; Ansal *et al.*, 2004; Mishra, 2004; Boncio *et et al.*, 2011; Vaccari *et al.*, 2011), but the final stage of all this study deals with the connection between the information coming from hazard study (first step), to determine the rock outcrop motion, the seismic site characterization (second step), through seismic site response in term of amplifications in the study area, and vulnerability analysis of buildings (third step). Microzonation is important because, as above described in the **Seismic site effect** (**Chapter II**), seismic waves transmitted through the ground material may be increased in amplitude, in frequency content, and in time duration. Many methods which can be grouped into experimental, numerical, empirical and semi-empirical methods exist to determine the seismic site response.

2.4.1. Experimental methods

The most common site response estimation technique using earthquake data, is standard spectral ratio (SSR) that it consists in comparing recordings at nearby sites one on a soft sediment recording site (target site) and one on a nearby recording site on rock called "reference site" (Borcherdt, 1970) (**Fig. 2.4.1.1**).

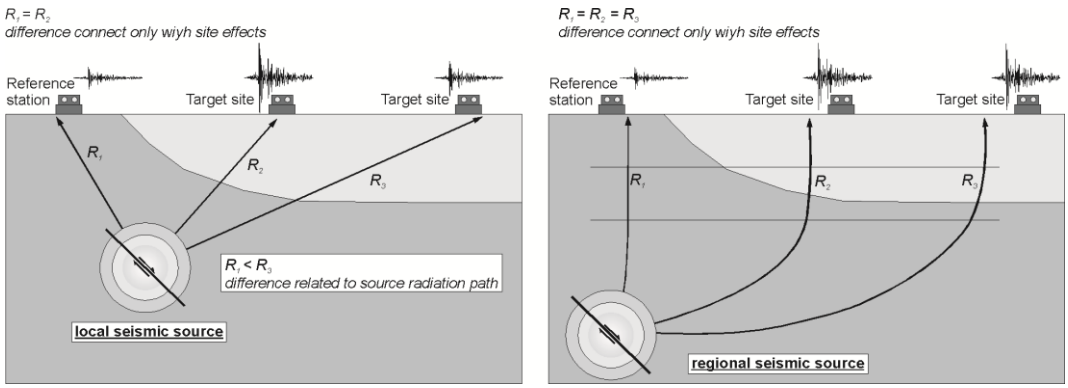

Fig. 2.4.1.1. *Schematic illustration of the station scheme use for the standard spectral ratios technique*

The SSR method provides a reliable estimate of site response if the "reference site" is free of any site effect, which is the case when the reference site is located on an un-weathered, horizontal bedrock. Moreover, it should be located near to the examined station to ensure that differences between each site are only due to site conditions, and not to differences in source radiation or travel path. This last condition is generally warranted for distances to the reference site is small compared to the source-to-site distance or as demonstrated by Steidl *et al.* (1996) for distances of about 20 km from the two considered stations considering regional events (**Fig. 2.4.1.1**). The site effect estimated by means of SSR techniques, often for non-linearity effects linked to the use of weak motion earthquake, may be considered as an overestimation or upper limit of the actual site effects at high frequencies, and, correlatively, a slight underestimation at frequencies below the "elastic" fundamental frequency, (Lacave *et al.*, 1999).

The method may be described as follows: for a network of I sites having recorded J events, the amplitude spectrum of the ground motion $S_{ij}(f)$ recorded at site i during the event j can be written as:

$$S_{ij}(f) = G_j(f) \,.\, R_{ij}(f) \,.\, T_i(f) \qquad (2.9)$$

with $G_j(f)$ source function, $R_{ij}(f)$ source-to-site path and $T_i(f)$ local site effects contribution. The terms $G_j(f)$ and $R_{ij}(f)$ can be considered site independent and the ratio of the amplitude spectra between target and reference sites give the transfer function.

In 1954, Kanai introduced the application of the Fourier amplitude spectra method on microtremor data to investigating the site response. The amplitude of these microtremors is generally very small (displacements are in the order of 10^{-4} to 10^{-2} mm). Although they are very weak, they always represent a useful source to researchers of earthquakes seismology as demonstrated by many authors (e.g. Alcook, 1974; Kats, 1976; Bard *et al.*,1999). The capability of this method strictly depends on two main assumptions: ambient seismic noise solely is composed of vertically incident shear waves (S waves) and the source spectrum of microtremors is characterized by white noise, which means that its power spectral density is constant with frequency. As demonstrated by several authors (e.g.

Lermo and Chávez-García, 1994; Tokimatsu, 1995) both assumptions do not correspond to the truth, because microtremors are mainly composed of surface waves, and each spectrum based on free field noise data is not white, being influenced by band-limited perturbing signals and temporal variations.

Since early seventies several Japanese scientists (Nogoshi and Igarashi, 1970; Nakamura, 1989) introduced the ratio between the Fourier spectra of the horizontal and vertical components of ambient vibrations noise (HVNR). The principal two basic hypothesis explanation for using ambient noise are two. Nogoshi and Igarashi (1970) showed through their investigations that HVNR on microtremors are directly related to the ellipticity curve of Rayleigh waves because of the predominance of Rayleigh waves in the vertical component. Nakamura (1989) instead, asserted that the H/V-ratio on microtremors gives a good estimate of the *S* waves site response function. Dividing the horizontal component of surface ground motion by the vertical, a removal of the source as well as the Rayleigh wave effects can be obtained. In particular, the theoretical background of Nakamura (1989) about the body-wave interpretation has been contradicted in several articles highlighting the relationship between the HVNR and the ellipticity of fundamental Rayleigh-wave mode, which is associated to an inversion of the direction of Rayleigh waves rotation (Lachet and Bard, 1994; Kudo, 1995; Bard, 1998; Fäh *et al.*, 2001; Bonnefoy-Claudet *et al.*, 2006). However, the amplitude of fundamental resonant frequency is not well correlated with the S wave amplification at the site's resonant frequency (Mucciarelli, 1998; Al Yuncha and Luzon, 2000; Rodriguez and Midorikawa, 2002;Maresca *et al.*, 2003), but the stability as well as plausibility of results are almost convincing (e.g. Lermo and Chavez-Garcia 1993; Gitterman *et al.*, 1996; Seekins *et al.*, 1996). The amplitude of the HVNR peak, moreover, seem to be correlated to the position and depth of the source (**Fig. 2.4.1.2**).

Another important aspect is linked to the fact that the H/V ratios from ambient vibrations are sometimes "non-informative". This seems to be true particularly in the case of significant lateral heterogeneity, that originates 2D/3D effects, and velocity inversion, which influence the vertical component of motion too (Di

Giacomo *et al.*, 2005 Castellaro and Mulargia, 2009). Nevertheless, the method proved to be the most inexpensive and convenient technique to estimate fundamental frequencies of soft deposits.

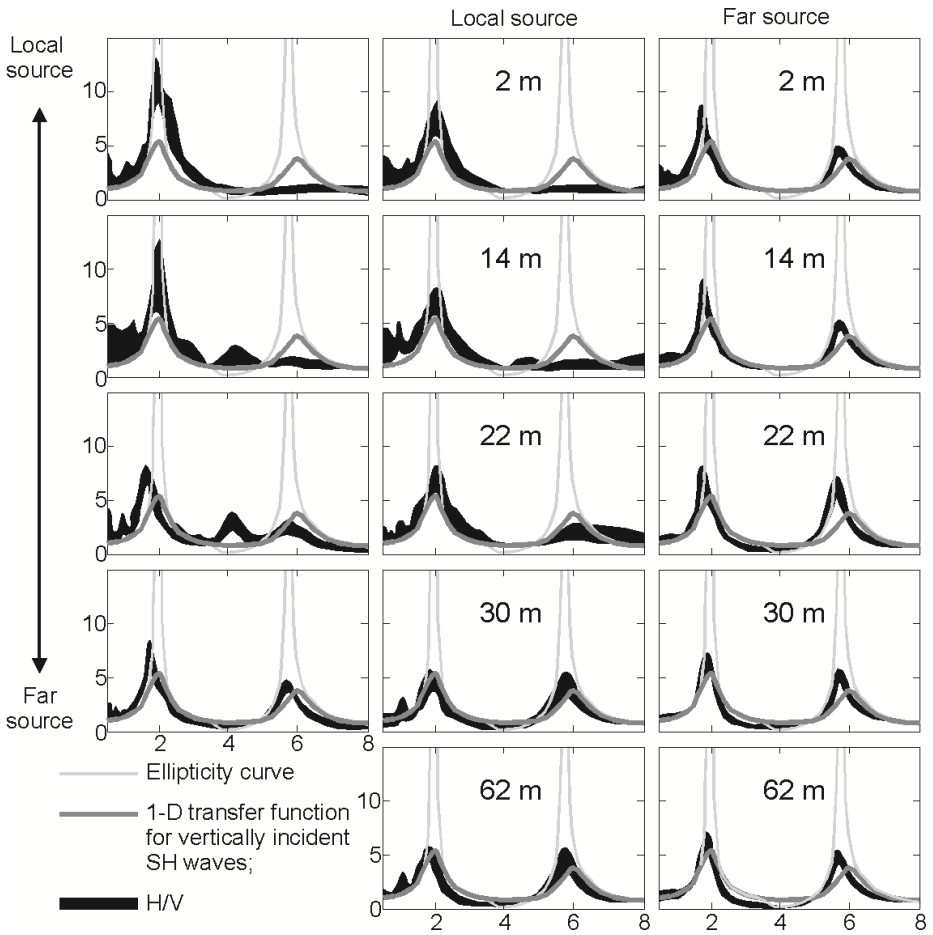

Fig. 2.4.1.2. *Changing in H/V ratios using different position and depth of the source, ellipticity of fundamental mode of Rayleigh wave and 1-D transfer function (modified from Bonnefoy-Claudet et al., 2006).*

Another very widespread technique, that does not need a reference station, consists in the spectral ratio between the horizontal and the vertical components of the shear wave part of the earthquake recordings (HVSR). This method is a combination of Langston's (1979) "*receiver-function*" technique for determining the velocity structure of the crust from the horizontal to vertical spectral ratio of teleseismic P waves, and the HVNR. It was first applied by Lermo and Chavez-Garcia (1993) at three different sites in Mexico. The HVSR exhibits very encouraging similarities between the SSR, GIT (Generalized Inversion

Technique) and the HVNR (**Fig. 2.4.1.3**), with a good fit especially in frequencies of the resonant peaks when the *S*-wave part of the seismograms is used (Chavez-Garcia *et al.*, 1996; Bonilla *et al.*, 1997; Castro *et al.*, 1998; Riepl *et al.*, 1998; Triantafyllidis *et al.*, 1999; Parolai *et al.*, 2000, 2001). These observations permit to conclude that HVSR is well correlated with surface geology, and much less sensitive to source and path effects. However, the amplitude of the peak depends on the type of incident waves (**Fig. 2.4.1.3**) consequently the determination of the absolute level of amplification from only HVSR is not straightforward (Field and Jacob, 1995). The HVSR was applied also to P wave but generally provide contradictory results. In the case of significant lateral heterogeneity, that origin 2D/3D effects, the vertical component of motion may be affected by the site effects and therefore the HVSR might became "non-informative" as demonstrated by several authors (Riepl *et al.*, 1998; Raptakis *et al.*, 1998 and 2000; Triantafyllidis *et al.*, 1999; Parolai *et al.*, 2004; Bindi *et al.*, 2009).

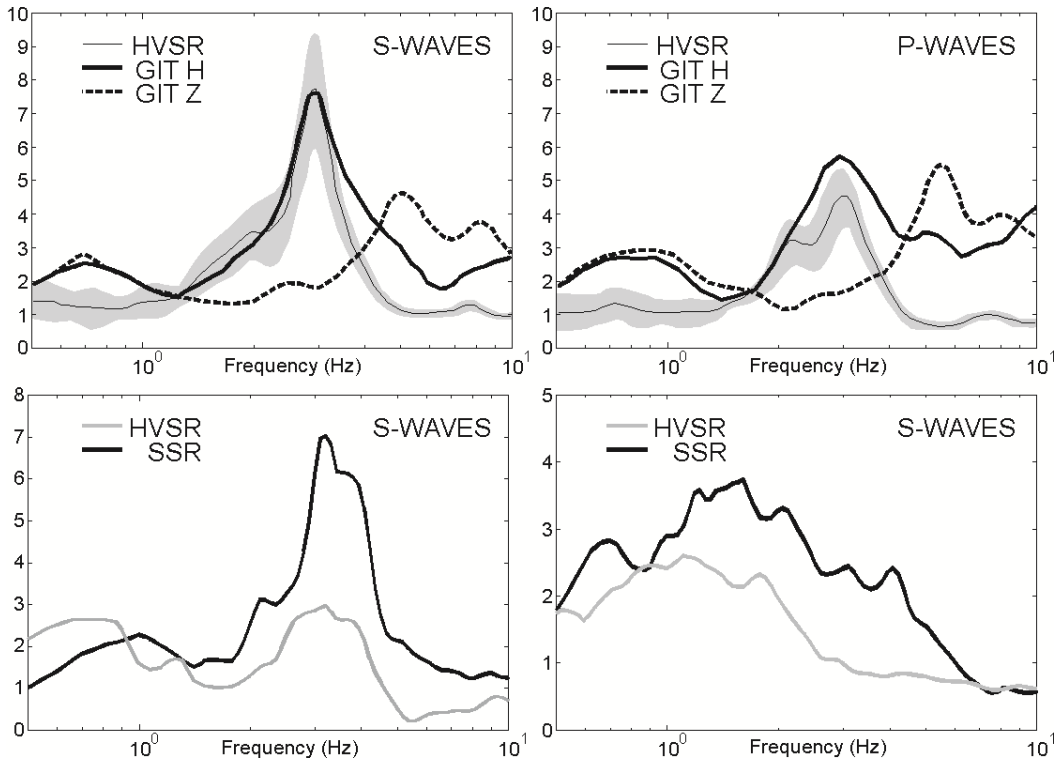

Fig. 2.4.1.3. *Upper panel HVSR ±1 standard deviation (gray shaded area) and GIT methods to S- and P-wave windows (modified from Parolai et al., 2004). Lower panel HVSR and SSR techniques to S-wave windows(modified from Panzera et al., 2011b).*

2.4.2. Numerical methods

The numerical methods allow to increase the degree of accuracy in predicting the seismic site response, because they are also able to model situations very complex in terms of topographic, stratigraphic and dynamic behaviour of soils (**Fig. 2.4.1.4**). The numerical analysis is performed using computer codes that simulate the propagation of seismic waves within a soil deposit of which there are known the geotechnical characteristics.

There exists a number of simple analytical methods which allow computation of the seismic site response of a given site in term of amplification function, response spectrum, acceleration, velocity, displacement, shear strain and stress time histories. The most widely used considers the response of a1-D soil column associated to the multiple reflection vertically incident S waves in horizontally layered deposits. The parameters required for such analysis are shear-wave velocity, density, damping and thickness of each layer. These parameters may be obtained through geotechnical abacus, direct *in situ* (e.g. drillings, down-hole, Standard Penetration Test) and subsequent laboratory measurements. These code may work considering a linear or non-linear behavior of the soil. Non-linearity for different types of material, usually, is approximated using shear modulus and damping reduction curves as function of the shear strain (see **Fig. 2.1.2**). Some of these software are SHAKE (Schnabel *et al.*, 1972), EERA (Bardet *et al.*, 2000), DEEPSOIL (Hashash, 2009) and NERA (Bardet and Tobita, 2001).

Earthquake engineers have traditionally evaluated seismic site response using simple models based on a 1D description of local soil profile and seismic wave propagation, with reasonable success. However, recent events such as the 2009 L'Aquila (Abruzzo, Italy) earthquake with its narrow "intensified damage", have disclosed a remarkable complexity in seismic amplification patterns due to unfavorable combinations of seismic source and near-surface geology. All numerical methods have the same base, but many different models have been proposed to investigate complex phenomena connect to 2-D/3-D structure geometry. Complex site effects (2D/3D) tend to occur on deeply incided, sediment filled valleys and basins, where cities are located, or on steep

topography, where some of the oldest downtown are found. To analyze seismic wave propagation in this complex geological structures, various numerical methods are available such as boundary element method (BEM), finite element method (FEM) and finite difference method (FDM). The BEM allows a very good description of the radiation conditions but is preferably dedicated to weak heterogeneities and linear constitutive models (Beskos, 1997; Bonnet, 1999; Dangla, 1988; Dangla *et al.,* 2005; Sanchez-Sesma and Luzon, 1995; Semblat, 2000b; Semblat *et al.*, 2008). The FEM is efficient to deal with complex geometries and numerous heterogeneities, but has several drawbacks such as numerical dispersion and numerical damping (Hughes, 1987 and 2008; Ihlenburg and Babuška, 1995; Semblat, 2000a; Semblat et *al.*, 2008; Bonilla, 2000) and consequently numerical cost in 3D elastodynamics. The FDM is accurate in elastodynamics but is mainly adapted to simple geometries (Bohlen, 2006; Frankel; 1992; Moczo, 2002; Virieux, 1986). Each method have specific advantages and shortcomings, it is consequently often more interesting to combine two methods to take advantage of their peculiarities (Semblat, 2010).

It is important to note that numerical methods require detailed geotechnical and geophysical investigations for the investigated sites to provide valid results and they can be applied only to some limited cases (Lacave *et al.*, 1999).

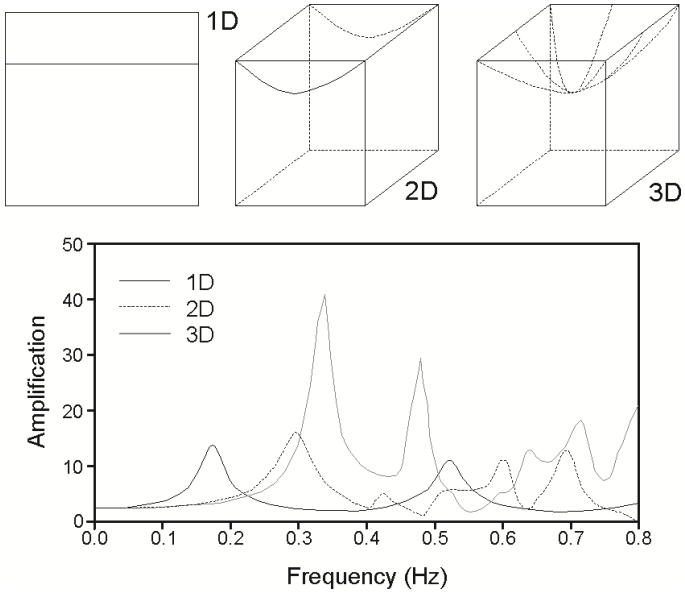

Fig. 2.4.1.4. *Variation in amplification functions considering a simple valley geometry in the cases 1D, 2D and 3D (modified from Bard and Riepl-Thomas, 1999).*

2.4.3. Empirical methods and soil parameter

Apart from the possible amplification effects due to the local subsoil, the amplitude level of seismic action decreases as the distance to the seismic source increases. This field of interest is covered by the elaboration of empirical attenuation laws for permanent ground displacements (PGD), spectral accelerations (S_a), at discrete periods, peak ground acceleration (PGA) and velocity (PGV). Many empirical attenuation laws have been derived on the basis of available strong motion recordings (e.g. Ambraseys et al., 2005; Akkar and Bommer, 2007; Boore and Atkinson, 2008; Cauzzi and Faccioli, 2008; Bindi et al., 2009). Other given empirical ground motion parameter are earthquake time duration, Arias (I_a, 1970) and Housner (I_h, 1959) intensities:

$$I_a = \frac{\pi}{2g}\int_0^{T_d} a^2(t)dt \qquad (2.10)$$

$$I_h = \int_{0.1}^{2.5} S_v\,(T, \xi = 0.05)dT \qquad (2.11)$$

where in *(2.10)* g is the gravity acceleration, T_d is the earthquake time duration and $a(t)$ is the acceleration time history. Besides in *(2.11)* S_v is the pseudo velocity spectrum, T is the vibration period and ξ is the viscous damping.

The attenuation laws, especially, take into account a site parameter that it is a simple descriptor factor, such as "rock" and "non-rock". Rarely this is a more refined indicator of the site geology characteristic, for instance with distinction between thin and thick deposits, or with S-wave velocity values. In this way it is possible to modify the ground motion parameters according to the site geology. However, these modifications are based on a very simple classification of soils, and on statistical studies which smooth out the extreme values, such an approach may lead to a dangerous underestimation or overestimation of amplifications at the study sites. A widely used parameter is the mean value of shear wave velocity over the last 30 m (V_{S30}) as defined by EUROCODE 8 (2003):

$$V_{S30} = \frac{30}{\sum_{i=1,N}\frac{h_i}{V_i}} \qquad (2.12)$$

where h_i and V_i are the thickness (m) and shear-wave velocity of the *i-th* formation or layer, in a total of N, existing in the top 30 meters, respectively. Such

criterion certainly has some drawbacks, since it does not take into account the velocity profile at greater depths, which may have a prominent influence on the low frequency response. In **Table 2.1** are shown the soils classification in term of V_{S30}, N_{SPT} (number of shot in standard penetration test) and C_U (equivalent un-drained shear resistance).

Tab. 2.1. *Classification of ground conditions according to EUROCODE 8 (2003)*

Site Class	Description of stratigraphic profile	V_{S30} (m/s)	N_{SPT} (bl/30cm)	C_U (kPa)
A	Rock or other rock-like geological formation, including at most 5 m of weaker material at the surface	>800	-	-
B	Deposits of very dense sand, gravel, or very stiff clay, at least several tens of m in thickness, characterised by a gradual increase of mechanical properties with depth	360-800	>50	>250
C	Deep deposits of dense or medium – dense sand, gravel or stiff clay with thickness from several tens to many hundreds of m	180-360	15-50	70 –250
D	Deposits of loose-to-medium cohesionless soil (with or without some soft cohesive layers), or of predominantly soft-to-firm cohesive soil	<180	<15	<70
E	A soil profile consisting of a surface alluvium layer with V_{S30} values of class C or D and thickness varying between about 5 m and 20 m, underlain by stiffer material with V_{S30} > 800 m/s	-	-	-
S_1	Deposits consisting – or containing a layer at least 10 m thick – of soft clays/silts with high plasticity index (PI > 40) and high water content	<100	-	10-20
S_1	Deposits of liquefiable soils, of sensitive clays, or any other soil profile not included in classes A-E or S1	-	-	-

Conventional methods for determining shear-wave velocity are borehole methods (down-hole, up-hole, cross-hole), active seismic methods (refraction, multichannel surface wave analysis, seismic analysis of surface waves) and passive seismic methods (refraction microtremor, *f-k* analysis of noise array measurements). In this thesis the method used are multichannel surface wave analysis (MASW) and refraction microtremor (ReMi), which will be widely discussed in other chapters.

Chapter III

Seismic Hazard Assesment: the study cases of Catania and Siracusa, Italy

3.1. Issues of the chapter

Catania and Siracusa are located on the eastern coast of Sicily (southern Italy). The high level of seismicity that affects the area, together with the considerably high density of inhabitants, contribute to classifying these towns amongst those with the highest seismic risk in Italy. The potential severity of damage to which their historic-architectural patrimony could be subjected to is also not negligible. The seismic activity of the investigated area is particularly high as testified by the historical earthquakes that occurred in 1169, 1542, 1693, 1818, 1908 as well as the recent one that occurred in 1990, all having intensity ranging between the VI and XI MCS scale (Working Group CPTI, 2004).

The seismic hazard assessment (SHA) consists in evaluating the possible effects due to future earthquakes (and the related uncertainties) to which a study area can be subjected. It can be performed using either a deterministic (DSHA) or a probabilistic (PSHA) approach. The DSHA uses individual earthquake sources and single-valued events to establish a particular scenario that describes the hazard. Typically, a seismic source location, an earthquake of specified size and a ground motion attenuation relationship are required. However, this approach does not provide information on the occurrence probability of an earthquake parameter (acceleration, magnitude) during a finite period of time (e.g., the useful lifetime of a particular structure or facility). PSHA, being a statistical approach, needs to identify a suitable time interval having good completeness of information. On the other hand, PSHA allows to estimate the probability when an intensity measurement (e.g., peak acceleration) could exceed a defined value during a given time (e.g., 50 years) (McGuire, 2004). It accounts for all possible combinations of

magnitude-location of shocks and models describing the effects and the occurrence rate of all earthquakes that could affect an area.

Recently, the SHA in eastern Sicily has been performed by several authors (Azzaro *et al.*, 1999; Zollo *et al*., 1999; Azzaro and Barbano, 2000; Decanini and Panza, 2000; Faccioli and Pessina, 2000; Barbano and Rigano, 2001; Barbano *et al.*, 2001; Azzaro *et al.*, 2008; Fiorini *et al.* 2008) who used either the DSHA or the PSHA approaches, taking into account different source areas of the major historical earthquakes that are mostly located on the Malta Hyblean fault system. In recent years, a national seismic hazard map was produced by the Working Group MPS04 (2004) and a new hypothesis was proposed for the source locations in Eastern Sicily. On the basis of the macroseismic fields, the authors thus moved the epicenters of the major earthquakes inland. The identification of the causative faults of such events is, however, still unclear and different hypotheses have been reported in literature (e.g. Argnani and Bonazzi, 2005; Gutscher *et al.*, 2006; Basili *et al.*, 2008).

The aim of the present study is to carry out a detailed probabilistic seismic hazard analysis for the towns of Catania and Siracusa using two probabilistic approaches. The results of the "site" method (Albarello and Mucciarelli, 2002) and the "seismotectonic" methodology (Cornell, 1968; Esteva, 1967) were compared taking also into account different seismogenic sources. Therefore, the SASHA code (D'Amico and Albarello, 2008) and the CRISIS2007 code (Ordaz *et al.*, 2007) were used to estimate seismic hazard through the above mentioned methods, respectively.

3.2. Seismotectonic features of the south-eastern Sicily

The seismicity of the study area is linked to the collision between the African and European plates. **Figure 3.1** shows the major tectonic domains and the main active faults in eastern Sicily and the southern Calabria area.

As far as the Calabria region is concerned, the major shocks that affected the area are located in the Crati, Savuto and Mesima basins, including the Messina straits. Among these events, the sequences of 1783, 1905 and 1908 earthquakes

stand out. Details about their features, such as epicentral location, geometry and source dimensions are described by Boschi *et al.* (2000), Monaco and Tortorici (2000) and Valensise and Pantosti (2001).

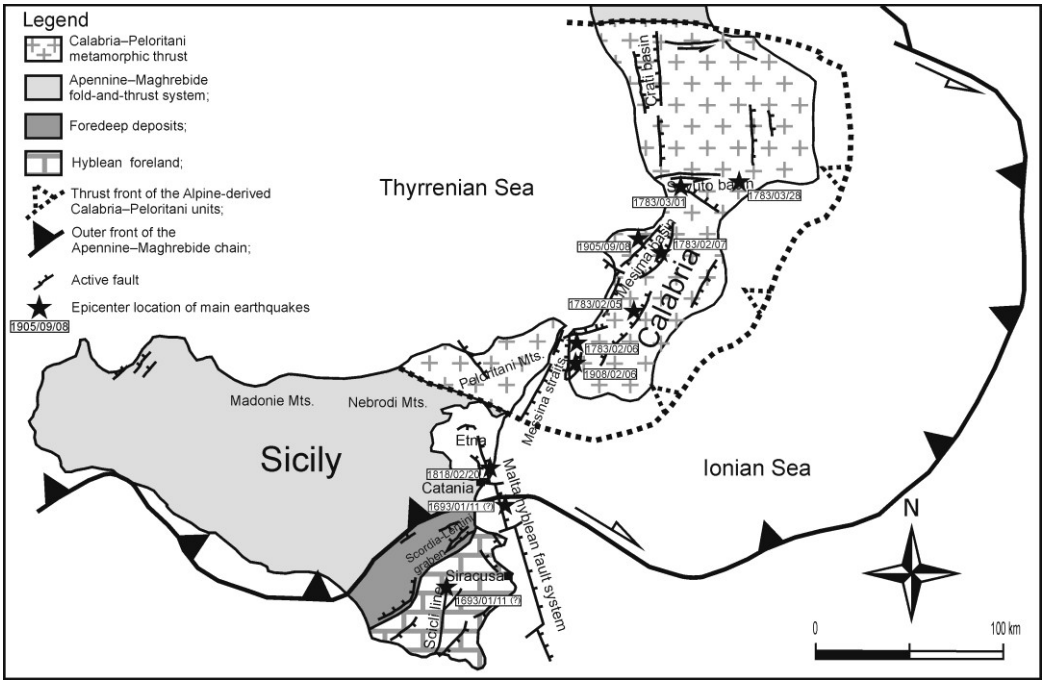

Fig. 3.1. *Tectonic framework of the study area with major structural domains of southern Italy (Lavecchia et al., 2007, modified) and active faults identified through surface geological evidence (Galadini et al., 2001, modified).*

In western and central Sicily, the compressional and transpressional faults are the dominant tectonic features. The Madonie–Nebrodi–Peloritani Mt. chain, that outlines northern Sicily, as well as the Tyrrhenian offshore area, are characterized by Plio-Quaternary extensional structures which are formed by N-to-NW dipping normal and normal-oblique faults, that dislocate the pre-existing compressional structures (Monaco and Tortorici, 2000; Pepe *et al.*, 2000). Eastern Sicily is delineated by the crossing of lithosphere structures that give rise to the origin of Mt. Etna and by the presence of the Malta Hyblean fault system that goes down to the Sicilian coast towards the Ionian Sea.

The definition of seismic sources in eastern Sicily is a quite debated problem due to the lack of clear evidence of surface faulting and to the few high-magnitude

instrumental earthquakes. For example, the location, size and kinematics of the January 11, 1693 earthquake (M_W = 7.4, Working Group CPTI, 2004) is particularly uncertain and debated in literature. Some authors locate the source inland, whereas others locate it off-shore. The inland source models are based on geologic, geomorphologic and macroseismic intensity analyses and they address either a WSW-ENE striking normal fault within the Scordia-Lentini graben (D'Addezio and Valensise, 1991; Tinti and Armigliato, 2003) or a blind NNE-SSW striking transcurrent fault, parallel to the Scicli line (Sirovich and Pettenati, 1999; Basili *et al.*, 2008). The models that adopt an offshore source are mainly based on results of seismic prospecting at sea and on tsunami modeling which suggests either the rupture of a segment of the NNW-SSE Malta fault escarpment (Piatanesi and Tinti, 1998; Azzaro and Barbano, 2000; Jacques *et al.*, 2001; Argnani and Bonazzi, 2005) or the rupture of a locked subduction fault plane (Gutscher *et al.*, 2006). Recently, Lavecchia *et al.* (2007), have suggested associating the 1693 earthquake to the Sicilian basal thrust, to which they also link the 1818 Catania event (M_W = 6.2, Working Group CPTI, 2004).

In eastern Sicily, in addition to the seismicity related to these regional sized tectonic structures, there is an intense seismic activity linked to the Etna volcano. Its seismicity is characterized by low magnitude events and shallow hypocenters that produce destructive effects only at local scale.

3.3. Site approach method

The seismic hazard estimate through the "site" approach was performed using the SASHA code. It was developed in order to handle the intensity data taking into account the macroseismic information of past earthquakes included in the DBMI04 (Working Group DBMI04, 2005) and used for compiling the parametric earthquake catalogue CPTI04 (Working Group CPTI, 2004). To build the seismic site histories of Catania and Siracusa, the felt data in the 217 b.c. – 2002 a.d. time interval, considering an intensity threshold of IV MCS, were taken into account.

A logic tree for the site approach (**Fig. 3.2**) was built up, taking into account all the options provided by the code to reduce the statistical uncertainties. The first

elements of the logic tree are the CPTI04 and the DBMI04. Three possible site seismic histories were considered. The first kind of seismic history uses only felt data. The second one adopts felt data integrated with "virtual" intensities obtained through a Gaussian attenuation relationship (Pasolini *et al.*, 2008), and the third takes into account felt data integrated with "virtual" intensities coming out from a binomial empirical attenuation relationship (Albarello *et al.*, 2007). The above-mentioned attenuation laws were taken into account for all events having epicentral distance within 200 km from each considered site and epicentral intensity $I_0 \geq$ V-VI MCS. As regards the Etnean earthquakes, instead of using the Gaussian and binomial attenuation relationships, the attenuation model proposed by Azzaro *et al.* (2006) was adopted in order to consider the geologic setting of the volcanic area. Macroseismic intensities I_S were converted into PGA values using both the Faccioli and Cauzzi (2006) and Gómez Capera *et al.* (2007) relationships. According to the study of Faenza and Michelini (2010), a higher weight was assigned to the PGA-intensity conversion law of Gomez Capera *et al.* (2007) with respect to Faccioli and Cauzzi (2006). This choice comes from the observation that Gomez Capera *et al.* (2007) used only Italian earthquake data and adopted the orthogonal distance regression technique, which is a more appropriate technique whenever dependent and independent variables are both affected by uncertainties. Faccioli and Cauzzi (2006) relations were obtained by integrating Italian and non-Italian earthquakes and using the least squares fitting technique.

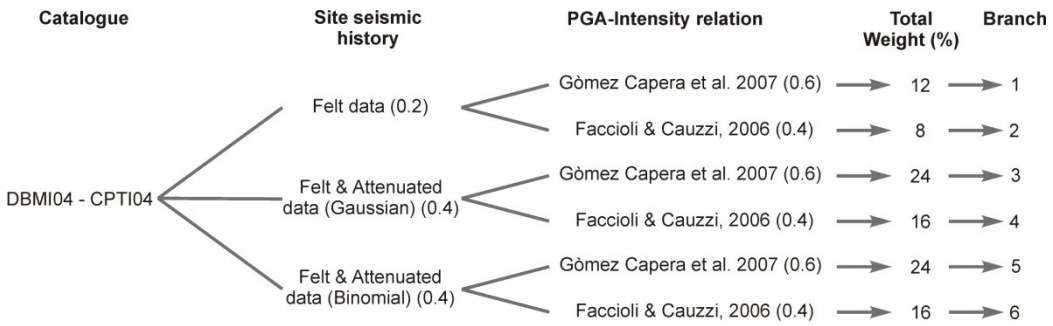

Fig. 3.2. *Logic tree site and weighted values used in the "site" approach.*

The highest total weight in the logic tree (**Fig. 3.2**) were given to branches 3 to 6 which concern felt data with attenuated effects. Such option was preferred so as to take into account the lack of historical information (see **Fig. 3.3**) that often affects the seismic site history catalogues (Albarello *et al.*, 2007), especially at moderate to low intensity values (I = IV-V MCS).

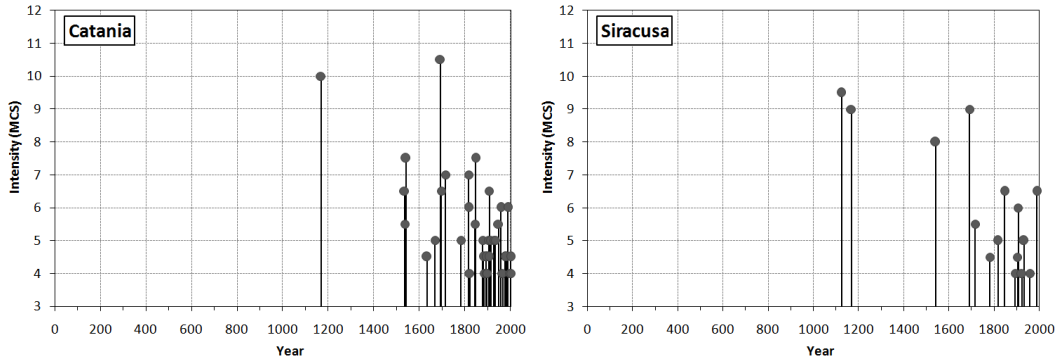

Fig. 3.3. *Seismic site histories for Catania and Siracusa considering only felt data (DBMI04, 2005).*

The first step of the hazard estimation with SASHA is to build up the seismic history at each site. Moreover, before evaluating the seismic hazard, a completeness analysis has to be performed. In the site approach, the completeness of the local catalogue used for hazard computation is assessed through a statistical methodology. According to Albarello *et al.* (2001), three assumptions were adopted: a) the seismogeneic process is stationary, b) the most recent part of the catalogue is complete, c) the catalogue is statistically representative of the long-term stationary seismogenic process. At this stage, the SASHA code provides the seismic hazard for an intensity threshold and exposure time (e.g. 50 years). Resulting hazard values, computed for each intensity degree, represent the hazard curve at the studied site. A reference intensity I_{ref} is then derived from this curve corresponding to the higher intensity value that can be reached for a given exceedence probability during the considered exposure time. Finally, using the above mentioned PGA-intensity relationships, the code converts the hazard estimates from intensity to peak ground acceleration (PGA) providing a reference value for the last one (see D'Amico and Albarello, 2008).

3.4. Esteva–Cornell method

An SHA based on the Esteva–Cornell method, was performed using the open source code CRISIS2007. Such code requires as input data a source-zone model where the seismic rate of each considered zone and a ground motion predictive equation are described. According to current international conventions for SHA (SSHAC, 1997), a logic tree approach was followed to consider and evaluate the epistemic uncertainties that affect the hazard estimates (**Fig. 3.4**). Special care was devoted to defining alternative source-zone models to take into account the possibility of different seismogenic sources in south-eastern Sicily. This permits to consider the uncertainties in the source location and in the fault mechanisms of

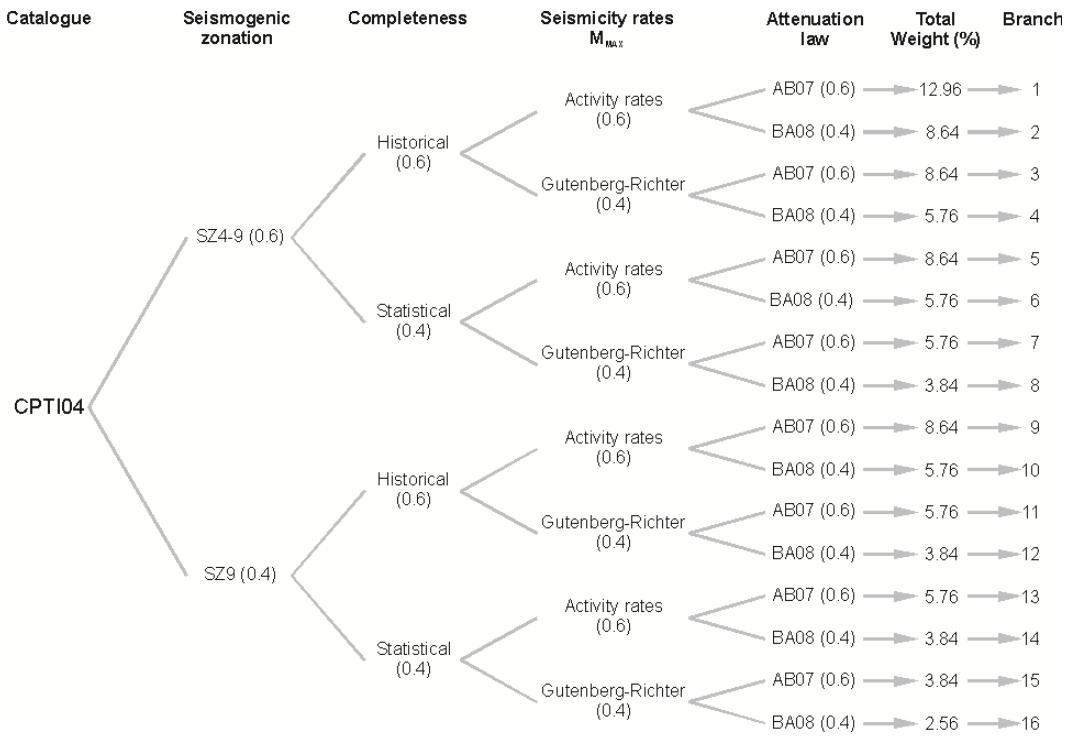

Fig. 3.4. *Logic tree used for the SHA through the CRISIS2007 code.*

the major earthquakes of the area. Two different models were therefore considered (**Fig. 3.5**). The first, based on SZ9 (Working Group MPS04, 2004; Meletti *et al.*, 2008), locates the source of the 1693 earthquake, inland. The other model (SZ4-9), which differs only locally in the definition of the seismogenic zones of south-eastern Sicily, discriminates two seismotectonic zones (78, 79) so

that, according to Meletti *et al.* (2000), the possibility of the Malta escarpment being a potential source was taken into account. In the Esteva-Cornell logic tree, the highest weight was given to the branches concerning SZ4-9, since recent studies (Brancato *et al.*, 2009) demonstrate that the Malta escarpment is an active fault system that likely gave origin to the tsunami of the 1693 earthquake (Gerardi *et al.*, 2008; Visini *et al.*, 2009).

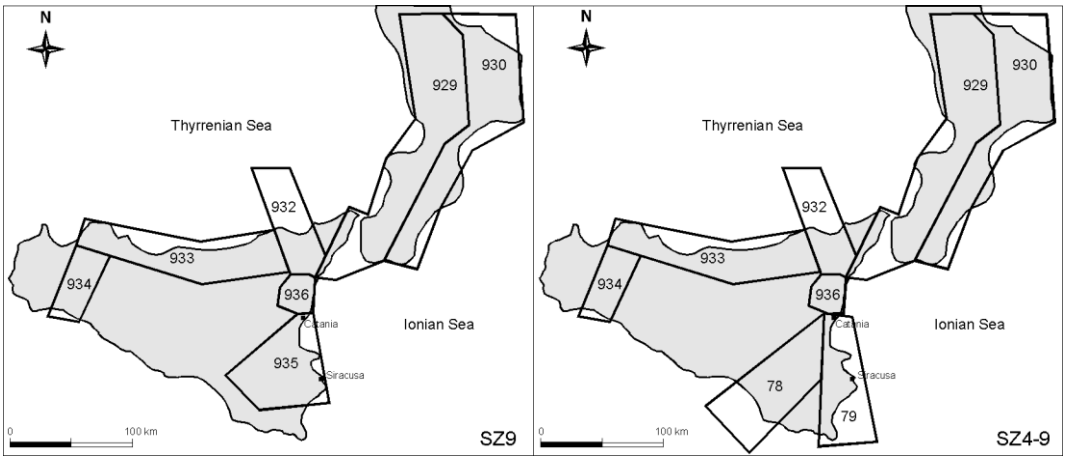

Fig. 3.5. *Source zone models considered for the SHA withthe Esteva-Cornell method, SZ9 (from Working Group MPS04, 2004) and SZ4-9 (modified from Meletti et al., 2000).*

The Gutenberg-Richter b-value coefficients, the maximum moment magnitude (M_w) and its seismic rates (λ), as well as the seismogenic depth (H) and the faulting style (see **Tab. 3.1**), were taken from the MPS04 hazard map for each of the source zones assumed in the Meletti *et al.* (2008) model. The same parameters for the SZ78 and 79 (SZ4-9 model in **Fig. 3.5**) were estimated using the CPTI04 and the same methodology proposed by the Working Group MPS04 (2004). Consequently, the activity rates (AR) were obtained by dividing the number of seismic events, of each magnitude class (twelve of $0.23M_W$ with minimum magnitude equal 4.76) for the completeness time. According to Working Group MPS04, two completeness time intervals, historical and statistical, were used. As concerns the parameters of Gutenberg-Richter, they were obtained by interpolating the AR values with a least square method.

Table. 3.1. *Maximum magnitude (MW-max), b-value, seismic rate (λ), style of faulting and depth parameter (H) for each seismogenic zone (from Working Group MPS04, 2004); the same parameters obtained in the present study for SZ 78 and 79 are reported in bold.*

SZ	Gutenberg-Richter					Activity Rates			Style of faulting	H (km)
	$M_{W\text{-}max}$	Historical		Statistical		$M_{W\text{-}max}$	Historical	Statistical		
		b	λ	b	λ		λ	λ		
929	7.29	-0.82	0.17	-0.79	0.17	7.29	0.17	0.17	Normal	10
930	6.60	-0.98	0.17	-0.89	0.21	6.60	0.17	0.21	Unspecified	10
932	6.14	-1.21	0.21	-1.08	0.33	6.14	0.21	0.33	Strike-slip	13
933	6.14	-1.39	0.20	-1.24	0.31	6.14	0.21	0.33	Inverse	10
934	6.14	-0.96	0.20	-0.93	0.20	6.14	0.21	0.21	Inverse	10
935	7.29	-0.72	0.12	-0.69	0.17	7.29	0.12	0.18	Strike-slip	13
936	5.45	-1.63	0.33	-1.22	0.33	5.45	0.33	0.33	Unspecified	3
78	**5.68**	**-0.92**	**0.38**	**-1.14**	**0.28**	**5.68**	**0.42**	**0.33**	**Normal**	**13**
79	**7.29**	**-0.66**	**0.10**	**-0.66**	**0.13**	**7.29**	**0.12**	**0.18**	**Normal**	**13**

Two ground-motion predictive equations were taken into account. The first relationship AB07 (Akkar and Bommer, 2007a and 2007b) uses strong-motion data sets from Europe and Middle East events. The second, BA08 (Boore and Atkinson, 2008) is defined considering earthquakes worldwide. Both equations calculate different shaking parameters (PGA, PGV, SA, SD), using the M_W, the Joyner-Boore source distance (R_{JB}), the characteristic style-of-faulting and the site class. For both attenuation models, rock ($V_{S,30} \geq 800$ m/s) and soft soil ($183 \leq V_{S,30} \leq 366$ m/s) conditions were taken into account. As regards the Etna volcano seismic zone (SZ936), no specific attenuation law was used, but both the AB07 and BA08 relationships were applied, assuming to reduce, by standard deviation, the PGA and the SA values obtained.

Italian volcanic districts are characterized by insufficient earthquake recordings for the calibration of ground motion attenuation laws. For this reason, past studies of SHA in Italy had adopted either the commonly used attenuation laws, reducing them by a fraction of the standard deviation (e.g. Slejko *et al.*, 1998), or a specific attenuation law for the volcanic districts (Working Group MPS04, 2004) obtained through the random vibration theory (Cartwright and Lounguet-Higgins, 1956). On the Etna volcano, two classes of events are observed: a) volcano-tectonic earthquakes (VT), linked to shear fracture processes, having spectral features with

dominating high frequencies, and b) long period events (LP), characterized by an enrichment of long-period (1–10 s) components of the ground motion (Milana *et al.*, 2008). However, the LP events occur more rarely than the VT which represent the largest part of the seismic events recorded at the Mt. Etna volcano. In **Figure 3.6**, an example of acceleration spectra for VT and LP events is plotted together with the theoretical spectral acceleration obtained through AB07 and BA08 attenuation laws, considering an unspecified fault mechanism. These earthquakes were recorded at the Bronte seismic station, located on the western flank of Etna, in an A type soil category (Working Group ITACA, 2010). Especially for periods smaller than 0.1 s and greater than 0.5 s, the figure shows a fairly good agreement between the theoretical and the experimental spectral accelerations of the VT event, when the theoretical ones are reduced by a standard deviation. For long period events, there is a disagreement especially at periods greater than 1 s. Such evidence agrees with the findings of Faccioli and Rovelli (2007) and Milana *et al.* (2008) who observed that the VT earthquakes follow the same attenuation law valid for tectonic events, whereas the LP events diverge from expected values obtained with common attenuation laws. In the light of these considerations, in the present study, the attenuation law for the volcanic area was approximated, assuming to reduce the values of PGA and SA obtained through AB07 and BA08 relations by a standard deviation. Such assumption provides, in my opinion, quite a good solution for the Etna area, considering also that VT events are by far the more frequently recorded type of earthquakes.

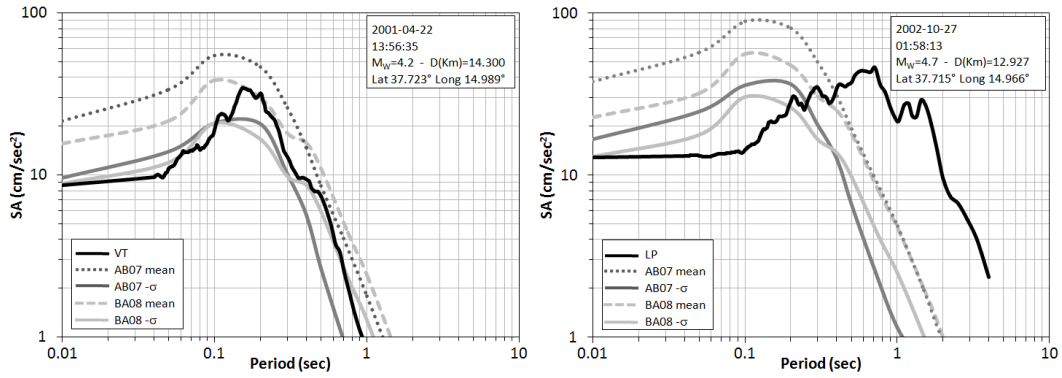

Fig. 3.6. *Comparison between response spectra of a VT (left panel) and an LP event (right panel) with the predicted theoretical spectral acceleration.*

Another important problem pertains to the site-to-source distance, especially for the disaggregation analysis. Disaggregation is used here to compute the contributions to the 10% exceedance probability in 50 years of peak ground horizontal acceleration. In the adopted attenuation laws the distance was measured with R_{JB}, whereas the SZ definition was done referring to epicentral locations. In CRISIS2007, the attenuation relationships can be specified in terms of 4 different measures of distance such as the focal, the epicentral, the Joyner and Boore or the closest distance to rupture area (R_{RUP}). If the R_{RUP} or the R_{JB} distances are used, the CRISIS2007 code needs to know the rupture area or the rupture length, as a function of magnitude, in order to compute the required distances. The code then assumes that the relation between area/rupture length and magnitude is:

$$A = K_1 e^{K_2 M}; L = K_3 e^{K_4 M} \qquad (3.1)$$

where A is the source area (in km^2), L is the rupture length (in km), M stands for the magnitude and K_1 , K_2, K_3 and K_4 are constants given by the user or chosen from a built-in set of constants. In this study, source area (A) and the Wells and Coppersmith (1994) constants were adopted, specifying these latter in the "source geometry" screen of the code. In such instances, CRISIS2007 will assume that the earthquake takes place in a plane defined by the source geometry, and that the rupture area will be a circle, within this plane, with an area A and a radius:

$$r = \sqrt{\frac{A}{\pi}} \qquad (3.2)$$

CRISIS2007 uses the type of distance adopted in the attenuation relationship for the hazard computation and, in addition, in the "global parameter" screen, it permit to specify which kind of distance the users would like to adopt for the disaggregation output. According to this possibility, the results of the disaggregation was chosen to be expressed in terms of epicentral distance.

3.5. Results and discussions

The use of the SASHA code provided, through a set of hazard curves, the estimation of a reference intensity (I_{ref}), which expresses a threshold indicating that, for a fixed exceedance probability level (e.g., 10% in 50 years), the observed

effects could be greater or equal to I_{ref}. It is interesting to observe (**Tab. 3.2**) that smaller values of I_{ref} come out for branches 1 and 2 of the logic tree in Fig. 2 (only felt data), whereas higher values are obtained in branches 5 and 6 (felt and "virtual" data). Such results are in good agreement with the observations of Albarello *et al.* (2007), pointing out that "virtual" intensities affect the SHA especially in areas where seismic site histories are particularly poor.

The hazard curves for all branches, at exceedance probability in 50 years (**Fig. 3.7**), were obtained taking into account the site intensity (I_S) values and the

Table 3.2. *I_{ref}, obtained for nine exceedance probabilities (E.P.) in 50 years, for each branch of the logic tree site adopted for Catania and Siracusa.*

Catania									
E.P.	**0.81**	**0.63**	**0.57**	**0.43**	**0.34**	**0.3**	**0.22**	**0.18**	**0.10**
Branch 1	5	6	6	6	7	7	7	7	8
Branch 2	5	6	6	6	7	7	7	7	8
Branch 3	6	6	7	7	7	7	7	8	8
Branch 4	6	6	7	7	7	7	7	8	8
Branch 5	7	7	7	7	7	7	8	8	8
Branch 6	7	7	7	7	7	7	8	8	8
Siracusa									
E.P.	**0.81**	**0.63**	**0.57**	**0.43**	**0.34**	**0.3**	**0.22**	**0.18**	**0.10**
Branch 1	4	5	5	5	6	6	6	7	8
Branch 2	4	5	5	5	6	6	6	7	8
Branch 3	5	6	6	6	6	6	7	7	8
Branch 4	5	6	6	6	6	6	7	7	8
Branch 5	6	6	7	7	7	7	7	8	8
Branch 6	6	6	7	7	7	7	7	8	8

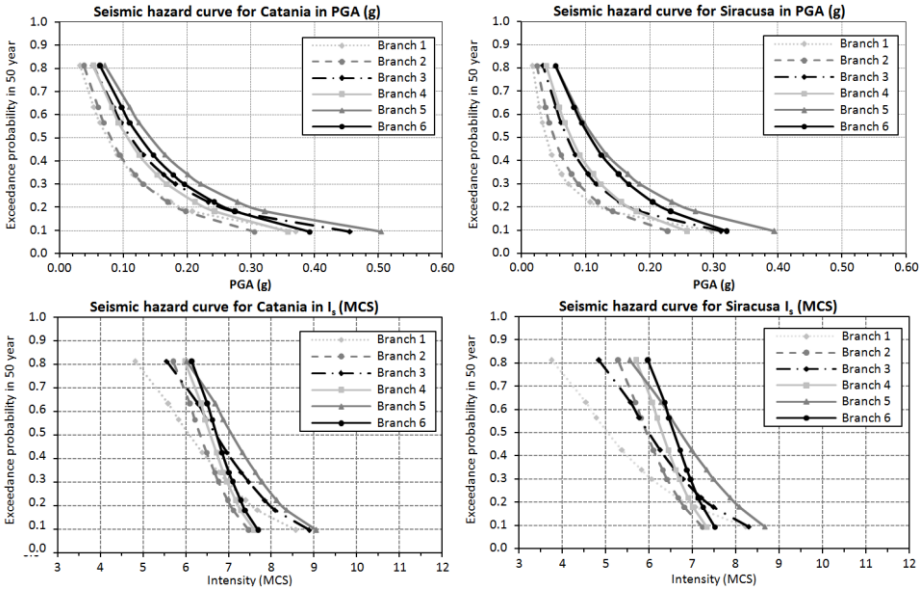

Fig. 3.7. *Hazard curves in PGA_{ref} (upper panels) and I_S (MCS) (lower panels) for each branch of the logic tree site.*

corresponding PGA_{ref} provided by the code, using the Gomez Capera *et al.* (2007) and the Faccioli and Cauzzi (2006) relationships. The higher values of PGA_{ref} and I_S were obtained when branch 5 of the logic three is followed, whereas lower values are observed for branches 1 and 2, both in Catania and Siracusa.

Table 3.3 summarizes the 16th, 50th, 84th percentiles and the mean values obtained by the logic tree for the site approach at nine exceedance probabilities in 50 years. **Figure 3.8** shows the mean and the percentile hazard curves, putting in evidence the fact that both PGA_{ref} and I_S attain slightly higher values in Catania rather than in Siracusa.

Table 3.3. *Mean, 16th, 50th (median) and 84th percentile values of PGA and I_S (MCS) for nine exceedance probabilities(E.P.) in 50 years.*

E.P.	Catania								Siracusa							
	PGA (g)				Intensity (MCS)				PGA (g)				Intensity (MCS)			
	16th	50th	84th	Mean	16th	50th	84th	Mean	16th	50th	84th	Mean	16th	50th	84th	Mean
0.10	0.35	0.38	0.46	0.42	7.6	8.1	8.9	8.4	0.25	0.30	0.33	0.32	7.3	7.9	8.4	8.0
0.18	0.21	0.26	0.28	0.27	7.2	7.5	8.2	7.8	0.14	0.18	0.24	0.20	7.0	7.2	7.6	7.4
0.22	0.17	0.22	0.25	0.23	7.1	7.3	7.9	7.6	0.12	0.15	0.21	0.17	6.7	7.0	7.3	7.2
0.30	0.13	0.18	0.20	0.18	6.9	7.0	7.5	7.3	0.09	0.12	0.17	0.13	6.3	6.7	7.1	6.9
0.34	0.12	0.16	0.18	0.16	6.8	6.9	7.4	7.2	0.08	0.11	0.15	0.12	6.2	6.6	7.0	6.7
0.43	0.09	0.13	0.15	0.13	6.5	6.8	7.0	6.9	0.06	0.09	0.13	0.10	6.0	6.3	6.8	6.4
0.57	0.07	0.09	0.11	0.10	6.1	6.5	6.7	6.5	0.04	0.06	0.09	0.07	5.6	6.0	6.5	6.0
0.63	0.06	0.08	0.10	0.09	6.0	6.3	6.5	6.3	0.04	0.06	0.08	0.06	5.4	5.9	6.3	5.8
0.81	0.04	0.05	0.07	0.06	5.4	5.8	6.0	5.8	0.02	0.04	0.05	0.04	4.6	5.4	5.8	5.2

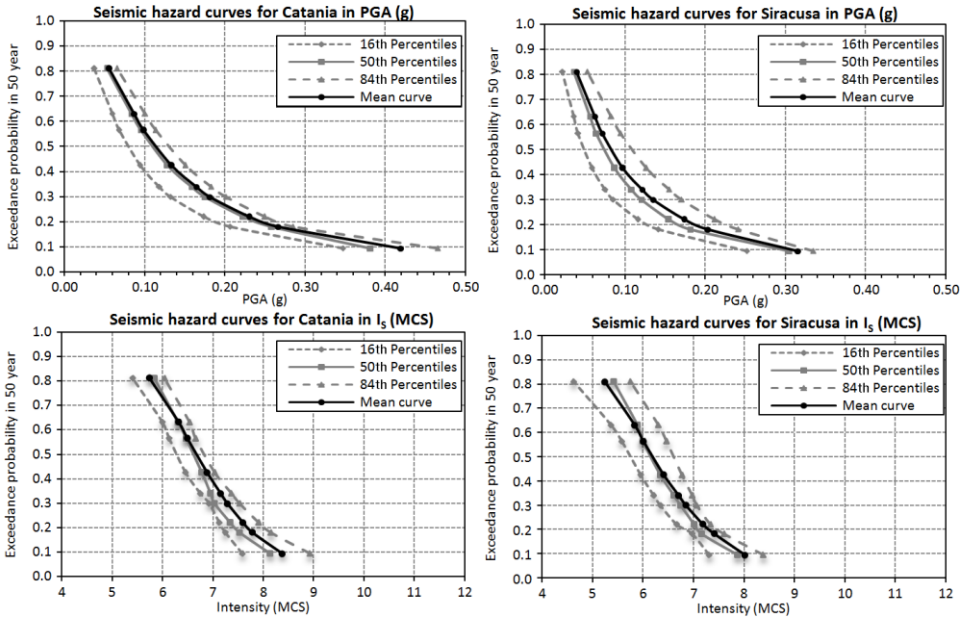

Fig. 3.8. *Mean, median (50th percentile), 16th and 84th percentiles hazard curves in PGA_{ref} (upper panels) and IS (MCS) (lower panels) for Catania and Siracusa.*

Seismic hazard, using the Esteva-Cornell approach, was computed for each branch of the logic tree considering rock and soft soils (**Fig. 3.9**). In **Table 3.4**, the mean and median PGA values obtained for the whole logic tree, as well as for SZ4-9 or SZ9 are shown, together with the related uncertainty, quantified through the 16th and 84th percentiles.

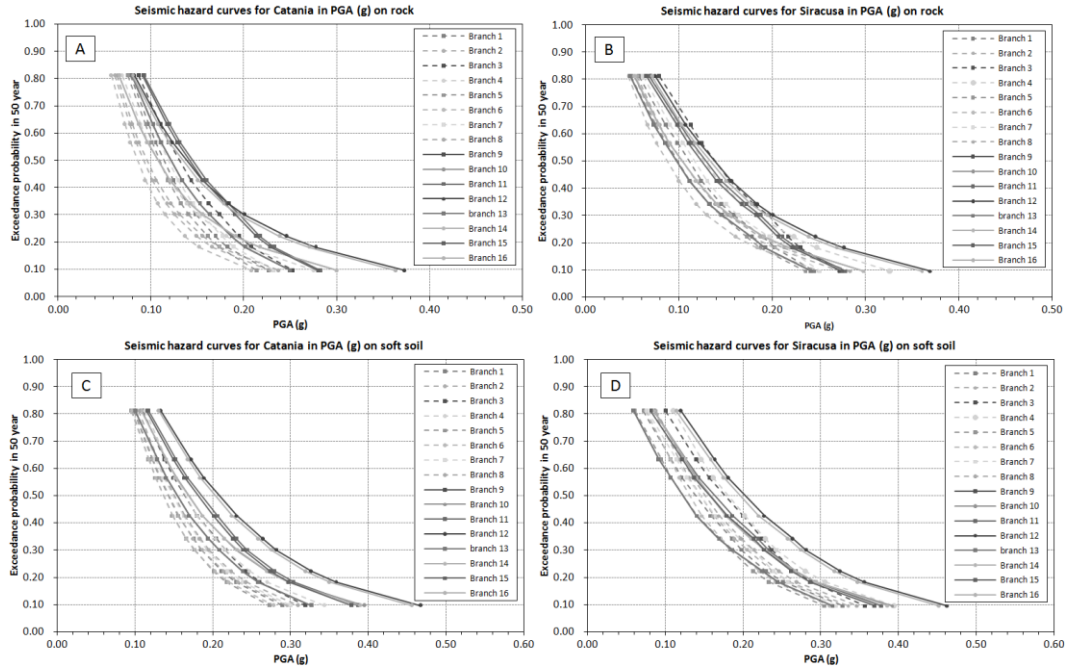

Fig. 3.9. *Hazard curves in PGA for each branch of the logic tree for rock (A, B) and soft soil (C, D).*

The mean, median, 16th and 84th percentiles hazard curves obtained for Catania and Siracusa on rock and soft soils, that in other words represent the reference hazard estimate, are shown in **Figure 3.10**. Inspection of the hazard curves puts in evidence small differences (±0.03 g) in PGA values. In particular, for exceedance probability smaller than 0.43 in 50 years, Catania has a slightly higher hazard than Siracusa, which, on the other hand, shows a slightly higher hazard for exceedance probability in 50 years greater than 0.43 (**Fig. 3.10 and Tab. 3.4**). Such results are, in my opinion, significantly affected by the location of the two towns with respect to the seismic zones considered. Catania is also very close to SZ936 that has a high seismicity rate at a relatively small magnitude with respect to SZ79 or SZ 935.

Table 3.4. *Mean, 16th, 50th (median) and 84th percentile values of PGA (g) for rock and for soft soil conditions obtained considering the whole logic tree, SZ4-9 and SZ9 seismogenic zonations.*

E.P.		CATANIA								SIRACUSA							
		ROCK				SOFT SOIL				ROCK				SOFT SOIL			
		16th	50th	84th	Mean	16th	50th	84th	Mean	16th	50th	84th	Mean	16th	50th	84th	Mean
LOGIC TREE	**0.10**	0.227	0.252	0.300	0.255	0.292	0.327	0.393	0.331	0.243	0.274	0.315	0.271	0.315	0.352	0.393	0.349
	0.18	0.174	0.203	0.231	0.199	0.231	0.260	0.302	0.260	0.193	0.217	0.241	0.213	0.245	0.278	0.301	0.271
	0.22	0.158	0.187	0.216	0.182	0.213	0.240	0.277	0.239	0.178	0.191	0.221	0.194	0.225	0.254	0.275	0.248
	0.30	0.135	0.156	0.193	0.156	0.186	0.213	0.243	0.209	0.146	0.157	0.192	0.163	0.187	0.220	0.241	0.214
	0.34	0.126	0.144	0.179	0.146	0.175	0.199	0.229	0.196	0.133	0.143	0.176	0.149	0.171	0.204	0.227	0.199
	0.43	0.111	0.127	0.154	0.127	0.156	0.175	0.204	0.173	0.111	0.121	0.149	0.126	0.143	0.173	0.201	0.169
	0.57	0.091	0.107	0.122	0.105	0.132	0.145	0.166	0.145	0.086	0.095	0.116	0.098	0.112	0.137	0.160	0.132
	0.63	0.083	0.100	0.111	0.097	0.123	0.134	0.151	0.133	0.074	0.083	0.103	0.086	0.100	0.122	0.144	0.118
	0.81	0.064	0.079	0.085	0.076	0.099	0.107	0.117	0.106	0.049	0.056	0.071	0.059	0.065	0.085	0.107	0.082
SZ4-9	**0.10**	0.216	0.230	0.251	0.233	0.280	0.298	0.318	0.299	0.246	0.262	0.282	0.263	0.313	0.332	0.355	0.335
	0.18	0.167	0.178	0.202	0.182	0.221	0.236	0.258	0.237	0.189	0.208	0.229	0.209	0.243	0.259	0.285	0.261
	0.22	0.150	0.166	0.181	0.167	0.204	0.217	0.240	0.219	0.174	0.189	0.215	0.191	0.222	0.239	0.264	0.240
	0.30	0.127	0.145	0.155	0.144	0.178	0.190	0.214	0.192	0.145	0.156	0.180	0.160	0.188	0.209	0.234	0.208
	0.34	0.117	0.136	0.145	0.135	0.167	0.179	0.201	0.181	0.133	0.143	0.166	0.147	0.173	0.192	0.222	0.194
	0.43	0.102	0.119	0.129	0.119	0.149	0.159	0.178	0.161	0.112	0.121	0.141	0.125	0.148	0.163	0.196	0.167
	0.57	0.085	0.099	0.109	0.100	0.127	0.135	0.149	0.136	0.086	0.095	0.112	0.098	0.119	0.129	0.154	0.131
	0.63	0.078	0.092	0.101	0.092	0.119	0.125	0.137	0.126	0.075	0.083	0.098	0.086	0.107	0.116	0.138	0.117
	0.81	0.062	0.072	0.081	0.073	0.096	0.101	0.109	0.102	0.050	0.056	0.069	0.059	0.072	0.081	0.099	0.082
SZ9	**0.10**	0.254	0.292	0.356	0.289	0.333	0.389	0.449	0.378	0.246	0.288	0.353	0.284	0.321	0.382	0.444	0.370
	0.18	0.203	0.223	0.266	0.224	0.263	0.298	0.345	0.294	0.196	0.220	0.264	0.220	0.250	0.293	0.341	0.285
	0.22	0.187	0.202	0.236	0.204	0.242	0.272	0.315	0.269	0.180	0.199	0.236	0.199	0.229	0.267	0.312	0.260
	0.30	0.157	0.177	0.195	0.175	0.211	0.236	0.272	0.234	0.148	0.169	0.194	0.166	0.191	0.228	0.270	0.222
	0.34	0.144	0.165	0.183	0.162	0.197	0.221	0.255	0.218	0.134	0.154	0.178	0.152	0.174	0.213	0.253	0.205
	0.43	0.122	0.142	0.156	0.140	0.172	0.194	0.223	0.192	0.112	0.130	0.150	0.128	0.144	0.179	0.216	0.173
	0.57	0.098	0.115	0.128	0.114	0.142	0.159	0.182	0.157	0.086	0.100	0.117	0.098	0.111	0.140	0.171	0.134
	0.63	0.089	0.105	0.117	0.104	0.130	0.145	0.166	0.144	0.074	0.088	0.103	0.086	0.095	0.126	0.154	0.119
	0.81	0.067	0.080	0.090	0.080	0.102	0.112	0.129	0.112	0.049	0.059	0.071	0.058	0.062	0.085	0.111	0.081

The choice of the source zone model for south-eastern Sicily seems to affect the hazard computation (**Fig. 3.9 and Tab. 3.4**) significantly. The trend of the Catania hazard curves, referring to the branches of SZ4-9 (see dashed lines in **Fig. 3.9** A, C), points out a lower hazard than that obtained when SZ9 is considered (see continuous lines in **Fig. 3.9** A, C). As matter of fact the b-values and the activity rates (λ) of SZ935 are slightly higher than those obtained for SZ79 (**Tab. 3.1**). The seismogenetic zones was extend (SZ935) to include all seismic data of the area, which provides an increase in the hazard estimates and smoothes the local differences. On the other hand, the use of small zones, with a minor seismic activity (SZ79) can imply a decrease in the hazard assessment. This is the consequence of the well known "hazard spreading effect" of the Cornell approach. The assumption of homogenous seismicity rates in a seismogenic zone tends, in actual fact to "distribute" throughout the entire zone extension, the hazard associated to the seismic activity observed in a limited portion (Del Gaudio *et al.*, 2009). Despite such considerations, the PGA values obtained by considering SZ4-

9 are not very different from those obtained when SZ9 is taken into account and the differences do not exceed ±0.05 g for all considered exceedance probabilities in 50 years.

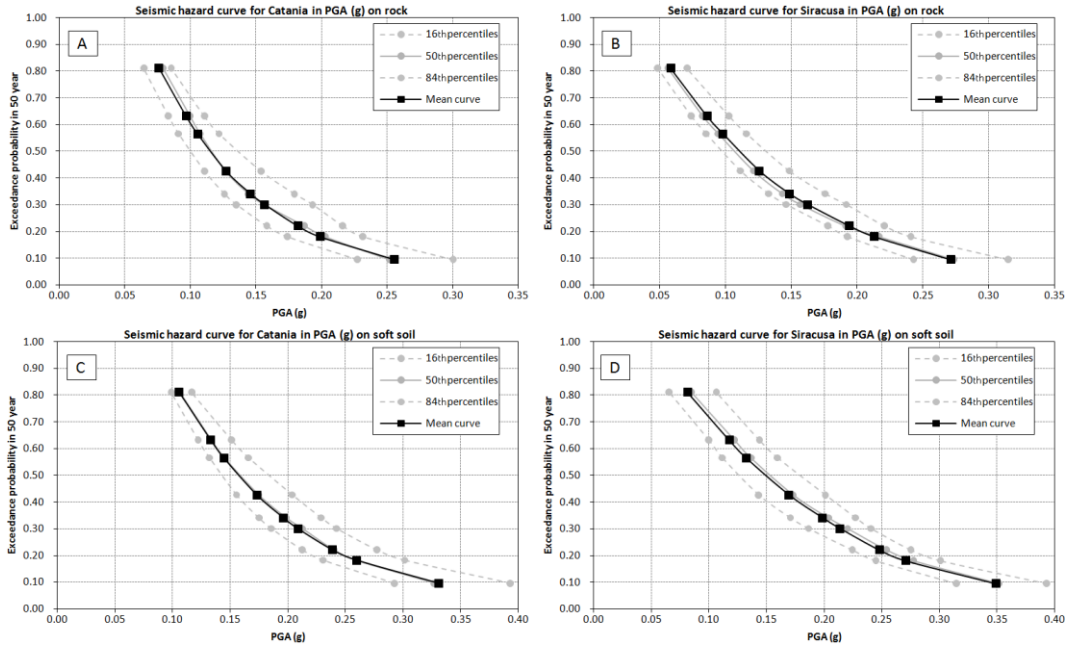

Fig. 3.10. *Mean, median (50th percentile), 16th and 84th percentiles hazard curves obtained for Catania and Siracusa on rock (A, B) and soft soil (C, D).*

Moreover, uniform hazard response spectra in acceleration (UHRSA), assuming rock-site conditions, were computed at both the Catania and Siracusa sites for 11 spectral periods ranging between 0.05 and 2.0 seconds. The mean UHRSA for the whole logic tree (**Fig. 3.11a, b**) were obtained for return periods of 475 and 975 years. It is generally found that large magnitude events affect the long period portion (>0.5 s) of a UHRSA whereas, small magnitude events affect the short-period section of the spectrum (Tselentis *et al.*, 2010). The graphs in **Figure 3.11 a and b**, show a high content at the short period in UHRSA, with picks ranging between 0.1-0.3 s. This indicates that both in Catania and Siracusa, the UHRSA are influenced by a great number of earthquakes having moderate magnitude and short source-to-site distance. A comparison of the UHRSA with the ones of the Italian hazard map (Working Group MPS04, 2004) shows that the response spectral accelerations for Catania are smaller than those obtained by the

Working Group MPS04, at periods greater than 0.2 s (see dotted lines **in Fig. 3.11 a, b**). The UHRSA computed for Siracusa are higher than the response spectra acceleration of Working Group MPS04 (2004) in short periods (<0.40 sec). Similarly to Catania, the UHRSA of the Working Group MPS04 (2004) exhibits larger values at long periods (>0.4 sec), therefore indicating a greater contribution over long periods due to larger magnitude events and to greater source-to-site distance. Such a difference, in my opinion, could be related to the fact that in the present study, only seismogenic sources located within a distance of about 300 km from south-eastern Sicily were considered. A suitable selection of the source zone models for south-eastern Sicily strongly influences the UHSRA as well. It is indeed evident (**Fig. 3.11c and d**) that the acceleration response spectra referring to SZ9 (full lines) always show PSA values greater than those referring to SZ4-9 (dashed lines).

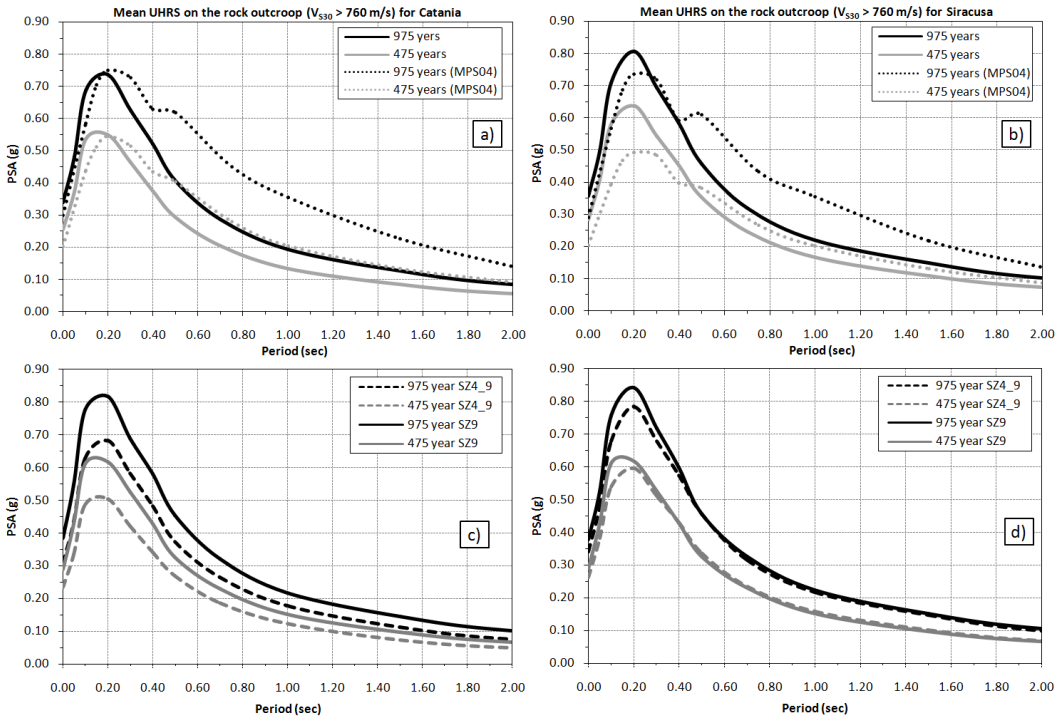

Fig. 3.11. *Mean UHRSA for 475- and 975-year return periods for the whole logic tree, corresponding UHRSA obtained by Working Group MPS04 (2004) (a, b) and UHRSA taking into account SZ4-9 and SZ9 separately (c, d).*

The UHRSA gives an appropriate probabilistic representation of the seismic action but does not, generally, correspond to the spectrum of a specific earthquake. For this reason a disaggregation analysis of the PSHA is necessary (Bazzurro and Cornell, 1999). A two dimensional disaggregation in magnitude and epicentral distance (R_{epi}) was performed for a 475-year return time. Such procedure permits to identify the design earthquake that characterizes the local seismic hazard. Similarly to the procedure used for obtaining the hazard curves and the response spectra, the disaggregation charts were obtained for the whole logic tree, for SZ4-9 and for SZ9 models (**Fig. 3.12a, b**). The dominant scenario earthquake can be defined using either the mean or the modal value of its magnitude (M) and source-to-site distance (R_{epi}) (see **Tab. 3.5**) coming out from the use of the different branches of the logic tree. Using the mean values, although they are simple to understand and to compute, not always represent a realistic

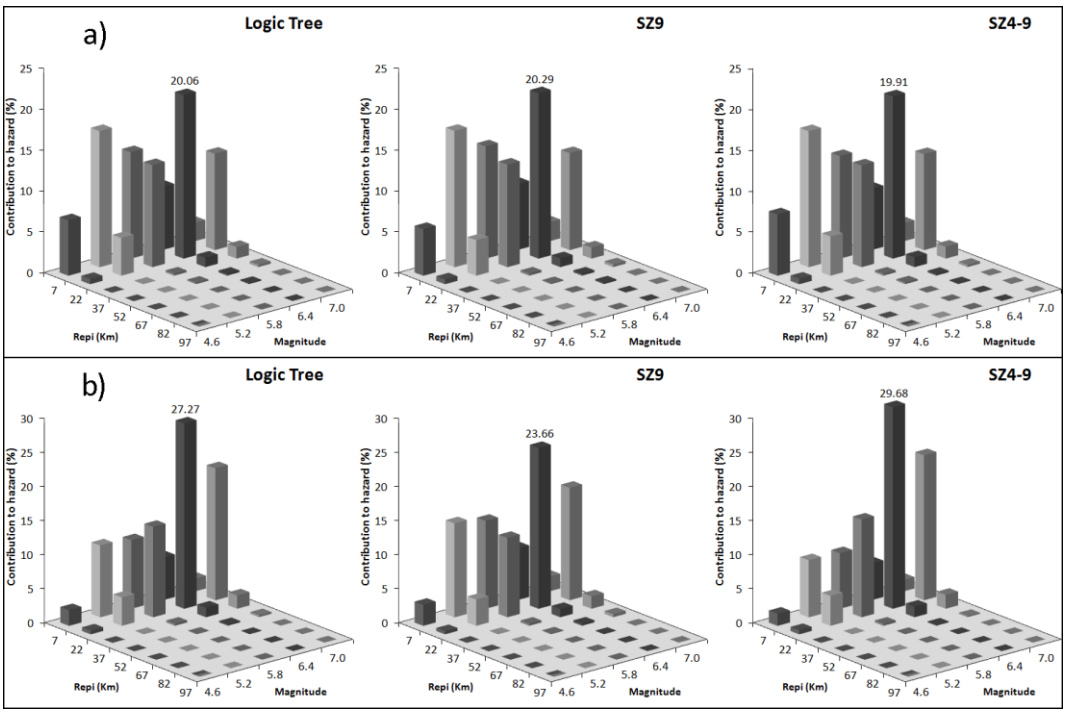

Fig. 3.12. *Disaggregation of the seismic hazard for Catania (a), and Siracusa (b) considering an exceedance probability of 10% in 50 years.*

scenario whereas, the mode corresponds to the M-R group that gives the largest contribution to the hazard and, consequently, corresponds to a more realistic source (Barani *et al.*, 2009). Inspection of the disaggregation graphs (**Fig. 3.12**) shows that, for all considered models, the major contribution to the dominant scenario is given by an earthquake having magnitude M=6.4 and R_{epi}= 22 km. Both mean and modal values obtained (see **Tab. 3.5**) do not show significant differences for all models unless the source-distance (R_{epi}) is taken into account. The mean values of M and R_{epi} obtained in the present study were compared with the ones calculated by the Working Group MPS04 (2004). The results obtained in this study are higher than those provided by the Working Group MPS04 both as concerns the magnitude (about 0.2 units) and the epicentral distance (about 5 km). It is, however, worth noting that as observed by Barani *et al.* (2009), these results show that the attenuation equation used in the hazard computation strongly affects the parameters of the dominant scenario earthquake.

Table 3.5. *Mean and modal values of magnitude (M) and distance (Repi), obtained by considering 10% exceedance probability, for SZ4-9, SZ9, for the complete logic tree and mean values found by the Working Group MPS04 (2004).*

CATANIA															
SZ4-9				**SZ9**				**LOGIC TREE**				**MPS04**			
Mean		**Modal**		**Mean**		**Modal**		**Mean**		**Modal**		**Mean**		**Modal**	
10%				**10%**				**10%**				**10%**			
M	D	M	D	M	D	M	D	M	D	M	D	M	D	M	D
5.9	15.7	6.2	14.4	6.2	15.6	6.3	14.4	6.0	15.7	6.3	14.4	5.8	9.3	-	-
SIRACUSA															
SZ4-9				**SZ9**				**LOGIC TREE**				**MPS04**			
Mean		**Modal**		**Mean**		**Moda**		**Mean**		**Modal**		**Mean**		**Modal**	
10%				**10%**				**10%**				**10%**			
M	D	M	D	M	D	M	D	M	D	M	D	M	D	M	D
6.2	18.8	6.4	19.1	6.1	16.7	6.4	16.9	6.2	18.0	6.4	18.2	5.9	11.4	-	-

Chapter IV

Seismic Urban Scenario and Seismic Site Response in Catania, Italy

4.1. Issues of the chapter

The town of Catania is located in the eastern coast of Sicily (southern Italy) to the south of Mt. Etna. The high level of seismicity that affects the city, together with the considerably high density of inhabitants living in its urban area, contributed to classify it as one of the town having the highest seismic risk in Italy. It is also not negligible the high potential damage to which its historic-architectural patrimony could undergo even at moderate to small magnitudes. The seismicity of this area is linked to the collisional processes between African and European plates. In particular, the earthquakes occurred in 1169, 1542, 1693, 1818, 1908 and more recently in 1990, having intensity ranging between VI and XI MCS scale (Working Group MPS, 2004) testify the high level of hazard in this area. The information on damage distribution during the past earthquakes is available for downtown Catania only. In the past 20 years residential areas were erected in the northern and southern parts of the town. It is therefore evident the importance of evaluating the local seismic effects in the whole Catania area assessing the ground motion amplification and damage distribution during earthquakes having different magnitude and source-to-site distance. A reliable evaluation of ground motion requires the analysis of the following three fundamental steps: seismic radiation released by the source; path and attenuation effects in the wave propagation from the source to the city; local effects linked to elastic and anelastic properties of soil deposits interposed between the bedrock and the "receivers" at the ground surface. Most of the researches about the seismic response of the Catania area were performed in the frame of two national research projects (see Faccioli and Pessina, 2000; Mucciarelli and Pacor, 2007). Seismic

sources in eastern Sicily were studied by several authors who estimated, also through numerical simulations, potential shaking parameters for different earthquake inputs (Langer *et al.*, 1999; Zollo *et al.*, 1999; Azzaro and Barbano, 2000; Barbano and Rigano, 2001; Laurenzano *et al.*, 2004; Laurenzano and Priolo, 2005). As regards the evaluation of the seismic input at the bedrock, taking into account both the source features of a scenario earthquake and the attenuation, studies were carried out by De Lorenzo *et al.* (2004), Giampiccolo *et al.* (2002, 2003, 2004). A significant improvement to the knowledge of the seismotectonic setting in south-eastern Sicily was achieved by the analysis of the 13 December 1990 earthquake and its aftershocks. These events are, indeed, the first digital set of seismic data for the area, therefore allowing investigations on the spectral source parameters and the estimate of attenuation and seismic scaling laws in south-eastern Sicily (Amato *et al.*, 1995; Di Bona *et al.*, 1995; Giardini *et al.*, 1995; Scognamiglio *et al.*, 2005). As a result of all these studies, reference seismic inputs at the bedrock were assessed and both the 1693 and 1818 shocks were taken into account as reliable scenario earthquakes for modelling seismic inputs in the Catania area (Laurenzano *et al.*, 2004; Lombardo *et al.*, 2004). The estimate of ground motion features at the surface was performed using numerical modeling as well as noise measurements. In particular, Biondi and Maugeri (2005), Lombardo *et al.*, (2004, 2006), Catalano *et al.*, (2005), Lombardo and Rigano (2007) evaluated the local seismic response in test sectors of the urban area, whereas preliminary estimates of site response in the whole Catania area were obtained by Giampiccolo *et al.*, (2001), Lombardo *et al.*, (2001), Priolo *et al.*, (2005). Further investigations on the local effects due to fault zones (Rigano *et al.*, 2008) as well as to natural cavities (Lombardo and Rigano, 2009; Lanzo *et al.*, 2006; Sgarlato *et al.*, 2011) have been recently performed and others are still in progress. All these studies, besides identifying the coarse features of the elements needed to assess the seismic hazard of the area, have focused their attention on some modelling of geological site conditions and interpreting ambient noise recordings. Nevertheless, studies so far performed do not consider exhaustively the complexity of phenomena causing site amplification. The contribution of

topographic effects and the existence, in the sedimentary deposits, of engravings filled up by quaternary and historic lava flows, are often neglected. Moreover, none of the afore mentioned studies carried out a comparison and validation of obtained results with findings coming from earthquake recordings. Present study therefore aims at dealing with such aspect combining numerical and experimental approaches as well, in order to validate the findings so far obtained.

4.2. Tectonic features and geologic setting of Catania

At regional scale, the tectonics of Eastern Sicily is quite complex. Seismotectonic information and interpretations available for south-eastern Sicily suggest the existence of two groups of possible sources for the seismicity that affected the town of Catania in different time. The sources are located either close to the Ionian coast (Messina Straits and Malta-Hyblean escarpment), or inland, both in the Hyblean foreland and Etnean areas (**Fig. 4.1**). The Malta-Hyblean escarpment, a normal fault system trending NNW-SSE, is in particular considered (Azzaro and Barbano, 2000) as the possible source of the destructive earthquakes ($M \approx 7.0$) that struck in past centuries the Catania area.

The geo-lithologic map of the Catania urban area is shown in **Fig. 4.1**. It is the result of assembling information coming from data and surveys performed by several authors (Monaco and Tortorici, 1999; Monaco *et al.*, 2000; Lombardo *et al.*, 2001; Carbone *et al.*, 2009). The surface geology of the town derives from the combination of three processes linked to the volcanic, tectonic and human activities. As a consequence of this, the main feature of the area is a complex sedimentary sequence interbedded between a clay basement and an upper volcanic formation with lava flows and pyroclastics that sometimes is surmounted by detritus and ruins due to past earthquakes. The bedrock of the area is composed of a Lower-Middle Pleistocene succession of marly clays, having thickness up to about 600 m. In the upper part of this succession, levels of sand and sandy clays are frequently present. These deposits are indeed followed upwards by some tens meters of fluvial-deltaic yellowish sandy clay, sand and coarse gravel, referred to the Middle Pleistocene, called *"Terreforti"* formation. This formation is alluvial

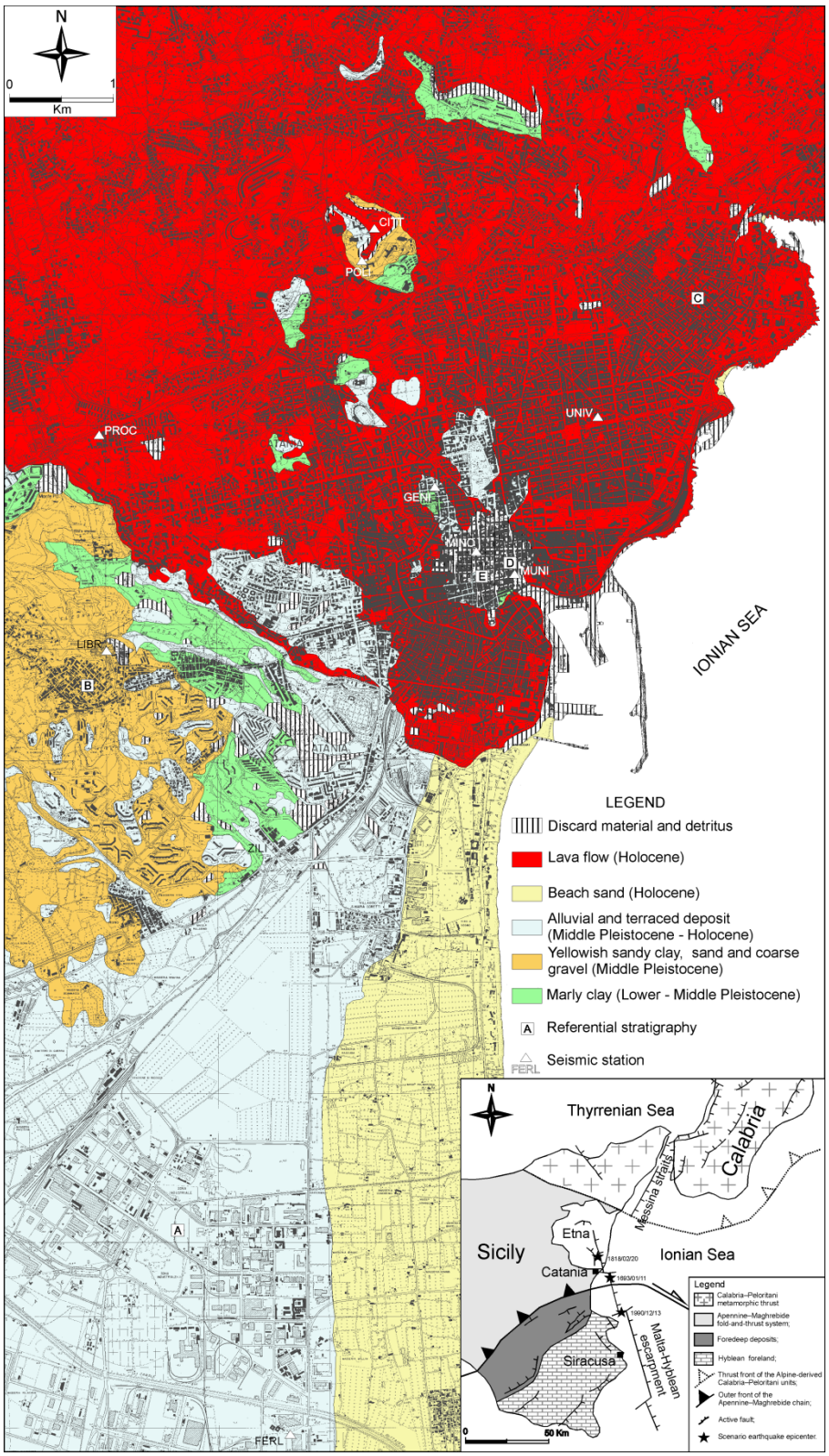

Fig. 4.1. *Geolithologic map of Catania urban area . The inset map shows the main structural features in Eastern Sicily (modified from Lavecchia et al., 2007 and Galadini et al., 2001) and the location of the considered scenario earthquakes.*

deposits (Middle Pleistocene—Holocene), that outcrop in some places in the northern and western part of the urban area, and are characterized by several meters thick sands, gravels and silty clays. Recent alluvial deposits (Holocene) formed by levels of sands, silt and sometimes gravelly sands, outcrop in the southern part of the urban area and pertain to the Simeto river plain. Such deposits grade upwards to Holocene coastal sand deposits. However, the lithotype more frequently cropping out in the study area is the basaltic lava that in pre-historical and historical times flowed onto the valleys originally existing in the sedimentary formations. The flows have an extremely variable thickness and often are formed by alternating levels of massive lava and more or less weathered scoriae. Finally, in several parts of the historic centre, discard building materials, having thickness up to ten–fifteen meters, mostly resulting from ruins due to historical earthquakes, are present. These materials were not distinguished from the slope detritus in the geo-lithologic map of **Fig. 4.1**.

4.3. Methodology

The evaluation of local seismic response was performed by combining a numerical approach with experimental observations. The numerical study was carried out using equivalent-linear earthquake site response analyses (EERA, Bardet, 2000). This code requires: (a) simplified geological model to individuate macro-layers, down to the bedrock; (b) shear wave velocity profile for the elastic properties of the macro-layers and bedrock; (c) the shear strain (γ) non linearity of the shear modulus G and damping ratio D of macro-layers and bedrock. Moreover, a reference earthquake has to be chosen. In this study, based on the seismic history of Catania (Azzaro *et al.*, 1999), three scenarios earthquakes were selected as examples of destructive (return period ≈500 years), strong (return period ≈200–250 years) and moderate (return period ≈ 50–60 years) inputs for hazard evaluation. **Table 4.1** lists the parameters of the 1693, 1818 and 1990 earthquakes that were selected as representative of a destructive, strong and moderate scenario, respectively. The Malta-Hyblean escarpment was considered as the seismic source for both 1693 and 1990 earthquakes. As regards the 1693

earthquake, in particular, the seismic source was selected according to recent studies based on the results coming from seismic prospecting at sea and to tsunami modeling which suggest the rupture of a segment of the Malta-Hyblean fault escarpment (Gerardi *et al.*, 2008; Brancato *et al.*, 2009). The Sicilian basal

Table 4.1. *Features of scenario earthquakes; h = hypocentral depth; M_W = moment magnitude. Epicentral distance (R_{epi}), hypocentral distance (R_{hyp}), focal mechanism and fault strike were taken from studies quoted in the reference column.*

Earthquake	h* (Km)	M_W**	R_{epi} (Km)	R_{hyp} (Km)	Focal Mechanism	Fault Strike	Reference
1990-Dec-13	13	5.68	25	28.18	Strike slip	E-W	Amato *et al.*, 1995
1818-Feb-20	13	6.20	12	17.69	Thrust	ENE-WSW	La Vecchia *et al.*, 2007
1693-Jan-11	13	7.00	15	19.85	Normal fault	NNW-SSE	Priolo, 1999
*Working Group MPS, 2004; **Working Group CPTI, 2004							

thrust was considered as the possible source for the 1818 earthquake, as stated by Lavecchia *et al.* (2007), through the analysis of structural and geophysical data (see epicentre locations in **Fig. 4.1**). The magnitude (M_W), the hypocentre distance (R_{hyp}) and the focal mechanism (**Table 4.1**) stand for the input of the Cauzzi and Faccioli (2008) attenuation law in order to define the target spectra. The authors calibrated this attenuation law using intraplate events, focal depth within about 22 km and moment magnitude ranging from 5.0 to 7.2. Such features are consistent with the seismic activity of the Italian region. The authors derived an empirical equation for the prediction of displacement response spectra (DRS) in the range 0.05–20 s, considering the geometric mean of the horizontal components of motion at a given period. The empirical equation for the prediction of the DRS ordinates, considering an outcropping bedrock and the focal mechanism, was taken in the form:

$$Log_{10}DRS(T;\xi) = a_1 + a_2 M_W + a_3 Log_{10}R + a_N E_N + a_R E_R + a_S E_S + \varepsilon \quad (4.1)$$

where a_i (i = 1. . .S) are the numerical coefficients depending on the period (T) and the damping ratio (ξ) to be determined through regressions, R is the focal distance in km, E_x (x = N, R, S) are dummy variables for normal, reverse, and

strike-slip fault mechanisms, respectively, and ε denotes a random error term. Using the relation:

$$PSA = (T;\xi) = \left(\frac{2\pi}{T}\right)^2 DRS(T;\xi) \qquad (4.2)$$

pseudo-acceleration spectra (PSA) were obtained. The PSA and the spectral acceleration (Sa) were found by the authors to be substantially coincident in the range 0.05–10 s. Seven strong motion accelerograms, for each considered scenario, were selected from the European Strong Motion Database (Ambraseys *et al.*, 2002) through the REXEL code (Iervolino *et al.*, 2010) (see **Fig. 4.2**).

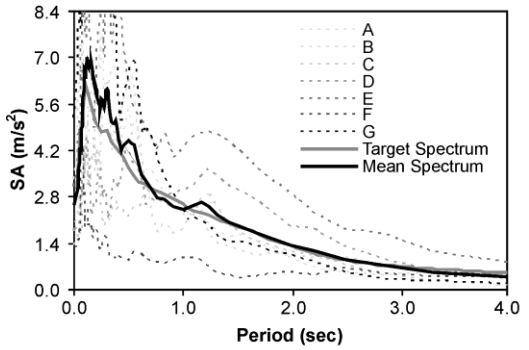

	Earthquake Name	Date	Mw	Fault Mechanism	Epicentral Distance [km]	EC8 Site class
A	Montenegro	1979-04-15	6.9	thrust	21	A
B	Campano Lucano	1980-11-23	6.9	normal	23	A
C	Campano Lucano	1980-11-23	6.9	normal	23	A
D	South Iceland (aftershock)	2000-06-21	6.4	strike slip	24	A
E	Tabas	1978-09-16	7.3	oblique	12	A
F	South Iceland	2000-06-17	6.5	strike slip	5	A
G	South Iceland (aftershock)	2000-06-21	6.4	strike slip	6	A
	Mean:		6.8		16.3	

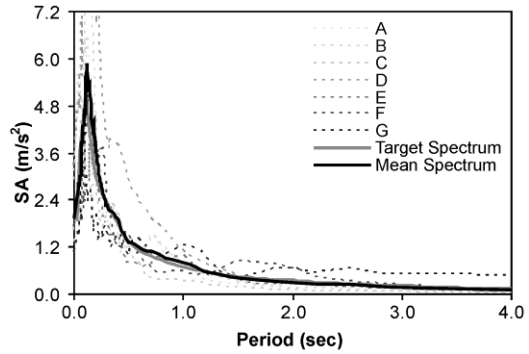

	Earthquake Name	Date	Mw	Fault Mechanism	Epicentral Distance [km]	EC8 Site class
A	Friuli (aftershock)	1976-09-15	6.0	thrust	12	A
B	SE of Tirana	1988-01-09	5.9	thrust	7	A
C	Umbria Marche	1997-09-26	5.7	normal	23	A
D	South Iceland (aftershock)	2000-06-21	6.4	strike slip	14	A
E	South Iceland (aftershock)	2000-06-21	6.4	strike slip	24	A
F	Umbria Marche (aftershock)	1997-10-06	5.5	normal	10	A
G	Umbria Marche (aftershock)	1997-10-14	5.6	normal	12	A
	Mean:		6.0		14.6	

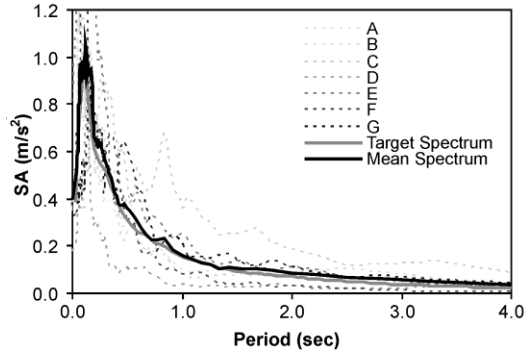

	Earthquake Name	Date	Mw	Fault Mechanism	Epicentral Distance [km]	EC8 Site class
A	Umbria	1984-04-29	5.6	normal	27	A
B	Umbria	1984-04-29	5.6	normal	27	A
C	Umbria Marche (aftershock)	1997-10-14	5.6	normal	23	A
D	Mt. Vatnafjoll	1987-05-25	6.0	oblique	24	A
E	Umbria Marche (aftershock)	1997-10-06	5.5	normal	29	A
F	Golbasi	1986-05-05	6.0	oblique	29	A
G	Umbria Marche (aftershock)	1997-10-14	5.6	normal	29	A
	Mean:		5.7		26.9	

Fig. 4.2. *Compatible combination of accelerograms found for the considered scenarios; upper panel refers to the destructive scenario (1693), middle and lower panels refer to strong (1818) and moderate (1990) scenarios, respectively.*

The use of real seismic inputs was preferred to synthetic ones since the basic problem with spectrum-compatible artificial records is that they have an excessive number of cycles of strong motion and consequently they possess unreasonably high energy content (Bommer and Acevedo, 2004). According to Cauzzi and Faccioli (2008) a scaling factor of $1/R_{hyp}$ was adopted to correct the peak ground acceleration (PGA_{ref}) and the spectral acceleration ($Sa_{g(ref)}$), obtained at the bedrock through parameters reported in **Table 4.1**. This procedure allowed to scale the selected accelerograms at each site. The elastic parameters of main geological formations coming out as a result of the "Catania Project" of CNR-GNDT (Faccioli and Pessina, 2000) were used in order to model the input stratigraphic sequence (**Table 4.2**). Experimental curves of the shear modulus reduction (G) and the material damping (D) as a function of shear strain (γ) are shown in **Fig. 4.3**. They were taken from Carrubba and Maugeri (1988) for cohesive soils (clay) and from Cavallaro *et al.* (2001) for weathered lava and non cohesive soils (sand). As regards the compact lava, strain-dependent damping and shear modulus degradation curves were taken from Seed and Idriss (1970),

Table 4.2. *Elastic parameters of main geological formations in the Catania area. The acronyms in the first column refer to the soil deposits listed in the legend of Fig. 1: MC=Marly Clay; Y=Yellowish sandy clay, sand and coarse gravel; AT=Alluvial and terraced deposit; L=Lava deposit; S=Sand; D=Discard material and detritus.*

	Lithotype	ρ (Kg/m^3)	V_P (m/s)	V_S (m/s)	σ	Q (s-1)
MC	Marly Clay	2000	1235	650	0.308	35
Y	Sandy Clay	1950	490	250	0.324	15-20
	Coarse Sand and Gravel	2000	2000	450	0.31	20
	Gravelly Sand/Sandy Clay	1940	640	330	0.319	22
AT	Fine Alluvial deposits	1900	370	190	0.321	15
	Coarse Alluvial deposits	1850	408	210	0.32	12
S	Beach deposits (Sand)	1830	430	220	0.323	12
L	Massive Lava	2300	2300	1000	0.249	50-100
	Scoriaceous/fractured Lava	1800	1800	230	0.267	15
	Pyroclastics	1700	1700	300	0.288	30
	Massive/Scoriaceous Lava	1950	750	400	0.301	20
D	Discard material - Detritus	1800	1800	210	0.31	12

according to Bessason and Kaynia (2002) that estimated site amplification in lava rock on soft sediments sites. The local seismic response with EERA was calculated in 194 sites randomly distributed in the Catania urban area. The stratigraphy of selected sites was inferred from data of the "Catania Project"

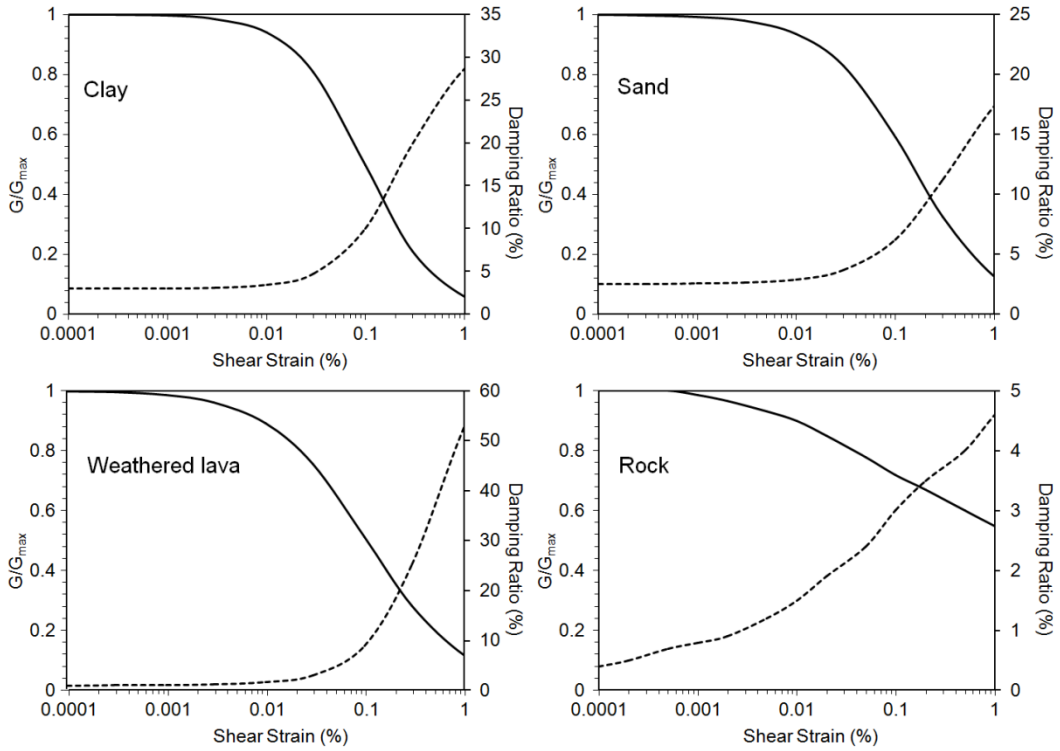

Fig. 4.3. *Behavior of shear modulus, G, and damping factor, D, dependent on shear strain, γ used in this study.*

dataset. The most representative of main lithotypes as well as those drilled to a depth reaching the bedrock were selected from a dataset formed by 860 boreholes. The EERA code provides as output results the PGA values, at different depth, and both the theoretical transfer function and the response spectra. The iso-acceleration maps for the considered scenarios were drawn using the computed value of PGA and acceleration spectra at the 5% critical damping, for the periods 0.2, 0.5 and 1.0 s, at the surface (**Figs. 4.4**, **4.5** and **4.6**). The above mentioned periods were selected since they represent the range of natural periods commonly observed for 2–3 storeys up to tall buildings (about 10 storeys).

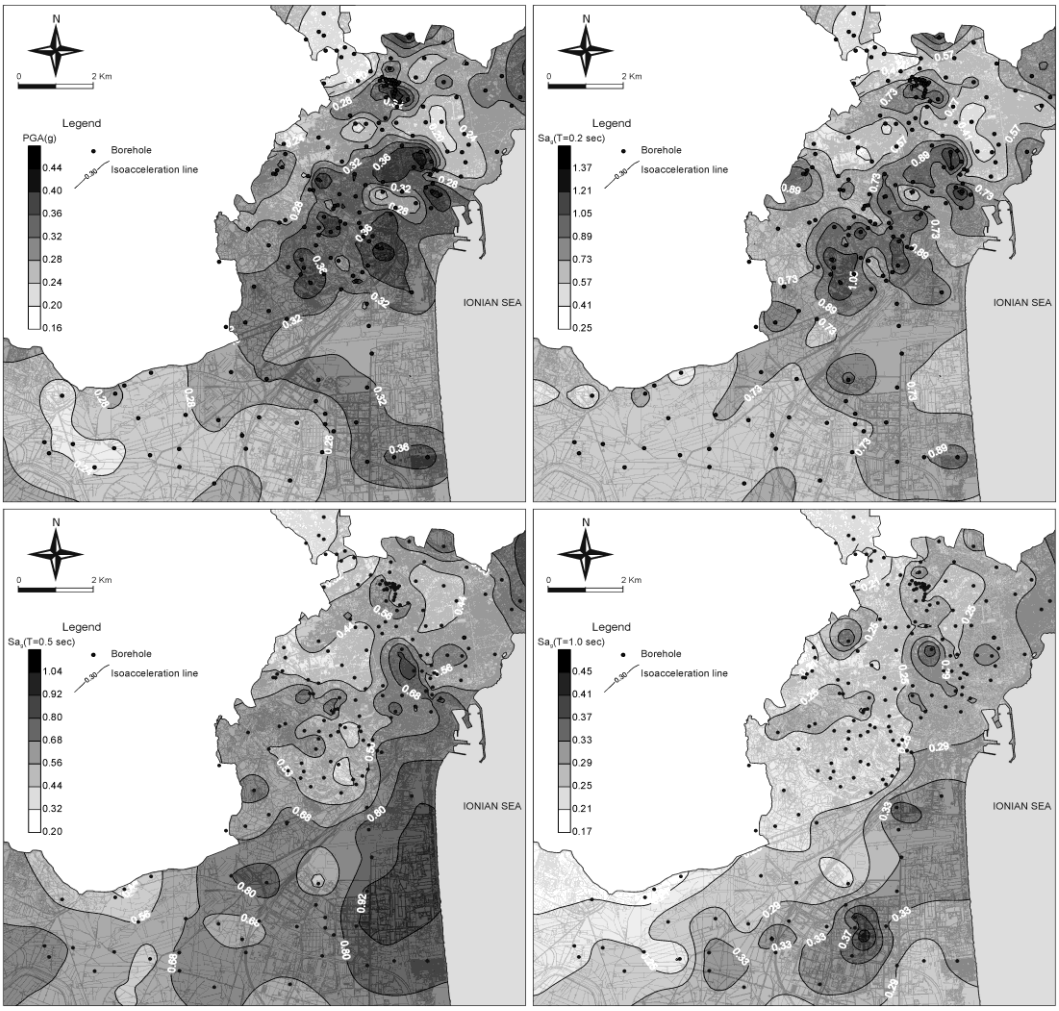

Fig. 4.4. *Contour of PGA and ground motion distribution in term of acceleration response spectral ordinates at 0.2 sec, 0.5 sec and 1 sec period, 5% damping, obtained for a destructive scenario (1693 earthquake).*

Further maps were drawn in order to summarize the local amplifications, considering three classes of increments and decrements with respect to PGA_{ref} and $Sa_{g(ref)}$ (**Fig. 4.7**). Statistical analysis shows that the probability distribution of ground-motion spectral acceleration at individual periods can be well approximated by log-normal distributions (e.g. Wang 2010). These maps were therefore obtained by calculating the log-normal mean deviations, at each site, for the three considered scenarios. The contouring of all maps was performed through the *Kriging* algorithm. It is a widely adopted geo-statistical gridding method that produces reliable maps from irregularly spaced data. Since for a correct

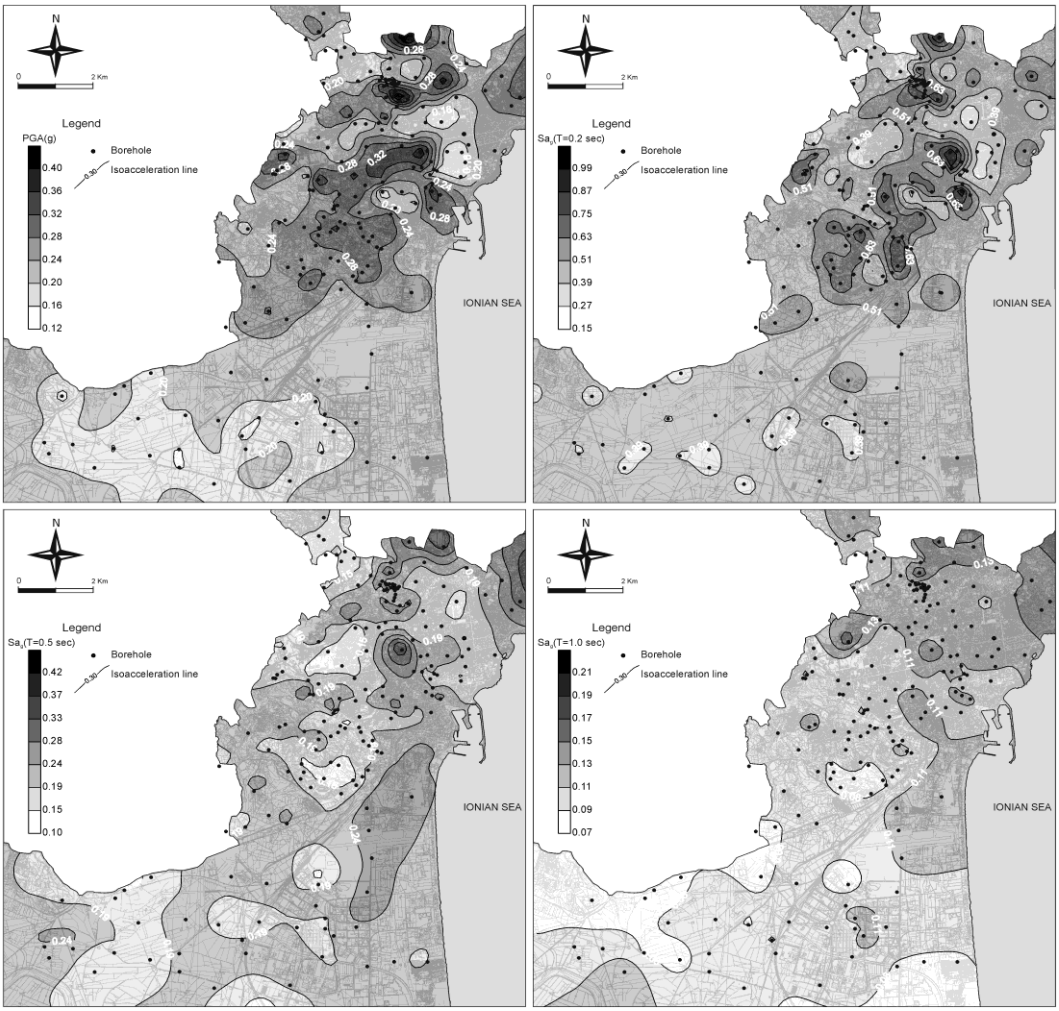

Fig. 4.5. *Contour of PGA and ground motion distribution in term of acceleration response spectral ordinates at 0.2 sec,0.5 sec and 1 sec period, 5% damping, obtained for a strong scenario (1818 earthquake).*

application of *Kriging* an appropriate variogram model has to be defined, the *Variowin* software (Pannatier 1996) was used for estimating the variogram parameters ruling the contouring procedure. Moreover, in the frame of a collaboration between researchers of the Istituto Nazionale di Geofisica e Vulcanologia (INGV) of Rome and of the Department of Geological Science of the University of Catania, ten sites were instrumented with broad-band seismometers (**Fig. 4.1**). Stations were located taking into account the outcropping lithology and the logistics facilities. The stations were deployed in groups of four that were simultaneously recording for some months. The area was however

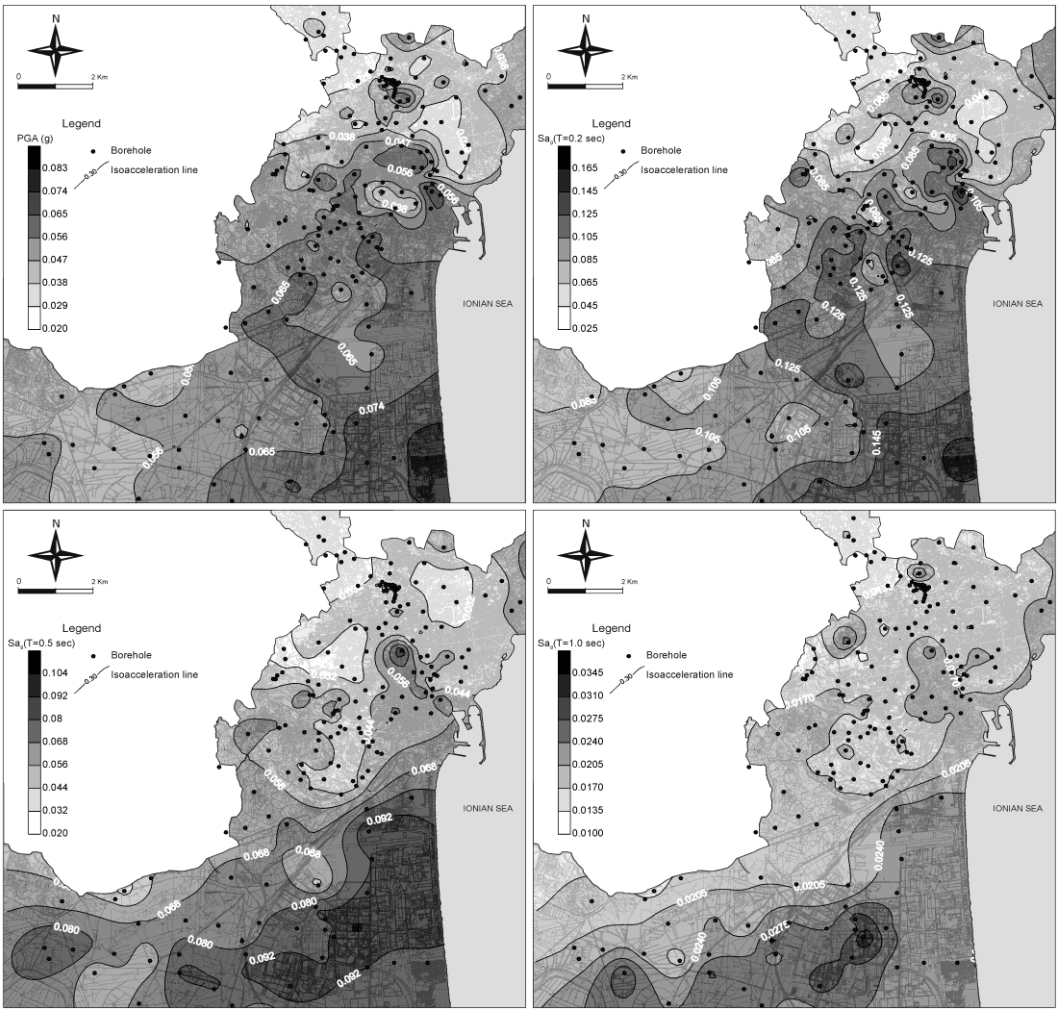

Fig. 4.6. *Contour of PGA and ground motion distribution in term of acceleration response spectral ordinates at 0.2 sec, 0.5 sec and 1 sec period, 5% damping, obtained for a moderate scenario (1990 earthquake).*

monitored for about 2 years and half, from 1999 till 2001. A set of about 850 local and regional seismic events was collected for data processing through different experimental techniques. The location and magnitude of recorded events was taken from the INGV bulletin. The signal-to-noise ratio, in a 10 s time window close to the S-waves onset, was calculated for the whole set of recorded earthquakes. In order to select good quality events, only those having a ratio greater than three, in the frequency band 0.5–10 Hz, were taken into account. The considered interval (0.5–10 Hz) accounts for the frequency boundaries which are significant for engineering purposes. The 172 seismic events that went through the

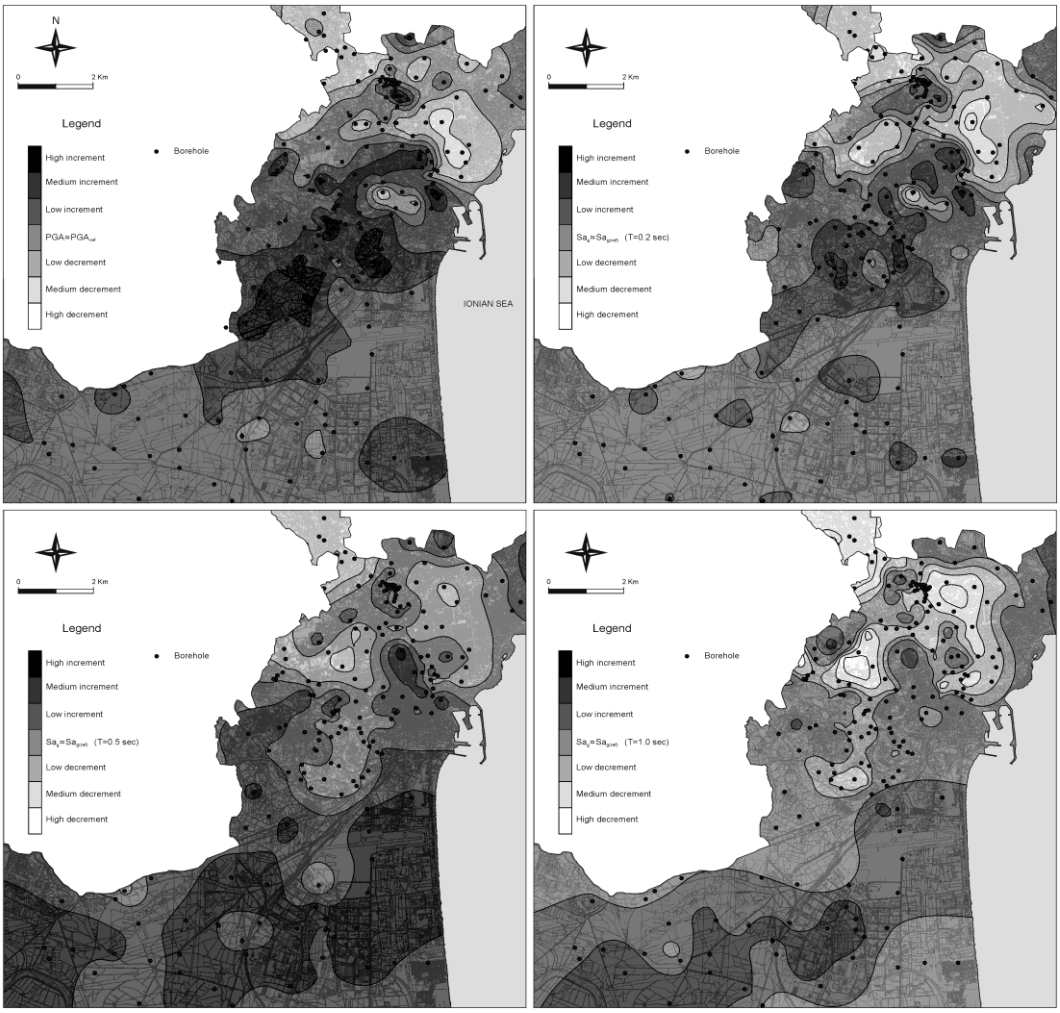

Fig. 4.7. *Map of increments/decrements with respect to the reference peak ground acceleration (PGAref) and acceleration response spectral ordinates at 0.2 sec, 0.5 sec and 1 sec period, 5% damping (Sag(ref)) at the bedrock obtained for the three considered scenarios.*

above mentioned selection (**Table 4.3**), were processed using the standard spectral ratio (SSR) and earthquake's horizontal to vertical spectral ratio (HVSR). Time windows of 10 s, starting from S-waves onset, were considered and both a base-line correction and a high pass filter (>0.05Hz) were used in order to remove spurious offsets and low-frequency trends. The signals were cosine-tapered before using the FFT algorithm. Spectra obtained were smoothed with a 0.15 Hz running frequency box. Finally, all the spectral ratios obtained at each site, were averaged in order to get the mean spectral ratio in the NS and EW component of motion.

Table 4.3. *List of selected events recorded at each seismic station located in the geolithologic map; M_D = duration magnitude.*

#	yy-mm-dd	hh/mm	Lat. N	Long. E	Depth (Km)	M_D	CITT	FERL	GENI	LIBR	MINO	MUNI	POLI	PROC	UNIV	ZILI
1	1999/02/08	19:24	37.66	14.99	5	2.7	*							*	*	
2	1999/02/08	21:06	37.65	14.98	10	2.3	*									
3	1999/02/09	05:24	37.66	14.99	10	2.6	*							*		
4	1999/02/13	22:58	38.19	15.02	10	3.3	*								*	
5	1999/02/14	06:23	38.15	15.05	7	3.0	*							*	*	
6	1999/02/14	11:45	38.09	15.06	9	4.3	*							*	*	
7	1999/02/14	15:10	38.21	15.03	7	3.3	*								*	
8	1999/02/14	15:43	38.17	15.04	12	3.2	*									
9	1999/02/16	08:54	37.59	15.11	10	2.4	*							*	*	
10	1999/02/16	10:29	37.61	15.16	10	2.1	*							*	*	
11	1999/02/16	10:34	37.60	15.13	10	2.6	*								*	
12	1999/02/16	10:36	37.63	15.09	10	2.8	*									
14	1999/02/16	10:58	37.62	15.10	10	2.5	*								*	
16	1999/03/09	00:17	37.77	14.92	5	2.4								*		
17	1999/03/12	01:50	37.93	14.11	12	2.6								*		
18	1999/03/18	10:47	37.75	15.09	6	3.1								*		
19	1999/05/23	11:53	37.90	14.99	4	3.3	*	*					*		*	
20	1999/05/23	12:33	37.68	14.99	5	2.8	*						*			
21	1999/05/24	02:50	37.76	14.55	16	2.7	*									
22	1999/06/02	10:37	38.50	14.08	21	4.0	*	*					*		*	
23	1999/06/02	11:52	38.56	14.01	11	3.8	*									
24	1999/06/02	11:56	38.55	13.99	7	3.8	*									
25	1999/06/02	18:14	37.70	14.96	5	2.8	*									
26	1999/06/07	03:37	38.55	14.17	18	3.5	*									
27	1999/06/13	17:46	37.79	15.96	44	3.2	*	*					*		*	
28	1999/06/13	18:10	37.72	15.12	3	2.8	*						*			
29	1999/06/14	20:36	37.29	15.00	10	2.1	*						*			
30	1999/06/20	23:06	37.67	15.01	6	2.7	*						*		*	
31	1999/06/22	04:11	37.68	14.95	10	2.5	*						*			
32	1999/07/02	22:40	37.68	14.95	10	2.4	*									
33	1999/08/21	01:38	37.75	15.16	10	3.3	*	*					*			
34	1999/08/26	08:50	37.79	15.15	10	3.3	*						*			
35	1999/08/26	08:56	37.78	15.16	10	3.2	*						*			
36	1999/09/16	13:23	37.58	14.92	5	2.7	*						*			
37	1999/09/20	06:57	38.42	15.65	173	3.4	*	*					*			
38	1999/09/24	04:57	37.74	15.13	10	2.5	*									
39	1999/09/25	00:51	38.57	16.62	26	3.6	*									
40	1999/09/27	20:46	38.64	16.43	24	3.6	*									
41	1999/09/28	10:55	37.72	14.95	10	2.5	*									
42	1999/09/30	14:52	37.73	15.18	4	2.9	*						*			
43	1999/10/01	07:27	37.76	15.20	10	2.7	*						*			
44	1999/10/12	01:21	37.70	15.01	5	2.9	*						*			
45	1999/10/12	01:56	37.69	15.01	5	2.8	*						*		*	
46	1999/10/12	03:27	37.70	15.00	5	2.8	*						*		*	

#	yy-mm-dd	hh/mm	Lat. N	Long. E	Depth (Km)	M_D	CITT	FERL	GENI	LIBR	MINO	MUNI	POLI	PROC	UNIV	ZILI
47	1999/10/12	04:59	37.69	15.02	5	2.8	*						*			
48	1999/10/21	10:40	37.48	14.92	5	3.0									*	
49	1999/12/26	14:19	37.67	15.18	5	3.0	*								*	
50	1999/12/27	04:54	38.41	14.24	10	3.3	*								*	
51	2000/12/06	06:13	37.79	15.14	3	2.6			*	*	*					*
52	2000/12/27	20:57	37.55	14.95	5	3.2			*	*	*					*
53	2001/01/04	22:20	38.73	14.95	356	3.5			*	*					*	*
54	2001/01/08	14:33	37.78	14.93	5	3.0			*	*						
55	2001/01/09	02:51	37.67	15.13	5	3.3			*	*	*					*
56	2001/01/09	03:32	37.67	15.13	5	2.7			*	*	*					*
57	2001/01/09	04:31	37.66	15.17	5	2.8			*	*	*					*
58	2001/01/23	16:55	37.13	15.33	15	3.3			*	*	*				*	*
59	2001/01/26	08:20	37.75	14.98	10	2.8			*	*					*	*
60	2001/01/26	08:20	37.73	14.99	5	3.2			*	*					*	*
61	2001/01/28	14:40	37.53	15.28	10	2.3			*	*					*	*
62	2001/02/10	17:46	37.16	14.99	12	2.1										*
63	2001/02/24	01:23	37.72	14.98	5	2.8			*	*					*	*
64	2001/03/07	17:20	37.89	14.87	27	2.9										*
65	2001/03/27	18:12	37.78	15.14	5	2.5										*
66	2001/03/30	18:40	37.69	15.06	5	2.8			*						*	
67	2001/04/06	07:52	37.74	15.12	5	2.6									*	
68	2001/04/18	17:35	37.73	15.01	5	3.0									*	
69	2001/04/22	13:56	37.70	15.02	5	3.5									*	
70	2001/04/23	00:36	37.71	15.01	5	2.9									*	
71	2001/04/23	22:26	37.73	14.99	5	2.4			*							
72	2001/04/24	04:03	37.71	15.02	5	2.8			*						*	
73	2001/04/25	19:33	37.72	15.10	2	3.0			*						*	*
74	2001/04/27	21:08	37.71	15.02	7	2.4			*						*	
75	2001/04/27	21:09	37.70	15.10	5	3.1			*						*	*
76	2001/04/29	20:00	37.77	14.96	11	3.1			*						*	*
77	2001/05/03	21:41	37.59	15.03	5	3.3			*		*				*	
78	2001/05/03	21:46	37.62	15.01	10	2.8			*		*				*	
79	2001/05/04	04:42	37.61	15.11	10	3.0			*		*				*	
80	2001/05/07	20:07	37.79	14.98	8	2.4			*							
81	2001/05/08	03:52	38.14	14.91	9	3.3			*							
82	2001/05/19	16:15	37.76	14.89	14	3.0			*		*				*	
83	2001/05/19	20:47	37.74	14.92	9	2.9			*		*				*	
84	2001/05/20	20:08	37.74	14.92	5	2.9			*							
85	2001/05/26	06:02	37.45	16.05	13	3.6			*		*				*	
86	2001/06/09	17:50	37.73	15.20	5	2.9			*							
87	2001/06/21	01:26	37.75	14.72	9	2.6			*						*	
88	2001/07/08	06:29	38.52	16.79	48	3.3			*							
89	2001/07/12	22:45	37.62	15.17	5	2.7			*						*	
90	2001/07/13	00:09	37.77	15.05	5	2.8			*							
91	2001/07/13	01:30	37.67	15.09	5	2.5			*						*	
92	2001/07/13	01:36	37.64	15.13	5	2.7			*						*	
93	2001/07/13	01:39	37.65	15.03	5	2.4			*							

#	yy-mm-dd	hh/mm	Lat. N	Long. E	Depth (Km)	M_D	CITT	FERL	GENI	LIBR	MINO	MUNI	POLI	PROC	UNIV	ZILI
94	2001/07/13	02:51	37.51	15.17	5	2.5			*							
95	2001/07/13	03:12	37.65	15.11	5	4.0			*						*	
96	2001/07/13	03:15	37.67	15.01	5	3.9			*						*	
97	2001/07/13	03:24	37.66	15.04	5	2.5			*							
98	2001/07/13	04:34	37.66	15.09	5	2.8			*						*	
99	2001/07/13	04:46	37.68	15.06	5	2.9			*						*	
100	2001/07/13	04:49	37.66	15.11	5	2.7			*						*	
101	2001/07/13	04:56	37.68	15.06	5	3.3			*						*	
102	2001/07/13	05:11	37.66	15.06	5	3.2			*						*	
103	2001/07/13	05:25	37.69	15.13	5	3.0			*						*	
104	2001/07/13	05:49	37.64	15.08	5	2.6			*							
105	2001/07/13	11:55	37.66	15.09	5	2.6			*							
106	2001/07/13	12:33	37.66	15.11	5	3.0			*						*	
107	2001/07/14	01:20	37.68	15.05	5	2.6			*							
108	2001/07/14	03:04	37.65	15.10	5	3.0			*						*	
109	2001/07/14	04:19	37.67	14.99	5	3.0			*						*	
110	2001/07/14	04:41	37.65	15.00	5	2.7			*							
111	2001/07/14	04:47	37.64	15.01	5	2.9			*						*	
112	2001/07/14	05:53	37.63	15.02	5	3.3			*						*	
113	2001/07/14	07:38	37.66	15.09	5	3.1			*						*	
114	2001/07/14	08:54	37.65	15.15	5	2.8			*							
115	2001/07/14	08:57	37.63	15.09	5	2.5			*							
116	2001/07/14	10:42	37.52	15.04	5	2.9			*						*	
117	2001/07/14	13:36	37.67	15.03	5	3.0			*						*	
118	2001/07/14	16:52	37.67	15.10	5	2.7			*						*	
119	2001/07/14	18:50	37.64	14.98	5	2.7			*						*	
120	2001/07/15	00:09	37.84	15.01	5	2.7			*						*	
121	2001/07/15	07:45	37.69	15.05	5	3.6			*						*	
122	2001/07/15	08:06	37.72	15.07	5	2.9			*						*	
123	2001/07/15	09:00	37.70	14.93	5	3.3			*						*	
124	2001/07/15	13:25	37.84	15.15	4	3.1			*						*	
125	2001/07/15	15:02	37.65	15.05	5	2.9			*						*	
126	2001/07/15	23:38	37.68	15.12	5	2.5			*							
127	2001/07/16	00:37	37.83	14.98	5	2.8			*						*	
128	2001/07/16	02:44	37.68	15.12	5	2.9			*						*	
129	2001/07/16	04:00	37.67	15.04	5	2.8			*						*	
130	2001/07/16	07:27	37.71	15.08	5	2.8			*							
131	2001/07/16	09:24	37.76	15.09	5	3.2			*							
132	2001/07/16	15:08	37.47	15.12	10	2.9			*							
133	2001/07/16	17:04	37.68	15.14	5	3.4			*							
134	2001/07/16	20:27	37.67	15.05	5	3.2			*							
135	2001/07/16	23:19	37.67	15.03	5	3.3			*							
136	2001/07/17	00:59	37.63	15.13	5	2.8			*							
137	2001/07/17	02:39	37.64	15.09	5	2.5			*							
138	2001/07/17	05:33	37.67	15.05	5	3.5			*							
139	2001/07/17	08:25	37.54	14.94	5	2.6			*							
140	2001/07/17	10:08	37.89	15.00	5	2.6			*							

#	yy-mm-dd	hh/mm	Lat. N	Long. E	Depth (Km)	M_D	CITT	FERL	GENI	LIBR	MINO	MUNI	POLI	PROC	UNIV	ZILI
141	2001/07/17	13:46	37.73	15.17	5	2.6			*							
142	2001/07/18	20:00	37.71	14.92	5	2.7			*							
143	2001/07/18	21:38	37.67	14.88	5	2.7			*							
144	2001/07/22	12:32	37.63	15.11	5	3.2			*						*	
145	2001/07/23	20:42	37.61	15.04	10	2.4			*						*	
146	2001/07/31	18:47	38.49	15.16	6	3.5			*						*	
147	2001/08/17	03:15	38.34	14.73	232	3.1									*	
148	2001/08/20	22:44	37.67	15.13	5	3.4									*	
149	2001/09/14	18:53	37.52	16.11	17	3.4						*			*	
150	2001/10/05	13:29	37.24	15.8	10	3									*	
151	2001/10/15	20:44	37.58	15.17	5	2.6									*	
152	2001/10/18	11:02	39.26	16.28	5	3.6									*	
153	2001/10/18	18:08	38.49	15.13	246	3.7									*	
154	2001/10/26	05:38	37.59	15.18	5	2.7									*	
155	2001/10/28	09:03	37.59	15.17	5	3.7						*			*	
156	2001/10/28	11:00	37.62	15.19	10	2.4									*	
157	2001/10/28	15:05	37.61	15.14	5	3.3						*			*	
158	2001/10/31	22:06	37.61	15.18	5	2.5									*	
159	2001/10/31	23:44	37.62	15.14	5	2.5									*	
160	2001/11/01	02:46	37.74	14.66	21	2.5										
161	2001/11/03	14:53	37.75	14.73	6	2.7										
162	2001/11/03	18:29	37.76	14.76	12	2.6										
163	2001/11/05	10:17	37.12	14.77	19	2.7										*
164	2001/11/25	18:26	37.81	13.95	7	3.3										*
165	2001/11/25	19:33	37.76	13.98	1	4						*				*
166	2001/11/28	10:43	37.79	13.95	5	3.5										*
167	2001/11/29	16:36	37.92	14.9	27	2.4										*
168	2001/12/02	04:08	37.41	16.53	14	3.2						*				
169	2001/12/07	04:05	37.2	16.71	100	2.8									*	
170	2001/12/12	11:06	37.6	15.16	10	2.5									*	
171	2001/12/22	10:42	37.85	14.72	26	2.6									*	
172	2001/12/26	08:43	37.78	16.11	49	2.9									*	
Total number of seismic event for each stations							44	5	89	12	12	5	19	9	90	22

The analysis of the modifications to which the seismic input undergoes, when it propagates from the bedrock to the surface through the shallower deposits, was performed, in the frequency domain, using the SSR and HVSR approaches. The SSR technique (Borcherdt, 1970) consists in computing the Fourier's spectral ratio of the same seismic waves simultaneously recorded by the horizontal components of two seismic stations, one of which is located on a bedrock outcrop. The earthquake's HVSR, or receiver function technique, do not need a reference station and consists in the computation of the spectral ratio between horizontal and vertical components of motion recorded at one seismic station only (Lermo

and Chavez-Garcia, 1993). The correct use of the SSR technique implies that the distance (*d*) between test and reference sites has to be significantly smaller than the epicentral distance. Steidl *et al.* (1996) demonstrated that a distance *d* of about 20 km can be considered acceptable, providing that regional events are taken into account. In this study, all seismic stations have *d* less than 5 km from the reference site, except station FERL ($d \approx 9$Km). However, only regional events, having their source located at about 150–200 km from Catania, were used in evaluating the standard spectral ratio at FERL. The station UNIV, which was installed on a 30 m thick compact lava rock overlaying the marly clays formation that can be considered as the bedrock in the Catania area, was selected as reference site (**Fig. 4.8**). According to Steidl *et al.* (1996), the features of the reference site were tested performing the Fourier spectral analysis of the horizontal components as well as the HVSR spectral ratio. **Figure 8a** shows that in the frequency band 0.5–10 Hz the Fourier spectrum of a sample earthquake is free from both spectral holes and peaks, and the average HVSR, obtained by

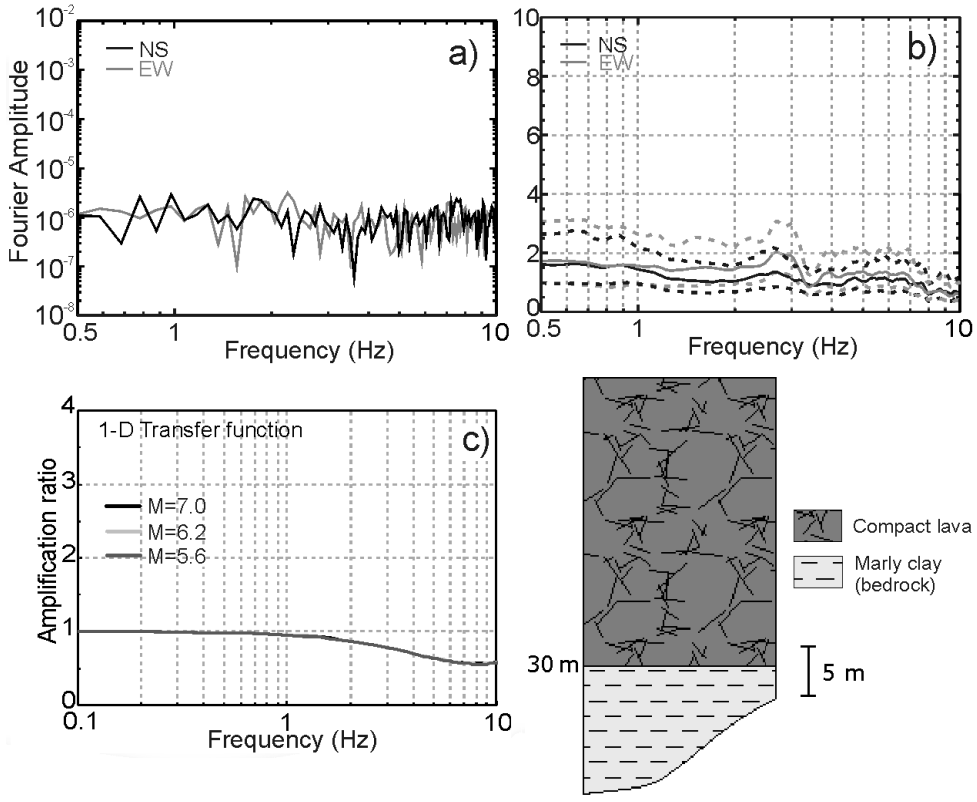

Fig. 4.8. *Litho-stratigraphic sequence at the reference station UNIV with an example of Fourier spectrum (a), HVSR (b) and theoretical transfer function (c).*

91 seismic events, shows no significant amplification (**Fig. 4.8b**). A further validation of this choice comes out from the average of all the theoretical transfer functions obtained through the EERA numerical code for all considered scenarios (**Fig. 4.8c**). According to these results, only peaks having amplitude greater than 3 units in the HVSRs were considered as significant for local seismic effects.

4.4. Results and discussion

T he local seismic response in Catania was evaluated through the EERA software using several borehole data although their distribution do not spreads homogeneously over the study area. The obtained maps show the contouring of PGA and Sa_g at the 5% critical damping, for the periods 0.2, 0.5 and 1.0 sec, values (**Figures 4.4** to **4.7**) that are in good agreement with results of various authors (Langer *et al.*, 1999; Priolo, 1999; Zollo *et al.*, 1999; Laurenzano *et al.*, 2004) which evaluated the local response in Catania area through numerical approaches based on synthetic seismic inputs.

The PGA distribution obtained for destructive scenario shows values ranging between 0.16-0.50 g (**Fig. 4.4**) whereas, PGA values ranging in the intervals 0.12-0.44 g and 0.02-0.10 g, are observed for strong and moderate scenarios, respectively (**Figs. 4.5** and **4.6**). It is worth noting that the site-to-source distance strongly affects the PGA values. The destructive and the strong reference shocks used in the present study have epicentral distance of about 15 Km and 12 Km, respectively, from downtown Catania (see **Tab. 4.1**). This implies that the obtained values of PGA are sometimes comparable (**Fig. 4.9**), although the difference of magnitude is high (M_w=7.0 for the destructive event and M_w=6.2 for the strong one). However, the accelerogram of the 1990 earthquake, recorded on the Catania alluvial plane, showed a PGA of 0.21 g (Working group ITACA, 2008). Such a value, although is far greater than that obtained through EERA 1-D numerical modelling (0.06-0.10 g), could be explained as linked to the existence of 2D or 3D site response effects connected to the complexity in the alluvial deposits. Although instrumental records of seismic events having a magnitude

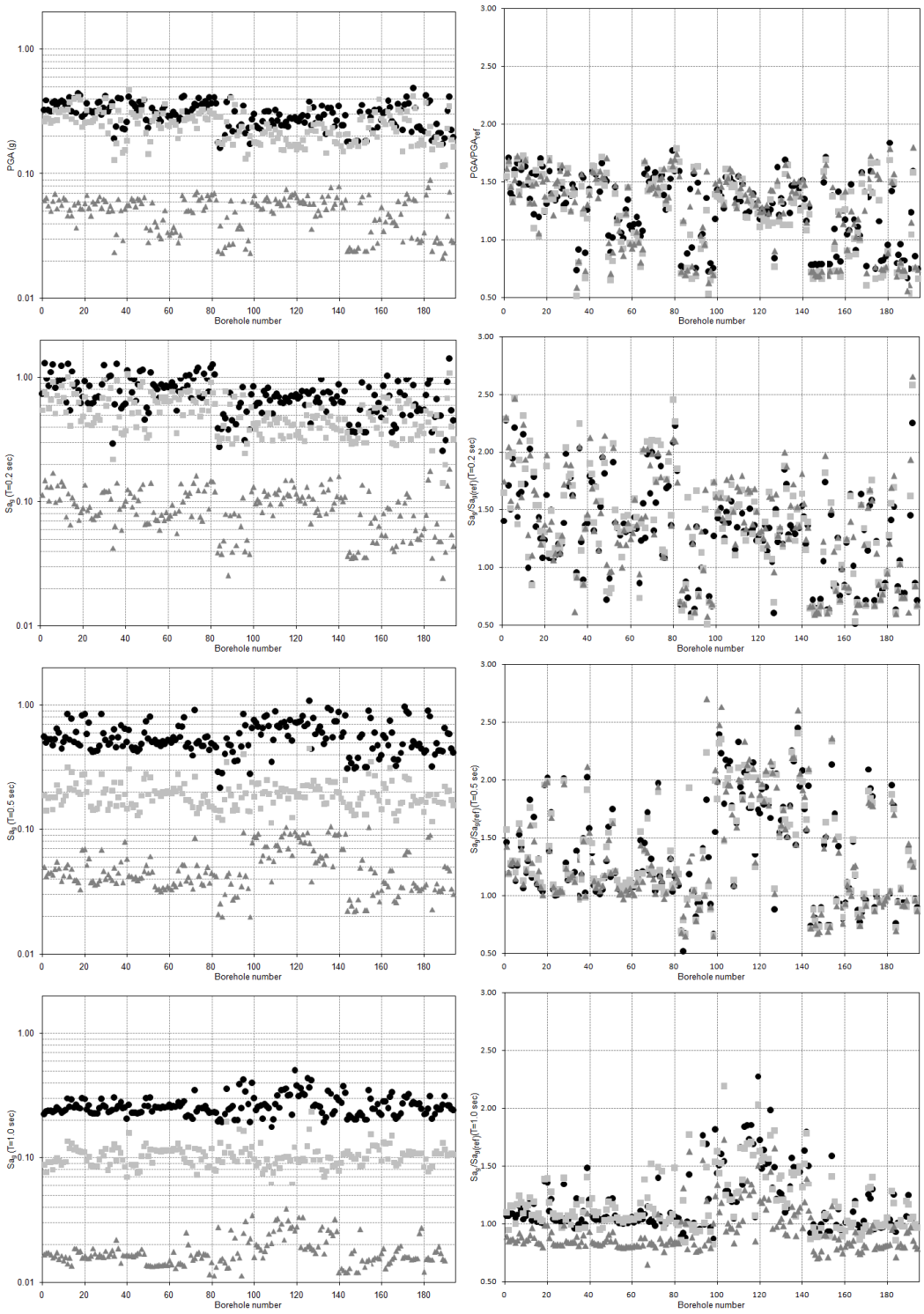

Fig. 4.9. *PGA values and Sag ordinates at 0.2 sec, 0.5 sec and 1.0 sec period, 5% damping (left column). PGA to PGAref ratio and Sag to Sag(ref) (right column) obtained at each borehole site; black circles, gray squares and light gray triangles, respectively refers to destructive, strong and moderate scenario earthquakes.*

comparable with that of 1818 and 1693 shocks are not available, the above mentioned PGA estimates suggest that, in the Catania area, the shaking level might be greater than that obtained in a theoretical approach.

Peak spectral acceleration, for considered periods, varies from 1.37 to 0.17 g for destructive scenarios (**Fig. 4.4**), 1.10 to 0.07 g for strong scenarios (**Fig. 4.5**) and 0.20 to 0.01 g for moderate scenarios (**Fig. 4.6**). Spectral acceleration response values appear quite dependent on the frequency content of the scenario earthquakes. As a matter of fact, they decrease more rapidly with increasing period (from 0.2 to 1.0 sec, see left panels in **Fig. 4.9**), when strong and moderate earthquake scenarios are taken into account, with respect to the destructive scenario which produce larger ground motions and longer periods. Moreover the observed amplification ratio (right panels in **Fig. 4.9**) increases as the magnitude decreases, especially in soft soils. This might be explained in terms of non-linear behavior connected to the soil typology, the magnitude of the earthquake and the different source-to-site distances of selected scenarios (**Fig. 4.10**).

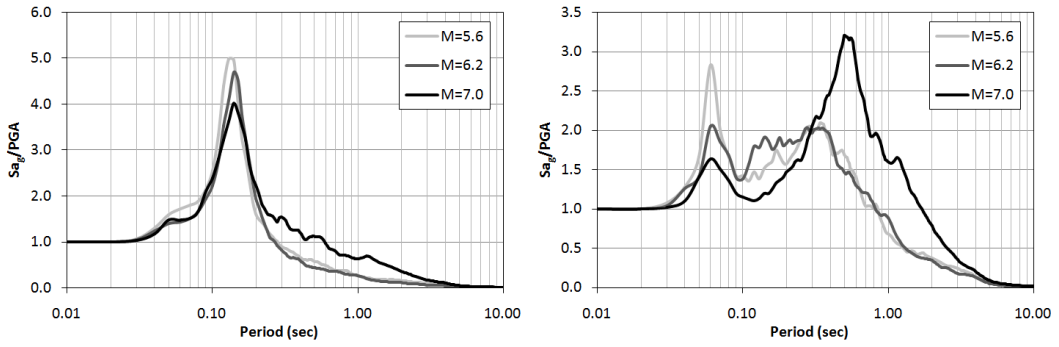

Fig. 4.10. *Normalized response spectra for each considered scenario that show non-linearity and magnitude dependence.*

It is interesting to observe that amplification factor calculated for PGA and Sa_g (**Fig. 4.9**), for the periods 0.2, 0.5 and 1.0 sec, never exceeds 3. The amplification factor at each site mainly depends on the impedance ratio (*I*). In the Catania area, frequently the impedance ratio is relatively low, as in the case of the soil deposits overlaying the marly-clay bedrock ($I \approx$ 2-3). In a few cases, when the soil deposits cover the compact lava, *I* exceed 2-3 up to 5-6.

Despite such considerations, it is quite evident that the accelerations coming out from the three scenario maps spread in a similar way throughout the study area and show a quite comparable distribution of both maximum and minimum values.

Preliminary to the description of PGA and Sa_g distribution, the information coming out from both surface geology and available boreholes has to be summarized. Five ideal stratigraphies (**Fig. 4.11a**) describing the most widespread sequences of lithotypes present in the Catania urban area, were therefore drawn. **Figure 4.11b** shows the theoretical transfer functions obtained, through the EERA numerical code, for such ideal stratigraphies.

In the southern part of the urban area, the clayey basement is mostly covered by sandy and gravelly sediments together with alluvial deposits (A and B in **Figs. 4.1** and **4.11a**). The theoretical transfer functions (A and B in **Fig. 4.11b**) show fundamental frequencies in the range 1.0-3.0 and 1.5-4.5 Hz that appear linked to the presence of soft sediments laying on the clayey basement. The not pronounced amplification peaks observed, could be related to the low impedance ratio between such sediments and the clayey basement underneath. However, the PGA values in this part of the area, are quite pronounced in all the three scenarios maps (0.05-0.10 g moderate, 0.20-0.36 g strong and 0.24-0.48 g destructive shocks) especially where terraced alluvial deposits outcrop. The spectral amplitude observed in this area are among the highest values for the destructive (0.57-1.53 g for T=0.2 sec, 0.44-1.16 g for T=0.5 sec and 0.25-0.50 g for T=1.0 sec) and moderate scenarios (0.08-0.19 g for T=0.2 sec, 0.056-0.12 g for T=0.5 sec and 0.02-0.04 g for T=1.0 sec), whereas they are the lowest values for the strong scenario (0.27-0.63 g for T=0.2 sec, 0.15-0.28 g for T=0.5 sec and 0.07-0.13 g for T=1.0 sec). The distribution of Sa_g in the southern part of the urban area, therefore, sets into evidence the important role played, besides the lithologic setting, also by the different azimuth and the source-to-site distances (see inset map in **Fig. 4.1** and **Tab. 4.1**).

In the northern part of Catania, the basement is mostly covered by volcanic soils having thickness up to 50 m (C in Figs. **4.1** and **4.11a**). Field surveys and

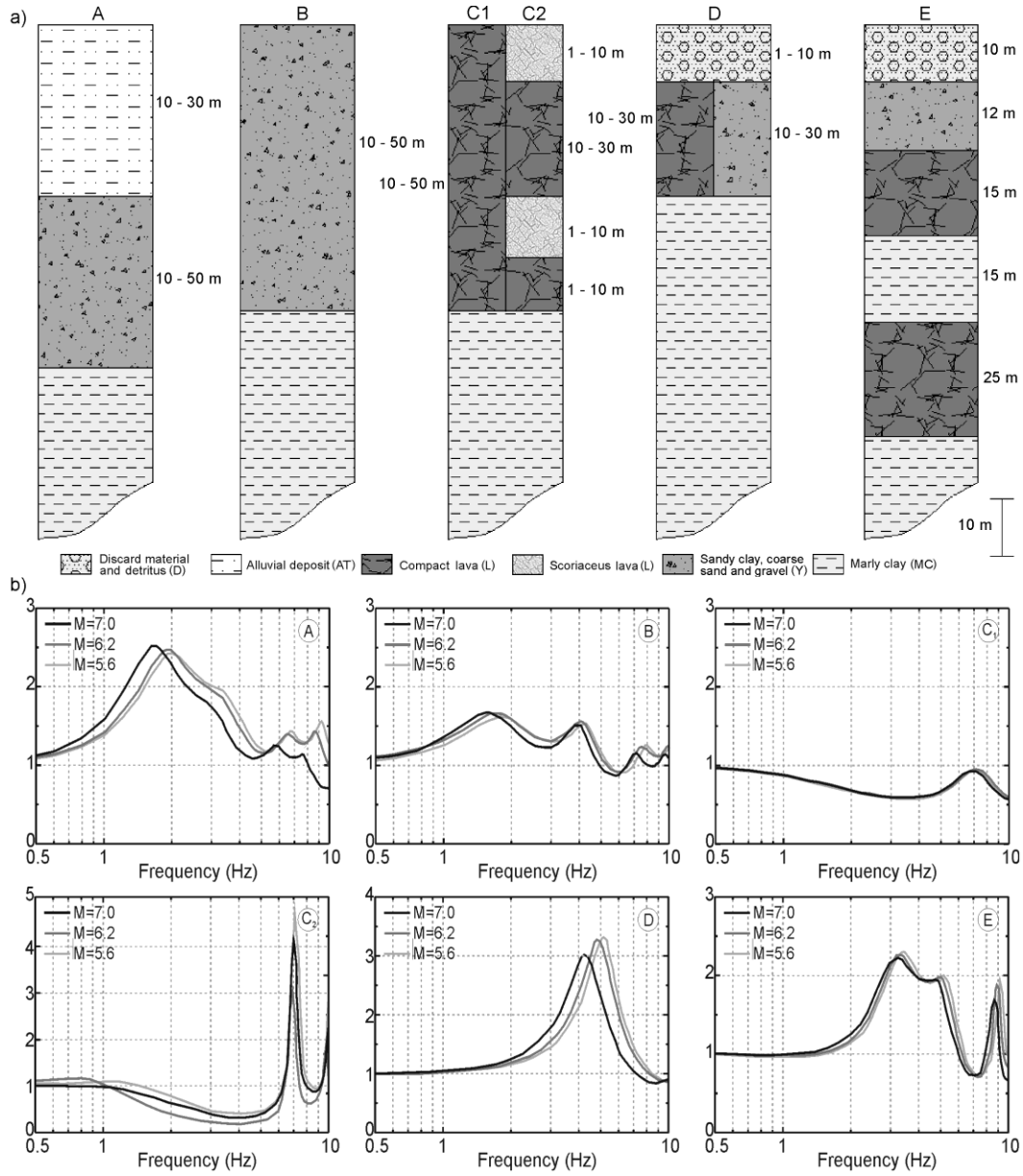

Fig. 4.11. *a) Ideal stratigraphies describing the main lithotype sequences characterizing the study area; in brackets are reported the same acronyms quoted in Table 2. b) Theoretical transfer functions, for each considered scenario, obtained taking into account the ideal stratigraphic sequence.*

borehole data (Monaco *et al.*, 2000), as well as both geotechnical (Faccioli, 1997) and geophysical evidences (Lombardo *et al.*, 2001) point out that lava flows are not homogeneous and usually massive lavas alternate with several meters of fractured and scoriaceous levels and pyroclastic deposits (see C1 and C2 in **Fig.**

4.11a) This implies some variability in the resulting theoretical transfer functions (**Fig. 4.11b**), so that, even if the lava formations overlaying the clayey basement generally do not show significant amplifications (C1 in **Fig. 4.11b**), the presence of fractured and scoriaceous lavas can cause the amplification peaks observed at about 6 Hz in the transfer function C2 in **Fig. 4.11b**. As a consequence of this, the lowest PGA values observed in the three maps (0.02-0.04 g, 0.12-0.24 g and 0.16-0.28 g, for the moderate, strong and destructive scenarios, respectively), account for the presence of quite compact lavas, whereas the relatively higher acceleration values (0.04 g, 0.24 g and 0.28 g) observed in some spots of the northern area (**Figs. 4.4** to **4.6**), can be referred to significant thickness levels of highly fractured and scoriaceous lavas. A similar behavior is observed for the spectral acceleration with the lowest values for destructive (0.25-0.57 g for T=0.2 sec, 0.20-0.56 g for T=0.5 sec and 0.17-0.29 g for T=1.0 sec), strong (0.15-0.51 g for T=0.2 sec, 0.10-0.24 g for T=0.5 sec and 0.07-0.13 g for T=1.0 sec) and moderate scenarios (0.025-0.065 g for T=0.2 sec, 0.020-0.044 g for T=0.5 sec and 0.010-0.017 g for T=1.0 sec) The lithologic setting, in this part of the study area, seems to have a prevailing role with respect to the different azimuth and the source-to-site distances.

In the historic centre of the city, discard material and either gravelly sands or volcanic product overlay the clayey basement (D and E in **Figs. 4.1** and 4.**11a**). The existence of discard materials and ruins, having thickness up to 12 metres, above either coarse sand deposits or scoriaceous lava levels overlaying the basement, can account for the pronounced amplification peaks (D in **Fig. 4.11b**) at frequencies between 4.0 and 5.0 Hz. In some cases the existence of alternating soft and rigid lithotypes (see E in **Fig. 4.11a**) was proved by borehole data and this may produce the slightly reduced amplification peaks observed in the associated theoretical transfer function. In downtown Catania, however, the highest values of peak ground accelerations (0.05–0.07 g, 0.32-0.40 g and 0.36-0.50 g) are observed for the three considered scenarios (**Figs. 4.4** to **4.6**). Similarly, the spectral accelerations obtained in Catania downtown are higher than the ones observed in all the study area, especially for 0.2 and 0.5 sec. It is worth

nothing that most of the masonry buildings erected in downtown consist of 2-4 stories so that their fundamental period is in the range 0.2-0.5 sec (Grasso *et al.*, 2004). Consequently, they might suffer significant damage especially when destructive and strong scenario earthquakes are considered.

In order to summarize previous results and interpret them in a geological sense, the maps of **Figure 4.7** were drawn. Such maps set into evidence a strong relationship between the spreading of the log-normal mean deviations of increments/decrements of the above mentioned values and the near surface geology. The highest increments are observed in the historic centre and in some spots where discard materials and detritus outcrop, as well as in some sedimentary deposits prevailing to the south of the study area. Medium and low increments prevail in the sectors not covered by lava flows. On the other hand, higher decrements are typical of areas where massive lavas overlay the basement (see **Fig. 4.7**). Hence, major increments of peak ground acceleration and spectral acceleration are linked to sites where detritus, loose sediments and/or alluvial deposits outcrop. Conversely, decrements and consequently low potential damage, attain to sites where the outcropping compact lava flows directly overlay the basement.

In order to check and validate the reliability of the results so far described, a comparison was made with experimental findings from earthquake recordings. The use of spectral ratio techniques (SSR and HVSR) allowed a trustworthy estimate of fundamental frequencies in the selected sites, although the inferred spectral amplitudes do not give univocal clues. The spectral ratio amplitudes from the HVSRs are indeed often lower than the SSRs. According to Fäh *et al.*, (2001) this finding is a consequence of the moderate velocity contrast between the bedrock and the overlaying soft sediments, as observed in this area by Lombardo *et al.*, (2001) from ambient noise measurements. Moreover, the vertical component could be strongly affected by local amplification effects when pronounced heterogeneities characterize the local geology (Riepl *et al.*, 1998; Raptakis *et al.*, 1998 and 2000; Triantafyllidis *et al.*, 1999; Bindi *et al.*, 2009).

In **Figure 4.12a** the litho-stratigraphic sequences of the sites where the seismic stations were located, are shown. These characteristics were used as input data in EERA code for the theoretical transfer function evaluation. The comparison between the experimental results, obtained through spectral ratios, and the theoretical 1D transfer function provided by the EERA code are shown in **Figure 4.12b**.

The seismic stations FERL, LIBR and ZILI are located in the southern part of the area, where alluvial deposits and gravelly sands are present. In the three stations, both experimental spectral ratios and the 1D modelling approach set into evidence the existence of amplification effects in the frequency range 1.5-5.0 Hz, therefore confirming the findings previously described for the southern part of Catania urban area. It is interesting to point out that differences between SSR and HVSR are mainly observed at FERL. Such station is located in the Catania alluvial plain which, as demonstrated by field and borehole data (Accordi and Francaviglia, 1960; AGIP, 1977; Carbone *et al*., 2008) is formed by highly heterogeneous sediments characterized by pronounced lateral discontinuities. These irregularities can affect the amplitude of the vertical component of motion, because of the presence of diffracted Rayleigh waves (Field and Jacob, 1995; Raptakis *et al.*, 1998 and 2000), thus causing differences between the SSRs and HVSRs. Moreover, the spectral ratios at both LIBR and ZILI show amplifications gradually increasing in a wide frequency range. Such effect could be interpreted as a consequence of the already mentioned low velocity contrast that characterizes the sedimentary sequence. A strong impedance contrast, between hard and soft soils is indeed needed to obtain pronounced fundamental frequencies either when earthquakes or ambient noise (Fäh *et al.*, 2001) are used as input signals.

The results of the experimental approach at the stations CITT and GENI, located on the central and northern part of the town, show moderate amplifications in the range 1.5 – 4.0 Hz. These values, which are in quite good agreement with the ones of the theoretical transfer function, could be interpreted as amplification effects linked to soft soils, having thickness of about 15-20 m. Such amplifications appear in the "sedimentary windows" remaining among the

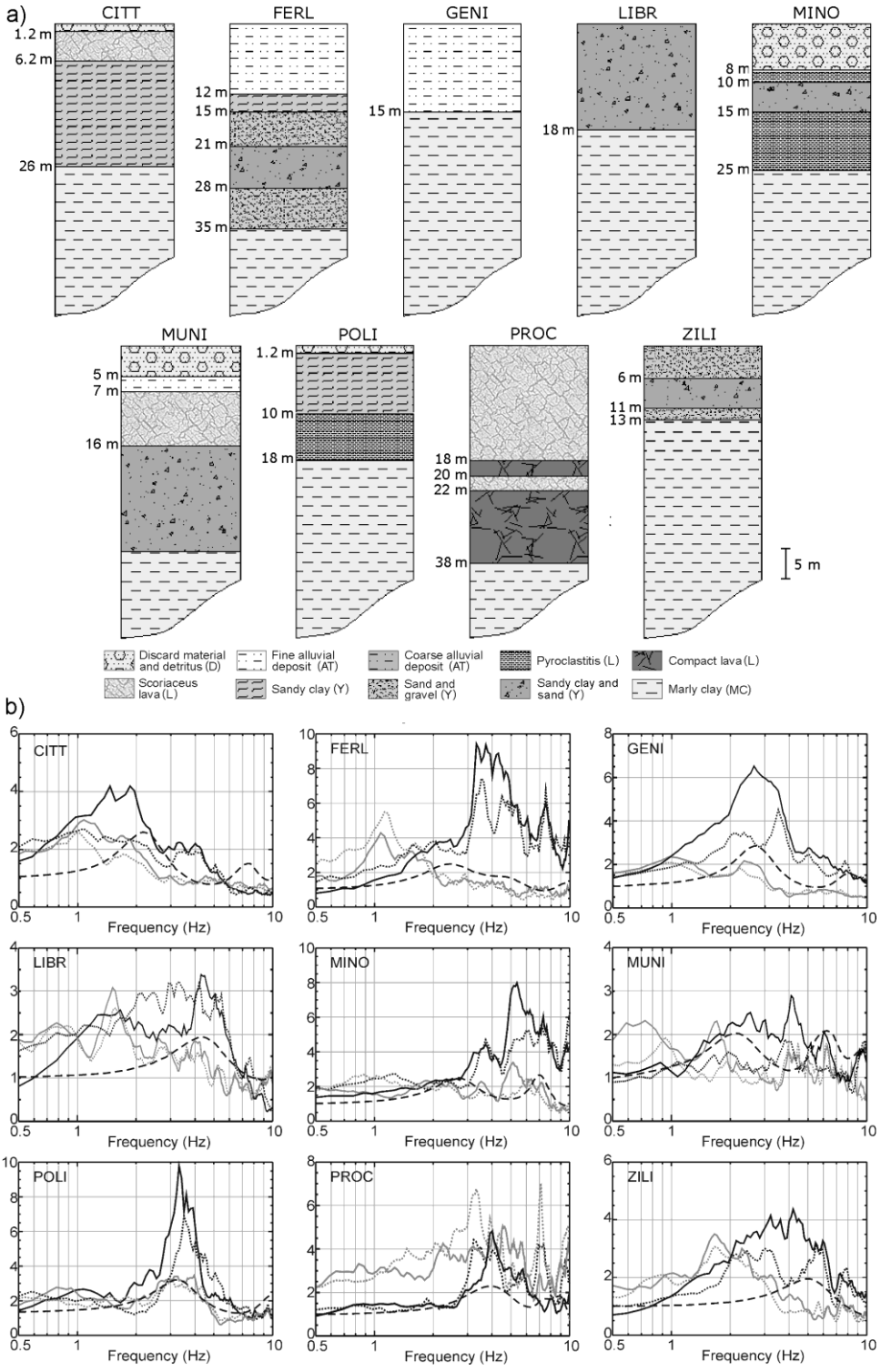

Fig. 4.12. *a) Litho-stratigraphic features of the recording station site; in brackets are reported the same acronyms quoted in Table 2. b)..Experimental and theoretical transfer functions at each seismic station; solid and dotted black lines refer to the N-S and E-W components of motion of the SSR respectively; solid and dotted grey lines refer to the N-S and E-W components of motion of the HVSR respectively; dashed black line refers to the 1D theoretical transfer function.*

lava flows covering the clayey basement (GENI) as well as when a scoriaceous component prevails in the lava flows (CITT). On the other hand, when the basaltic lavas are somewhat compact and directly lay over the bedrock, they do not produce amplification effects as observed for the reference site UNIV (**Fig. 4.8**).

As far as the other recording sites are concerned, they are located either on spots of soft sediments and pyroclastics surrounded by lava flows (POLI, MINO), or they are sited on fairly fractured and scoriaceous basaltic lavas (PROC) sometimes covered by coarse detritus and sand (MUNI). Therefore, quite pronounced amplification peaks are observed. At POLI and MINO stations, peaks in the ranges 2.5-5.0 Hz and 3.0-8.0 Hz, respectively, are shown in both SSR and HVSR. Such ranges of values, observed in the theoretical transfer function too, are more pronounced in the SSR rather than in the HVSR. It has to be specified that both stations are located almost at the top of a small sedimentary hill surrounded by lava flows. This topographic setting could be responsible for the pronounced amplification effects, therefore, in my opinion, further investigations are needed to corroborate the hypothesis of such effects in the ground motion.

A good match between the experimental and theoretical approach is also found at station PROC. Here, spectral peaks in the 2.5-7.0 Hz frequency band occur. This, as the results of 1D modelling indicate, can be interpreted as linked to the presence of alternating massive and scoriaceous/fractured lavas. A similarly good match is found between the experimental and theoretical transfer functions obtained at MUNI, where moderate amplification peaks in the range 2.0-6.0 Hz, related to about 35 m thick alternating levels of soft materials and fractured lavas, are observed.

Chapter V

Seismic properties of lithotypes cropping out in the Siracusa city, Italy

5.1. Issues of the chapter

In recent years, a number of methodologies aims at evaluating the shear wave velocity profile, down to about thirty meters of thickness, have been proposed and tested. Not invasive geophysical prospecting techniques, based on surface wave dispersion properties in vertically heterogeneous media, were largely adopted. As well known, the surface waves velocity varies as a function of frequency and wavelength, therefore controlling their penetration depth (Aki and Richards, 2002). This dispersion property can be used to derive Vs versus depth through inversion processes (Herrmann, 1994; Wathelet *et al.*, 2005).

The spectral analysis of surface waves (SASW), introduced by Nazarian and Stokoe (1984), is amongst the most used methods, together with the MASW technique (*Multichannel Analysis of Surface Waves*, proposed by Park *et al.* (1999). More recently, the passive source method ReMi (*Refraction Microtremors*), proposed by Louie (2001), combines the most effective components of the SASW and MASW methods with microtremor techniques.

A quick estimate of the surface geology effects on seismic motion is provided by the horizontal to vertical noise spectral ratio technique (HVNR). This technique firstly introduced by Nogoshi and Igarashi (1971), was put into practice by Nakamura (1989) and became in recent years widely used since it provides a reliable estimate of the fundamental frequency of soft soil deposits (Lermo and Chavez-Garcia 1993; Gitterman *et al.*, 1996; Seekins *et al.*, 1996). Although the scientific community has questioned the existence of simple direct correlation between HVNR amplitude values and the actual site amplification (see Mucciarelli, 1998; Al Yuncha *et al.*, 2000; Maresca *et al.*, 2003; Rodriguez and

Midorikawa, 2002), such method is widely used since it significantly reduces field data acquisition time and costs. The basic hypothesis for using ambient noise is that the resonance of a soft layer corresponds to the fundamental mode of Rayleigh waves, which is associated with an inversion of the direction of Rayleigh waves rotation (Nogoshi and Igarashi, 1971; Lachet and Bard, 1994). The reliability of such an approach has been asserted by many authors (e.g. Lermo and Chávez-García, 1993), who have stressed its significant stability in local seismic response estimates. It is commonly accepted that, although the single components of ambient noise can show large spectral variations as a function of natural and cultural disturbances, the HVNR spectral ratio tends to remain invariant, therefore preserving the fundamental frequency peak (Cara *et al.*, 2003).

The damage to buildings are tightly linked, besides their vulnerability, to both the characteristics of the maximum acceleration and frequency of the ground motion, as well as to the features of surface geology. From this point of view, the geophysical and geotechnical characterization of the soil conditions, down to the bedrock, is very important in order to identify the site effects, in term of fundamental frequencies, for a correct planning of earthquake resistant structures.

In this study the dynamic properties of main lithotypes outcropping in the Siracusa area and the features of the local seismic response were investigated. The town of Siracusa is located in the south-eastern coast of Sicily and its downtown, called Ortigia, forms a low hill, shaped as a peninsula surrounded by the sea. Two non-invasive seismic prospecting techniques (MASW and ReMi), using the vertical component of surface waves, were applied in four sites, selected among the mostly outcropping lithotypes, to estimate the dispersion curves and the shear-wave velocity profiles through the neighborhood algorithm (Sambridge, 1999; Wathelet *et al.*, 2005; Wathelet, 2008). Moreover, the site response was evaluated in thirty-two sites, using ambient noise measurements processed through spectral ratio techniques (HVNR).

5.2. Geologic Setting

In the study area the substratum outlines a horst structure formed by a Meso-Cenozoic carbonate sequence with interbedded volcanics (Grasso and Lentini, 1982) cropping out in the northern part of Siracusa (**Fig. 5.1**). The Cretaceous volcanics, having thickness up to 500 m, locally represent the deepest term (Tortorici, 2000) which is unconformably covered by sub-horizontal carbonate sequences that stand for the lithotypes more frequently cropping out in the Siracusa town. The above mentioned carbonate sequence is distinguished in two main units, having similar geotechnical features, known in the literature as Mt. Climiti and Mt. Carruba formations. The former, having thickness ranging between 20 and 80 m, lays on the Cretaceous volcanics and consists of compact and well cemented calcarenites, the latter, with an average thickness of about 20 m, is characterized by alternating calcarenites and marlstones. In some sites the carbonate sequence is directly overlaid by sub-horizontal poorly consolidated calcarenites up to 20 m thick (Tortorici, 2000), whereas, in the southern part of the study area, sands and sandy clays, up to 20 m thick, overlay the Meso-Cenozoic carbonate bedrock. Finally, alluvial deposits fill out the graben of the "Pantanelli" plain (see **Fig. 5.1**) whilst detritus, having thickness of about 6-8 m due to anthropic activity and historical ruins, is mainly outcropping in the downtown Ortigia area.

5.3. Methodology

The dynamic properties of the main lithotypes outcropping in the study area were evaluated through the non-invasive techniques MASW and ReMi. According to suggestions of Park *et al.* (2005) a combined use of both methods has been made to compare and check the obtained results trying to overcome the limitations of each approach.

The MASW technique needs a suitable location of the seismic source as well as a correct choice of transducers spacing in order to define a reliable wave-length range in the measurements. The dispersion curves are always obtained in a relatively high frequency range (5–50 Hz), that implies a maximum depth of

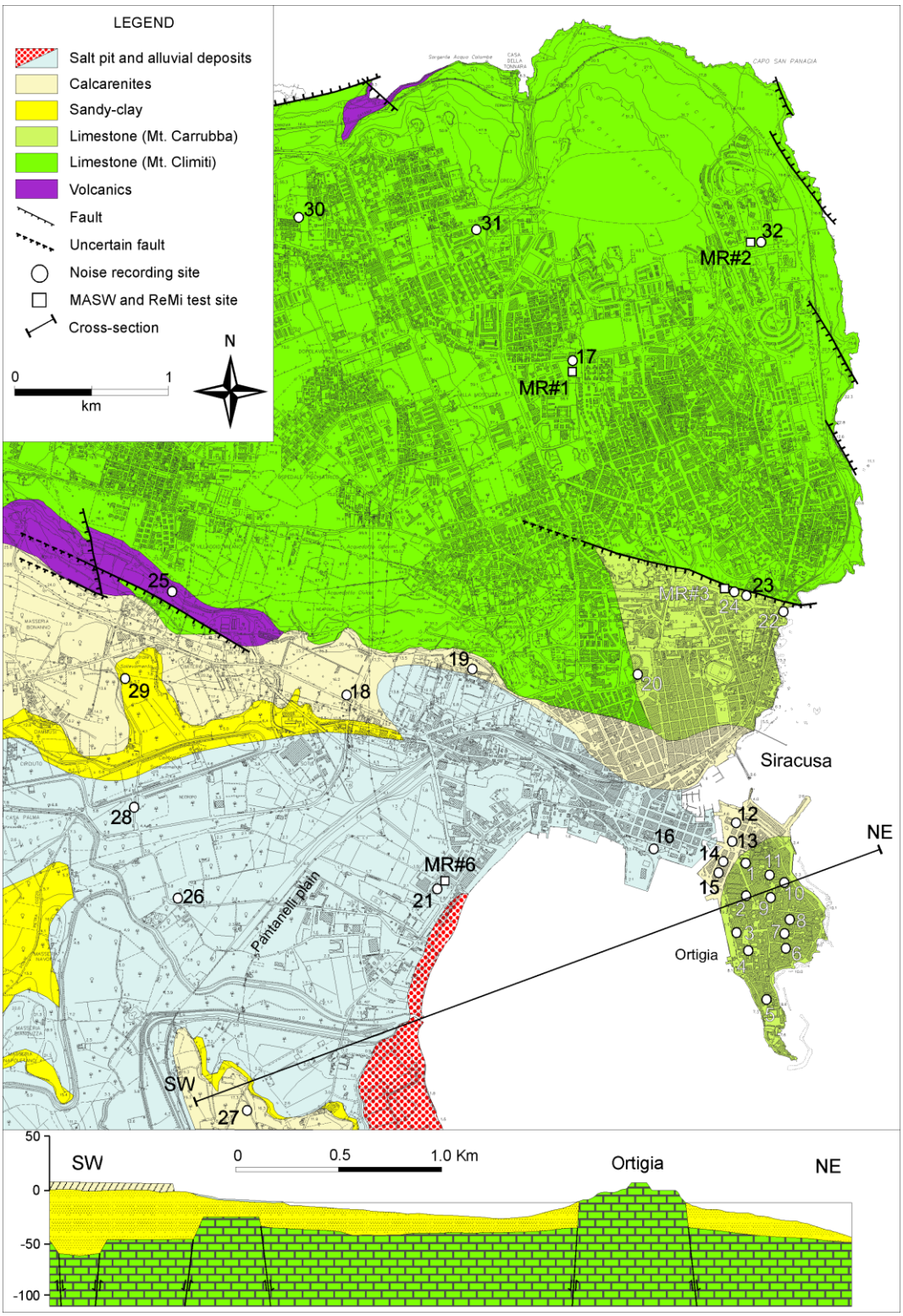

Fig. 5.1. *Geo-lithologic map of the Siracusa area (modified from Lentini et al., 1986) and cross section of Piana dell'Anapo-Ortigia (modified from Aureli et al., 2010).*

investigation usually not exceeding 30 m, depending on the lithotype features and the active sources used. It is also of crucial importance to adopt the ideal distance for the nearest offset (source-to-nearest receiver distance) and for the maximum offset (source-to-farthest receiver distance) for a correct investigation depth (Park *et al.*, 2002). A longer receiver spread is, indeed, necessary for the lower frequencies component of surface waves, but if the maximum receiver offset is too large (> 100 m), the high-frequency components of surface-wave energy will be poorly defined in the spectrum (Park *et al.*, 1999). MASW tests, in this study, were performed using a 12-channel seismograph equipped with 4.5 Hz geophones. A linear array having a length of 36-48 m, depending on the available free space at each site, was deployed using a 2-4 m interval pitch between the sensors. A 8 Kg hammer source, with a fixed 8 m offset distance was used, recording five shots, 3 s length, with a sample rate of 512 Hz.

The same kind of linear array was used for the ReMi measurements, recording 10 minutes of ambient noise. The passive techniques based on ambient noise recordings, such as the ReMi, provide reliable dispersion curves in the low frequency range as well, taking advantage from the use of natural sources and cultural noise having wavelengths ranging from a few kilometers to a few tens or hundreds of meters, respectively (Okada, 2003). The refraction microtremor technique offers the advantage of not requiring triggered source of wave energy and it will work best in a seismically noisy urban setting, analyzing the surface waves produced by traffic vehicles, wind responses of trees and buildings (Louie, 2001). However, special care must be used in processing the ReMi data because the presence of a omni-directional source may lead to the estimation of apparent S waves velocities not coincident with the real shear wave velocity (Louie, 2001; Park and Miller, 2008).

MASW and ReMi experimental dispersion curves were carried out using the Grilla 6.1 software (www.tromino.it). The software calculate the *f-k* spectrum of a seismic section, having the travel time (t) and the distance (x) as the vertical and the horizontal coordinates, respectively. The transform of t gives the frequency spectrum and the transform of the x coordinate gives the wavenumber k spectrum

(Lacoss *et al.*, 1969; Kvaerna and Ringdahl, 1986). From the *f-k* spectrum the phase velocity vs. frequency contour plot, was obtained. This analysis was carried out to calculate dispersion curves of the fundamental mode on the recorded seismograms for MASW (**Fig. 5.2a, b, c** and **d**). In the ReMi technique, time windows of 5, 10, 15 and 20 s were considered in order to test the effect of increasing record length. The dispersion curves were computed by a simple average (**Fig. 5.2a', b', c'** and **d'**), not including in the computation all the curves showing a not clear dispersion and/or dominant higher modes. The obtained dispersion curves were automatically picked from the displayed trends, sampling a large number of apparent phase velocities.

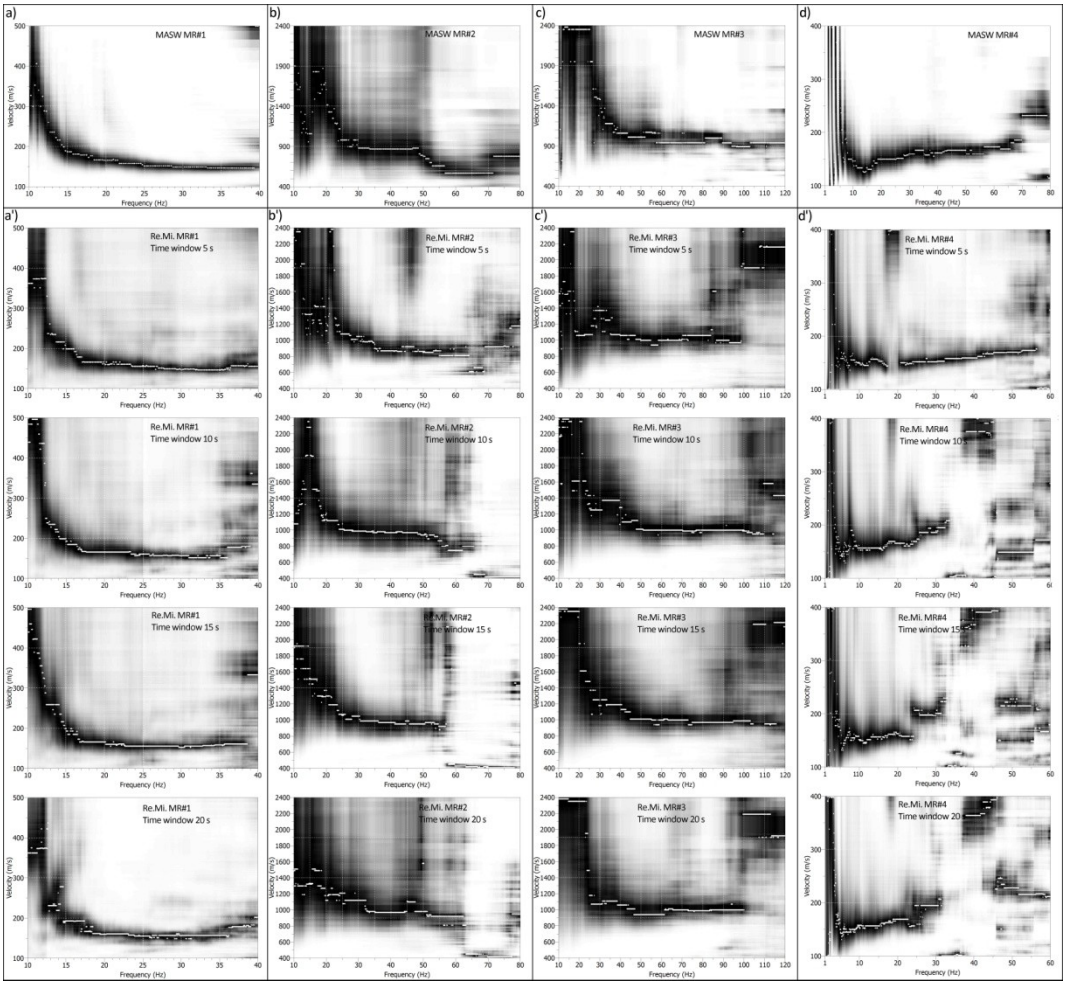

Fig. 5.2. *Phase velocity vs. frequency contour plot spectra for MASW (a, b, c, d) and ReMi (a',b', c', d') tests.*

The derivation of one-dimensional shear-wave velocity profiles from surface wave dispersion curves is a classical inversion problem in geophysics. The inversion of dispersion curves is known to be strongly nonlinear and is affected by non-uniqueness of solutions (Dal Moro *et al.*, 2006). In this study, the Rayleigh wave dispersion curves, obtained from the experimental setup, were inverted using the DINVER software (www.geopsy.org) which provided a set of dispersion curve models compatible with the observed dispersion curve. This inversion tool uses a directed-search method, called *"neighbourhood algorithm"* (Sambridge, 1999; Wathelet *et al.*, 2005; Wathelet, 2008), for nonlinear inversion that employs the Voronoi cells to investigate the multidimensional model and to compute the misfit function across the parameter space. The misfit function between experimental and computed dispersion curves is defined for each inverted model as:

$$misfit = \sqrt{\sum_{i=0}^{n_f} \frac{(x_{exp} - x_{cal})^2}{\sigma_i^2 n_f}}$$

where x_{exp} and x_{cal} are the phase velocities of the experimental and the calculated curves at frequency f_i, σ_i is the uncertainty of the considered frequency samples and n_f is the number of frequency samples. As suggested by Wathelet (2005), since in this study the uncertainty was not considered, σ_i was replaced by x_{exp}.

The experimental dispersion curves were inverted following a method similar to the one proposed by Coccia *et al.* (2010). The automatic picking of the dispersion curve of each site was approximated through a regression to a polynomial curve of fifth/sixth degree according to the observed trend (**Fig. 5.3**). To invert the dispersion curve, a set of 1 to 8 uniform layers with homogeneous properties was considered, taking into account five parameters: shear waves velocity (V_S), thickness, compressional waves velocity (V_P), Poisson's ratio and density (ρ). The most influent parameter in the surface wave inversion proces is V_S, that for all layer was considered as ranging between 100-2000 m/s. The influence of the other parameters is relatively small (Xia *et al.*, 1999; Xia *et al.*, 2003; Wathelet, 2008). For this reason, consistently with its low influence on surface wave dispersion, the

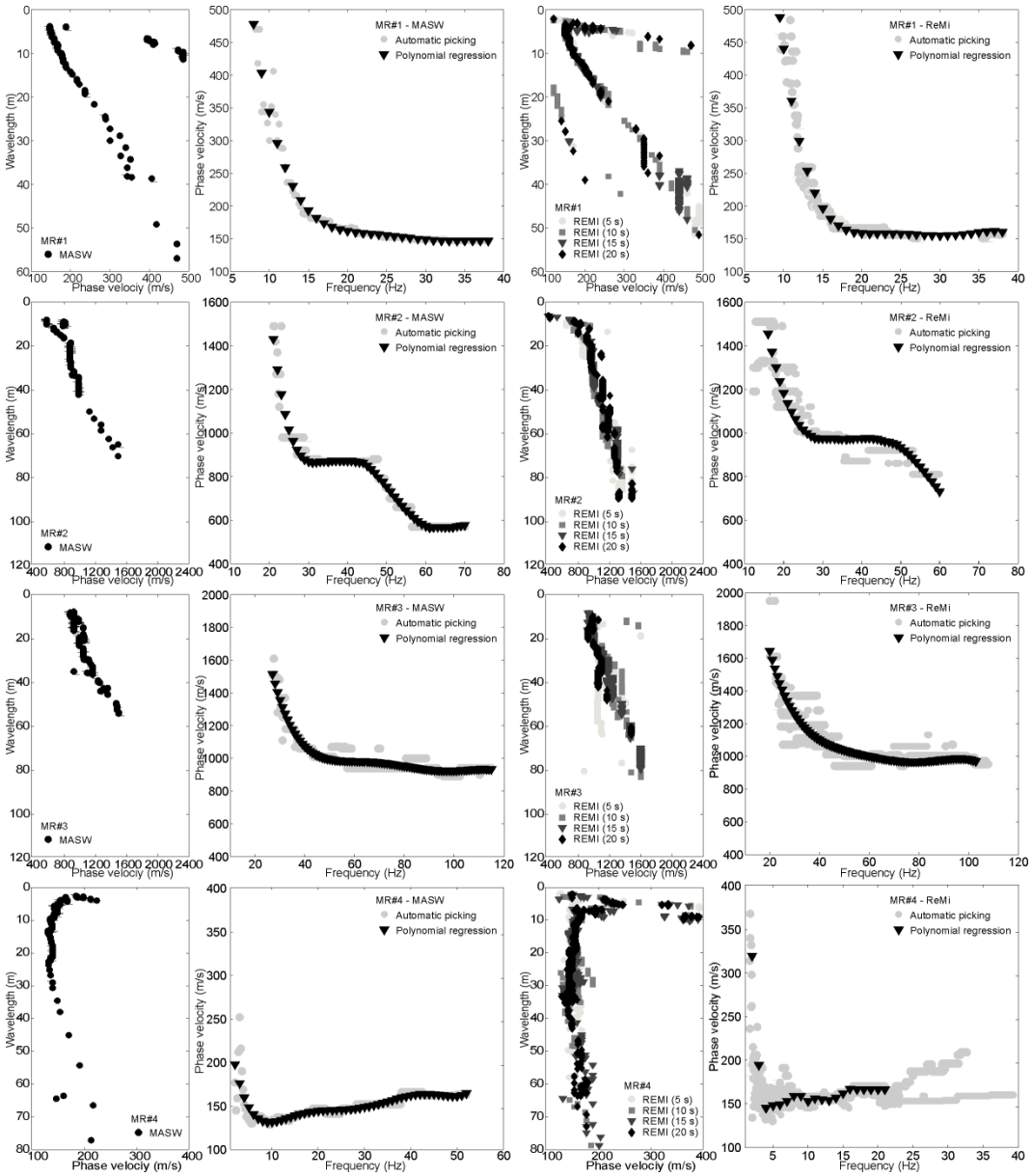

Fig. 5.3. *Rayleigh waves phase velocities as a function of wavelength and corresponding polynomial regression curves obtained from the automatic picking of Figure 2 spectra plots at each site.*

density (ρ) was fixed at a constant value of 2000 kg/m^3 in each layer. The compressional velocity (Vp) was varied from 200 to 5000 m/s and the Poisson's ratio (ν) was ranging between 0.2 and 0.5. As regards the thickness (H) it was constrained by fixing the bottom depths of some layers. Generally, the thickness limits are defined through the wavelengths (λ) derived from the frequencies and

phase-velocities of the experimental dispersion curves. The thickness range was obtained considering λ/4 and λ /2 for the minimum and maximum bottom depth, respectively. In **Table 5.1** the inversion parameters used for each layer are reported.

Tab. 5.1. *Input parameters used for the inversion of the experimental dispersion curves at each investigated site.*

MASW						
SITE	**N° Layer**	**V_P (m/s)**	**σ**	**V_S (m/s)**	**H (m)**	**ρ (Kg/m^3)**
MR#1	**1** Linear increase (n° 5)	200-5000	0.2-0.5	100-250	1.0-7.5	2000
	2 Uniform	200-5000	0.2.0.5	250-1000	∞	2000
MR#2	**1** Uniform	200-5000	0.2-0.5	500-700	1.0-5.0	2000
	2 Uniform	200-5000	0.2-0.5	500-700	2.0-5.0	2000
	3 Uniform	200-5000	0.2-0.5	800-1200	5.0-30.0	2000
	4 Uniform	200-5000	0.2-0.5	1000-2000	∞	2000
MR#3	**1** Linear increase (n° 5)	200-5000	0.2-0.5	750-950	1.0-5.0	2000
	2 Uniform	200-5000	0.2-0.5	900-1000	5.0-20	2000
	3 Uniform	200-5000	0.2-0.5	1200-2000	∞	2000
MR#4	**1** Uniform	200-5000	0.2-0.5	150-250	1.0-3.0	2000
	2 Uniform	200-5000	0.2-0.5	130-150	2.0-4.0	2000
	3 Uniform	200-5000	0.2-0.5	100-200	10.0-30.0	2000
	4 Uniform	200-5000	0.2-0.5	150-400	∞	2000
ReMi						
SITE	**N° Layer**	**V_P (m/s)**	**σ**	**V_S (m/s)**	**H (m)**	**ρ (Kg/m^3)**
MR#1	**1** Linear increase (n° 5)	200-5000	0.2-0.5	100-250	1.0-7.5	2000
	2 Uniform	200-5000	0.2.0.5	250-1000	∞	2000
MR#2	**1** Linear increase (n° 5)	200-5000	0.2-0.5	500-800	1.0-5.0	2000
	2 Uniform	200-5000	0.2-0.5	800-1000	5.0-10.0	2000
	3 Uniform	200-5000	0.2-0.5	900-1200	5.0-30.0	2000
	4 Uniform	200-5000	0.2-0.5	1200-2000	∞	2000
MR#3	**1** Linear increase (n° 5)	200-5000	0.2-0.5	900-1100	1.0-5.0	2000
	2 Uniform	200-5000	0.2.0.5	900-1400	10-20	2000
	3 Uniform	200-5000	0.2-0.5	1400-2000	∞	2000
MR#4	**1** Uniform	200-5000	0.2-0.5	150-250	1.0-5.0	2000
	2 Uniform	200-5000	0.2-0.5	100-150	5.0-10.0	2000
	3 Uniform	200-5000	0.2-0.5	100-200	10.0-40.0	2000
	4 Uniform	200-5000	0.2-0.5	150-500	∞	2000

The HVNR method is a common tool, used for site effect investigations, based on the ratio of horizontal over vertical components of motion. Generally, this spectral ratio exhibits a peak, that corresponds more or less to the fundamental frequency of the site (Bonnefoy *et al.*, 2006). However, the ambient noise wavefield is the result of the combination of unknown portions of both body and surface waves. If the first are prevailing, the ratio is mainly induced by S_H

resonance in the superficial layers whereas, if Rayleigh surface waves predominate, the theoretical ellipticity dictates the observed curves (Nogoshi and Igarashi, 1971; Fäh *et al.*, 2001; Scherbaum *et al.*, 2003). This is especially true when a great shear-wave contrasts between the shallow layer and the bedrock does exist, as theoretically confirmed by Malischewsky and Scherbaum (2004). Although experimental data peaks usually fit quite well the frequency of the theoretical curves and are poorly reliable in amplitude, the HVNR however contains valuable information about the underlying structure, especially as the relationship is concerned between V_S of the sediments and their thickness (Ibs-Vonseth and Wholenberg, 2000; Scherbaum *et al.*, 2003).

The ambient noise was recorded in thirty-two sites (**Fig. 5.1**) using Tromino (www.tromino.it), a compact 3-component velocimeter. Time series of ambient noise, having a length of 30 minutes, were recorded with a sampling rate of 128 Hz. Following the guidelines suggested by the SESAME project (2004) the recorded signal was divided in time windows of 30 s not overlapping. For each window a 5% cosine taper was applied and the Fourier spectra were calculated in the frequency range 0.5 - 64.0 Hz. The spectra of each window were smoothed using a Konno-Ohmachi window (Konno and Ohmachi, 1998) fixing the parameter *b* to 40. Finally the resulting HVNR was computed estimating the logarithmic average of the spectral ratio obtained for each time window, selecting only the most stationary and excluding transients associated to very close sources. Moreover, the HVNR obtained for selected sites (#17, #21, #24 and #32), were used to estimate the ellipticity curves to improve the final solution of the MASW and ReMi dispersion curve inversion. It is well known that the HVNR information usually controls the deeper part of the estimated Vs profiles, but because the absolute amplitude of the curve cannot be directly compared to the S_H transfer function amplitude or to the ellipticity, only the fit with the frequency of the peak is here taken into account.

The HVNR were also subdivided into groups showing a similar shape using the cluster analysis. Several studies have tried to correlate the information coming out from the HVNR to identify homogeneous areas in term of site response and local

geology in order to find relationships with the damage pattern due to ground shaking (Rodriguez and Midorikawa, 2002; Bragato *et al.*, 2007; Cara *et al.*, 2008; Strollo *et al.*, 2011). In particular, Bragato *et al.*, (2007) and Cara *et al.*, (2008), clustered the sites by considering the similarities in the HVNR function, without associating to each cluster any site response function obtained from earthquake data. Strollo *et al.* (2011), tested the reliability of the HVNR with a general inversion technique and standard spectral ratio obtained by analyzing earthquake data.

The clustering technique includes different algorithms and methods for grouping objects in a set of categories with relatively homogeneous characteristics. In this study, the cluster analysis was computed in the frequency range 0.5 – 10.0 Hz, not including the higher frequency values, being not interesting from the engineering point of view. The analysis was performed taking into account the thirty-two HVNR (i=1…32) whose amplitude was computed at sixty-three frequency values (M) in the range 0.5-10.0 Hz, expressing them by a vector y_{iM}. The degree of similarity between the HVNR observed at two sites (e.g. i and j) was calculated using the Euclidean distance:

$$d_{ij} = \sqrt{\sum_{M=1}^{63} \left(y_{iM} - y_{jM}\right)^2}$$

Finally, the use of *k-means* clustering approach (MacQueen, 1967) led to the recognition of the clusters. This technique consists in ranking into N_C clusters, chosen by the user, the N_K measurement points and evaluating the quality of the clustering by computing the sum of the squared error (SSE):

$$SSE = \sum_{i=1}^{N_K} \sum_{j=1}^{M} \left(y_{ij} - y_{C_{kj}}\right)^2$$

where y_{Ck} is the centroid of the vectors y_i in the cluster, calculated through:

$$y_{C_{kj}} = \frac{1}{N_K} \sum_{i=1}^{N_K} y_i$$

The *k-means* algorithm directly attempts to minimize the SSE, assessing each measurement point to its nearest cluster and repeating the computation until the points do not change the cluster any longer.

The detection of the optimal number of clusters in a dataset is a general problem (Burnham and Anderson, 2002), that can be solved through several methods. In this study the identification of the best solution from a group of acceptable models was achieved through the Akaike Information Criterion (AIC, Akaike, 1974). This procedure does not require particular assumptions on the experimental data and it is suitable for solving the model decision problem in many applications (Burnham and Anderson, 2002). To find the optimal partition, the cluster analysis was run for increasing values of N_C (ranging from 5 to 15) and selecting the N_C value for which the AIC is minimized. Assuming that the model error is normally distributed, the AIC formula is:

$$\mathrm{AIC} = N_K ln\left(\frac{RSS}{N_K}\right) + 2k + \frac{2k(k+1)}{(N-k-1)}$$

where N_K is the total number of HVNR, *ln* indicates the natural logarithm, *RSS* is the residual sums of squares and *k* indicates the number of free parameters as N_C-1. In this study *RSS* is defined as the sum of the *SSE* of all the clusters of each partition. Eventually, each group of the HVNR so far obtained by the analysis, was associated to the features of the main lithotypes outcropping in the Siracusa area.

5.4. Results and discussion

Inspection of the dispersion curves for MASW and ReMi (**Fig. 5.2**), obtained at each considered site, shows that only slight differences in the quality of the obtained phase velocity – frequency plots, are present. The comparison of the two methodology clearly shows the contribution of high frequencies in the definition of the dispersion curves obtained with the MASW technique, while the phase velocity - frequency curves obtained by ReMi approach, appear to be better defined at lower frequency. In the MASW technique, being an active source method, it is generally difficult to generate low frequency waves, whereas the

passive source method (ReMi), which makes use of microtremor, has a wide range of low frequencies. The various plots of the ReMi dispersion curves, obtained for different window length, were also compared and no significant differences in their definition was observed. In some cases (i.e. **Fig. 2b'** and **d'** for time windows greater than 15 s), a slightly poor quality of the dispersion curves could be explained as due to a transient increase of the background ambient noise energy at certain frequencies, rather than the result of the time window recording lengths changes (Pancha *et al.*, 2008). A further important aspect in the surface wave method interpretations, is that these techniques tend to overestimate of about 5-15% the average V_S with respect to other techniques such as the down-hole (Stephenson *et al.*, 2005). For these reason the soil category assessment, performed at each investigated site, following the EC8 code, was made by considering a 15% reduction of the $V_{S,30}$ value.

The dispersion curves estimated by MASW and ReMi methods for the site MR#1 show comparable results, although the ReMi dispersion curve, obtained considering a 20 s time window, appears less clear at low frequencies (between 10 to 17 Hz) (**Fig. 5.2**). The curves are well defined in the frequency range 10-40 Hz, with velocities approximately between 150 and 450 m/s (**Fig. 5.3**). In **Figure 5.4**, the results of the dispersion curve inversion with *"neighborhood algorithm"* method are shown. A good fit between experimental and theoretical dispersion curves was obtained and the $V_{S,30}$ values, 414.31 m/s and 429.89 m/s, obtained from the MASW and the ReMi prospections, respectively, so that the site was classified in the B soil category. Reducing this value by the 15%, make possible to classify this lithotype in a C soil category. At the MR#1 site, the resonance frequency is clearly indicated by a pronounced peak in the HVNR curve at about 6.5 Hz and the ellipticity of the theoretical fundamental mode of Rayleigh waves, obtained considering the best inverted model from both MASW and ReMi, is consistent in terms of fundamental frequency with the HVNR peak (**Fig. 5.4**). This indicate that the MR#1 site is characterized by a simple 1D layering with a strong velocity contrast between the soft sediments outcropping, belonging to the detritic-clay formation, and the bedrock boundary formed by the limestone.

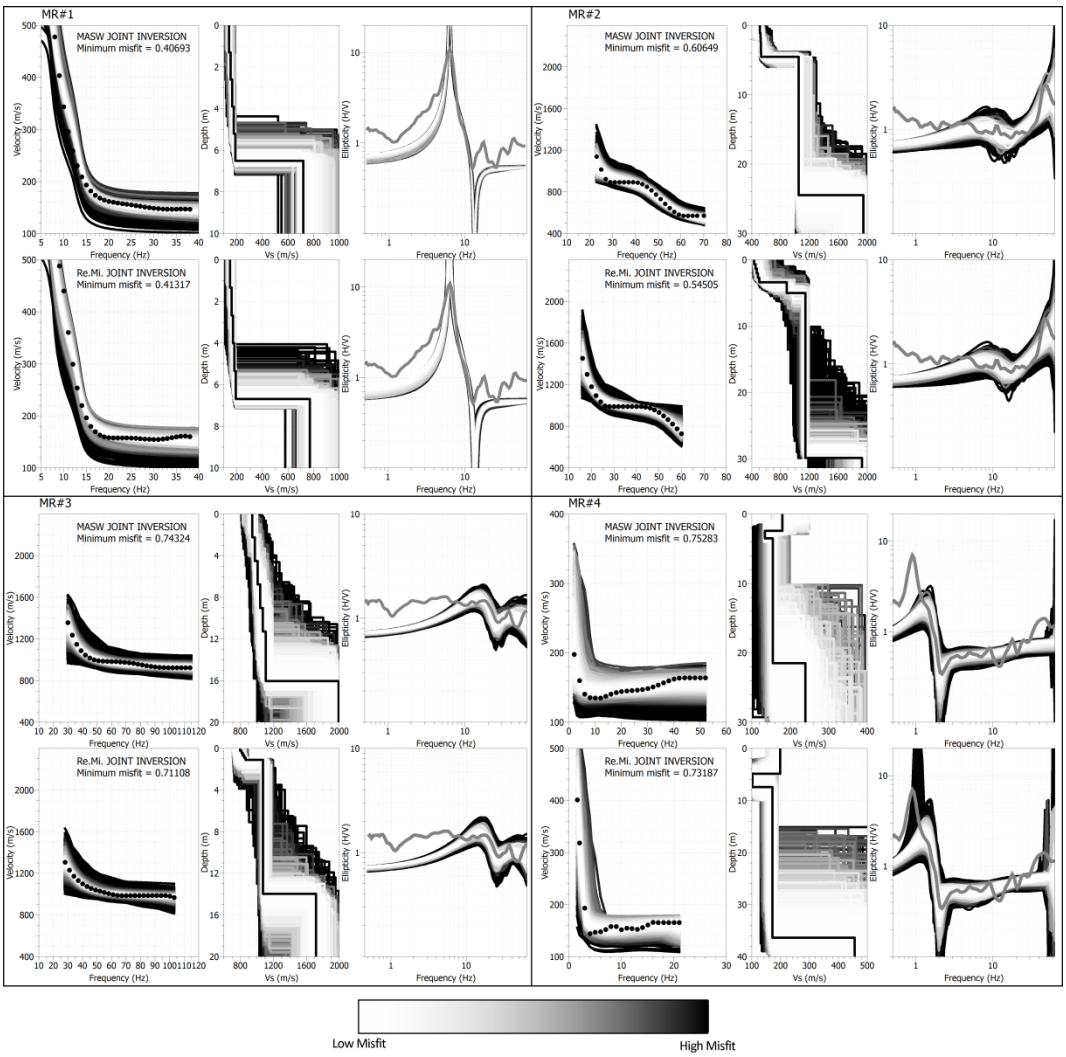

Fig. 5.4. *Dispersion curves, shear wave velocity profiles and ellipticity curves obtained from the joint inversion of the experimental phase velocities (black circles) and the HVNR curves (grey lines); black line in the Vs profiles indicates the best estimated model.*

At the site MR#2 both the MASW and ReMi dispersion curves cover the frequency range 10-80 Hz and the shear waves velocity ranges from 500 to 1800 m/s (**Fig. 5.3**). The results of the two techniques show significant differences at high (50-80 Hz) and low frequencies (10-20 Hz). In particular, the ReMi dispersion curve appears better defined at about 10-20 Hz, especially considering 10-15 s time window, whereas the MASW one is more detailed at higher frequencies (50-80 Hz) (**Fig. 5.2**). The inversion in terms of the fundamental Rayleigh mode indicates for this site the A class soil category, with a $V_{S,30}$,

obtained from the inverted models, of 983.18 m/s and 980,01 m/s for the MASW and the ReMi, respectively. The soil class category does not change after the 15% reduction, giving values of 833.01 m/s and 835.71 m/s, respectively (**Fig 5.4**). The experimental HVNR curves are not fully matched from the theoretical ellipticity, especially at low frequency, mainly because there is lack of phase velocities estimates at low frequency values (**Fig. 5.4**). This site seems to be characterized by the presence of a relatively soft thin layer (3-4 m) having a V_S of about 500 m/s, overlaying the limestone bedrock.

The phase velocity–frequency spectrum obtained for the site MR#3 ranges from 10 to 120 Hz with a phase velocity between 800-2000 m/s (**Fig. 5.3**). The ReMi dispersion curve appears better defined for the time window of 15 s, whereas a poorer quality is observed for the other time windows (**Fig. 5.2**). A good match between experimental and theoretical dispersion curves is observed (**Fig. 5.4**) and the inverted model provides a $V_{S,30}$ of 1300 m/s for the MASW and 1283 m/s for the ReMi experiments. The 15% reduction of the $V_{S,30}$ values gives 1090.73 m/s and 1130.52 m/s, therefore confirming the A class soil category for this site. The results of ellipticity are similar to those obtained for the site MR#2 with a low quality matching at low frequency and a better match at high frequency (**Fig. 5.4**). The results of both the HVNR and the S waves velocity profile, confirm that this site is characterized by outcropping limestone.

The MASW and ReMi dispersion curves obtained for the site MR#4 (**Fig. 5.3**), appear quite unclear. The observed frequency ranges are 1-80 and 1-30 Hz, for the MASW and ReMi dispersion curves, respectively, with velocity phase ranging between 150-300 m/s. Moreover, a mode splitting phenomenon, affecting mainly the ReMi dispersion curves (**Fig. 5.2**), seems to be present in this site. Such effect is typical of a complex energy distribution due to velocity inversions and high values of the Poisson ratio (O'Neill and Matsuoka, 2005). The shape of both MASW and ReMi experimental dispersion curves (**Fig. 5.3**) suggest the presence of a low velocity layer. As a matter of fact, in this area a lithologic sequence formed by alluvial deposits overlaying about 10 m thick calcarenites, having higher shear wave velocity with respect the underlying sandy clays, is present.

The results of the dispersion curves inversion suggest a D class soil category for this site (**Fig. 5.4**). A $V_{S,30}$ of 173.98 m/s for the MASW and 166.88 m/s for the ReMi data, is indeed observed, and reducing them by the 15% they became 147.89 m/s and 141.85 m/s, respectively. The MASW and ReMi dispersion curves constrain the estimated models to depths of about 20–40 m and the obtained ellipticity do not totally fit the HVNR peak. This could be explained as a consequence of a bedrock depth greater than that obtained through the experimental dispersion curve. Underneath a 30-40 m depth, the inverted velocity profile is not well constrained, considering the used experimental setup. A longer linear array spacing and the use of lower frequency geophones could have improved the resolution of the obtained dispersion curve.

The HVNRs obtained from measurements performed in the Siracusa area were subdivided in different groups through a cluster analysis. The optimal partition, for which the AIC is minimized, was obtained for N_C equal to 12 (see lower right panel in **Fig. 5.5**).

The cluster (a) consist of six measurement points (#1, #2, #3, #4, #12 and #13), performed in the Ortigia area on outcropping limestone, characterized by peaks in the frequency range 1.0-3.0 Hz (see panels (a) in **Figs. 5.5** and **5.6**). In a recent work by Panzera *et al.* (2011a) these peaks appeared to be consistent with a topographic effect. Such HVNR peaks, indeed, cannot be justified in terms of stratigraphic features, considering also the physical properties of the limestone (V_S > 900 m/s), as obtained from both the MASW and ReMi experiments (see MR#2 and MR#3 in **Fig. 5.4**). The HVNRs obtained for the sites #5, #9, #14 and #15 form the clusters (b) and (e) (see **Figs. 5.5** and **5.6**). They show two dominant peaks in the frequency ranges 1.0-3.0 and 4.0-10.0 Hz. Following Panzera *et al.* (2011a), the first frequency range can be ascribed to the particular seismic site response observed in the Ortigia peninsula, similarly to the cluster (a) whereas the spectral ratio peaks in the frequency range 4.0-10.0 Hz could be linked to some local shallow lithologic features. It has to be remembered, indeed, that high frequency ground motion can be controlled by the vibration of smaller blocks therefore implying different resonant frequencies (Burjànek *et al.*, 2010). In the

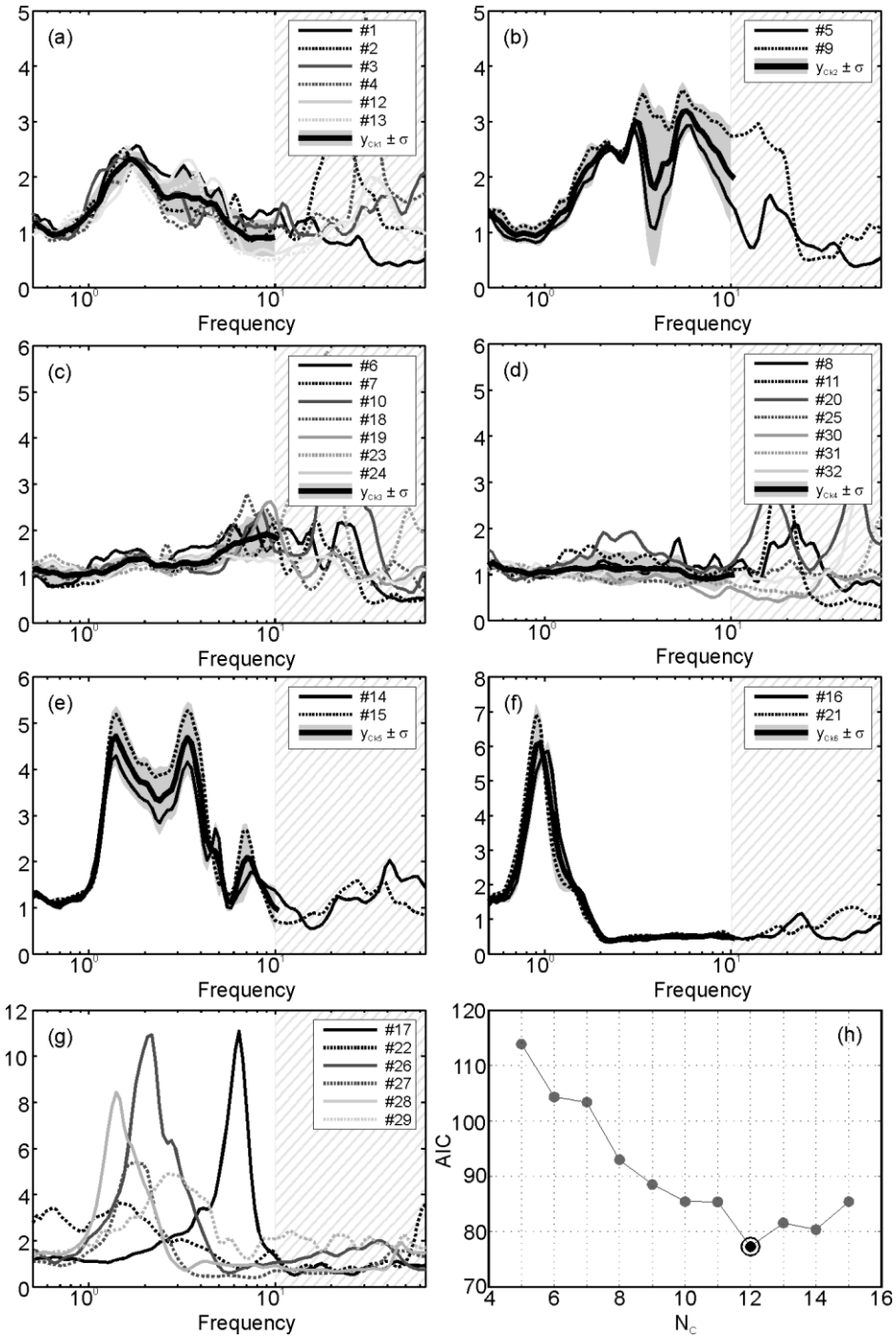

Fig. 5.5. *HVNRs forming each cluster (continuous and dotted thin lines) found out for the Siracusa area; thick black lines show the average HVNR for each cluster, grey area delimitate the corresponding $\pm\sigma$ standard deviations (a, b, c, d, e, f, g). Akaike Information Criterion parameter vs. the number of clusters for the Siracusa area (h).*

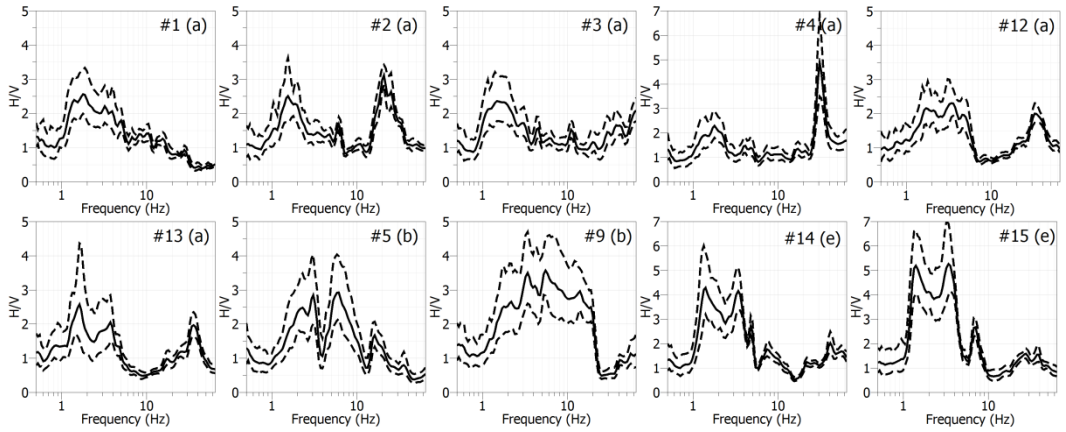

Fig. 5.6. *HVNR and the corresponding ±σ for the clusters (a), (b) and (e).*

cluster (c) the spectral ratio curves show a tendency towards a slight and constant increase in amplitude that reach a value of 2-3 units at frequencies greater than 7.0 Hz (see in **Figs. 5.5** and **5.7**). This moderate amplitude increases, in my opinion, could be related to the modest velocity contrast existing between the calcarenites (#18 and #19) or the slightly fractured limestones (#6, #7, #10, #23 and #24) with respect to the massive limestone forming the underlying bedrock. Slightly fractured limestones are characterized by a V_S of about 500 m/s, as shown in site MR#3, whereas no experimental values of V_S were calculated for the calcarenites

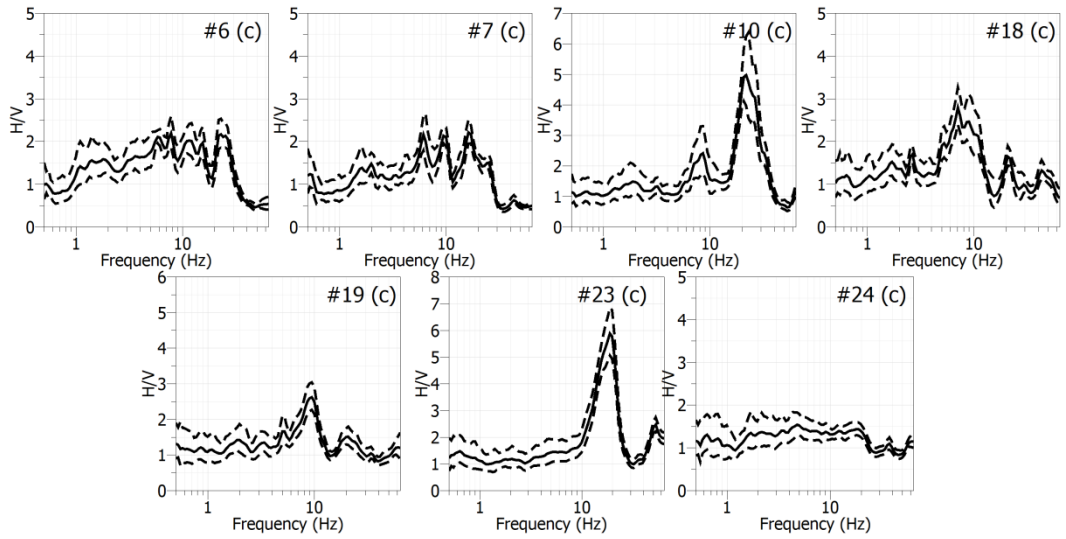

Fig. 5.7. *HVNR and the corresponding ±σ for the cluster (c).*

but an average V_S value of about 350 m/s is available from literature (Tortorici, 2000). The HVNRs obtained for the carbonate sequence (#8, #11, #20, #30, #31 and #32) and the volcanics (#25), constitute the cluster (d) which shows a flat spectral ratio plot (see **Figs. 5.5** and **5.8**). After all, these formations represent the local bedrock as confirmed by the shear waves velocities obtained through the MASW and ReMi experiments (see MR#2 and MR#3 in **Fig. 5.4**). The cluster (f) is formed by the Nakamura spectral ratios obtained from measurements points #16 and #21. They show pronounced spectral peaks at about 1.0 Hz (see **Figs. 5.5** and **5.9**) which can be related to the presence of thick (40-50 m) alluvial deposits and soft sandy-clay sediments having a V_S of about 170-180 m/s (see MR#4 in **Fig. 5.4**). Finally, the group (g) includes all the measurement points (#17, #22,

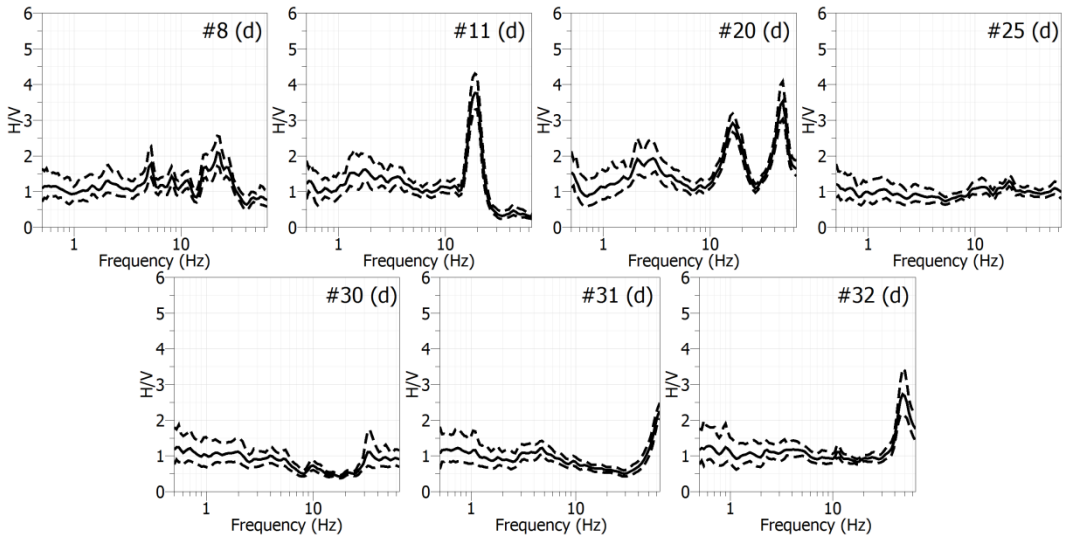

Fig. 5.8. *HVNR and the corresponding ±σ for the cluster (d).*

#26, #27, #28 and #29) each outlining a cluster (see **Figs. 5.5** and **5.10**). The measurement point #17 represents an anomaly in the limestone formation, but this behaviour could be related to the high velocity contrast existing between the detritus and the limestones, as demonstrated by the MASW and ReMi measurements performed in the same site of the ambient noise recording (see MR#1 in **Fig 5.4**). The spectral ratio #22 shows a wide standard deviation at low

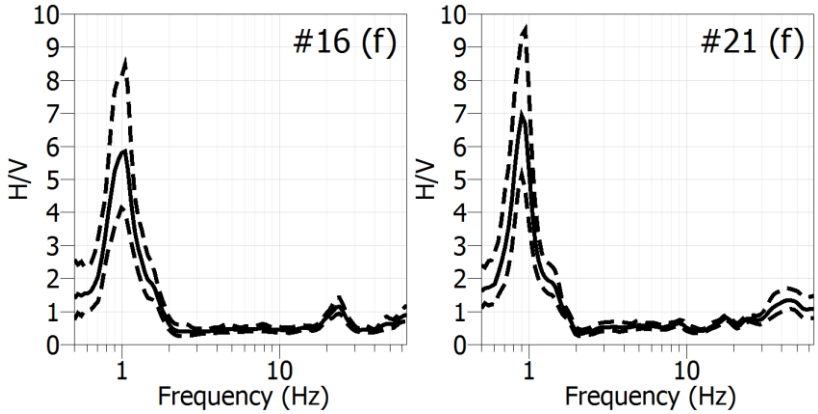

Fig. 5.9. *HVNR and the corresponding ±σ for the cluster (f).*

frequency values (0.5-4.0 Hz), therefore indicating an effect that could be ascribed to the interaction between the sea waves and the cliff nearby the measurement point, that imply a significant increment of the amplitude (3-4 unit) at relatively small frequency. The results obtained for the site #26 and #28 located in the

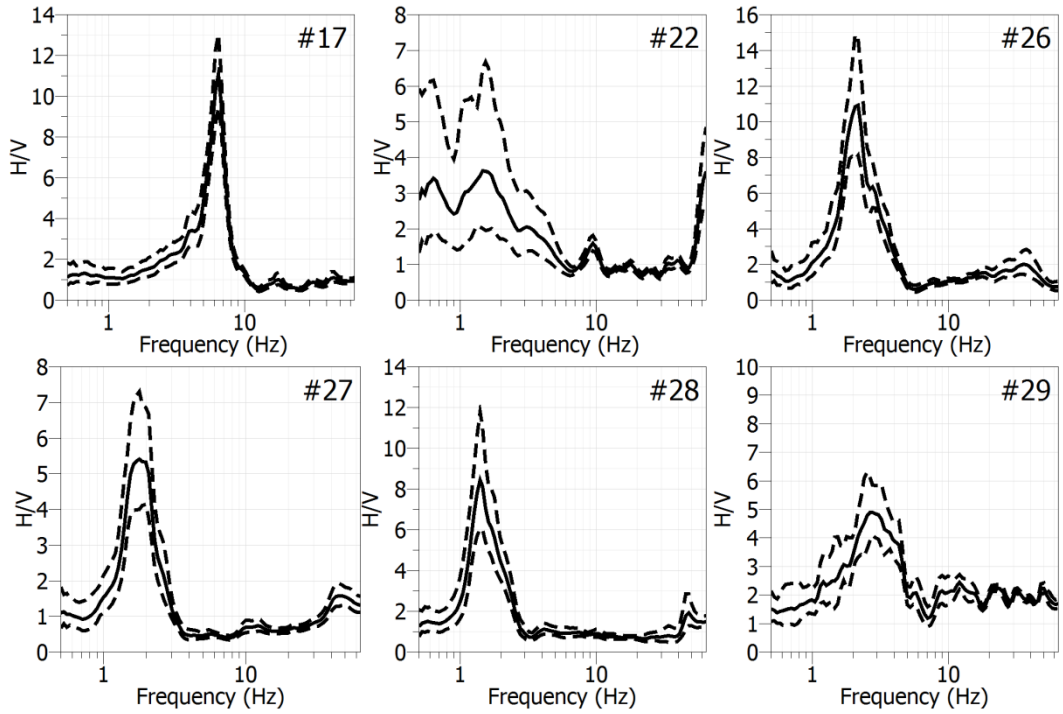

Fig. 5.10. *HVNR and the corresponding ±σ for six measurement sites, each outlining a cluster, and forming the group (g).*

southern part of the study area show pronounced spectral peaks, at about 2.5 Hz and 1.5 Hz, respectively. These H/V peaks can be related to the presence of thick alluvial deposits and soft sandy-clay sediments. The HVNR #27 was performed from records on calcarenites and shows a significant peak at about 2.0 Hz. Such peak, as it can be inferred from geologic observations (see cross-section in **Fig. 5.1**), could be ascribed to the existence of a thick layer of sandy clays inter-bedded between the calcarenites and the limestone. Lastly, the HVNR obtained from the measurement site #29, located in the sandy clay formation, shows a significant peak that could be interpreted as connected to the sharp velocity contrast with the underlying limestones.

Moreover, pronounced spectral peaks at frequencies higher than 10.0 Hz (not considered in the cluster analysis) are sometimes observed especially in the sites located on limestone and calcarenites (see **Figs. 5.6**, **5.7** and **5.8**). Such feature, in my opinion, could be interpreted as a consequence of the high velocity contrast existing between the limestones and the thin layers of detritus that often overlay them.

Chapter VI

The role of the lithology and topography on the seismic site response

6.1. Issues of the chapter

The structure of surface geology as well as the morphologic setting play a key role in controlling ground motion at the surface. Local changes of topography imply, indeed, the occurrence of diffraction as well as reflection and conversion of the incident seismic waves leading to significant modification of ground shaking. Generally, the amplification effects take place at the topmost part of a hill and they are frequency dependent so that resonance phenomena occur when the wavelength of the incident wave is comparable to the hill width (Bard, 1982). Another important aspect concerns the difficulty to distinguish between a purely topographic effect and the influence of different local lithology amplification. Performing measurements along a cross section in the French Alps, Pedersen et al. (Pedersen *et al.*, 1994) observed that ground motion amplitude caused by topography variations can be in some instances smaller than the amplification linked to stratigraphic effects. Slope inclination is however a sensitive feature of site response because it determines the angle of reflection and diffraction of seismic waves. Going into more details, steep slopes tend to pack and focus the reflected seismic waves at the slope crest, while gentle slopes scatter the diffracted seismic waves (Boore, 1973). Moreover, the effect of varying slope angles was investigated by numerical models by Ashford *et al.* (1997) who observed that amplification increases with the increase of the slope angle. The sharpness of the ridge crest, therefore may significantly influence the local ground motion (Bard and Riepl-Thomas, 1999). In recent years, many authors (Bonamassa and Vidale, 1991; Spudich *et al.*, 1996; Del Gaudio *et al.*, 2008; Rigano *et al.*, 2008; Burjànek *et al.*, 2010) have also reported cases of considerable directional variations of the

seismic site response linked to different geological and topographic conditions. In particular, significant directional effects, transverse to the major axis of the ridge, are often observed (e.g. Spudich *et al.*, 1996; Le Brun *et al.*, 1999; Massa *et al.*, 2010; Pischiutta *et al.*, 2010; Marzorati *et al.*, 2011).

In this study, a field experiment using ambient noise and moderate magnitude seismic events is performed on a small hill, named S. Sofia (see **Fig. 6.1**), located in the northern part of Catania (Italy), where the university campus stands. The S. Sofia hill has a gentle topography with a flat surface at the top (**Fig. 6.1b**), it is elongated for about 700 m in NW-SE direction with a maximum height of 40 m. Its longitudinal section (B-B' in **Fig. 6.1a**) is asymmetric, consequently the northwestern side is quite gentle with respect to the southeastern part. On the other hand, the transverse section is more regular and symmetric (A-A' in **Fig. 6.1a**), with a base having width of about 500 m. In the past, a preliminary study was performed in this area (Lombardo and Rigano, 2007), using ambient noise records and a small set of earthquakes recorded on stations operating for a few weeks. That study was devoted to investigate the local seismic response linked to the features of different lithotypes outcropping in the area. The aim of present experiment is to evaluate the effects of the topography on the seismic response of the study area, testing at the same time the reliability of the use of ambient noise for studying such phenomena in a rather complex geologic and topographic setting. The most commonly adopted techniques to evaluate site response properties, such as the standard spectral ratio (SSR), the horizontal to vertical spectral ratio (HVSR) and the horizontal to vertical noise ratio (HVNR) are therefore adopted. Techniques evaluating directional effects are also used as a test procedure for the identification of directional site response.

6.2. Geologic setting

The geo-lithologic map of the study area is shown in **Figure 6.1a**. The map is the result of assembling information coming from pulling together both geophysical data (Lombardo and Rigano, 2007) and geologic field surveys performed by several authors (Monaco *et al.*, 2000; Carbone *et al.*, 2009).

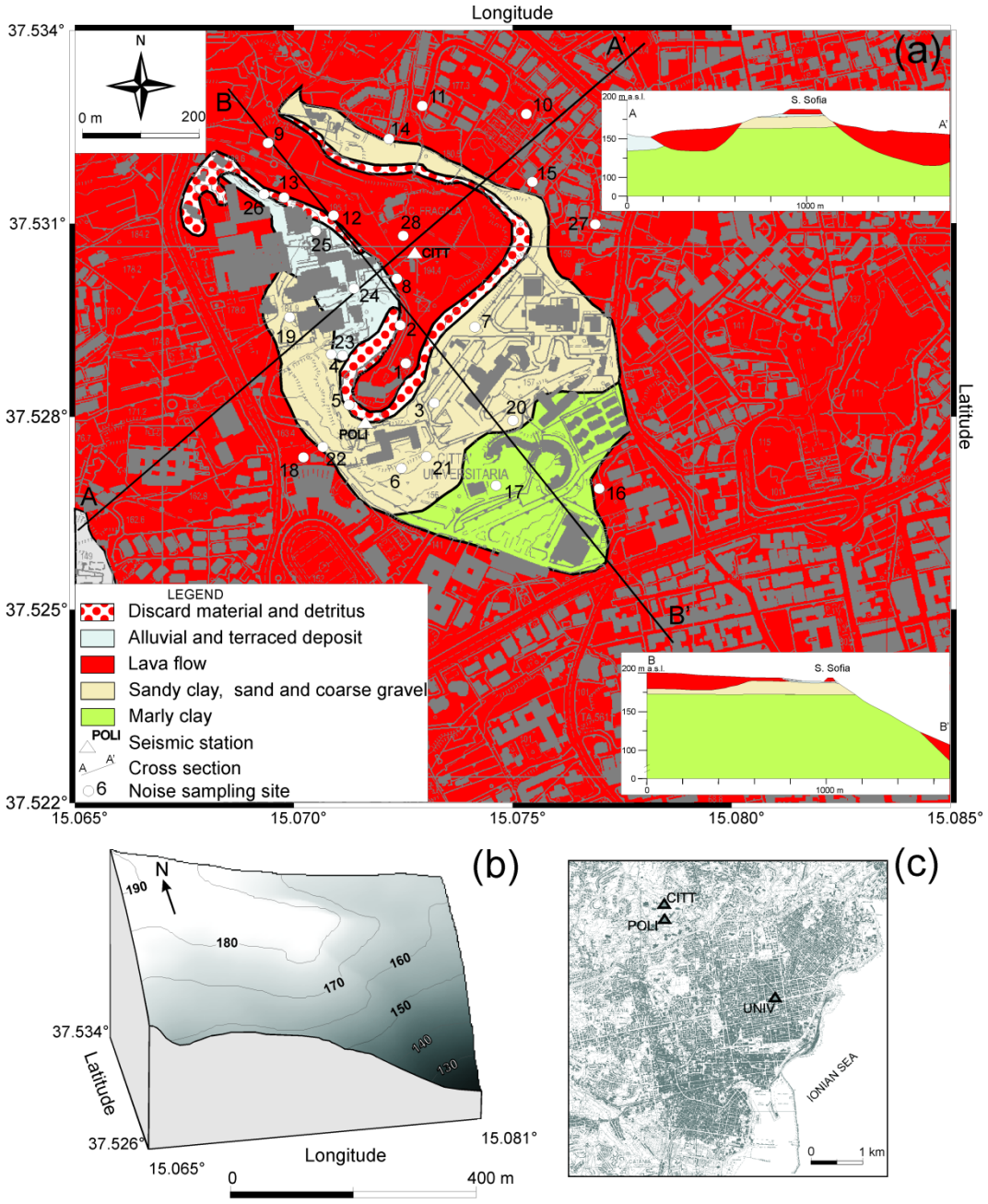

Fig. 6.1. *(a) Geo-lithologic map of the study area with cross sections of S. Sofia hill; the insets show the local geologic structure across the profiles AA' and BB'. (b) 3D surface model of the investigated area. (c) location of the reference station (UNIV) with respect to the permanent stations.*

The surface geology of Catania derives from the combination of processes linked to the volcanic and tectonic activities. The main feature of the study area is a complex sedimentary sequence laying between a clayey basement and an upper

volcanic formation with lava flows and pyroclastics. The bedrock of the area is represented by a succession of marly clays, having thickness up to about 600 meters. In the upper part of this formation, levels of sand and sandy clays are frequently present. These terrains are followed upwards by some tens meters of fluvial-deltaic sands and gravels called "Terreforti" formation. Such a formation is unconformably covered by terraced alluvial deposits that outcrop in different places inside the urban area. The most recent deposits are formed by slope detritus and ruins deriving from historical earthquakes.

In the study area the most frequently cropping out lithotype is basaltic lava that in pre-historical and historical times flowed onto the valleys originally existing in the sedimentary formations (see cross section A-A' in **Fig. 6.1a**). The lava flows have an extremely variable thickness and often are formed by alternating levels of massive lava and more or less weathered scoriae.

6.3. Methodology

The evaluation of local seismic response in the complex geologic situation of the study area was undertaken by integrating different experimental approaches. The data used in this study consist of both noise and earthquake recordings that were processed through spectral ratio techniques.

Three sites, located on the top (CITT), along the southwestern slope of the hill (POLI) and at about 3 Km from the study area (UNIV) (**Fig. 6.1a**, 6.**1c**), were selected and instrumented with Reftek seismic stations, equipped with broadband seismometers (Guralp40T).

The area was monitored for about two years, from 1999 till 2000. In this study, a set of 44 local and regional seismic events (**Tab. 6.1**), having a good signal-to-noise ratio was selected. Data were processed with horizontal to vertical spectra ratio (HVSR) and standard spectral ratio techniques considering horizontal (HSSR) and vertical (VSSR) components. It has to be noted that in case of complex structures there might be a broad range of amplification rather than a single frequency and it is also possible the existence of pronounced changes in the vertical component of the ground motion. This might therefore indicate that the

Table 6.1. *List of selected events recorded at each seismic station.*

#	yy-mm-dd	hh/mm	Lat. N	Long. E	Depth (Km)	M_D	CITT	POLI	UNIV
1	1999/02/08	19:24	37.66	14.99	5	2.7	*		*
2	1999/02/08	21:06	37.65	14.98	10	2.3	*		
3	1999/02/09	05:24	37.66	14.99	10	2.6	*		
4	1999/02/13	22:58	38.19	15.02	10	3.3	*		*
5	1999/02/14	06:23	38.15	15.05	7	3.0	*		*
6	1999/02/14	11:45	38.09	15.06	9	4.3	*		*
7	1999/02/14	15:10	38.21	15.03	7	3.3	*		*
8	1999/02/14	15:43	38.17	15.04	12	3.2	*		
9	1999/02/16	08:54	37.59	15.11	10	2.4	*		*
10	1999/02/16	10:29	37.61	15.16	10	2.1	*		*
11	1999/02/16	10:34	37.60	15.13	10	2.6	*		*
12	1999/02/16	10:36	37.63	15.09	10	2.8	*		
13	1999/02/16	10:58	37.62	15.10	10	2.5	*		*
14	1999/05/23	11:53	37.90	14.99	4	3.3	*	*	*
15	1999/05/23	12:33	37.68	14.99	5	2.8	*	*	
16	1999/05/24	02:50	37.76	14.55	16	2.7	*		
17	1999/06/02	10:37	38.50	14.08	21	4.0	*	*	
18	1999/06/02	11:52	38.56	14.01	11	3.8	*		*
19	1999/06/02	11:56	38.55	13.99	7	3.8	*		
20	1999/06/02	18:14	37.70	14.96	5	2.8	*		
21	1999/06/07	03:37	38.55	14.17	18	3.5	*		*
22	1999/06/13	17:46	37.79	15.96	44	3.2	*	*	
23	1999/06/13	18:10	37.72	15.12	3	2.8	*	*	
24	1999/06/14	20:36	37.29	15.00	10	2.1	*	*	
25	1999/06/20	23:06	37.67	15.01	6	2.7	*	*	*
26	1999/06/22	04:11	37.68	14.95	10	2.5	*	*	
27	1999/07/02	22:40	37.68	14.95	10	2.4	*		
28	1999/08/21	01:38	37.75	15.16	10	3.3	*	*	
29	1999/08/26	08:50	37.79	15.15	10	3.3	*	*	*
30	1999/08/26	08:56	37.78	15.16	10	3.2	*	*	
31	1999/09/16	13:23	37.58	14.92	5	2.7	*	*	
32	1999/09/20	06:57	38.42	15.65	173	3.4	*	*	
33	1999/09/24	04:57	37.74	15.13	10	2.5	*		
34	1999/09/25	00:51	38.57	16.62	26	3.6	*		
35	1999/09/27	20:46	38.64	16.43	24	3.6	*		
36	1999/09/28	10:55	37.72	14.95	10	2.5	*		
37	1999/09/30	14:52	37.73	15.18	4	2.9	*	*	
38	1999/10/01	07:27	37.76	15.20	10	2.7	*	*	
39	1999/10/12	01:21	37.70	15.01	5	2.9	*	*	
40	1999/10/12	01:56	37.69	15.01	5	2.8	*	*	*
41	1999/10/12	03:27	37.70	15.00	5	2.8	*	*	*
42	1999/10/12	04:59	37.69	15.02	5	2.8	*	*	
43	1999/12/26	14:19	37.67	15.18	5	3.0	*		*
44	1999/12/27	04:54	38.41	14.24	10	3.3	*		*
Total number of seismic event for each stations							44	19	18

structure of the site exhibits significant lateral variations, which will lead to significant 2D or 3D effects. HVSR technique, in particular, was proposed for 1D structures, then, the identification of main resonance frequencies through this technique can be very difficult in such situation. For this reason the ratios between the vertical component spectra of records at the local permanent stations and at the reference one were calculated as well. The station UNIV (**Fig. 6.1c**) was used as reference site since, as suggested by several authors (Bouchon and Barker, 1996; Catchings and Lee, 1996; Steidl *et al.*, 1996), it is important to adopt a reference station not significantly influenced by the topography itself. Such station was installed on a 30 meters thick compact lava rock overlaying the marly clays formation. The suitability of the reference site was tested, following Steidl et al. (Steidl *et al.*, 1996), by performing the HVSR which showed the lack of significant resonance phenomena (**Fig. 6.2**).

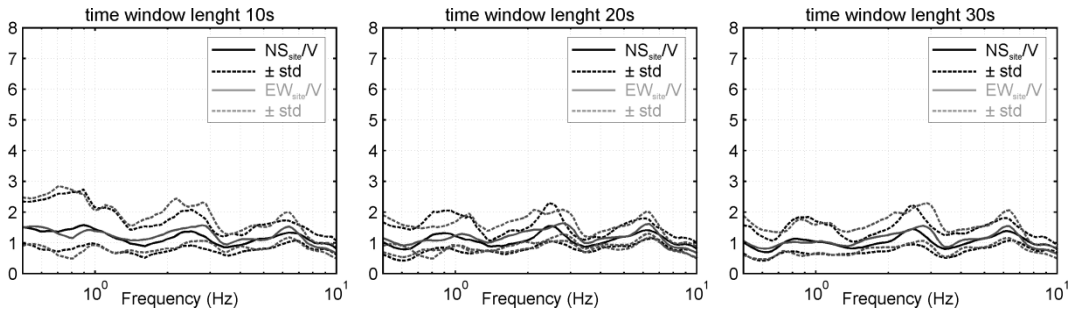

Fig. 6.2. *HVSR of the NS and EW components of motion at the reference site, computed by considering three different time window duration.*

The signals of the recorded earthquakes were base-line corrected, in order to remove spurious offsets and band-pass filtered in the range 0.08-20 Hz, with a fourth order causal Butterworth filter. In order to verify the contribution of the body and of the surface waves, in the seismic site response assessment, the analysis was performed considering different time windows (10, 20, 30 s), starting from S waves onset and using a 5% cosine-tapered window. The signal, indeed, should be long enough so that any resonant peaks in the spectral ratio can be adequately resolved. The obtained Fourier spectra, for each considered earthquake, were smoothed using a proportional 10% triangular window. For each

windows, the spectral ratio as a function of the frequency was computed, eventually performing the geometric mean.

The ambient noise was recorded in twenty eight sites (**Fig. 6.1a**) using Tromino (www.tromino.it). It is a compact 3-component velocimeter, designed for recording and processing ambient noise, having a response curve almost flat in the band of engineering interest (Castellaro and Mulargia, 2009). Time series of 30 minutes length were recorded using a sampling rate of 128 Hz and processed through spectral ratio technique (HVNR). According to the guidelines suggested by the SESAME project (2004), time windows of 30 s were considered and the most stationary part of the signal was selected excluding transients associated to very close sources. Fourier spectra were calculated and smoothed using a triangular average on frequency intervals of ± 5% of the central frequency. Following the criteria suggested by SESAME project (2004), only the spectral ratio peaks having amplitude greater than two units were considered significant.

The results obtained through the experimental techniques (HVSR, HSSR, VSSR and HVNR), at the permanent seismic stations, were compared with those coming out from numerical 1D modeling based on the knowledge of the subsurface geology. To acquire the theoretical HVSR and the amplification spectra, for S and P waves, the ModelHVSR Matlab routines (Herak, 2008) were adopted. This software, in its simplest formulation, consider a vertical incidence SH-waves and horizontally stratified soil layers. The soil model consists of a number of visco-elastic layers, stacked over a halfspace, each of them being defined by the thickness (h), the velocity of the body waves (V_P and V_S), the density (ρ), and the Q-factor, which controls the anelastic properties. To compute the synthetic HVNR the usually postulated ambient noise properties was adopted, therefore, assuming that the microtremor consists of Rayleigh waves in the fundamental mode (Fäh *et al.*, 2001), including the presence of Love waves (Bonnefoy-Claudet *et al.*, 2008) and adopting a 1-D layered viscoelastic solid, as in the Hermann (2002) formulation. The stratigraphy of the seismic station sites was inferred from borehole data and the input elastic parameters of main geologic formations (**Table 6.2**) were taken from the results of the CNR-GNDT "Catania

Project" (Faccioli and Pessina, 2000). Moreover, to improve the solution at low frequency (0.5-1.0 Hz), according to Priolo (1999), the presence of Pliocenic sediments (flysch, clay, silt and sand) was assumed beneath the marly clay bedrock.

Table 6.2. *List of elastic parameters of main lithotype outcropping in the study area, used for 1D modeling.*

Start 1D model used to compute the numerical earthquakes and noise spectral ratios at POLI						
Thickness (m)	V_P (m/s)	V_S (m/s)	ρ (kg/m^3)	σ	Q_P	Q_S
5	750	390	1900	0.320	42	50
5	858	450	1950	0.320	10	12
10	550	300	1700	0.288	13	16
120	1235	650	2000	0.320	21	25
∞	2365	1316	2200	0.260	250	300
Start 1D model used to compute the numerical earthquakes and spectral ratios at CITT						
Thickness (m)	V_P (m/s)	V_S (m/s)	ρ (kg/m^3)	σ	Q_P	Q_S
1.5	400	210	1800	0.310	8	10
10	1730	1000	2300	0.249	83	100
10	370	190	1900	0.320	10	12
25	640	330	1940	0.320	42	50
125	1235	650	2000	0.320	21	25
∞	2365	1316	2200	0.260	250	300

Experimental spectral ratios (HSSR, HVSR, HVNR) were also calculated after rotating the NS and EW components of motion by steps of 10 degrees starting from 0° (north) to 180° (south). This approach, firstly applied to earthquake recordings in studying the directional effects due to topographic irregularities at Tarzana, California (Spudich *et al.*, 1996), has also widely adopted, for similar purposes, using ambient noise signals (Del Gaudio *et al.*, 2008; Burjànek *et al.*, 2010; Panzera *et al.*, 2011a)

A direct estimate of the polarization angle, for both earthquakes and noise data, was achieved by using the covariance matrix method (Jurkevics, 1988). This technique is very efficient in overcoming the bias linked to the denominator behavior that could occur in the H/V's technique, and it is based on the evaluation of eigenvectors (u_1; u_2; u_3) and eigenvalues (λ_1; λ_2; λ_3) of the covariance matrix

obtained by three-component seismograms. Parameters describing the characteristics of the particle motion (rectilinearity L; azimuth A; incidence angle I; instantaneous horizontal to vertical ratio HV) are extracted using the attributes from the principal axes. In particular, the degree of rectilinearity is defined as:

$$L = 1 - \left(\frac{\lambda_2 + \lambda_3}{2\lambda_1}\right)$$

and it is equal to unity for pure body waves and zero for spherical waves. The azimuth of a wave can be estimated by:

$$A = \tan^{-1}\left(\frac{u_{21}(sign\mathrm{u}_{11})}{u_{31}(sign\mathrm{u}_{11})}\right)$$

where u_{j1} j=1, 2, 3 are the three direction cosines of eigenvector u_1 and the *sign* function is introduced to resolve the ambiguity of taking the positive vertical component of u_1. The apparent incidence angle of rectilinear motion may be obtained from the corresponding direction cosine of u_1:

$$I = \cos^{-1}|u_{11}|.$$

The polarization was calculated by running a moving window of 1 s with 20% overlap, using the whole noise record and, as concerns the earthquake records, by considering the signals from the P waves onset up to the late coda waves.

6.4. Results and discussion

The results coming out from HSSR, HVSR and VSSR analysis are shown in **Fig. 6.3**. The role of different window length was tested performing the spectral analysis using three different time windows (10, 20 and 30 s). It is interesting to note that the obtained results do not change significantly, the largest variation being observed in their standard deviations. In particular, at low frequencies the standard deviations show a tendency to diminish with increasing window length. This effect could be explained as a consequence of the low signal to noise ratio at frequencies closer to the lower limit of the analyzed frequency range, especially for small magnitude events. Therefore, long windows of signal may allow more stable spectral amplitudes of stationary low-frequency noise, therefore reducing the standard deviation. The test shows that if a 20 s window is used, a good

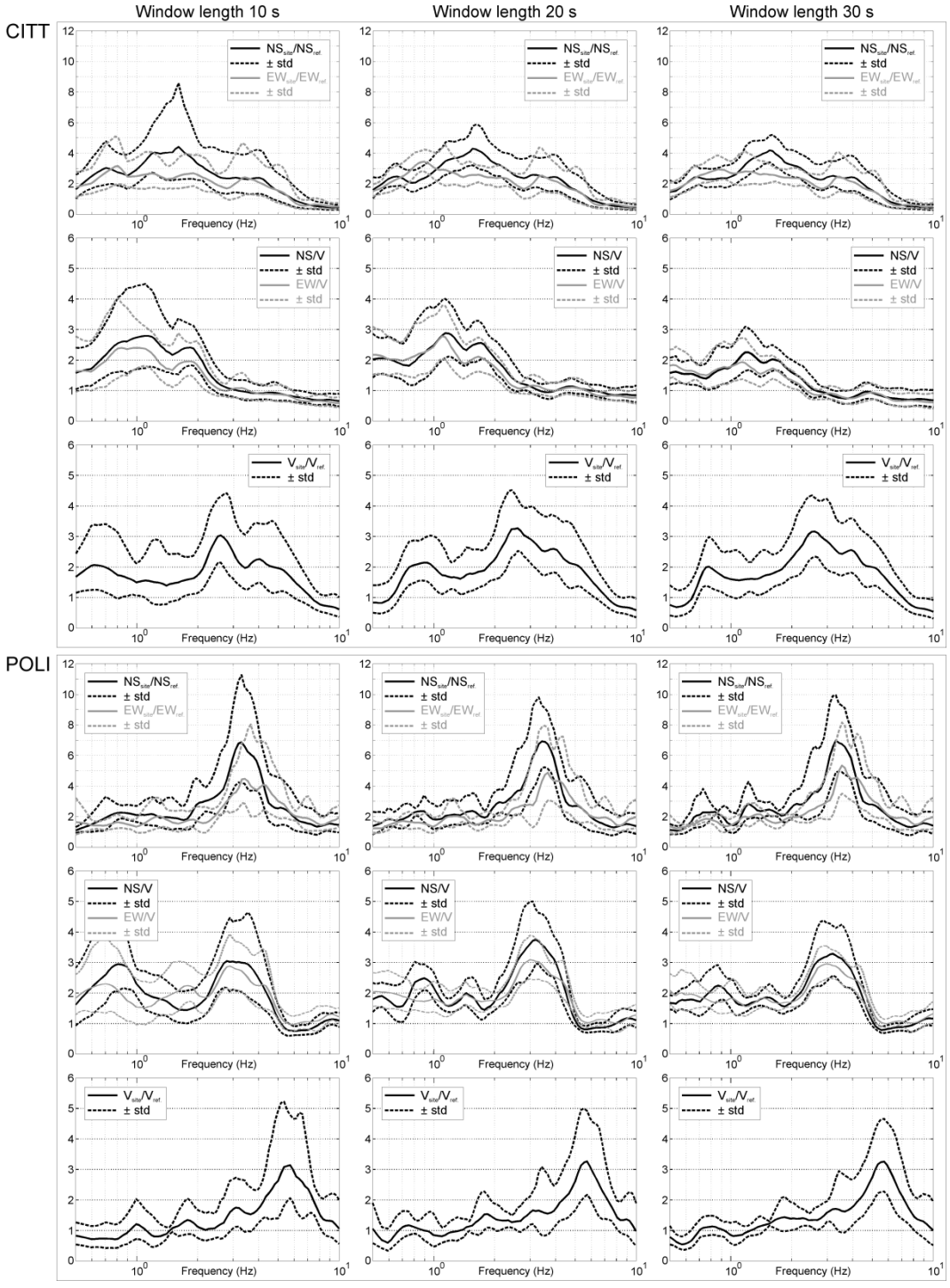

Fig. 6.3. *Spectral ratios (HSSR, HVSR and VSSR) at each permanent station (CITT upper panels, POLI lower panels), computed for 10 s, 20 s and 30 s time windows length.*

stability of spectral ratios, especially at low-frequency, is achieved. So that for further analysis in this study was adopted such window length.

Inspection of the HSSR (**Fig. 6.3**) points out that at the station CITT less pronounced spectral ratio peaks are observed with respect to the station POLI. At CITT, the horizontal standard spectral ratio do not show pronounced peaks, but a broad band of amplification, in the range 0.5-5.0 Hz, reaching 4 and 3 units in the NS and EW component of motion, respectively. At POLI, the HSSR highlights pronounced spectral ratio peaks, in the frequency band 2.0-5.0 Hz, with greater amplitude (about 7 units) in the NS component.

The spectral ratio amplitude obtained through the HVSR method appears underestimated in amplitude with respect to those obtained through the HSSR approach, however, especially at POLI, a good agreement between the two methodology is observed concerning the frequency range of the dominant peaks (**Fig. 6.3**). Moreover, it is interesting to observe that CITT and POLI stations show a flat spectral ratio peaks, with HVSR amplitude going down to values lower than 1 units at frequencies higher than about 3.0 and 5.0 Hz, respectively (**Fig. 6.3**). This appears related to the presence of a significant amplification of the vertical component of motion, as it can be observed in the V/V_{ref} plots (**Fig. 6.3**). Such an effect could be explained in terms of the complexity of the near-surface morphology and the existence of pronounced stratigraphic heterogeneities that, as postulated by many authors (Chavez-Garcia *et al.*, 1996; Raptakis *et al.*, 1998; Raptakis *et al.*, 2000; Bindi *et al.*, 2009), may affect the vertical component of motion. The presence of a complex morphologic and lithologic setting in the Catania area and, in the S. Sofia hill in particular, was indeed set into evidence in several studies (Lombardo *et al.*, 2001; Lombardo and Rigano, 2007; Panzera *et al.*, 2011b). Present results therefore, point out that major differences in the shape of HSSR and HVSR at both stations, occur in the higher frequencies portion of the spectral ratios. Such observations, as suggested by Parolai and Richwalski (2004) can be interpreted as due to both the influence of the incidence angle and the *S*-to-*P* waves conversion which imply amplification of the vertical component in the *S*-wave window analyzed and deamplification in the HVSR. Moreover, it has to be remembered that POLI is located along the slope of the hill whereas CITT is located on the top. The results obtain are therefore in contrast with

usually expected effects of amplification at the top of a hill. This behavior, in my opinion, could be related to the gentle slope of the S. Sofia hill. In such conditions the reflection angle between the direction perpendicular to the free surface topography and the upward propagating wavefront is smaller than in the case of a steep slope. Therefore, the focusing effects at the crest are shadowed by laterally propagating waves (Boore, 1973) and it is reasonable to observe only moderate amplifications at the top of the hill. Moreover, it must be remembered that POLI is set up on the sedimentary terrains whereas CITT is settled down on a compact lava flow. Such lithotype generally do not show significant spectral ratio peaks as already observed in studies concerning the local seismic response in the Catania area (Lombardo *et al.*, 2001; Lombardo and Rigano, 2007; Panzera *et al.*, 2011b).

Ambient noise was recorded, in different lithotypes, alongside the slopes of the hill at decreasing height from the top (**Fig. 6.1**), to remark possible topographical effects. The HVNRs show flat and, at times, deamplificated spectral ratios in several recording sites (#8, #9, #10, #11, #12, #13, #14, #15, #16, #18, #22, #26, #27, #28) where the local geology consists in a sequence of thick (10-20 m) massive lava flows that overlay the sand and coarse gravel sediments laying on the marly clay basement (**Fig. 6.4a**). Conversely, when the sedimentary terrains outcrop (#3, #4, #5, #6, #21, #23), significant spectral ratio peaks, are observed (**Fig. 6.4b**). Results obtained by the HVNR confirm the findings coming out from earthquake data analysis and set into evidence that the geological setting is more complex than a simple 1-D layered structure, for which the noise spectral ratio method was originally proposed. The presence of lava flows at the surface imply the existence of possible velocity inversions that gives origin to H/V spectral amplitude lower than one unit (Di Giacomo *et al.*, 2005; Castellaro and Mulargia, 2009) and the existence of amplification in the vertical component of the ground motion. The influence of lava thickness on the amplitude of HVNR peaks is also set into evidence by the results shown at sites #1, #2, #8 and #28 (**Fig. 6.5**), where the amplitude of spectral ratio peaks decreases as the thickness of the lava flow increases going from its boundaries to the inner part (top of the hill). A detailed study of lava thickness at S. Sofia hill was performed, using borehole data, by

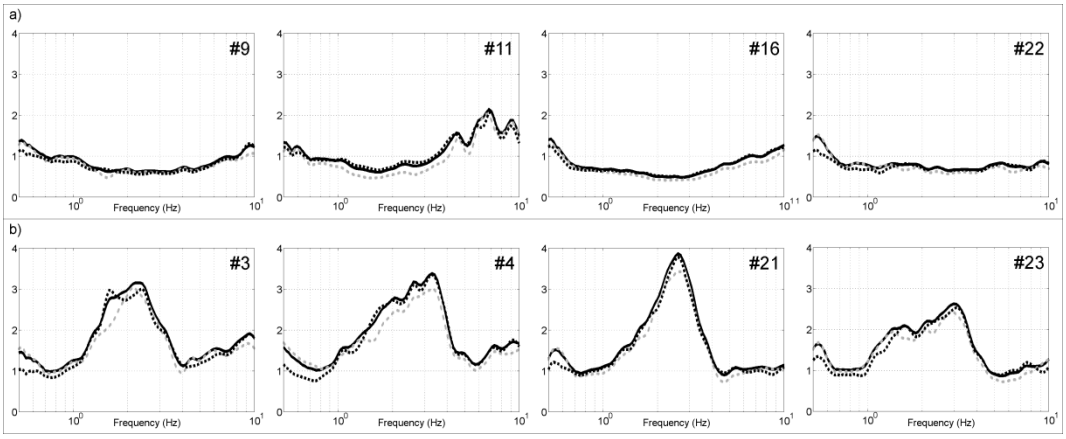

Fig. 6.4. *Examples of HVNR results at representative recording sites located on lava flows (a) and on sedimentary terrains (b); solid black lines refer to the average H/V spectra, dotted grey and black lines refers to NS/V and EW/V spectra, respectively.*

Lombardo and Rigano (2007). Besides the complex lithologic setting so far described, the presence of sedimentary terrains having a modest velocity contrast could significantly affect the shape of H/V amplitude (Fäh *et al.*, 2001). In some instances (#7, #17, #19, #20, #24, #25), no significant dominant peaks are indeed found (**Fig. 6.6**). This behavior, was already observed in the Catania area (Lombardo *et al.*, 2001) and it was ascribed to a fair velocity contrast between the sandy clay with coarse gravel layers and the marly clay basement. In the same figure are also depicted the results obtained on the marly clay (#17, #20) outcropping in the southern part of the study area that, as expected for a bedrock formation, show flat HVNRs.

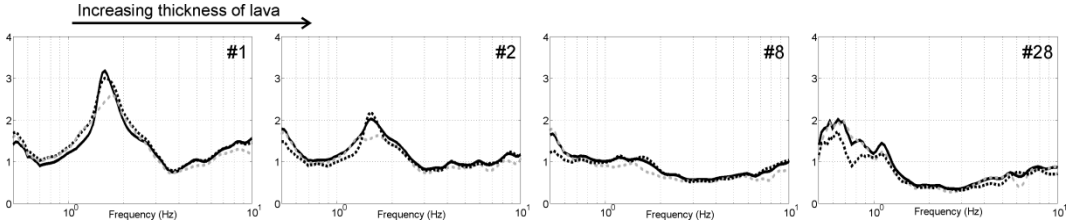

Fig. 6.5. *Amplitude of HVNR peaks as observed in sites located on different thickness of lava layers.*

In **Fig. 6.7** the HVNRs obtained from 30 minutes of the pre-event ambient noise, recorded at the stations POLI and CITT, are plotted together with the HVNRs from the measurements performed at the two mobile stations (#5 and

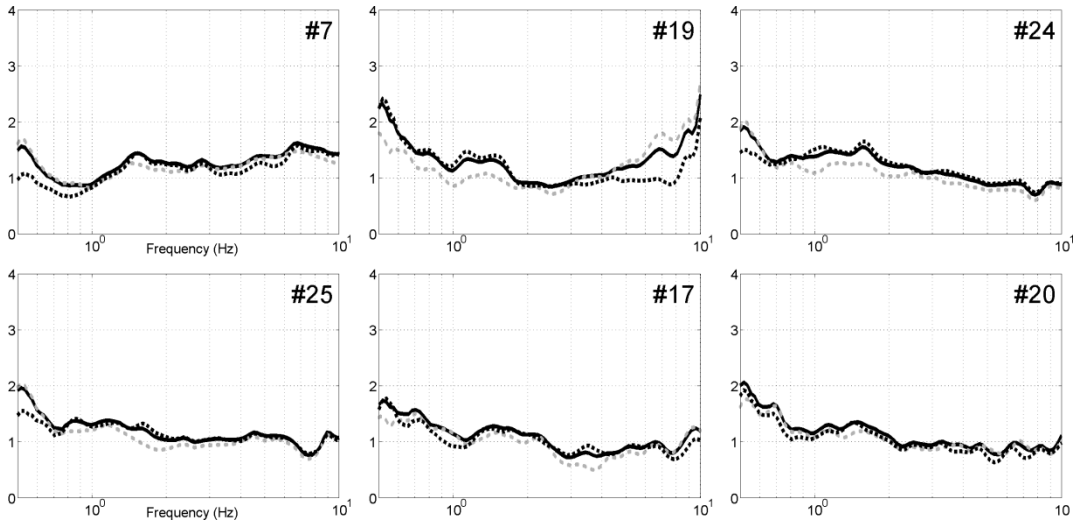

Fig. 6.6. *Examples of HVNR results at some recording sites located on sedimentary terrains having a low velocity contrast with respect to the clayey basement.*

#28, respectively) close to the permanent ones. It appear quite evident that both noise recordings, acquired with different instruments, show similar results. Such comparison allows us to assert that the significant differences in amplitude, sometimes observed between earthquake and noise data, cannot be ascribed to the use of different instruments but to the peculiarities of the noise and earthquake wavefields. Bonnefoy-Claudet *et al.* (2008) have indeed observed, by modeling the ambient noise wavefield, that HVNR peaks amplitude depends on the relative contribution of different types of seismic waves (body and surface waves) and on

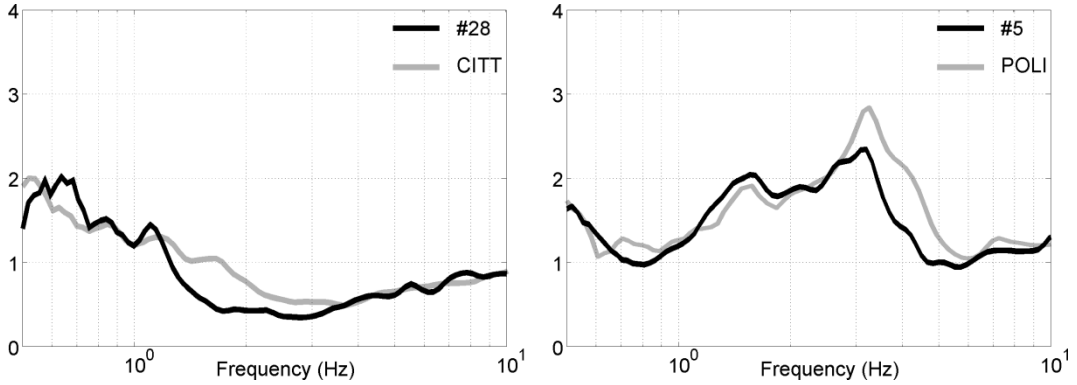

Fig. 6.7. *Comparison of the HVNR from pre-event at the two permanent stations with those obtained from records of mobile stations located at the same sites.*

the impedance contrast between sediment and bedrock. Consequently only an indirect correlation between the HVNR peak amplitude and the site amplification may exist and it is possible an underestimation of the amplitude with respect to the SSR techniques.

The experimental SSR, HVSR and HVNR at the two permanent seismic stations were compared with those obtained by modeling the site response to explain the observed spectral features from a lithologic point of view (**Fig. 6.8**).

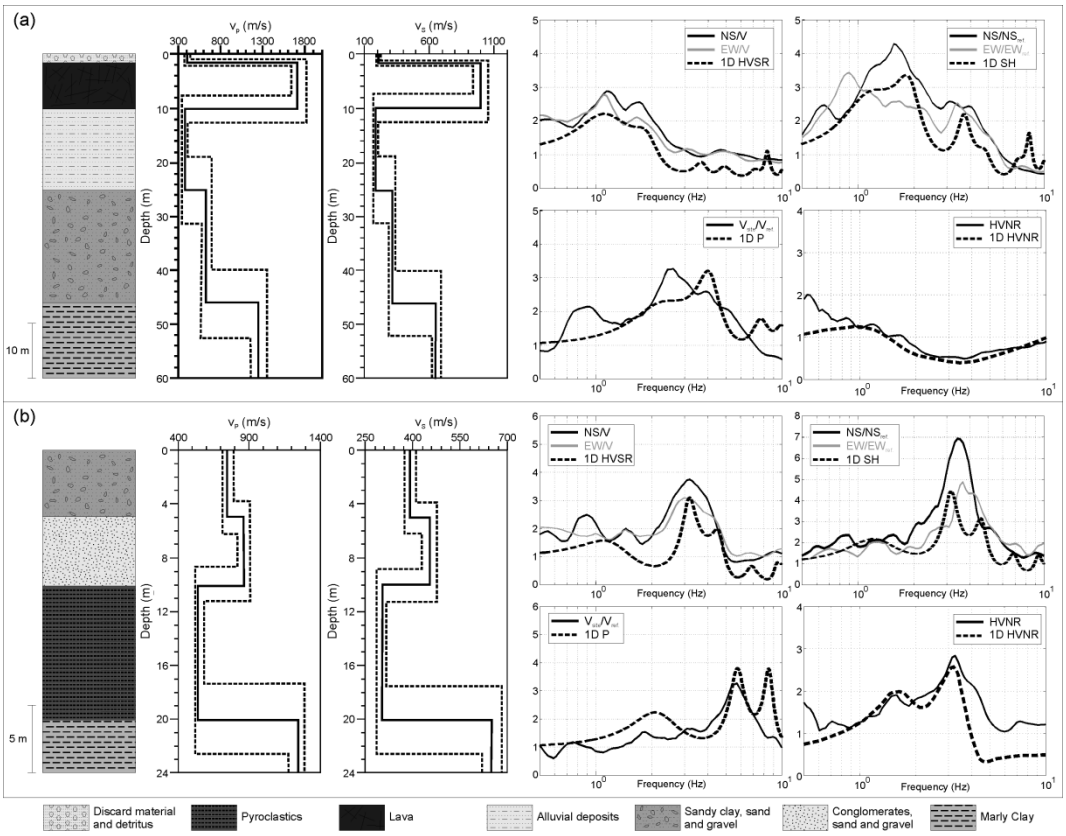

Fig. 6.8. *Stratigraphic sequences, velocity profiles and comparison of experimental spectral ratios with 1D theoretical modeling at CITT (a) and POLI (b) stations.*

The initial model of body wave velocities and layers thickness was perturbed by 5% and 25% respectively, to obtain a good fit with the experimental results. Despite the use of a simple 1D model, the theoretical results are in good agreement with the experimental techniques. At CITT (**Fig. 6.8a**), the theoretical modeling fit quite well the experimental results. The differences that can be observed between the SSR, HVSR and HVNR could be explained in terms of the

velocity inversion linked to the presence of the lava layer, which determines the differences in composition and propagation between the earthquakes and the noise wavefield (Di Giacomo et al., 2005; Castellaro and Mulargia, 2009). A quite good fit is also obtained at POLI (**Fig. 6.8b**). The differences observed in amplitude and shape between SSR, HVSR and HVNR may be attributed to the presence a velocity inversion at depth of about 10 m due to a low velocity layer of pyroclastics.

Although a good fitting between models and experimental data is in general observed, some differences in the spectral ratio shape are present. They could be related to the use of a simplified layer model, which is based on elastic properties valid on a large scale for the Catania area, and to the presence of directional effects as pointed out by the different spectral ratio shape of NS and EW components of motion.

To recognize the existence of directional amplifications, the horizontal components of each spectral ratio (HVSR, HSSR and HVNR) obtained at the two permanent stations, were rotated by steps of 10° starting from 0°N to 180°N (**Fig. 6.9**) and a direct estimate of the polarization angle in the time domain was performed as well (**Fig. 6.10**). The results obtained from the earthquakes data (**Fig. 6.9**) show, at the two stations, peaks in the frequency range 1.0 – 5.0 Hz with a prevailing direction in the range N0° - 50° that is more evident, both in frequency and amplitude, at POLI with respect to CITT which is located at the top of the hill. This directional effect is evident in both HVSR and HSSR, so that the influence of the reference site (UNIV) in the estimate of rotated HSSR appears negligible. The results obtained from the analysis of the pre-event ambient noise (HVNR in **Fig. 6.9**) appear comparable at the station POLI whereas at CITT not clear effects can be observed.

Inspection of the hodograms obtained in the frequency range 1.0 - 10.0 Hz (**Fig. 6.10**), confirms the evidences observed through directional analysis of the HVSR, HSSR and HVNR. Evidence of a less pronounced directivity effect at CITT are indeed observed, whereas clear polarization effects (at about 40°) appear at POLI. Such behavior is still observed in the hodograms obtained from the

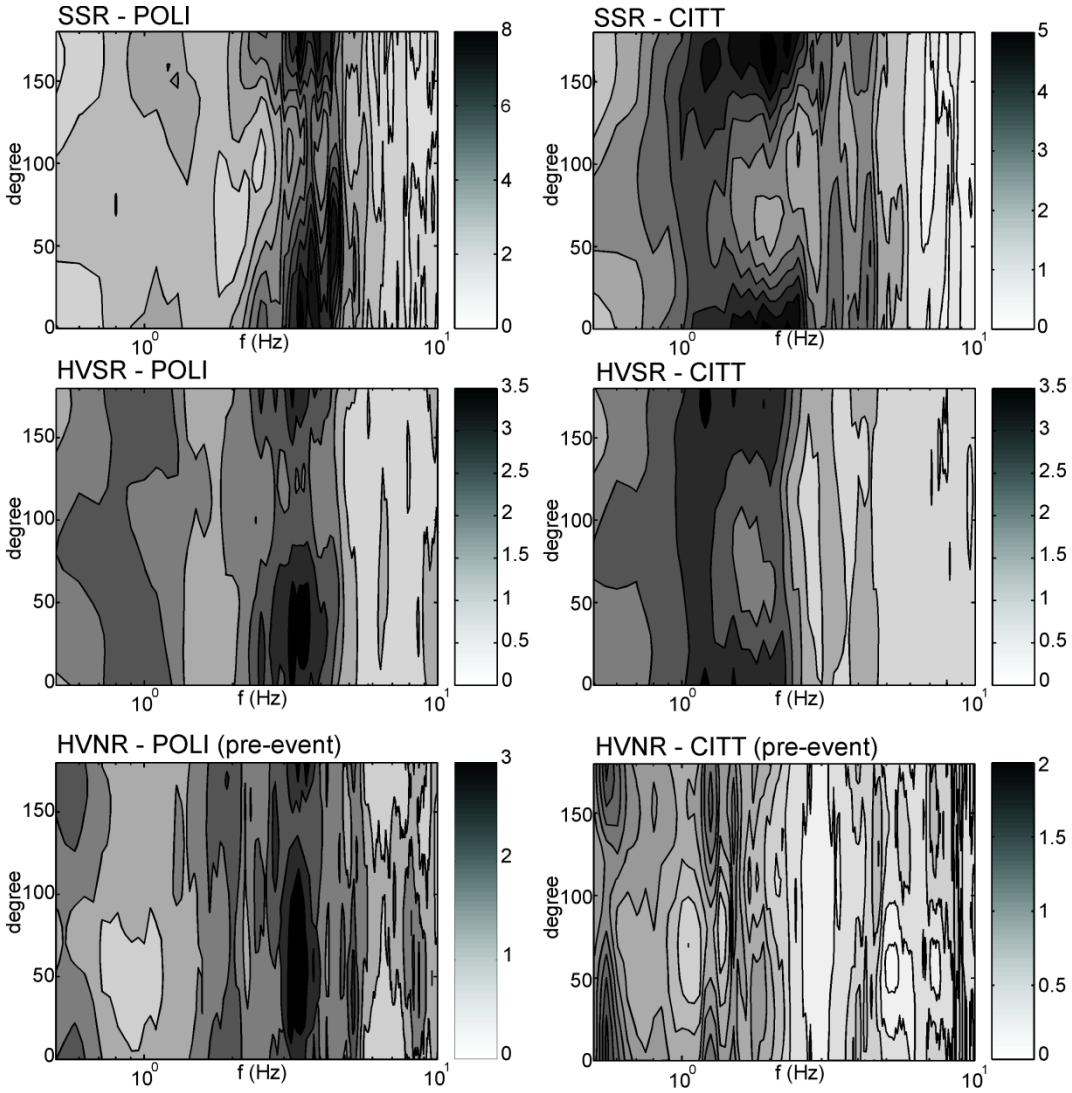

Fig. 6.9. *Contours of the geometric mean of the spectral ratios as a function of frequency (x axis) and direction of motion (y axis) for earthquakes and pre-event noise recorded at CITT and POLI.*

analysis of pre-event noise although, at POLI station, the rose diagram show greater (≈ 60°) azimuth values with respect to those obtained from the earthquake data. Slight differences between polarization angles obtained from the analysis of either earthquake or ambient noise data can be attributed to the contamination of the predominant direction of polarization by the isotropic distribution of the noise sources (Zheng and Stewart, 1992; Greenhalgh *et al.*, 2008). In **Fig. 6.10** the histograms of the occurrence (%) of the parameters describing the characteristics of the particle motion (rectilinearity *L*, incidence angle *I*, instantaneous horizontal to vertical ratio *HV*), are also reported. It appears evident that the plotted

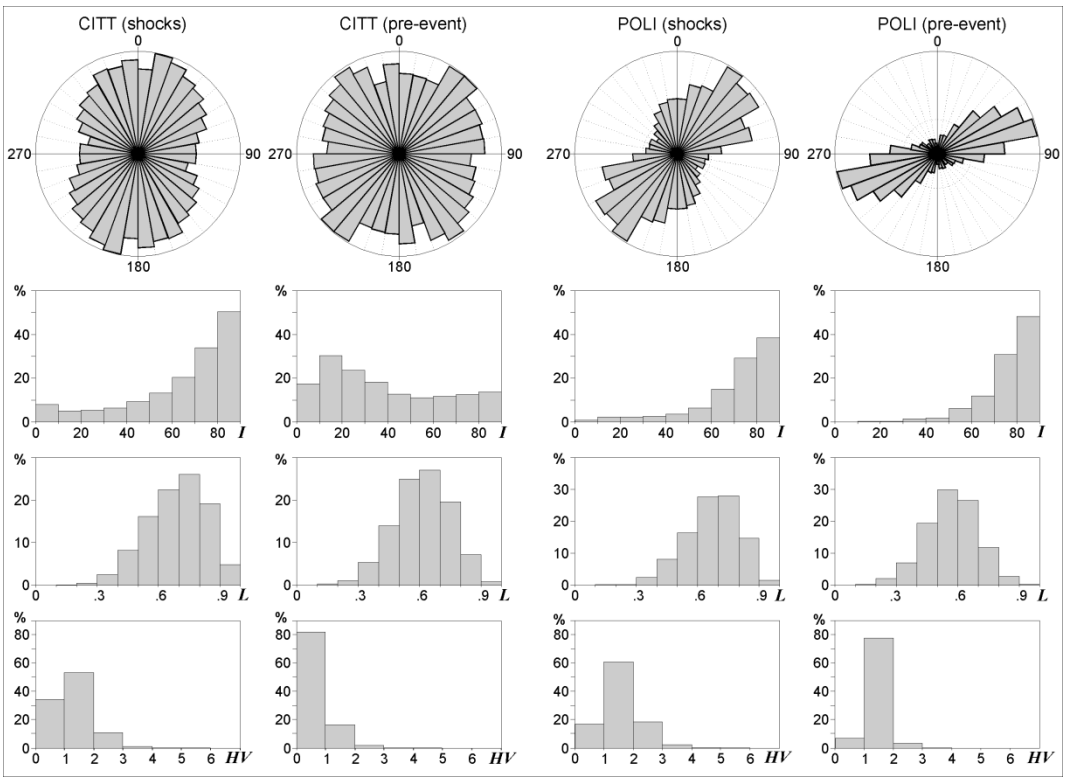

Fig. 6.10. *Rose diagrams and histograms of the particle motion parameters (incidence angle I, rectilinearity L and instantaneous horizontal to vertical ratio HV) for earthquakes and pre-event noise recorded at CITT and POLI.*

parameters show similar features at the two seismic stations, both for earthquake and pre-event noise. The only exceptions are observed in the *I* and *HV* values obtained from the analysis of pre-event noise at CITT, where a lack of any prevailing incidence *I* is observed, together with *HV* at prevailing values smaller than 1. This results are in good agreement with the observations coming from spectral ratio features (**Figs 6.3** and **6.4**), that pointed out a significant influence of the vertical component, particularly at the station CITT and in all measurement sites located on the lavas. The observed behavior, as already mentioned, could be interpreted in terms of the velocity inversion linked to the existence of a top rigid layer (basaltic lavas) overlaying the soft sedimentary terrains that imply the different features between the earthquake and the noise wavefields (Di Giacomo et al., 2005; Castellaro and Mulargia, 2009).

In order to verify that the directional effects observed at the two stations are

independent from back-azimuth, depth and distance from the source, the polarization parameters of three selected earthquakes (two local and one regional), are shown in **Fig. 6.11**. It is noteworthy to observe that the polarization azimuth during earthquakes is independent of the source position and it is well defined, at about 220° (equivalent to 40°+180°), at the station POLI with respect to CITT where it is more randomly distributed. Therefore, the observation of a persistent polarization direction, observed at POLI and a randomly distributed azimuth at CITT, using both noise and earthquakes, rules out a source effect and suggests a dependence of polarization on local properties of the site. It is also important to note that the incidence angle (*I*) is less stable at CITT rather than at POLI where, a few seconds after the P onset, it become stable at about 70°. Such behavior affects the instantaneous *HV* at CITT as well since, it can be observed that when *I* assumes values lower than 70°, *HV* values become lower than 1, therefore confirming, also for earthquake data, the presence of waves having a pronounced vertical direction of motion. No particular differences are observed, at the two stations, as far as the rectilinearity values are concerned (**Fig. 6.11**). The polarization azimuth, as observed by several authors (Spudich *et al.*, 1996; LeBrun *et al.*, 1999; Pischiutta *et al.*, 2010; Panzera *et al.*, 2011a), usually shows maxima in a direction perpendicular to the main elongation of the considered hill, and are frequently concentrated on the crest top. The present study shows that more evident polarization effects take place on the flanks of the hill (station POLI) rather than on its crest. Such a peculiar result could be explained, not only as due to an incidence angle in a hill with a slight slope, but taking also into account the influence of geologic factors. In the S. Sofia hill, the available borehole information set into evidence that in some sites, the lower levels of the lava flows, laying on the sedimentary terrains, are mostly formed by fractured lava with presence of water. In such conditions, a low layer zone having a modest quality factor can be postulated. A strong vertical and lateral variation in attenuation, as observed by Spudich *et al.* (1996), causes a reduction of high-frequency energy and the presence of scattered waves. These waves could propagate along multiple fractures corridors and therefore can explain the absence

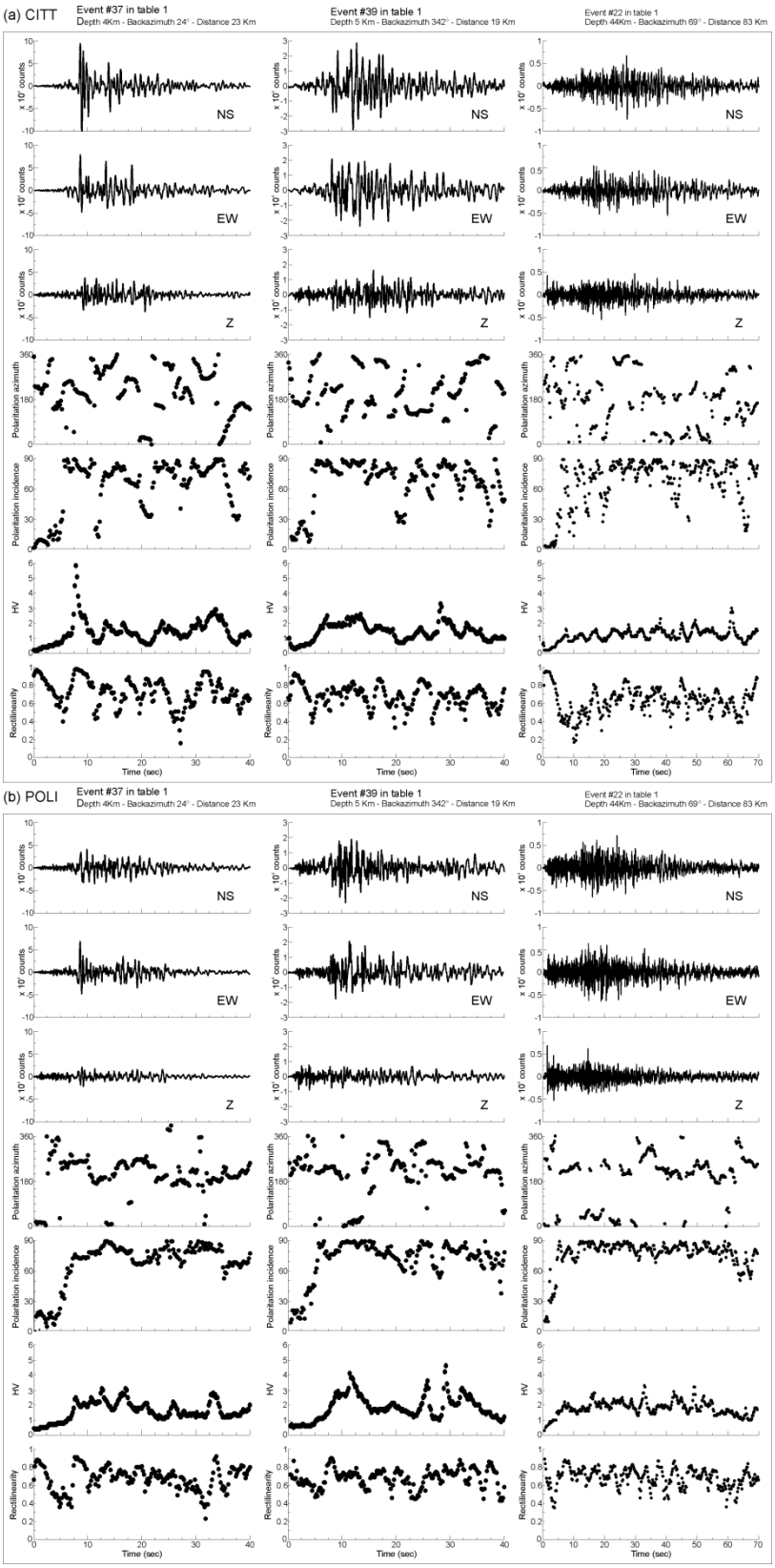

Fig. 6.11. *Examples of earthquakes recorded at CITT (a) and POLI (b) stations with instantaneous values of rectilinearity, polarization incidence, polarization azimuth and HV.*

of a clear polarization transversal to the hill at the crest. Such findings are not uncommon since the shear waves radiation can be deformed as a consequence of topographic irregularities and different wave propagation velocities in an anisotropic medium with cracks (Cary *et al.*, 2010).

Directional effects were further investigated, in the whole study are, through ambient noise records. The results obtained (see some examples in **Fig. 6.12**) confirm that the S. Sofia hill has not a simple 1D structure and it shows many oscillation modes making therefore not possible to find out a fundamental frequency of the study hill. The hodograms obtained from noise measurements, in

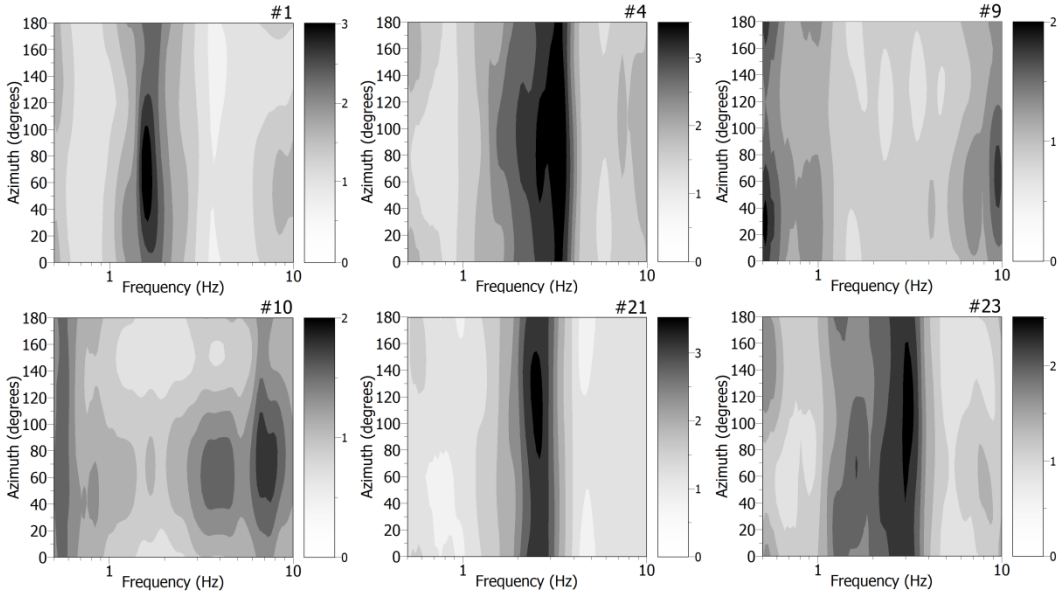

Fig. 6.12. *Examples of contours of the geometric mean of the spectral ratios as a function of frequency (x axis) and direction of motion (y axis) for noise measurements at some representative recording sites.*

the frequency range 1.0–10.0 Hz (**Fig. 6.13**), show that the polarization azimuths are similar to those obtained by processing the earthquake data. It appears indeed confirmed that at the top of the studied hill (#9, #12, #14 and #28) the pattern of polarization directions is similar to what observed at the station CITT. On the other hand, the noise rose diagrams obtained at the other recording sites point out polarization azimuths that seem to be in agreement with the slope directions of the hill flanks. Only few sites (#17, #21, #22, #25) make an exception to such a trend,

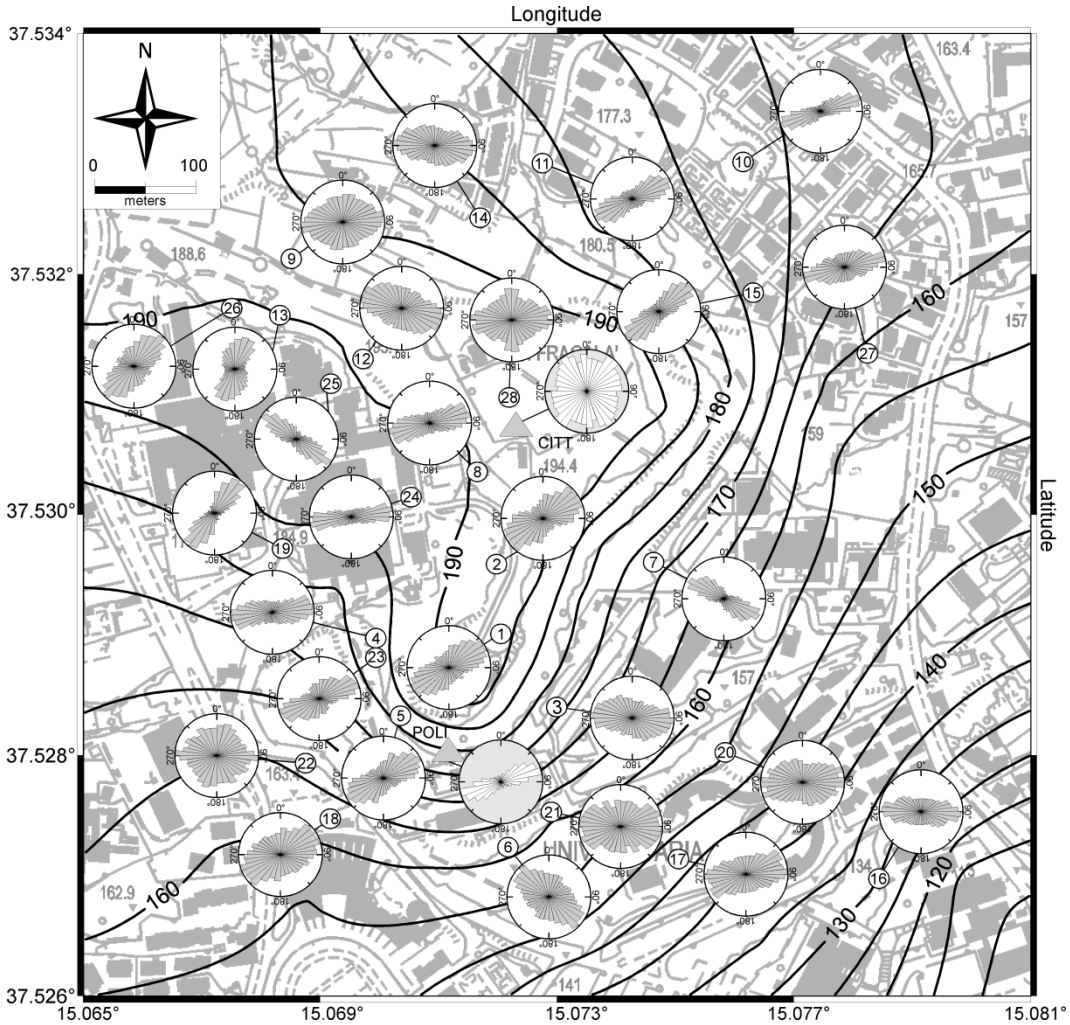

Fig. 6.13. *Rose diagrams from noise measurements in the S. Sofia hill area.*

showing a directional variability that cannot be easily interpreted. However, in my opinion, a possible explanation could be linked to the local shallow lithologic features since, in the study area, to reduce the hill slope, manmade terraces having variable thickness (2-10 m) were often build using massive block in sandy-clay matrix. As observed by Burjánek *et al.* (2010), the vibration of small blocks control high frequency ground motion implying both different resonant frequencies and directions.

In order to investigate on the influence of local geology and topographic setting of the study area on the noise wavefield, the features of the polarization parameters were analyzed in detail. In **Fig. 6.14** the percentage of time windows with polarization ellipsoids having high values of incidence angle (I≥45°),

instantaneous horizontal to vertical spectral ratio greater than one (HV≥1) and a high rectilinearity value (L≥0.5), are plotted, for each measurement site, on the geo-lithologic map. In this way all the windows not relevant for the definition of the azimuth in the horizontal plane were excluded. The maps obtained show that,

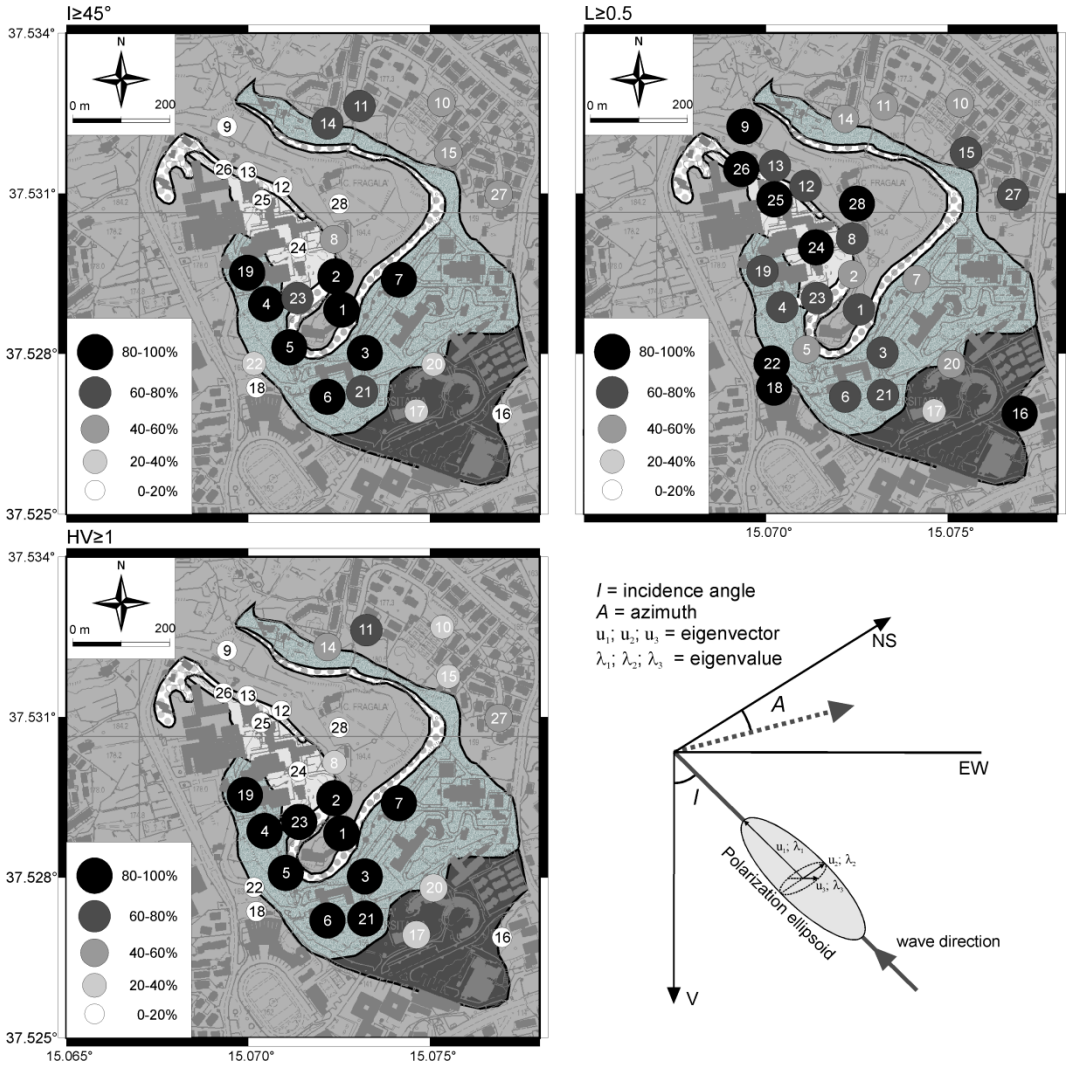

Fig. 6.14. *Geolithologic maps of the study area showing the values (%) of incidence angle I≥45°, rectilinearity L≥0.5 and instantaneous horizontal to vertical ratio HV ≥1. In the right lower corner a simplified sketch of the main polarization parameters is shown.*

besides the control of the topographic effects, a significant influence of the geo-lithologic features has to be taken into account. The results show that, as it is usually expected for ambient noise signals, all the measurement sites are characterized by high percentage of elliptical and rectilinear waves (L≥0.5 in **Fig.**

6.14). Moreover, it appears evident that the incidence angle and the horizontal to vertical spectral ratio (I≥45° and HV≥1 respectively, in **Fig. 6.14**), seem to be controlled by the surface geology. The higher percentage values were, indeed, observed along the hill slopes where the sedimentary terrains outcrop whereas, in the upper part of the hill and in all the measurement sites located on the lava flows, where a velocity inversion take place, their values attain a minimum.

Chapter VII

Evidence of topographic effects analysing ambient noise measurements

7.1. Issues of the chapter

Amplification of the ground motion in a topographic irregularity is generally linked to the focalization of seismic waves at its topmost part due to the existence of diffraction, reflection and conversion of the incident waves (Bard, 1982). The amplification effects at the topmost part of a hill are frequency dependent so that resonance phenomena occur when the wavelength of the incident wave is comparable to the horizontal dimension of the hill. Besides, the influence of the topography on ground motion is linked to the sharpness of the ridge crest (Géli *et al*., 1988; Bard and Riepl-Thomas, 1999). The upper part of a hill shows increasing resonant motion with respect to the whole of the structure. Such ground motion amplification mechanism taking place at ridge crests, is in principle similar to the well-known effects in the seismic design of buildings that therefore appears to apply at a larger scale to mountains, as well (Buech *et al*., 2010). Moreover, significant directional effects, transverse to the major axis of the ridge, are often observed (Spudich *et al.*, 1996).

Several analytical and numerical methods have been developed to study the interaction of incoming seismic waves with a hill shaped morphology (e.g. LeBrun *et al.*, 1999; Paolucci, 2002). On the other hand, experimental studies using earthquake instrumental records are relatively few and only in recent time data from small array start being commonly used (e.g. Buech *et al*., 2010; Pischiutta *et al.*, 2010). In a review article, Géli *et al.* (1988) point out that an important disagreement between observed and predicted amplification on a topographic feature often occurs. Several studies (Tucker *et al.,* 1984; *Catchings* and Lee, 1996; Steidl *et al.,* 1996; Bouchon and Barker, 1996) have shown that

this difference derives from the difficulty of adopting a reference station not significantly influenced by the topography itself. To resolve such difficulty for evaluating topographic site effects, studies of Spudich *et al.* (1996) and Chavez-Garcia *et al.* (1996 and 1997) propose the use of a non reference technique such as the earthquake horizontal-to-vertical spectral ratio (HVSR) and the generalized inversion scheme (GIS) method proposed by Andrews (1986) and Boatwright *et al.* (1991). Generally, the use of earthquake data has been shown to be a successful tool for the evaluation of topographic effects. However, artificial explosions and ambient noise records, processed with the horizontal to vertical noise ratio (HVNR) technique (Nakamura, 1989), can be a helpful alternative seismic input as supported by several studies (e.g. Borcherdt, 1970; LeBrun *et al.*, 1999; Poppeliers and Pavlis, 2002; Pagliaroli *et al.*, 2007].

The aim of this experiment was to estimate the seismic response in the area of downtown Syracuse (Sicily) and to test the reliability of ambient noise recordings, processed through HVNR techniques, to estimate topographic effects. Ambient noise has become in recent years widespread used for site amplification studies. Its use appear opportune for significant reductions in field data acquisition time and costs. The evaluation of site response using HVNR's technique is largely adopted since it requires only one mobile seismic station with no additional measurements at rock sites for comparison. Besides, it does not require the long and simultaneous deployment of several instruments to collect an useful data set of earthquake. The basic hypothesis of using ambient noise is that the resonance of a soft layer corresponds to the fundamental mode of Rayleigh waves, which is associated with an inversion of the direction of Rayleigh waves rotation (Nogoshi and Igarashi, 1970; Lachet and Bard, 1994). Thus, the ratio between the horizontal and vertical spectral components of motion can reveal the fundamental resonance frequency of the site. Reliability of such approach has been asserted by many authors (e.g. Lermo and Chavez-Garcıa, 1993; Duval, 1994; Bard, 1999) who have stressed its significant stability in local seismic response estimates and the reliaility of the H/V spectral ratio in estimating the fundamental frequency peak (Cara *et al*., 2003). Recently the use of HVNR methodologies was adopted for

investigating topographic effects, producing rather satisfactory results (Lermo and Chavez-Garcìa, 1993; Pagliaroli *et al.*, 2007), although no clear theoretical explanation was provided. A possible explanation could be that, contrary to alluvial deposits, the basic composition of the wave field is the same for earthquake and noise ground motion. There is, indeed, no reason to have Rayleigh waves due to the topography in the wave field of the noise and it has to be remembered that the topographic effect is much higher in the horizontal component of motion rather than in the vertical one (LeBrun *et al.*, 1999).

7.2. Geology of the Study Area

The study area (Ortigia peninsula) is located in the south-eastern coast of Sicily (southern Italy), in downtown Syracuse. It is elongated in the N-S direction, reaching a length of about 1500 m, with a maximum height of 30 m a.s.l. and its A-B transverse section has a width of about 700 m (**Fig. 7.1**).

In the Syracuse area, as previously described, the substratum is characterized by a Meso-Cenozoic carbonate sequence with interbedded volcanic levels (Grasso and Lentini, 1982) and the Cretaceous volcanics represent the deepest formation having a thickness of about 500 meters (Tortorici, 2000). Such formation is unconformably overlain by sub-horizontal carbonate sequences that are distinguished in two main units known in the literature as Mount Climiti and Mount Carruba formations, the latter outcropping in the Ortigia area (**Fig. 7.1**).

7.3. Experimental Setup

The dynamic site properties and, in particular, the shear wave velocity in the upper 30 m ($V_{(S, 30)}$) of the carbonate sequences were investigated through non-invasive techniques such as the Multichannel Analysis of Surface Waves (MASW) (Park *et al.*, 1999) and Refraction Microtremor (ReMi) (Louie, 2001). The combined use of both techniques permit to compare and check the obtained results going also all over the limitations of each methodology. In the MASW technique, being an active source method, it is generally difficult to generate low frequency waves. For this reason, the passive source method (ReMi), which make

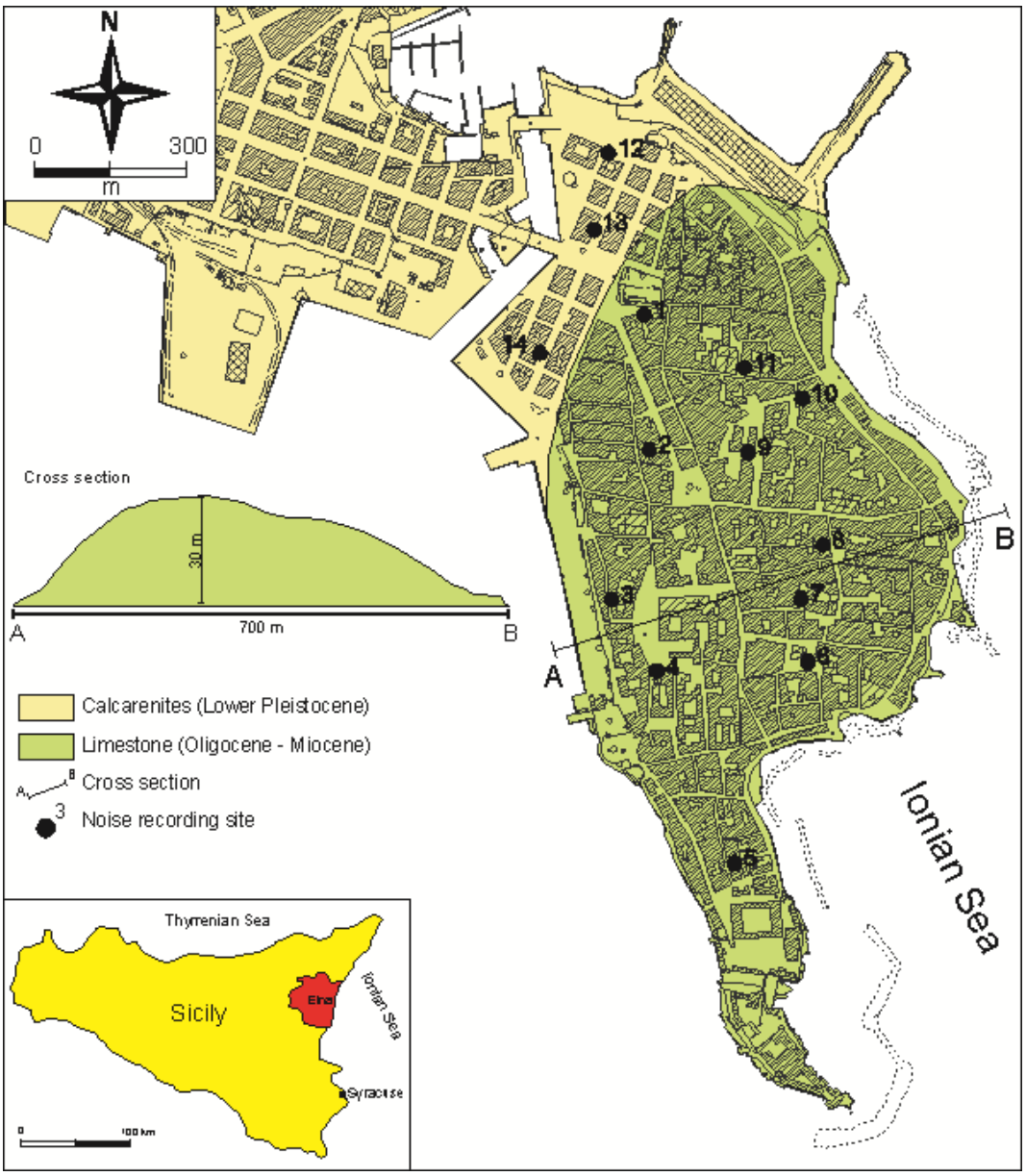

Fig. 7.1. *Geolithologic map of downtown Syracuse.*

use of microtremors and microseisms, therefore producing an input signal having a wide range of frequencies, was adopted as well. However, special care must be used in processing ReMi data because the presence of a omni-directional source may lead to the estimation of apparent S waves velocities not coincident with real shear wave velocity (Louie, 2001). On the other hand, in the MASW test, a suitable location of the seismic source together with an appropriate choice of the spacing between the receivers is needed. The offset of the source and the length of

the linear array itself, affects the largest reliable wavelength in the measurements (near field effects), whereas the receiver spacing and the sampling rate affect the smallest reliable wavelength in the test (Park *et al.*, 1999).

In the study area MASW tests were performed using a 12-channel seismograph and 4.5 Hz geophones. A linear array (**Fig. 7.2a**) having a length of 48 m was deployed with a 4 m interval pitch between sensors. Tests were made using a hammer source of 8 Kg, with a fixed offset distance of 8 m, recording five shots to reduce the possible interference with other sources in the vicinity, with a registration length of 3 s and sample rate of 512 Hz.

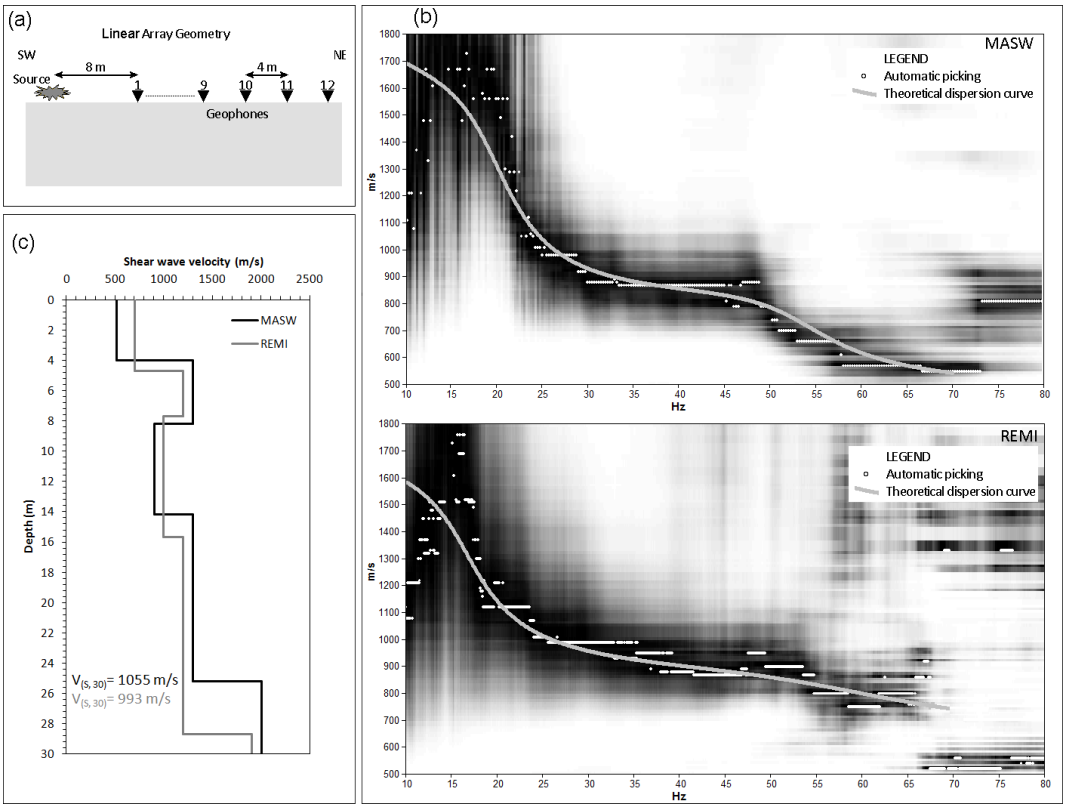

Fig. 7.2. *(a) Schematic configuration of the MASW and ReMi prospecting. (b) Phase velocity spectrum and theoretical dispersion curve. (c) Shear wave velocity-depth profile from the inversion of MASW and ReMi measurements.*

The same linear array was used for the ReMi measurements, recording 5 minutes of noise. Time windows of 10 s were considered to calculate dispersion curves of the fundamental mode and the average of the dispersion curves was

computed, excluding those not showing a clear dispersion or in which higher modes were dominant.

A $V_{(S, 30)}$ of about 1000 m/s, that is in good agreement with an A soil category, as shown by the Italian building code, was obtained as a result of both techniques (**Fig. 7.2b and 7.2c**).

7.4. Methodology

In this study ambient noise was recorded in fourteen sites (**Fig. 7.1**) using Tromino (www.tromino.it), a compact 3-component velocimeter with a quite reliable instrumental response in the frequency range 0.5-10 Hz. Time series, 30 minutes long, were recorded using a sampling rate of 128 Hz. The signals were processed evaluating spectral ratio through the HVNR technique. According to the guidelines suggested by the European SESAME (Site EffectS assessment using AMbient Excitations) project (SESAME, 2004), time windows of 30 s were considered, selecting the most stationary part and not including transients associated to very close sources. Fourier spectra were calculated and smoothed using a triangular average on frequency intervals of ± 5% of the central frequency.

HVNRs were also calculated after rotating the NS and EW components of motion by steps of 10 degrees from 0° (north) to 180° (south) and the contours of such spectral ratios amplitude were plotted as a function of frequency and direction of motion. This approach is powerful in enhancing, if any, the occurrence of site specific directional effects. It was first applied to earthquake data by Spudich *et al.* (1996) to study the directional resonance due to a topographic irregularity at Tarzana, California. A similar procedure was used for ambient noise signals by Del Gaudio *et al.* (2008) and Burjánek *et al.* (2009) for the identification of site response directivity in presence of a slope. A direct estimate of the polarization angle, for noise data, was achieved by using the method proposed by Jurkevics (1988). This technique is very efficient in overcoming the bias linked to the denominator behavior that could occur in the HVNR's technique. Polarization analysis makes full use of the three component vector field to characterize the particle motion and it is based on the evaluation of

eigenvectors and eigenvalues of the covariance matrix obtained by three-component seismograms. Signals at each site were band-pass filtered using the whole recordings and considering a moving window of 1 s with 20% overlap, therefore obtaining the strike of maximum polarization for each moving time windows.

7.5. Results and discussion

The HVNRs were computed dividing by the vertical component of motion (V) the NS and the EW components, separately (**Fig. 7.3**). It appears evident that the EW/V spectral ratios are more pronounced in amplitude than the NS/V ones, especially in the range 1.0-3.0 Hz.

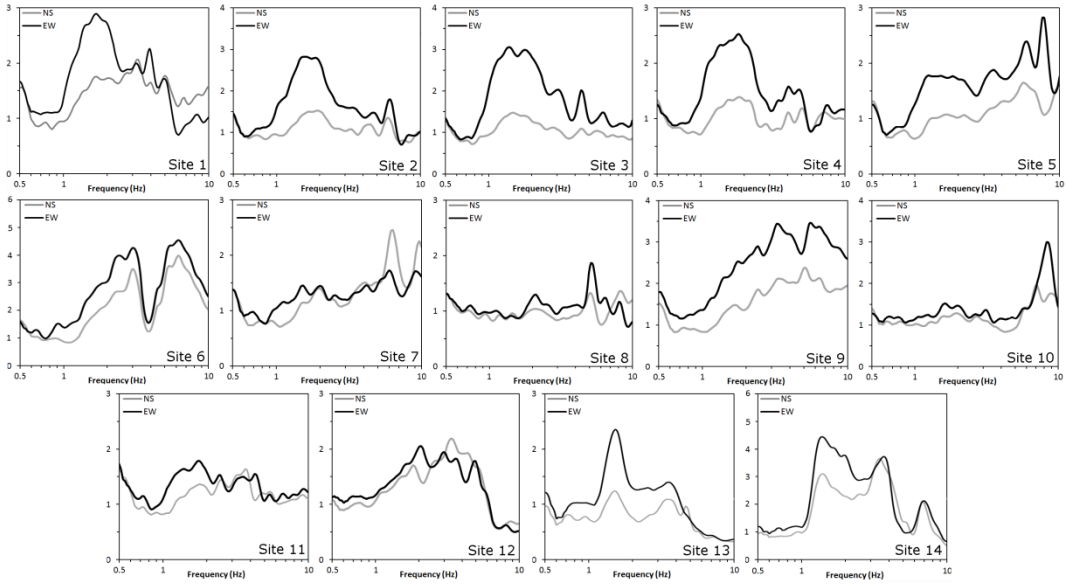

Fig. 7.3. *Spectral ratios (HVNR) obtained from ambient noise measurements performed in the Ortigia peninsula.*

In **Figure 7.4**, a direct comparison of the rotated HVNRs and the results of noise polarization analysis is shown for all recording sites. Both methodologies agree indicating, particularly in the frequency range 1.0-3.0 Hz, that maxima of HVNR amplitudes take place at 90-100° and maxima of the horizontal polarization strike in E-W direction. Spectral ratio peaks that can be observed in the frequency range 3.5-10 Hz (**Fig. 7.3**) show a more complex pattern of

directional effects. In **Figure 7.4**, for instance, a strong NW-SE directionality (site 1), as well as a N-S direction (sites 7 and 12) and a N-S direction together with a E-W one (site 8) are evident. Such high frequency directional variability cannot be easily interpreted. In my opinion a possible explanation could be linked to local shallow lithologic features. As observed by Burjánek *et al.* (2010), high frequency ground motion can, indeed, be controlled by the vibration of smaller blocks that imply both different resonant frequencies and directions.

Field data observations were compared with the theoretical resonance frequency (f_0) expected for the topographic effects in Ortigia hill. So that, the relationship $f_0 = Vs/L$, where L is the width of the hill (about 700 m) and Vs is the shear wave velocity of the limestone outcropping in the peninsula (1000 m/s) (Bouchon, 1973; Géli *et al*., 1988), was adopted. The predicted value, f_0 = 1.4 Hz, is consistent with the observed spectral peaks, in the range of 1.0-3.0 Hz.

In general, the amplification of ground motion connected to the surface topography is directly related to the sharpness of the topography (Bard, 1994). In such instances topographic effects become clearly detectable with experimental and numerical approaches. In present study, the gentle topography and the homogeneous lithology of the Ortigia peninsula make it an ideal and simple case study for investigating topographic effects using ambient noise records. The Ortigia hill has a natural frequency of about 1.4 Hz and shows an E-W preferential direction of vibration. The specific directional effects in ambient noise, well defined both in space and in a narrow frequency band (1.0-3.0 Hz), are signs of a normal mode of vibration of the hill (Roten *et al*., 2006).

It seems important to set into evidence that reliability of ambient noise records for studying topographic effects is supported by the concept that in a natural hill the horizontal component of the ground motion show an amplitude greater than the vertical one (LeBrun *et al.*, 1999). This behaviour is similar to what observed in civil structures providing that there is not significant soil–structure interaction and considering the building as a single-degree of freedom damped oscillator. In such instances the vertical component of motion travels through the building without amplification, whereas the horizontal components undergo a significant

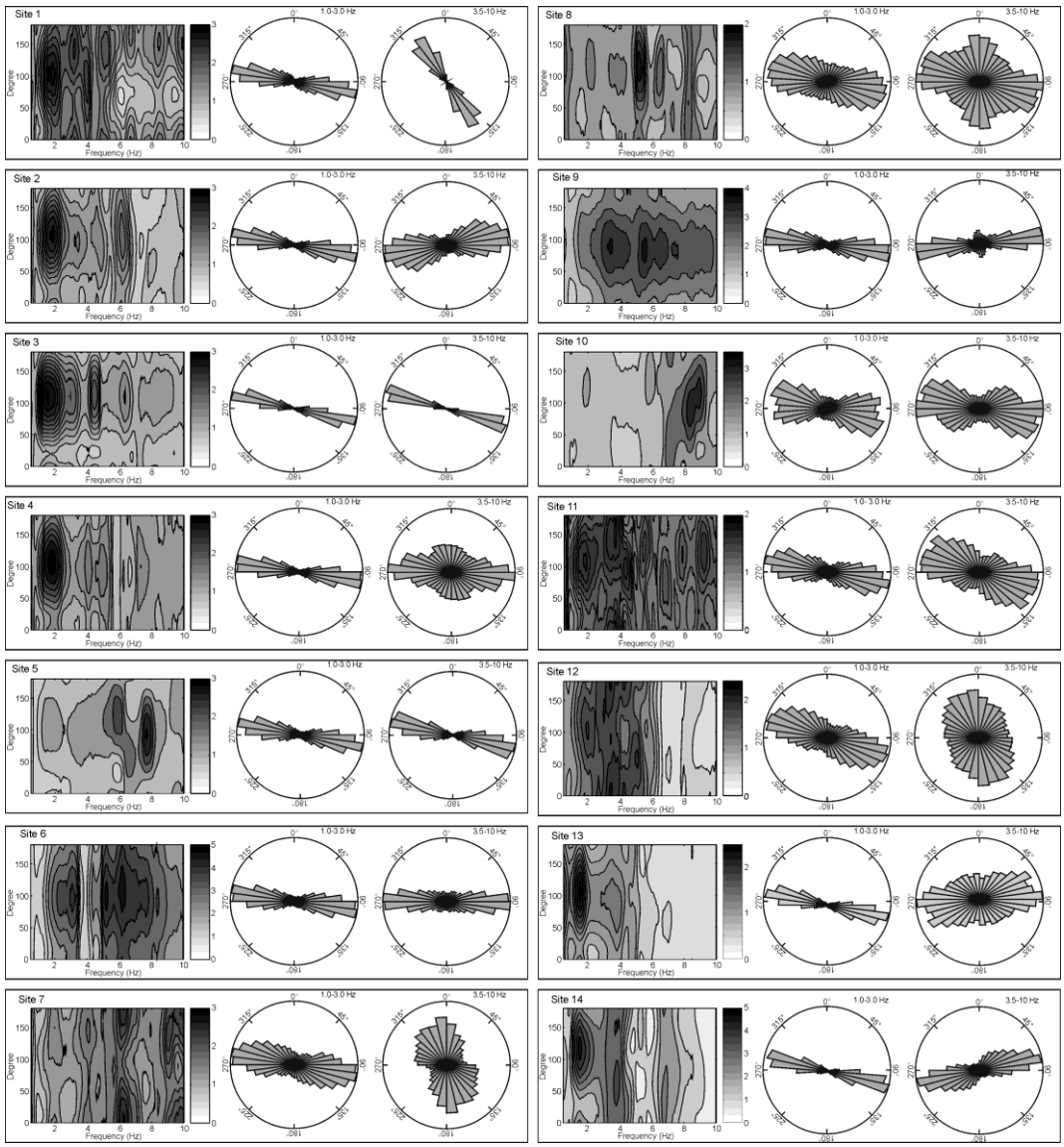

Fig. 7.4. *Contours of the geometric mean of the spectral ratios as a function of frequency (x axis) and direction of motion (y axis) and polarization rose diagrams calculated in the ranges 1–3 Hz and 3.5–10 Hz, respectively.*

amplification (Gallipoli *et al.*, 2009). It is common practice extracting the fundamental frequency of buildings, as well as their preferential direction of vibration using ambient noise records (Di Giulio *et al*., 2005). It can therefore be assumed that, especially when a simplified topography and lithology is present, data coming from ambient noise measurements can be worthwhile to characterize the topographic effects.

Concluding remarks

A detailed study about seismic hazard assessment southestern Sicily was performed. It provided interesting results for the Catania and Siracusa areas pointing out the differences deriving from the use of either the site or the seismotectonic approach. It can be observed that the site approach generally assigns a higher hazard for all the exceedance probabilities to Catania rather than to Siracusa. Such findings can be interpreted as the consequence of the higher damage suffered historically by this town and its average shorter distance from the seismogenic sources of major historical earthquakes as located by Azzaro and Barbano (2000). The Esteva-Cornell method puts in evidence that the hazard estimate for the two towns strongly depends on the size and geometry of the source zones postulated for south-eastern Sicily. Such features entail a spatial distribution of the seismic rates and a sort of "spreading" of the hazard, as well as the effect that all sites located in the inner part of the SZ will show a hazard greater than those located at its boundaries. Moreover, it appeared clear that the bigger the SZs, the greater the computed average hazard. It is evident that in the former instance (SZ9) the town of Catania has a higher hazard rather than in the latter case (SZ4-9) where it is located closer to the boundary of the seismogenic zone with respect to Siracusa. The "spreading effect" has also to be taken into account in order to explain the higher PGA and PSA values when SZ9 is used. It is worth noting that the PGA values obtained through the site method are quite similar to those computed by the Esteva-Cornell one only when the soft soil conditions are taken into account, whereas major differences occur when the rock site conditions are considered. Such differences could be a consequence of the intrinsic diversity between the two approaches used that makes a realistic comparison rather difficult. The site approach, in particular, uses macroseismic intensity data that are intrinsically linked to the dominant soil type which, in a relatively wide area, is reasonably soft soil. The results obtained from this seismic

hazard study, compared with those coming from the national hazard map (Working Group MPS04, 2004) show some differences that could be referred to the use of a different logic tree, as well as to the adoption of different attenuation laws and to taking into account local (within about 300 km) seismogenic sources only. The use of a combined approach, in the seismic hazard estimation, appears however advisable for a mutual validation of the obtained results and any choice is strictly linked to the knowledge of the local seismotectonic features.

The different quality and amount of the data on seismotectonic setting, as well as on seismicity and number of felt data at city scale, suggested the use of methodologies based on ground motion scenarios and/or on seismic soil characterization in the different urban contexts that have been investigated.

In the complex geological situation of Catania the evaluation of the local seismic response was undertaken using a twofold approach based on theoretical modelling, through an equivalent-linear numerical code (EERA), combined with local borehole information and experimental methods based on spectral ratio techniques. The joint use of numerical and experimental approaches allowed us to obtain quantitative indications about the site response in the study area and granted a mutual validation of results, thus making possible their interpretation into a geological framework. Data coming from about two hundred boreholes provided reliable stratigraphic sequences for modelling the investigated sites. To obtain contour maps of PGA and Sa_g, three different scenario earthquakes were assumed and seven real accelerograms were selected for each considered scenario. The numerical approach pointed out that all scenarios show comparable results in terms of local distribution of amplifications. The largest PGA and Sa_g values are concentrated in wide areas located in downtown Catania, where coarse materials and ruins of historical earthquakes are present, as well as in sectors where soft sediments and alluvial deposits outcrop among the basaltic lava flows. On the contrary, the lowest values are observed in all sectors of the urban area where lava flows directly cover the marly clay bedrock, as long as the basaltic lavas are not scoriaceous and/or fractured. The results obtained through spectral ratios techniques, processing the earthquake records, confirm the findings previously

described. Significant ground motion amplifications are indeed observed in the stations located either on spots of soft sediments, such as coarse detritus and sand surrounded by lava flows or when they are sited on fairly fractured and scoriaceous basaltic lavas. It is worth noting that both the SSR and HVSR techniques provide a reliable estimate of the fundamental frequencies at the investigated sites. Spectral ratios obtained through the HVSR method often appear less pronounced than those obtained through the SSR. Such evidence appears related to the role played by the pronounced lateral heterogeneities existing in the area, which affect the vertical component of motion, as well as to the complexity of near-surface morphology.

In the Siracusa area a detailed evaluation of the local seismic response was carried out using a twofold approach based on the interpretation of the Rayleigh waves dispersion curves obtained from MASW and ReMi prospections and on the Nakamura's technique. The use of techniques based on the propagation of surface waves made possible the $V_{S,30}$ characterization of the main outcropping lithotypes and consequently the classification, according to the EUROCODE8 (2003), of the investigated sites. As a result of this, a class C soil category was estimated for the the detritus, a class D was assigned to the alluvial deposits, whereas an A soil category was allocated to the sites placed on the limestone. The comparison of MASW and ReMi approaches has shown that the best defined surface waves dispersion curves are obtained when the active method is used. In particular, the MASW technique should be preferred when, as in the study case, the investigated depth do not exceeds about 30 m since, when the investigation has to reach a greater depth a longer linear array and a more energetic source are necessary. Information about the deeper part of the estimated V_S profiles was provided through the fitting between the HVNR frequency peaks and the theoretical ellipticity. This inversion strategy granted good results providing that the linear array configuration was optimal without relatively low velocity contrast between the existing lithotypes or not adequate length of the linear array to reach the bedrock depth. However, the combined use of prospections based on the surface wave analysis, together with the HVNR technique, has shown to be a remarkable

tool in order to better constrain possible deep horizons, reducing, at the same time, the problems related to non-uniqueness of the solutions in the dispersion curve analysis. The results of spectral ratios from measurements performed in thirty-two sites, show that pronounced spectral peaks are observed in the recording sites located on the alluvial deposits, as well as on the coarse detritus and sandy clay. On the contrary, no significant spectral ratio peaks are present both in all sectors of the urban area, where limestone and volcanics outcrop, and in all the sites where calcarenites directly cover the limestone. We can conclude that the limestone can be considered as the local bedrock since the higher shear waves velocity values are here observed.

Nevertheless, it is evident that further investigations are useful to take into account the complexity of the geological and morphologic context of Catania and Siracusa areas. The theoretical modelling and experimental methods based on spectral ratio analysis pointed out in the Catania area, indeed, the presence of strong heterogeneities linked to sedimentary paleo-valleys covered by lava flows and soft sediments hills surrounded by lava fields. On the other hand the spectral ratios obtained from noise measumerents performed in the Ortigia area (Siracusa), on outcropping limestone, showed significant spectral ratio peaks (in the frequency range 1.0-3.0 Hz) that appear not compatible with the H/V features expected for quite stiff lithotypes. For this reason, the S. Sofia hill and the Ortigia peninsula were selected as test sites to investigate the peculiar local seismic responses connected to the stratigraphic and topographic complexity of the study areas.

The characteristics of the site response at the S. Sofia hill, set into evidence that the observed local amplification and the directivity effects of the ground motion are strongly affected by the shape of the hill and the complexity of the near-surface geology. Findings of this study set into evidence that major amplification effects take place on the sedimentary terrains which outcrop along the flanks of the hill. On the contrary, on the lava flows, a significant amplification of the vertical component of motion, is observed as a consequence of velocity inversion effects. Although the results coming from processing earthquake and ambient

noise data appear comparable, it has to be remarked that the complex geologic setting of the study hill, being far from a simple 1D structure as theoretically postulated for H/V techniques, implies that such methodology reaches its limits in the estimation of the fundamental frequency. Directional resonances and polarization analysis have pointed out the existence of pronounced directional effects having azimuths that appear controlled by the directions of the hill slopes. At the top of the hill not pronounced polarization azimuths are observed. This result appears linked to the complex wavefield, generated by waves propagating along multiple fractures existing in the lower portion of the compact lava formation, and to the wide wedge angle of the hill, that reduces the focusing effects at the crest in favour of laterally propagating waves.

The findings coming out from the Ortigia test site have pointed out a good reliability of the HVNR technique for evaluating the influence of topography on the local seismic response. The H/V spectral ratios showed dominant frequency peaks in the range of 1.0-3.0 Hz that are in good agreement with the theoretical resonance frequency of the hill. Moreover, both the directional resonance and the polarization analysis, confirm the presence of a directional effect having azimuth 90-100 degrees, transverse to the major axis of the ridge. These results showed that, conversely to what is observed on the S. Sofia hill, the in Ortigia test site, being a calcareous ridge with a more homogeneous lithology, the topographic effects are predominant with respect to the stratigraphic ones.

Finally, as a practical implication of present study it can be set into evidence that hazard estimate and seismic microzonation investigations require multi-disciplinary approaches and the use of different tecniques based both on numerical and experimental processing of data in order to get a mutual validation of the obtained results. The results shown here clarify indeed that the simple use of an approach based on a $V_{S,30}$ study only, would fail to predict the observed site-response behaviour in the presence of a complex 2D/3D structures.

Research products

National conference presentations

- Lombardo G, Rigano R, **Panzera F**, Rovelli A, Cara F, Di Giulio G, Grasso S (2008). Valutazione della risposta sismica locale nell'area urbana di Catania tramite metodi sperimentali e numerici. *In: GNGTS 27° Convegno Nazionale. Gruppo Nazionale di Geofisica della Terra Solida. Trieste, 6-8 Ott. 2008, poster section, TRIESTE: Stella, p. 264-266, ISBN/ISSN: 88-902101-3-3*
- **Panzera F**, Lombardo G, Rigano R (2009). Seismic hazard assessment (SHA) using different approaches in Catania and Siracusa urban areas (Italy). *In: GNGTS 28° Convegno Nazionale. Gruppo Nazionale di Geofisica della Terra Solida. Trieste, 16-19 Nov. 2009, poster section, TRIESTE,: Stella, p. 394-398, ISBN/ISSN: 88-902101-4-1*
- **Panzera F**, Lombardo G, Rigano R, Cara F, Di Giulio G, Rovelli A, Azzara R (2009). Preliminary study of directivity in the local seismic response at a test site in Catania (Italy). *In: GNGTS 28° Convegno Nazionale. Gruppo Nazionale di Geofisica della Terra Solida. Trieste, 16-19 Nov. 2009, poster section, TRIESTE: Stella, p. 326-327, ISBN/ISSN: 88-902101-4-1*
- **Panzera F**, Lombardo G, Rigano R (2010). Site response in Ortigia peninsula (Siracusa, Italy). *In: GNGTS 29° Convegno Nazionale. Gruppo Nazionale di Geofisica della Terra Solida. Prato, 26-28 Ott.. 2010, oral section, TRIESTE: Stella, p. 278-281, ISBN/ISSN: 978-88-902101-5-0*
- **Panzera F**, Lombardo G, Rigano R (2010). Seismic characterization of main lithotypes outcropping in the Siracusa urban area. *In: GNGTS 29° Convegno Nazionale. Gruppo Nazionale di Geofisica della Terra Solida. Prato, 26-28 Ott.. 2010, poster section, TRIESTE: Stella, p. 281-283, ISBN/ISSN: 978-88-902101-5-0*

- Pace S, **Panzera F**, D'Amico S, Galea P, Lombardo G (2011). Modelling of ambient noise HVSR in a complex geological area: case study of the Xemxija bay area, Malta. *In: GNGTS 30° Convegno Nazionale. Gruppo Nazionale di Geofisica della Terra Solida. Trieste, 14-17 Nov. 2011, oral section, TRIESTE: Stella, p. 299-302, ISBN/ISSN: 978-88-902101-6-8*
- **Panzera F**, Lombardo G, Monaco C (2011). Ground motion polarization on fault zones: observations on Mt. Etna volcano and Hyblean area. *In: GNGTS 30° Convegno Nazionale. Gruppo Nazionale di Geofisica della Terra Solida. Trieste, 14-17 Nov. 2011, poster section, TRIESTE: Stella, p. 303-306, ISBN/ISSN: 978-88-902101-6-8*
- **Panzera** F, Pace S, D'Amico S, Galea P, Lombardo G (2011). Preliminary results on the seismic properties of main lithotypes outcropping on Malta. *In: GNGTS 30° Convegno Nazionale. Gruppo Nazionale di Geofisica della Terra Solida. Trieste, 14-17 Nov. 2011, poster section, TRIESTE: Stella, p. 306-308, ISBN/ISSN: 978-88-902101-6-8*
- D'Amico S, **Panzera** F, Pace S, Galea P, Lombardo G, Akingi A (2011). Stochastic ground motion simulations for seismic hazard assessment in the urban area of Xemxija, Malta. *In: GNGTS 30° Convegno Nazionale. Gruppo Nazionale di Geofisica della Terra Solida. Trieste, 14-17 Nov. 2011, poster section, TRIESTE: Stella, p. 356-357, ISBN/ISSN: 978-88-902101-6-8*

International conference presentations

- **Panzera F**, Lombardo G, Rigano R, Cara F, Di Giulio G, Rovelli A (2010). Topographic effects in the local seismic response at a test site in Catania (Italy). *In: EGU General Assembly 2010. Geophysical Research Abstract. Wien, 2010 May 2-8, poster section, Copernicus, Vol. 12, EGU2010-787-3, eISSN 1607-7962.*

- **Panzera F**, Lombardo G, Rigano R (2010). Seismic hazard assessment in the Catania and Siracusa urban areas (Italy) through different approaches. *In: EGU General Assembly 2010. Geophysical Research Abstract. Wien, 2010 May 2-8, poster section, Copernicus, Vol. 12, EGU2010-789-1, eISSN 1607-7962.*

Publications on ISI journals

- **Panzera F**, Rigano R, Lombardo G, Cara F, Di Giulio G, Rovelli A (2010). The role of alternating outcrops of sediments and basaltic lavas on seismic urban scenario: the study case of Catania, Italy. *Bulletin of Earthquake Engineering Vol. 9, n° 2, pp. 411-439. DOI: 10.1007/s10518-010-9202-x.*
- **Panzera F**, Lombardo G, Rigano R (2011). Evidence of topographic effects analysing ambient noise measurements: the study case of Siracusa, Italy. *Seismological Research Letters Vol. 82, n° 3, pp. 385 – 391. DOI: 10.1785/gssrl.82.3.385*
- **Panzera F**, Lombardo G, Rigano R (2011). Use of different approaches to estimate seismic hazard: the study cases of Catania and Siracusa, Italy. *Bollettino di Geofisica Teorica ed Applicata (Accepted)*
- **Panzera F**, Lombardo G, Cara F, Di Giulio G (2011). Influence of surface geology and topographic setting on the local seismic response at a test site in Catania, Italy. *Soil Dynamics and Earthquake Engineering (Submitted)*
- **Panzera F**, Lombardo G (2011). Seismic property delineation of lithotypes cropping out in the Siracusa urban area, Italy. *Engineering Geology (Submitted)*

References

Accordi B., Francaviglia A. (1960). La geologia del bacino del Simeto. Tecnica Agricola, XII(3): 221-244.

Akaike H. (1974). A new look at the statistical model identification. IEEE Trans. Automat. Contr., 19: 716-723.

Akkar S., Bommer J.J. (2007a). Prediction of elastic displacement response spectra in Europe and the Middle East. Earth. Eng. Struct. Dyn., 36: 1275-1301.

Akkar S., Bommer J.J. (2007b). Empirical prediction equations for peak ground velocity derived from strong-motion records from Europe and the Middle East. Bull. Seism. Soc. Am., 97: 511-530.

Aki K., Richards P. (2002). Quantitative Seismology. Second ed. University Science Books, Sausalito, California.

Albarello D., D'Amico V., Gasperini P., Pettenati F., Rotondi R., Zonno G. (2007). Nuova formulazione delle procedure per la stima dell'intensità macrosismica da dati epicentrali o da risentimenti in zone vicine. INGV-DPC Project S1, Deliverable D10: http://esse1.mi.ingv.it/d10.html.

Albarello D., Camassi R., Rebez A. (2001). Detection of space and time heterogeneity in the completeness of a seismic catalog by a statistical approach: an application to the Italian area. Bull. Seism. Soc. Am., 91: 1694-1703.

Albarello D., Mucciarelli M. (2002). Seismic hazard estimates using ill-defined macroseismic data at site. Pure Appl. Geoph. 159: 1289-1304.

Al Yuncha Z., Luzon F. (2000). On the Horizontal-to-Vertical Spectral Ratio in Sedimentary Basins. Bull. Seism. Soc. Am., 90(4): 1101–1106.

Al Yuncha Z., Luzon F., Posadas A., Martin J., Alguacil G., Almendros J., Sanchez S. (2004). The use of ambient seismic noise measurements for the estimation of surface soil effects: The Motril city case (Southern Spain). Pure appl. geophys., 161: 1549–1559.

Alcock E. D. (1974). Comments on "Comparison of earthquakes and microtremor ground motion in El Centro, California" by Udvadia and M. D. Trifunac. Bull. Seism. Soc. Am., 64, 495.

AGIP (1977). Temperature sotterranee. F.lli. Brugora eds., Milano

Amato A., Azzara R., Basili A., Chiarabba C., Cocco M., Di Bona M., Selvaggi G. (1995). Main shock and aftershocks of the December 13, 1990 Eastern Sicily earthquake. Ann. Geofis. 38(2): 255-266

Ambraseys N., Smit P., Sigbjornsson R., Suhadolc P., Margaris B. (2002). Internet-Site for European Strong-Motion Data. European Commission, Research-Directorate General, Environment and Climate Programme http://www.isesd.cv.ic.ac.uk/ESD/

Ambraseys N. N., Douglas J., Sarma S. K., Smit P. M. (2005). Equations for the estimation of strong ground motions from shallow crustal earthquakes using data from europe and the middle east: horizontal peak ground acceleration and spectral acceleration. Bulletin of Earthquake Engineering 3: 1–53

Andrews D.J. (1986). Objective determination of source parameters and similarity of earthquakes of different size. In Earthquake Source Mechanics: edited by Das et al., pp: 259-268, AGU, Washington, D.C.

Ansal A., Erdik M., Studer J., Springman S., Laue J., Buchheister J., Giardini D., Faeh D., Koksal D. (2004). Seismic microzonation for earthquake risk mitigation in turkey. 13th World Conference on Earthquake Engineering Vancouver, B.C., Canada August 1-6, 2004 Paper No. 1428.

Arias A. (1970). A measure of earthquake intensity. MIT Press, Cambridge, MA, 438-483.

Argnani A., Bonazzi C. (2005). Malta Escarpment fault zone offshore eastern Sicily: Pliocene-Quaternary tectonic evolution based on new multichannel seismic data. Tectonics, 24, Art. No. TC4009, 1-12.

Ashford S. A., Sitar N., Lysmer J., Deng N. (1997). Topographic effects on the seismic response of steep slopes. Bull. Seism. Soc. Am., 87(3): 701–709.

Aureli A., Dipasquale M., Privitera A.M.G. (2010). Hydrogeochemical study of water points and springs in Ortigia island (Siracusa). 3° International Symposium "Karst Evolution in the South Mediterranean area, May 29-31-2009, Ragusa, 14, 101-109.

Azzaro R., Barbano M. S. (2000). Seismogenic features of SE Sicily and scenario earthquakes for Catania, In The Catania Project: Earthquake damage scenarios for a high risk area in the Mediterranean. R. Faccioli and V. Pessina (Editors), CNR-GNDT, Roma, 225: 9-13.

Azzaro R., Barbano M.S. (2000). Analysis of seismicity of Southeastern Sicily: proposal of a tectonic interpretation. Ann. Geofis., 43: 1-18.

Azzaro R., Barbano M. S., Moroni A., Mucciarelli M., Stucchi M. (1999) The seismic history of Catania. J. Seism., 3(3): 235-252.

Azzaro R., Barbano M.S., D'Amico S., Tuvè T. (2006). The attenuation of seismic intensity in the Etna region and comparison with other Italian volcanic districts. Ann. Geofis., 49: 1003-1020.

Azzaro R., Barbano M.S., D'Amico S., Tuvè T., Albarello D., D'Amico V. (2008). First studies of probabilistic seismic hazard assessment in the volcanic region of Mt. Etna (southern Italy) by means of macroseismic intensities. Boll. Geofis. Teor. Appl., 49(1): 77-92.

Azzaro R., Barbano M.S., Moroni A., Mucciarelli M., Stucchi M. (1999). The seismic history of Catania. J. Seism., 3: 235-252

B

Barani S., Spallarossa D., Bazzurro P. (2009). Disagregation of probabilistic ground-motion hazard in Italy. Bull. Seism. Soc. Am., 99(5): 2638-2661.

Barbano M.S., Rigano R. (2001). Earthquake sources and seismic hazard in southerstern Sicily. Ann. Geofis., 44(4): 723-738.

Barbano M.S., Rigano R., Cosentino M., Lombardo G. (2001). Seismic history and hazard in some localities of south-eastern Sicily. Boll. Geofis. Teor. Appl., 42(1-2): 107-120

Bard P.Y. (1982). Diffracted waves and displacement field over two-dimensional elevated topographies. Geophys. J. Roy. Astron Soc., 71: 731-760.

Bard P.Y. (1994). Effects of surface geology on ground motion: recent results and remaining issues. In: G. Duma (ed), Proc. 10th European Conference on Earthquake Engineering. Wien, 28 Aug.-2 Sept., Balkema, Rotterdam, 1: 305-323.

Bard P.Y. (1997). Local effects on strong ground motion: Basic physical phenomena and estimation methods for microzoning studies. Advanced Study Course on Seismic Risk (SERINA), 21st-27th September 1997, Thessaloniki/Greece.

Bard P.-Y. (1998). Microtremor measurements: A tool for site effect estimation? Second International Symposium on the Effects of Surface Geology on seismic Motion - ESG98. Yokohama, Japan, December 1998.

Bard P.-Y. (1999). "Microtremor measurements: a tool for site estimation?", State-of the-art paper. Second International Symposium on the Effects of Surface geology on Seismic motion, Yokohama, December 1-3, 1998, Irikura, Kudo, Okada & Sasatani

Bard P.-Y., Bouchon M. (1985). The two-dimensional resonance of sediment-filled valleys. Bull. Seism. Soc. Am., 75: 519-541.

Bard P.Y., Riepl-Thomas J. (1999). Wave propagation in complex geological structures and their effects on strong ground motion. In Wave motion in Earthquake Engineering: edited by Kausel and Manolis, WIT Press, 2: 37-95.

Bardet J. P., Ichii K., Lin C. H. (2000). EERA. A computer program for Equivalent-linear Earthquake site Response Analyses of layered soil deposits. University of Southern California, Department of Civil Engineering, user's manual.

Bardet J. P., Tobita T. (2001). NERA: a computer program for nonlinear earthquake site response analysis of layered soil deposits. University of Southern California, Department of Civil Engineering, user's manual.

Basili R., Valensise G., Vannoli P., Burrato P., Fracassi U., Mariano S., Tiberti M.M., Boschi E. (2008). The Database of Individual Seismogenic Sources (DISS), version 3: summarizing 20 years of research on Italy's earthquake geology. Tectonophysics, doi:10.1016/j.tecto.2007.04.014.

Bazzurro P., Cornell C.A. (1999). Disaggregation of seismic hazard. Bull. Seism. Soc. Am., 89(2): 501-520.

Beskos D.E. (1997). Boundary elements methods in dynamic analysis: Part II (1986-1996). Appl. Mech. Rev. (ASME), 50(3): 149-197.

Bessason B., Kaynia A. M. (2002) Site amplification in lava rock on soft sediments. Soil Dyn. and Earthq. Eng., 22(7): 525–540.

Bindi D., Parolai S., Cara F., Di Giulio G., Ferretti G., Luzi L., Monachesi G., Pacor F., Rovelli A. (2009). Site amplifications observed in the Gubbio Basin, Central Italy: Hints for lateral propagation effects. Bull. Seism. Soc. Am., 99(2A): 741-760

Bindi D., Luzi L., Parolai S., Di Giacomo D., Monachesi G. (2011). Site effects observed in alluvial basins: the case of Norcia (Central Italy). Bull. Earthquake Eng. doi10.1007/s10518-011-9273-3

Biondi G., Maugeri M. (2005). Seismic response analysis of Monte Po hill (Catania). In "Seismic Prevention of Damage: a case study in a Mediterranean city", M. Maugeri (ed.), Vol 14, WIT Press, Southampton, 177-195

Boatwright J., Fletcher J. B., Fumal T. E. (1991). A general inversion scheme for source, site, and propagation characteristics using multiply recorded sets of moderate-sized earthquakes. Bull. Seism. Soc. Am., 81: 1754-1782.

Bohlen T., Saenger E. H. (2006). Accuracy of heterogeneous staggered-grid finite-difference modeling of rayleigh waves. Geophysics, 71: 109–115.

Bommer J. J., Acevedo A. B. (2004). The use of real earthquake accelerograms as input to dynamic analysis. J. Earth. Eng., 8(1) special issue: pp 43-91

Bonamassa O., Vidale J. E. (1991). Directional site resonances observed from aftershocks of the 18th October 1989 Loma Prieta earthquake. Bull. Seism. Soc. Am., 81: 1945–1957.

Boncio P., Pizzi A., Cavuoto G., Mancini M., Piacentini T., Miccadei E., Cavinato G.P., Piscitelli S., Giocoli A., Ferretti G., De Ferrari R., Gallipoli M.R., Mucciarelli M., Di Fiore V., Franceschini A., Pergalani F., Naso G., Working Group Macroarea3 (2011). Geological and geophysical characterisation of the Paganica - San Gregorio area after the April 6, 2009 L'Aquila earthquake (Mw 6.3, central Italy): implications for site response. Boll. Geofis. Teor. Appl., doi10.4430/bgta0014

Bonilla L.F., Steidl J.H., Lindley G.T., Tumarkin A.G., Archuleta R.J. (1997). Site amplification in the San Fernando valley, California: variability of site-effect estimation using the S-wave, coda, and H/V methods. Bull. Seism. Soc. Am. 87(3): 710-730.

Bonilla F. (2000). Computation of Linear and Nonlinear Site Response for Near Field Ground Motion. Ph.D., University of California at Santa Barbara.

Bonnefoy-Claudet S., Cornou C., Bard P.-Y., Cotton F., Moczo P., Kristek J., Fäh D., (2006). H/V ratio: a tool for site effects evaluation. Results from 1-D noise simulations. Geophys J. Int. 167 : 827–837.

Bonnefoy-Claudet S., Köhler A., Cornou C., Wathelet M., Bard P.Y. (2008). Effects of Love waves on microtremor H/V ratio. Bull. Seism. Soc. Am., 98(1): 288–300.

Bonnet M. (1999). Boundary integral equation methods for solids and fluids. Wiley.

Boore D.M. (1973). The effect of simple topography on seismic waves: implications for the accelerations recorded at Pacoima Dam, San Fernando valley, California. Bull. Seism. Soc. Am., 63(5): 1603–1609.

Boore D.M., Atkinson G.M. (2008). Ground-motion prediction equations for the average horizontal component of PGA, PGV, and 5%-damped PSA at spectral periods between 0.01 s and 10.0 s. Earthq. Spectra, 24: 99-138.

Boore D. M., Harmsen S. C., Harding S. T. (1981). Wave scattering from a step change in surface topography. Bull. Seism. Soc. Am., 86: 66–72.

Borcherdt R.D. (1970). Effects of local geology on ground motion near San Francisco Bay. Bull. Seism. Soc. Am. 60: 29–61.

Boschi E., Guidoboni E., Ferrari G., Gasperini P., Mariotti D., Valensise G.; 2000: Catalogue of strong Italian earthquakes from 461 B.C. to 1997. Ann. Geofis. 43: 843-868 and CD-ROM.

Bouchon M. (1973). Effect of topography on surface motion. Bull. Seism. Soc. Am. 63: 615-632.

Bouchon M., Barker J.S. (1996). Seismic Response of a Hill: The example of Tarzana, California. Bull. Seism. Soc. Am., 86: 66–72.

Bragato P.L., Laurenzano G., Barnaba C. (2007). Automatic zonation of urban areas based on the similarity of H/V spectral ratios. Bull. Seism. Soc. Am., 97 (5): 1404–1412.

Brancato A., Hole J. A., Gresta S., Beale J. N. (2009). Determination of Seismogenic Structures in Southeastern Sicily (Italy) by High-Precision Relative Relocation of microearthquakes. Bull. Seism. Soc. Am., 99(3): 1921-1936.

Burjànek J., Gassner-Stamm G., Poggi V., Moore J. R., Fäh D. (2010). Ambient vibration analysis of an unstable mountain slope. Geophys. J. Int., 180(2): 820-828.

Buech F., Davies T. R., Pettinga J. R. (2010). The little red hill seismic experimental study: topographic effects on ground motion at a bedrock-dominated mountain edifice. Bull. Seism. Soc. Am., 100 (5A): 2219–2229.

Burnham K. P., Anderson D. R. (2002). Model Selection and Multimodel Inference: A Practical-Theoretic Approach. Second Ed., Springer-Verlag, New York.

C

Cara F., Cultrera G., Azzara R. M., De Rubeis V., Di Giulio G., Giammarinaro M. S., Tosi P., Vallone P., Rovelli A. (2008). Microtremor measurements in the city of Palermo, Italy: Analysis of the correlation with local geology and damage. Bull. Seism. Soc. Am., 98: 1354-1372.

Cara F., Di Giulio G., Rovelli A. (2003). A study on seismic noise variations at Colfiorito, Central Italy: implications for the use of H/V spectral ratios. Geophys. Res. Lett., 30(18): 1972-1976.

Carbone S., Branca S., Lentini F., Barbano M. S., Corsaro M. A., Di Stefano A., Ferrara V., Monaco C., Longhitano S., Platania I., Zanini A., De Beni E., Ferlito C. (2009). Note Illustrative della Carta Geologica d'Italia alla scala 1:50000, foglio 634 Catania. ISPRA, Servizio Geologico d'Italia, Organo Cartografico dello Stato, S.EL.CA. s.r.l., Firenze.

Carrubba P., Maugeri M. (1988). Determinazione delle proprietà dinamiche di un'argilla mediante prove di colonna risonante. Rivista italiana di geotecnica 22(2): 101-113

Cary P., Li X., Popov G., Zhang C. (2010). Shear wave splitting in compliant rocks. The leading Edge, 29(10): 1278, doi 10.1190/1.3496918

Cartwright D.E., Longuet-Higgins (1956). The statistical distribution of the maxima of a random function. Proc. Roy. Soc. London A 237: 212-232.

Castellaro S., Mulargia F. (2009). The Effect of Velocity Inversions on H/V. Pure appl. geophys. 166: 567–592, doi 10.1007/s00024-009-0474-5

Castro R. R., RESNOM Working Group (1998). *P*- and *S*-wave site response of the seismic network RESNOM determined from earthquakes of northern Baja California, Mexico. Pure Appl. Geophys., 1052: 125–138.

Catalano S., De Guidi G., Gresta S., Langer H., Lombardo G., Monaco C., Rigano R., Tortorici L. (2005). Geolithological features and site response in the town of Catania. In "Seismic Prevention of Damage: a case study in a Mediterranean city", M. Maugeri (ed.), Advances in Earthquake engineering Vol 14, WIT Press, Southampton: 103-114.

Catchings R. D., Lee W. H. K. (1996). Shallow velocity structure and Poisson's ratio at the Tarzana, California, strong-motion accelerometer site. Bull. Seism. Soc. Am., 86, 1704-1713.

Cauzzi C., Faccioli E. (2008). Broadband (0.05 to 20 s) prediction of displacement response spectra based on worldwide digital records. J. Seismol., 12(4): 453-475.

Cavallaro A., Grasso S., Maugeri M. (2001). A dynamic geothechnical characterization of soil at Saint Nicola alla Rena Church damaged by South Eastern Sicily Earthquake of 13 December 1990. Proceedings of the 15th International conference on soil mechanics and geotechnical engineering, satellite conference "Lessons learned from recent strong earthquake. Istanbul, 25 august 2001, pp 243-248

Chávez-García F. J., Sanchez L. R., Hatzfeld D. (1996). Topographic site effects and HVSR. A comparison between observations and theory. Bull. Seism. Soc. Am., 86: 1559-1573.

Chávez-García F. J., Rodríguez M., Field E. H., Hatzfeld D. (1997). Topographic site effects. A comparison of two nonreference methods. Bull. Seism. Soc. Am., 87(6): 1667-1673.

Coccia S., Del Gaudio V., Venisti N., Wasowski J. (2010). Application of Refraction Microtremor (ReMi) technique for determination of 1-D shear wave velocity in a landslide area. J. Appl. Geophys., 71: 71–89.

Cornell C.A. (1968). Engineering seismic risk analysis. Bull. Seism. Soc. Am., 58: 1583–1606.

D

D'Amico V., Albarello D. (2008). SASHA: A computer program to assess seismic hazard from intensity data. Seismol. Res. Lett., 79: 663-671.

D'Addezio G., Valensise G. (1991). Metodologie per l'individuazione della struttura sismogenetica responsabile del terremoto del 13 dicembre 1990. In: Boschi, E., Basili, A. (Eds.), Contributi allo studio del terremoto della Sicilia orientale del 13 dicembre 1990. Int. Rep. 537, ING, Rome: 115–125.

Decanini L., Panza G.F. (Eds) (2000). Scenari di pericolosità sismica ad Augusta, Siracusa e Noto. CNR-Gruppo Nazionale per la Difesa dai Terremoti - Roma, 2000: 200 pp.

Dal Moro G., Pipan M., Gabrielli P. (2006). Rayleigh wave dispersion curve inversion via genetic algorithms and marginal posterior probability density estimation. Geophysics, 61: 39–55.

Dangla P. (1988). A plane strain soil-structure interaction model. Earthquake Eng. Struct. Dynam., 16: 1115-1128.

Dangla P., Semblat J.F., Xiao H., Delépine N. (2005). A simple and efficient regularization method for 3D BEM: application to frequency-domain elastodynamics. Bull. Seism. Soc. Am., 95: 1916-1927.

Del Gaudio V., Coccia S., Wasowski J., Gallipoli M. R., Mucciarelli M. (2008). Detection of directivity in seismic site response from microtremor spectral analysis. Nat. Hazards Earth Syst. Sci., 8: 751–762.

Del Gaudio V., Pierri P., Calcagnile G. (2009). Seismogenic zonation and seismic hazard estimates in a Southern Italy area (Northern Apulia) characterised by moderate seismicity rates. Nat. Hazards Earth Syst. Sci., 9(1): 161–174.

De Lorenzo S., Di Grazia G., Giampiccolo E., Gresta S., Langer H., Tusa G., Ursino A. (2004). Source and Qp parameters from pulse width inversion of low magnitude earthquake data in the Southeastern Sicily. J. Geophys. Res.: doi10.1029/2003JB002577.

Di Bona M., Cocco M., Rovelli A., Berardi R., Boschi E. (1995). Analysis of strong-motion data of the 1990 Eastern Sicily earthquake. Ann. Geofis. 38(2): 283-300.

Di Giacomo D., Gallipoli M. R., Mucciarelli M., Parolai S., Richwalski S. M. (2005). Analysis and Modeling of HVSR in the Presence of a Velocity Inversion: The Case of Venosa, Italy. Bull. Seism. Soc. Am., 95(6): 2364–2372.

Di Giulio G., Rovelli A., Cara F., Azzara R. M., Marra F., Basili R., Caserta A. (2003). Long-duration asynchronous ground motions in the Colfiorito plain, central Italy, observed on a two-dimensional dense array. J. Geophys. Res. 108(B10): 2486, doi:10.1029/2002JB002367.

E

Esteva L. (1967). Criterios para la construcción de espectros para diseño sísmico. Proc. of XII Jorn. Sudamericanas de Ingen. Estruc y III Simp. Panamericano de Estruc., Caracas.

EUROCODE8 (2003). Design of structures for earthquake resistance—Part 1: general rules, seismic actions and rules for buildings, EN 1998. European Committee for Standardization, Brussels.

F

Faccioli E., Battistella C., Alemani P., LoPresti D., Tibaldi A. (1991). Seismic microzoning and soil dynamics studies in San Salvador,12th ICSMFE, Rio de Jenerio, Brazil.

Faccioli E. (coordinator) (1997). Geotechnical earthquake engineering by characterisation of the Catania municipal area. Technical report and CD-Rom prepared by Ingegneria Geotecnica for CNR–Gruppo Nazionale Difesa Terremoti, Milan, Italy (in Italian), 33 pp + encl.

Faccioli E., Cauzzi C. (2006). Macroseismic intensities for seismic scenarios estimated from instrumentally based correlations. Proc. First Europ. Conference on Earth. Eng. and Seism., 569.

Faccioli E., Pessina V. (Eds.) (2000). The Catania Project: earthquake damage scenarios for high risk area in the Mediterranean. CNR- Gruppo Nazionale per la Difesa Terremoti, Roma, 225 pp.

Faccioli E., Pessina V. (2003). WP2 – Basis of a handbook of earthquake ground motions scenarios, Report number, 99 pp. (57 Figs., 12 Tables, 3 Appendices).

Faccioli E., Rovelli A. (2007). Project S5 – Seismic input in terms of expected spectral displacements. http://progettos5.stru.polimi.it/

Faenza L., Michelini A. (2010). Regression analysis of MCS Intensity and ground motion parameters in Italy and its application in ShakeMap. Geoph. J. Int., 180(3): 1138-1152.

Fäh D., Kind F., Giardini D. (2001). A theoretical investigation on H/V ratios. Geophys. J. Int. 145(2): 535-549.

Field E. H., Jacob K. (1995). A comparison and test of various site response estimation techniques. Bull. Seism. Soc. Am., 85(4): 1127-1143.

Fiorini E., Onida M., Borzi B., Pacor F., Luzi L., Meletti C., D'Amico V., Marzorati S., Ameri G. (2008). Microzonation study fora n industrial site in Southern Italy. The 14th World Conference on Earthquake Engineering, October 12-17, 2008, Beijing, China.

Frankel A., Vidale J. (1992). A Three-Dimensional Simulation of Seismic Waves in the Santa Clara Valley, California, from a Loma Prieta Aftershock. Bull. Seism. Soc. Am., 82: 2045-2074.

G

Galadini F., Meletti C., Vittori E. (2001). Major active fault in Italy: available surface data. Netherlands. J. Geosc., 80(3-4): 273-296.

Gallipoli M. R., Mucciarelli M., Vona M. (2009). Empirical estimate of fundamental frequencies and damping for Italian buildings. Earthq. Eng. Struct. Dynam.: doi10.1002/eqe.878.

Géli L., Bard P.-Y., Jullien B. (1988). The effect of topography on earthquake ground motion: a review and new results. Bull. Seism. Soc. Am., 78, 42-63.

Gerardi F., Barbano M. S., De Martini P. M., Pantosti D. (2008). Discrimination of Tsunami Sources (Earthquake versus Landslide) on the Basis of Historical Data in Eastern Sicily and Southern Calabria. Bull. Seism. Soc. Am. 98(6): 2795- 2805.

Giampiccolo E., Gresta S., Ganci G., (2003). Attenuation of body waves in Southeastern Sicily (Italy). Phys. Earth Planet Int. 135(4): 267 – 279.

Giampiccolo E., Gresta S., Mucciarelli M., De Guidi G., Gallipoli M. R. (2001). Information about subsoil geological structure in the city of Catania: Eastern Sicily from microtremor measurements. Ann. Geofis. 44(1): 1-12.

Giampiccolo E., Gresta S., Rasconà F., (2004). Intrinsic and scattering attenuation from observed seismic codas in Southeastern Sicily, Italy. Phys. Earth Planet. Int .145(1-4): 55-66.

Giampiccolo E., Tusa G., Langer H., Gresta S. (2002). Attenuation in Southeastern Sicily (Italy) by applying different coda methods. J. Seismol., 6(4): 487-501.

Giardini G., Palombo B., Pino N. A. (1995). Long period modelling of the MEDNET waveforms for the December 13, 1990 Eastern Sicily earthquake. Ann. Geofis. 38(2): 267-282.

Gitterman Y., Zaslavsky Y., Shapira A., Shtivelman V. (1996). Empirical site response evaluations: case studies in Israel. Soil Dyn. Earthquake Eng., 15 (7): 447–463.

Gómez Capera A.A., Albarello D., Gasperini P. (2007). Aggiornamento relazioni fra l'intensità macrosismica e PGA. Progetto DPC-INGV S1, http://esse1.mi.ingv.it/d11.html

Grasso M., Lentini F. (1982). Sedimentary and tectonic evolution of the eastern hyblean plateau (South-Eastern Sicily) during Late Cretaceous to Quaternary time. Paleoecology 39, 261-280.

Grasso S., Lombardo G., Maugeri M., Rigano R. (2004). Site effects evaluation in monumental and civil residence buildings in the urban area of Catania. In: Atti XI Convegno Nazionale ANIDIS "L'ingegneria sismica in Italia", Genova (Italia), 25-29 January 2004, CD-ROM.

Greenhalgh S. A., Zhou B., Rutty M. (2008). Effect of coherent noise on single-station direction of arrival estimation. J. Seismol., 12: 377–385.

Gutscher M.-A., Roger J., Baptista M.-A., Miranda J.M., Tinti S. (2006). Source of the 1693 Catania earthquake and tsunami (southern Italy): new evidence from tsunami modeling of a locked subduction fault plane. Geophys. Res. Lett., 33: doi:10.1029/2005GL025442.

H

Hashash Y. M. A. (2009). "DEEPSOIL V 3.7, Tutorial and User Manual. 2002-2009." University of Illinois at Urbana-Champaign, Urbana, Illinois.

Herak M. (2008). ModelHVSR—A Matlab_ tool to model horizontal-to-vertical spectral ratio of ambient noise. Comput. Geosci. 34: 1514–1526.

Herrmann R. B. (1994). Computer programs in seismology. Vol. 4 St Louis University.

Herrmann R.B. (2002). Computer programs in seismology. Vol. 4 St. Luis University.

Housner G.W. (1959). Behaviour of structures during earthquakes. J. Eng. Mech. Div., ASCE, 85(EM14): 109-129.

Hughes T. J. R. (1987). Linear static and dynamic finite element analysis, Prentice-Hall, Englewood Cliffs, N-J.

Hughes T. J. R., Reali A., Sangalli G. (2008). Duality and Unified Analysis of Discrete Approximations in Structural Dynamics and Wave Propagation: Comparison of p-method Finite Elements with k-method NURBS. Computer Meth. in Applied Mech. and Eng., 197(49-50): 4104-4124.

I

Ibs-Von Seth M., Wohlenberg J. (1999). Microtremor measurements used to map thickness of soft sediments. Bull. Seism. Soc. Am., 89: 250–259.

Iervolino I., Galasso C., Cosenza E. (2010). REXEL: computer aided record selection for code-based seismic structural analysis. Bull. Earthq. Eng. 8(2): 339-362.

Ihlenburg F., Babuška I. (1995). Dispersion analysis and error estimation of Galerkin finite element methods for the Helmholtz equation. Int. J. Numer. Meth. Eng., 38: 3745-3774.

J

Jacques E., Monaco C., Tapponier P., Tortorici L., Winter T. (2001). Faulting and earthquake triggering during the 1783 Calabria seismic sequence. Geophys. J. Int., 147: 499-516.

Jurkevics A. (1988). Polarization analysis of three component array data. Bull. Seism. Soc. Am.**,** 78: 1725-1743.

K

Kramer S.L. (1996). Geotechnical Earthquake Engineering. Prentice-Hall civil engineering and engineering mechanics series, New Jersey, 1996.

Kawase H. (1996). The cause of the damage belt in Kobe: 'the basin edge effect,' constructive interference of the direct S-wave with the basin induced diffracted/Rayleigh waves. Seismol. Res. Lett., 67(5): 25–34.

Kanai K., Tanaka T. (1961). On microtremors: Bull. Earthqu. Res. Inst., Tokyo University, 39: 97-114.

Katz L. J. (1976). Microtremor analysis of local geological conditions. Bull. Seism. Soc. Am., 66: 45-60.

Konno K., Ohmachi T. (1998). Ground-motion characteristics estimated from spectral ratio between horizontal and vertical components of microtremor. Bull. Seism. Soc. Am., 88 (1): 228–241.

Kudo K. (1995). Practical estimates of site response: state-of-art report, in 5th Int. Conf. on Seismic Zonation, Nice, France.

Kvaerna T., Ringdahl F. (1986). Stability of various fk-estimation techniques, in Semiannual Technical Summary, 1 October 1985 - 31 March 1986, In NORSAR Scientific Report, 1-86/87, Kjeller, Norway, 29-40.

L

Lacave C., Bard P.-Y., Koller M.G. (1999). "Microzonation: techniques and examples" In: Block 15: Naturgefahren-Erdbebenrisiko, (electronic book on the Internet; www.ndk.ethz.ch/pages/publ/Koller.pdf), 23 pp.

Lachet C., Bard P.-Y. (1994). Numerical and theoretical investigations on the possibilities and limitations of Nakamura's techniques. J. Phys. Earth**,** 302(42): 377– 397.

Lacoss R.T., Kelly E.J., Toksöz M.N. (1969). Estimation of seismic noise structure using arrays. Geophysics, 34: 21-38.

Lang D. H., Schwarz J. (2000). A comparison of site response estimation techniques: Case studies in earthquake-affected areas. Proceedings of the 6th International Conference on Seismic Zonation, Palm Springs/USA, 2000.

Langer H., Catalano S., Cristaldi M., De Guidi G., Gresta S., Monaco C., Tortorici L. (1999). Strong ground motion simulation in the urban area of Catania on the basis of a detailed geological survey, In: Earthquake Resistant Engineering Structures, (G. Oliveto and C.A. Brebbia eds.), WIT Press, Southampton, 343-352.

Langston C.A. (1979). Structure under Mount Rainier, Washington, inferred from teleseismic body waves. J. Geophys. Res., 84: 4749-4762.

Lanzo G., Lombardo G., Pagliaroli A., Rigano R. (2006). Effects of natural and artificial cavities in the evaluation of local seismic response. 25° Convegno Nazionale GNGTS, Roma, poster section: 244-246.

Lanzo G., Silvestri F. (1999). Risposta sismica locale – Teoria ed esperienze. Hevelius edizioni.

Lavecchia G., Ferrarini F., de Nardis R., Visini F., Barbano M. S. (2007). Active thrusting as a possible seismogenic source in Sicily (Southern Italy): Some insights from integrated structural–kinematic and seismological data. Tectonophysics, 445(3-4): 145-167.

Laurenzano G., Priolo E. (2005). Numerical modelling of the December 13, 1990, M=5.8 Eastern Sicily earthquake. Bull. Seis. Soc. Am., 95(1): 241-251.

Laurenzano G., Priolo E., Kline P., Vuan A. (2004). Near fault earthquake scenarios for the February 20, 1818 M=6.2 "Catanese" event. In "Proceedings of the Fourth Int. Conf. on Computer simulation in Risk Analysis and Hazard Mitigation, Risk Analysis IV", Rhodes, Greece, (C.A. Brebbia ed.), WIT Press, Southampton: 81-91.

LeBrun B., Hatzfeld D., Bard P.Y., Bouchon M. (1999). Experimental study of the ground motion on a large scale topographic hill at Kitherion (Greece). J. of Seism., 3: 1–15.

Lentini F., Carbone S., Cugno G., Grasso M., Scamarda G., Sciuto F. (1986). Carta geologica del settore nord-orientale ibleo (Sicilia S.E.), S.E.L.CA. editrice.

Lermo J., Chavez-Garcia F. J. (1993). Site effect evaluation using spectral ratio with only one station. Bull. Seism. Soc. Am. 83: 1574-1594.

Lermo J., Chavez-Garcia F. J. (1994). Are microtremor useful in site response evaluation? Bull. Seism. Soc. Am., 84: 1350-1364.

Lombardo G., Coco G., Corrao M., Imposa S., Azzara R., Cara F., Rovelli A. (2001). Results of microtremor measurements in the urban area of Catania (Italy). Boll. Geofis. Teor. Appl., 42(3-4): 317-334.

Lombardo G., Langer H., Gresta S., Rigano R., Monaco C., De Guidi G. (2006). On the importance of geolithological features for the estimate of the site response: the case of Catania metropolitan area (Italy). Natural Hazards 38(3): 339-354.

Lombardo G., Rigano R. (2007). Local seismic response in Catania (Italy): a test area in the northern part of the town. Eng. Geol. 94(1-2): 38-49.

Lombardo G., Rigano R. (2009). Local seismic response evaluation in natural and artificial cavities. Proceeding of the 3° International Symposium "Karst Evolution in the South Mediterranean Area", Ragusa, Italy May 2009, in print.

Lombardo G., Rigano R., Gresta S., Langer H., Monaco C., De Guidi G. (2004). Evaluation of the local seismic response in the area of Catania (Italy). In "Proceedings of the Fourth Int. Conf. on Computer simulation in Risk Analysis and Hazard Mitigation, Risk Analysis IV", Rhodes, Greece, (C.A. Brebbia ed.), WIT Press, Southampton: 103-114.

Louie J.L. (2001). Faster, Better: Shear-wave velocity to 100 meters depth from refraction microtremor arrays. Bull. Seism. Soc. Am., 91: 347-364.

M

MacQueen J. B. (1967). Some Methods for classification and Analysis of Multivariate Observations, Proceedings of 5-th Berkeley Symposium on Mathematical Statistics and Probability, Berkeley, University of California Press, 1: 281-297.

Malischewky P. G., Scherbaum F. (2004). Love's formula and H/V ratio (ellipticity) of Rayleigh waves. Wave Motion, 40: 57–67.

Maresca R., Castellano M., De Matteis R., Saccorotti G., Vaccariello P. (2003). Local Site Effects in the Town of Benevento (Italy) from Noise Measurements. Pure appl. geophys., 160: 1745–1764.

Marzorati S., Ladina C., Falcucci E., Gori S., Saroli M., Ameri G., Galadini F. (2011). Site effects "on the rock": the case of Castelvecchio Subequo (L'Aquila, central Italy). Bull. Earth. Eng.: doi 10.1007/s10518-011-9263-5.

Massa M., Lovati S., D'Alema E., Ferretti G., Bakavoli M. (2010). An experimental approach for estimating seismic amplification effects at the top of a ridge, and the implication for ground-motionpredictions: the case of Narni, central Italy. Bull. Seism. Soc. Am., 100(6): 3020–3034.

McGuire R. K. (2004). Seismic hazard and risk analysis. EERI, Oakland, 105-142.

Meletti C., Galadini F., Valensise G., Stucchi M., Basili R., Barba S., Vannucci G., Boschi E. (2008). A seismic source zone model for the seismic hazard assessment of the Italian territory. Tectonophysics 450: 85-108.

Meletti C., Patacca E., Scandone P. (2000). Construction of a seismotectonic model: the case of Italy. Pure and Appl. Geoph., 157: 11-35.

Milana G., Rovelli A., De Sortis A., Calderoni G., Coco G., Corrao M., Marsan P. (2008). The Role of Long-Period Ground Motions on Magnitude and Damage of Volcanic Earthquakes on Mt. Etna, Italy. Bull. Seism. Soc. Am., 98(6): 2724-2738.

Mishra P. S. (2004). Seismic Hazard and Risk Microzonation of Jabalpur. Paper presented at the workshop on seismic hazard and risck microzonation of Jabalpur, National Research Institute, Hyderabad, India.

Monaco C., Tortorici L. (2000). Active faulting in the Calabrian arc and eastern Sicily. J. Geod., 29: 40-424.

Monaco C., Tortorici L. (1999). Carta geologica dell'area urbana di Catania. S.E.L.C.A., Firenze, Italy.

Moczo P., Kristek J., Vavrycuk V., Archuleta R.J., Halada L. (2002). 3D Heterogeneous Staggered-Grid Finite-Difference Modeling of Seismic Motion with Volume Harmonic and Arithmetic Averaging of Elastic Moduli and Densities. Bull. Seism. Soc. Am., 92(8): 3042-3066.

Mucciarelli M. (1998). Reliability and applicability of Nakamura's technique using microtremors: an experimental approach. J. Earth. Eng., 2: 625–638.

Mucciarelli M., Pacor F. (2007). Progetti sismologici di interesse per il DPC, progetto S3 - Scenari di scuotimento in aree di interesse prioritario e/o strategico, task 2 - effetti di sito - deleverables D3-D4-D5. http://portale.ingv.it/temi-ricerca/terremoti

Monaco C., Catalano S., De Guidi G., Gresta S., Langer H., Tortorici L. (2000). The geological map of the urban area of Catania (Eastern Sicily): morphotectonic and seismotectonic implications. Mem. Soc. Geol. It., 55: 425-438.

N

Nazarian S., Stokoe K.H. (1984). In situ shear wave velocity from spectral analysis of surface waves. Proc. of the 8th World Conf. on Earthquake Engineering, 3: 31–38.

Nakamura Y. (1989). A method for dynamic characteristics estimation of subsurface using microtremor on the ground surface. Q.R. Railway Tec. Res. Inst. Rept., 30: 25-33.

Nogoshi M., Igarashi T. (1970). On the propagation characteristics of microtremors. J. Seism. Soc. Japan**,** 23: 264–280.

Norme tecniche per le costruzioni (2008). Azioni sulle costruzioni. In Nuove norme tecniche per le costruzioni. Edit by Ministero delle infrastrutture, Ministero dell'interno e Capo del Dipartimento della Protezione Civile, Gazzetta Ufficiale n° 29 del 4 febbraio 2008, pp. 11-46.

O

Okada H. (2003). The Microseismic Survey Method: Society of Exploration Geophysicists of Japan. Translated by Koya Suto, Geophysical Monograph Series No. 12, Society of Exploration Geophysicists, Tulsa.

O'Neill A., Matsuoka T. (2005). Dominant Higher Surface-wave Modes and Possible Inversion Pitfalls. J. Environ. Eng. Geophys., 10: 185-201.

Ordaz M., Aguilar A., Arboleda J. (2007). Crisis 2007: Program for computing seismic hazard. Version 5.4. Mexico City: UNAM.

Özel O., Cranswick E., Meremonte M., Erdik M., Safak E. (2002). Site effects in Avcilar, west of Istanbul, Turkey, from strong- and weak-motion data. Bull. Seism. Soc. Am., 92(1): 499-508.

P

Pagliaroli A., Pitilakis K., Chávez-García F. J., Raptakis D., Apostolidis P., Ktenidou O.-J., Manakou M., Lanzo G. (2007). Experimental study of topographic effects using explosions and microtremors recordings, paper presented at 4th International Conference on Earthquake Geotechnical Engineering, Thessaloniki, Greece.

Pancha A., Anderson J. G., Louie J. N., Pullammanappallil S. K. (2008). Measurement of shallow shear wave velocities at a rock site using the ReMi technique. Soil Dyn. Earthquake Eng., 28: 522–535.

Pannatier Y (1996) Variowin – Software for Spatial Data Analysis in 2D, Springer-Verlag, New York, 91 pp., ISBN 0-387-94579-9.

Panzera F., Lombardo G., Rigano R. (2011a). Evidence of Topographic Effects through the Analysis of Ambient Noise Measurements. Seism. Res. Lett., 82(3): 413-419.

Panzera F., Rigano R., Lombardo G., Cara F., Di Giulio G., Rovelli A. (2011b). The role of alternating outcrops of sediments and basaltic lavas on seismic urban scenario: the study case of Catania, Italy. Bull. Earth. Eng. 9: 411-439.

Paolucci R. (2002). Amplification of earthquake ground motion by steep topographic irregularities. Earthq. Eng. Struct. Dyn., 31: 1831–1853.

Parolai S., D. Bindi, Augliera P. (2000). Application of the generalized inversion technique (GIT) to a microzonation study: numerical simulations and comparison with different site-estimation techniques. Bull. Seism. Soc. Am**.,** 90(2), 286–297.

Parolai S., Bindi D., Troiani L. (2001). Site response for the RSM seismic network and source parameters in the central Apennines (Italy). Pure Appl. Geophys., 158: 695–715.

Parolai S., Richwalski S. M. (2004). The importance of converted waves in comparing H/V and RSM site response estimates. Bull. Seism. Soc. Am., 94(1): 304-313.

Park C. B., Miller R.D., Xia J. (1999). Multichannel analysis of surface waves. Geophysics, 64 (3): 800–808.

Park C. B., Miller R. D., Miura H. (2002). Optimum field parameter of an MASW survey, Extended Abstract, Society of Exploration Geophysicists of Japan, Tokio, May 22-23.

Park C. B., Miller R. D., Ryden N., Xia J., Ivanov J. (2005). Combined use of active and passive surface waves. J. Environ. Eng. Geophys., 10: 323–334.

Park C. B., Miller R. D. (2008). Roadside Passive Multichannel Analysis of Surface Waves (MASW). J. Environ. Eng. Geophys., 13(1): 1–11.

Pasolini C., Albarello D., Gasperini P., D'Amico V., Lolli B. (2008). The attenuation of seismic intensity in Italy part II: modeling and validation. Bull. Seism. Soc. Am., 98: 692-708.

Pedersen H. A, Le Brun B., Hatzfeld D., Campillo M., Bard P.Y. (1994). Ground motion amplitude across ridges. Bull. Seism. Soc. Am., 84: 1786-1800.

Pepe F., Bertotti G., Cella F., Marsella E. (2000). Rifted margin formation in the South Tyrrhenian Sea; a high-resolution seismic profile across the North Sicily passive continental margin. Tectonics 19(2): 241-257.

Piatanesi A., Tinti S. (1998). A revision of the 1693 eastern Sicily earthquake and tsunami. J. Geophys. Res. 103: 2749–2758.

Pischiutta M., Cultrera G., Caserta A., Luzi L., Rovelli A. (2010). Topographic effects on the hill of Nocera Umbra, central Italy. Geophys. J. Int., 182(2), 977-987.

Poppeliers C., Pavlis G. L. (2002). The seismic response of a steep slope: high-resolution observations with a dense, three-component seismic array. Bull. Seism. Soc. Am., 92(8): 3102–3115.

Priolo E. (1999). 2-D spectral element simulations of destructive ground shaking in Catania (Italy). J. Seism., 3(3): pp 289-309

Priolo E., Michelini A., Laurenzano G., Addia R., Puglia A. (2005). Seismic response from microtremors in Catania (Sicily, Italy). In "Seismic Prevention of Damage: a case study in a Mediterranean city", M. Maugeri (ed.), Advances in Earthquake engineering Vol. 14, WIT Press, Southampton, 33-61.

R

Raptakis D., Chavez-garcia F.J., Makra K., Pitilakis K. (2000). Site effects at Euroseistest – I. Determination of the valley structure and confrontation of observations with 1D analysis. Soil Dyn. Earthq. Eng., 19: 1-22.

Raptakis D., Theodulidis N., Pitilakis K. (1998). Data analysis of the Euroseistest Strong Motion Array in Volvi (Greece): standard and horizontal-to-vertical spectral ratio techniques. Earthquake Spectra, 14(1): 203-224.

Riepl J., Bard P.-Y., Hatzfeld D., Papaioannou C., Nechtschein S. (1998). Detailed evaluation of site response estimation methods accros and along the sedimentary valley of Volvi (EUROSEISTEST). Bull. Seism. Soc. Am 88(2): 488-502.

Rigano R., Cara F., Lombardo G., Rovelli A. (2008). Evidence for ground motion polarization on fault zones of Mount Etna volcano. J. Geophys. Res. 113: B10306, doi: 10.1029/2007JB005574.

Rodriguez V. H., Midorikawa S. (2002). Applicability of the H/V spectral ratio of microtremors in assessing site effects on seismic motion. Earthqu. Eng. Struct. Dyn., 31(2): 261–279.

Roten D., Cornou C., Fäh D., Giardini D. (2006). 2D resonances in Alpine valleys identified from ambient vibration wavefields. Geophys. J. Int., 165, 889-905.

S

Sambridge M. (1999). Geophysical inversion with a neighbourhood algorithm: I. Searching a parameter space. Geophys. J. Int., 138: 479– 494.

Sanchez-Sesma F. J., Luzon F. (1995). Seismic Response of Three-Dimensional Alluvial Valleys for Incident P, S and Rayleigh Waves. Bull. Seism. Soc. Am., 85: 269-284.

Seed H. B., Idriss I. M. (1970). Soil moduli and damping factors for dynamic response analyses. Report No. EERC-70-10, University of California, Berkeley

Seed H.B., Idriss I.M. (1982). Ground motions and soil liquefaction during earthquakes. Earthquake Engineering Research Institute, Berkeley/CA, 1982.

Seekins L. C., Wennerberg L., Marghereti L., Liu H.-P. (1996). Site amplification at five locations in San Fransico, California: a comparison of S waves, codas, and microtremors. Bull. Seism. Soc. Am., 86(3): 627–635.

Semblat J. F. (2010). Modeling seismic wave propagation and amplification in 1D/2D/3D linear and nonlinear unbounded media. Int. Jal of Geomechanics (ASCE), doi:10.1061/(ASCE)GM.1943-5622.0000023

Semblat J. F., Kham M., Bard P.Y. (2008). Seismic wave propagation in alluvial basins and influence of site-city interaction. Bull. Seism. Soc. Am., 98(6): 2665-2678.

Semblat J. F., Brioist J.J. (2000a). Efficiency of higher order finite elements for the analysis of seismic wave propagation. Journal of Sound and Vibration, 231(2), 460-467

Semblat J. F., Duval A. M., Dangla P. (2000b). Numerical analysis of seismic wave amplification in Nice (France) and comparisons with experiments. Soil Dyn. Earthq. Eng., 19(5): 347-362.

Scherbaum F., Hinzen K. G., Ohrnberger M. (2003). Determination of shallow shear wave velocity profiles in the Cologne, Germany area using ambient vibrations. Geophys J. Int., 152: 597–612.

Schnabel P. B., Lysmer J., Seed H. B. (1972). SHAKE A computer program for equation response analysis of horizontally layered sites. Rep. No. EERC 72-12, University of California, Berkeley.

Scognamiglio L., Malagnini L., Akinci A. (2005). Ground-Motion Scaling in Eastern Sicily, Italy. Bull. Seism. Soc. Am. 95(2): 568-578.

SESAME (2004). Guidelines for the implementation of the H/V spectral ratio technique on ambient vibrations: Measurements, processing and interpretation. SESAME European Research Project WP12, deliverable D23.12, http://sesame-fp5.obs.ujf-grenoble.fr/Deliverables/Del-D23-HV_User_Guidelines.pdf.

Sgarlato G., Lombardo G., Rigano R. (2011). Evaluation of seismic site response nearby underground cavities using earthquake and ambient noise recordings: A case study in Catania area, Italy. Eng. Geol., 122(3-4): 281-291.

Sirovich L., Pettenati F. (1999). Seismotectonic outline of South-Eastern Sicily: an evaluation of available options for the earthquake fault rupture scenario. J. Seismol., 3: 213–233.

Slejko D., Peruzza L., Rebez A. (1998). Seismic hazard maps of Italy. Ann. Geof., 41: 183–214.

Spudich P., Hellweg M., Lee W. H. K. (1996). Directional topographic site response at Tarzana observed in aftershocks of the 1994 Northridge, California, earthquake: implications for mainshock motions. Bull. Seism. Soc. Am., 86(1B): S193–S208.

SSHAC (Senior Seismic Hazard Analysis Committee) (1997). Recommendations for probabilistic seismic hazard analysis: guidance on uncertainty and use of experts. NUREG/CR-6372.

Steidl J. H., Tumarkin A. G., Archuleta R. J. (1996). What is a reference site? Bull. Seism. Soc. Am., 86, 1733-1748.

Stephenson W. J, Louie J. N., Pullammanappallil S., Williams R. A., Odum J. K. (2005). Blind shear wave velocity comparison of ReMi and MASW results with boreholes to 200 m in Santa Clara Valley: implications for earthquake ground motion assessment. Bull. Seism. Soc. Am., 95(6): 2506–2516.

Strollo A., Parolai S., Bindi D., Chiauzzi L., Pagliuca R., Mucciarelli M., Zschau J. (2011). Microzonation of Potenza (Southern Italy) in terms of spectral intensity ratio using joint analysis of earthquakes and ambient noise. Bull. Earthq. Eng.: doi10.1007/s10518-011-9256-4

T

Tinti S., Armigliato A. (2003). The use of scenarios to evaluate the tsunami impact in southern Italy. Mar. Geol., 199: 221-243.

Tokimatsu K. (1995). Geotechnical site characterization using surface waves. In: K. Ishihara (ed.): Proceedings of the 1st International Conference on Earthquake Geotechnical Engineering, IS-Tokyo 1995. Balkema Rotterdam, 3: 1333-1365.

Tortorici L. (2000). Geologia delle aree urbane della Sicilia Orientale. In Scenari di pericolosità sismica ad Augusta, Siracusa e Noto: edit by L. Decanini and G.F. Panza, CNR-Gruppo Nazionale per la Difesa dai Terremoti, Roma: 43-54.

Triantafyllidis P., Hatzidimitriou P. M., Theodulidis N., Suhadolc P., Papazachos C., Raptakis D., Lontzetidis K. (1999). Site effects in the city of Thessaloniki (Greece) estimated from acceleration data and 1-D local soil profiles. Bull. Seis. Soc. Am., 89(2): 521-537.

Tselentis G.-A., Danciu L., Sokos E. (2010). Probabilistic seismic hazard assessment in Greece – Part 2: Acceleration response spectra and elastic input energy spectra. Nat. Haz. Earth Syst. Sci., 10: 41–49.

Tucker B. E., King J. L., Hatzfeld D., Nersesov I. L. (1984). Observations of hard-rock site effects. Bull. Seism. Soc. Am., 74: 121-136.

V

Vaccari F., Walling Y., Mohanty W. K., Nath S. K., Verma A. K., Sengupta A., Panza G. F. (2011). Site-Specific Modeling of SH and P-SV Waves for Microzonation Study of Kolkata Metropolitan City, India. Pure Appl. Geophys,168: 479–493

Valensise G., Pantosti D. (2001). The investigation of potential earthquake sources in peninsular Italy: a review. J. Seism., 5: 287-306.

Virieux J. (1986). P-SV Wave Propagation in Heterogeneous Media: Velocity-Stress Finite-Difference Method. Geophysics, 51: 889-901.

Visini F., De Nardis R., Barbano M. S., Lavecchia G. (2009). Testing the seismogenic sources of the January 11th 1693 Sicilian earthquake (Io X/XI): some insights from macroseismic field simulations. Ital. J. Geosci., 128(1): 147-156.

Z

Zheng Y., Stewart R. R. (1992). Polarization filter: design and testing. CREWES Research Report, 4(8): 1-19.

Zollo A., Emolo A., Herrero A., Improta L. (1999). High frequency ground motion modelling in the Catania area associated with the Ibleo-Maltese fault system. J. Seism., 3(3): 279-288.

W

Wang J. G. Z. Q., Law K. T. (1994). Siting in earthquake zones. A.A. Balkema/Rotterdam/Brookfield.

Wang G. (2010). A ground motion selection and modification method preserving characteristics and aleatory variability of scenario earthquakes. 9th US National and 10th Canadian Conference on Earthquake Engineering: Reaching Beyond Borders, Toronto (Canada) 25-29 July 2010

Wathelet M. (2008). An improved neighborhood algorithm: parameter conditions and dynamic scaling. Geophys. Res. Lett., 35: L09301.

Wathelet M., Jongmans D., Ohrnberger M. (2005). Direct Inversion of Spatial Autocorrelation Curves with the Neighborhood Algorithm. Bull. Seism. Soc. Am., 95: 1787-1800.

Wells D. L., Coppersmith K. J. (1994). New Empirical Relationships among Magnitude, Rupture Length, Rupture Width, Rupture Area, and Surface Displacement. Bull. Seism. Soc. Am., 84(4): 974-1002.

Working Group CPTI (2004). Catalogo Parametrico dei Terremoti Italiani, versione 2004 (CPTI04). INGV, Bologna. http://emidius.mi.ingv.it/CPTI04

Working Group DBMI04 (2005). DBMI04, il database delle osservazioni macrosismiche dei terremoti italiani utilizzate per la compilazione del catalogo parametrico CPTI04. http://emidius.mi.ingv.it/DBMI04/. Quaderni di Geofisica, INGV, 49: 1-38.

Working Group ITACA (2010). Data Base of the Italian strong motion records. http://itaca.mi.ingv.it

Working Group MPS (2004). Redazione della mappa di pericolosità sismica prevista dall'Ordinanza PCM del 20 marzo 2003. Rapporto Conclusivo per il Dipartimento della Protezione Civile, INGV, Milano-Roma, April. 65 pp.+5 appendixes. http://zonesismiche.mi.ingv.it

X

Xia J., Miller R. D., Park C. B. (1999). Estimation of near-surface shear-wave velocity by inversion of Rayleigh wave. Geophysics, 64: 691-700.

Xia J., Miller R. D., Park C. B., Tian G. (2003). Inversion of high frequency surface waves with fundamental and higher modes. J. Appl. Geophys., 52 (1): 45–57.

Y

Yokota K., Imai T., Konno M. (1981). Dynamic deformation characteristics of soils determined by laboratory tests. OYO Tec. Rep. 3: pp. 13-37.